

**DYNAMIC BEHAVIOR OF CONTINUOUS FLOW STIRRED
SLURRY REACTORS IN BORIC ACID PRODUCTION**

**A THESIS SUBMITTED TO
THE GRADUATE SCHOOL OF NATURAL AND APPLIED SCIENCES
OF
MIDDLE EAST TECHNICAL UNIVERSITY**

BY

GAYE Ö. YÜCEL ÇAKAL

**IN PARTIAL FULFILLMENT OF THE REQUIREMENTS FOR THE DEGREE OF
DOCTOR OF PHILOSOPHY**

IN

THE DEPARTMENT OF CHEMICAL ENGINEERING

JUNE 2004

Approval of the Graduate School of Natural and Applied Sciences

Prof. Dr. Canan Özgen
Director

I certify that this thesis satisfies all the requirements as a thesis for the degree of Doctor of Philosophy.

Prof. Dr. Timur Doğu
Head of Department

This is to certify that we have read this thesis and that in our opinion it is fully adequate, in scope and quality, as a thesis and for the degree of Doctor of Philosophy.

Prof. Dr. İnci Eroğlu
Supervisor

Examining Committee Members

Prof. Dr. Hayrettin Yücel (METU CHE) _____

Prof. Dr. İnci Eroğlu (METU CHE) _____

Prof. Dr. Saim Özkar (METU CHEM) _____

Prof. Dr. Nusret Bulutcu (ITU CHE) _____

Prof. Dr. Nurcan Baç (METU CHE) _____

I hereby declare that all information in this document has been obtained and presented in accordance with academic rules and ethical conduct. I also declare that, as required by these rules and conduct, I have fully cited and referenced all material and results that are not original to this work.

Name, Last name : Gaye Ö. Yücel Çakal

Signature :

ABSTRACT

DYNAMIC BEHAVIOR OF CONTINUOUS FLOW STIRRED SLURRY REACTORS IN BORIC ACID PRODUCTION

Yücel Çakal, Gaye Ö.

Ph.D., Department of Chemical Engineering

Supervisor: Prof. Dr. İnci Eroğlu

June 2004, 213 pages

One of the most important boron minerals, colemanite is reacted with sulfuric acid to produce boric acid. During this reaction, gypsum (calcium sulfate dihydrate) is formed as a byproduct. In this study, the boric acid production was handled both in a batch and four continuously stirred slurry reactors (4-CFSSR's) in series system.

In this reaction system there are at least three phases, one liquid and two solid phases (colemanite and gypsum). In a batch reactor all the phases have the same operating time (residence time), whereas in a continuous reactor all the phases may have different residence time distributions. The residence time of both the reactant and the product solids are very important because they affect the dissolution conversion of colemanite and the growth of gypsum crystals.

The main aim of this study was to investigate the dynamic behavior of continuous flow stirred slurry reactors. By obtaining the residence time distribution of the solid and liquid components, the non-idealities in the reactors can be found. The experiments performed in the continuous flow stirred slurry reactors showed that the reactors to be used during the boric acid production experiments approached an ideal CSTR in the range of the stirring rate (500-750 rpm) studied.

The steady state performance of the continuous flow stirred slurry reactors (CFSSR's) in series was also studied. During the studies, two colemanites having the same origin but different compositions and particle sizes were used.

The boric acid production reaction consists of two simultaneous reactions, dissolution of colemanite and crystallization of gypsum. The dissolution of colemanite and the gypsum formation was followed from the boric acid and calcium ion concentrations, respectively. The effect of initial $\text{CaO}/\text{SO}_4^{2-}$ molar ratio (1.00, 1.37 and 2.17) on the boric acid and calcium ion concentrations were searched. Also, at these initial molar ratios the colemanite feed rate was varied (5, 7.5, 10 and 15 g/min) to change the residence time of the slurry.

Purity of the boric acid solution was examined in terms of the selected impurities, which were the magnesium and sulfate ion concentrations. The concentrations of them were compared at the initial molar ratios of 1.00 and 1.37 with varying colemanite feed rates. It was seen that at high initial $\text{CaO}/\text{SO}_4^{2-}$ molar ratios the sulfate and magnesium ion concentrations decreased but the calcium ion concentration increased.

The gypsum crystals formed in the reaction are in the shape of thin needles. These crystals, mixed with the insolubles coming from the mineral, are removed from the boric acid slurry by filtration. Filtration of gypsum crystals has an important role in boric acid production reaction because it affects the efficiency, purity and crystallization of boric acid. These crystals must grow to an appropriate size in the

reactor. The growth process of gypsum crystals should be synchronized with the dissolution reaction.

The effect of solid hold-up (0.04–0.09), defined as the volume of solid to the total volume, on the residence time of gypsum crystals was investigated and the change of the residence time (17-60 min) on the growth of the gypsum was searched. The residence time at each reactor was kept constant in each experiment as the volumes of the reactors were equal. The growth of gypsum was examined by a laser diffraction particle size analyzer and the volume weighted mean diameters of the gypsum crystals were obtained. The views of the crystals were taken under a light microscope. It was observed that the high residence time had a positive effect on the growth of gypsum crystals. The crystals had volume weighted mean diameters of even 240 μm .

The gypsum crystal growth model was obtained by using the second order crystallization reaction rate equation. The residence time of the continuous reactors are used together with the gypsum growth model to simulate the continuous boric acid reactors with macrofluid and microfluid models. The selected residence times (20-240 min) were modeled for different number of CSTR's (1-8) and the PFR.

The simulated models were, then verified with the experimental data. The experimentally found calcium ion concentrations checked with the concentrations found from the microfluid model. It was also calculated that the experimental data fitted the microfluid model with a deviation of 4-7%.

Key words: Gypsum Crystallization, Boric Acid, Colemanite Dissolution, Slurry Reactors, Residence Time Distribution, Macrofluid Model, Microfluid Model

ÖZ

BORİK ASİT ÜRETİMİNDE KULLANILAN SÜREKLİ AKIŞLI KARIŞTIRMALI ÇAMUR REAKTÖRLERİNİN DİNAMİK DAVRANIŞI

Yücel Çakal, Gaye Ö.

Doktora, Kimya Mühendisliği Bölümü

Tez Yöneticisi: Prof. Dr. İnci Eroğlu

Haziran 2004, 213 sayfa

Önemli bor minerallerinden biri olan kolemanitin, sülfürik asit ile reaksiyona girmesi sonucunda borik asit üretilmektedir. Bu reaksiyon esnasında jips (kalsiyum sülfat dihidrat) yan ürün olarak oluşmaktadır. Bu çalışmada, borik asit üretimi hem kesikli hem de dörtlü seri bağlantılı sürekli akışlı karıştırmalı çamur reaktörleri sisteminde ele alınmıştır.

Bu reaksiyon sisteminde en az üç tane faz vardır, bir sıvı ve iki katı faz (kolemanit ve jips). Kesikli reaktörde bütün fazlar aynı işletme zamanına (reaktörde kalış süresine) sahiptir. Bunun yanısıra, sürekli reaktörde hem reaksiyona giren katının hem de ürün olan katının reaktörde kalış süresi çok önemlidir çünkü bu kolemanitin çözünme dönüşümünü ve de jips kristallerinin büyümesini etkilemektedir.

Bu çalışmanın esas amacı, sürekli akışlı karıştırmalı çamur reaktörlerinin dinamik davranışını incelenmektir. Katı ve sıvı bileşenlerin reaktörde kalış süresini elde ederek, reaktördeki ideal olmayan koşullar saptanabilmektedir. Sürekli akışlı karıştırmalı çamur reaktörlerinde yapılan çalışmalar borik asit üretimi deneylerinde kullanılan reaktörlerin çalışılan karıştırma hızlarında (500-750 rpm) ideal karıştırmalı tank reaktörlerine yaklaştığını göstermektedir.

Seri bağlantılı sürekli akışlı karıştırmalı çamur reaktörlerinin yatışkinhal performansı da çalışılmıştır. Bu çalışmalar esnasında, aynı yerden gelen fakat farklı kompozisyonlara ve parça boyutuna sahip iki kolemanit kullanılmıştır.

Borik asit üretim reaksiyonu iki birbirini takip eden reaksiyondan oluşmaktadır, kolemanitin çözünmesi ve jipsin kristalizasyonu. Kolemanit çözünmesi ve jips oluşumu, sırasıyla, borik asit ve kalsiyum iyon konsantrasyonu ile takip edilmektedir. Başlangıç $\text{CaO}/\text{SO}_4^{2-}$ mol oranının (1.00, 1.37 ve 2.17) borik asit ve kalsiyum iyon konsantrasyonuna etkisi araştırılmıştır. Bu başlangıç mol oranlarında, çamurun reaktörde kalış süresini değiştirmek için farklı kolemanit besleme hızları (5, 7.5, 10 ve 15 g/dak) kullanılmıştır.

Borik asit çözeltisinin saflığı, seçilen safsızlıklar, magnezyum ve sülfat iyonları konsantrasyonları, ile incelenmiştir. Bu konsantrasyonlar, başlangıç mol oranı 1.00 ve 1.37 olduğu durumlarda, kolemanit besleme hızlarını değiştirerek karşılaştırılmıştır. Yüksek başlangıç $\text{CaO}/\text{SO}_4^{2-}$ mol oranında sülfat ve magnezyum iyon konsantrasyonlarının azaldığı fakat kalsiyum iyon konsantrasyonunun arttığı görülmüştür.

Reaksiyonda oluşan jips kristalleri ince iğneler şeklindedir. Bu kristaller, mineralden gelen çözünmemişlerle karışıp, borik asit çamurundan filtrasyonla uzaklaştırılır. Jips kristallerinin filtrasyonunun borik asit üretim reaksiyonunda önemli bir yeri vardır çünkü bu işlem, verimi, saflığı ve borik asidin kristalizasyonunu etkilemektedir. Bu kristaller reaktörde uygun bir boyuta büyütülmek zorundadır. Jips kristallerinin büyüme prosesi çözünme reaksiyonu ile senkronize bir şekilde çalışmalıdır.

Katı tutma oranının (0.04-0.09) jips kristallerinin reaktörde kalış süresine etkisi araştırılmış ve reaktörde kalış süresi değişimi (17-60 min) ile jipsin büyümesi

incelenmiştir. Katı tutma oranı, katı hacminin toplam hacime oranı şeklinde ifade edilir. Deneyler esnasında, her reaktördeki kalış süresi, reaktörlerin hacmi eşit olduğundan sabit kalmıştır. Jips büyümesi lazer kırınım parça boyut analiz cihazı ile incelenmiş ve jips kristallerinin hacimce ortalama çapları elde edilmiştir. Kristal görüntüleri ışık mikroskobu ile çekilmiştir. Yüksek reaktörde kalış süresinin jips kristal büyümesine pozitif bir etkisi olduğu gözlemlenmiştir. Kristallerin hacimce ortalama çapları 240 µm'a kadar varmıştır.

Jips kristal büyüme modeli, ikinci dereceden kristalizasyon reaksiyonu hız denklemi ile elde edilmiştir. Sürekli borik asit reaktörlerinin makroakışkan ve mikroakışkan modeli ile simulasyonu için, sürekli reaktörlerdeki reaktördeki kalış süresi jips büyüme modeli ile birlikte kullanılmıştır. Değişik sayıdaki sürekli karıştırılmalı tank reaktörleri (1-8) ve piston akış reaktörler, seçilen reaktörde kalış süreleri (20-240 dak) ile modellenmiştir.

Simule edilen modeller, daha sonra deneysel veri ile doğrulanmıştır. Deneysel olarak bulunan kalsiyum iyon konsantrasyonları mikroakışkan modeli ile bulunan konsantrasyonlarla uyumuştur. Deneysel verinin mikroakışkan modelinden % 4-7 oranında saptığı bulunmuştur.

Anahtar Kelimeler: Jips Kristalizasyonu , Borik Asit, Kolemanit Çözünmesi, Çamur Reaktörleri, Kalış Süresi Dağılımı, Makroakışkan Modeli, Mikroakışkan Modeli

ACKNOWLEDGMENTS

It is a great pleasure for me to have the opportunity to express my deepest gratitude to my supervisor Prof. Dr. İnci Erođlu for her invaluable supervision, continuous support and helpful suggestions throughout the course of this investigation.

I also wish to express my gratitude to my examining committee members Prof. Dr. Saim Özkar and Prof. Dr. Hayrettin Yücel for their encouragement and comments during the course of the study.

Special thanks are due to Prof. Dr. Nusret Bulutcu and Funda Altun for the valuable discussions and advise.

I would like to thank Eti Maden İşletmeleri for the colemanite, sulfuric acid and boric acid supports and METU for the financial support with the BAP Project with the number BAP- 2001-07-02-02.

I wish to thank Prof. Dr. Zeki Aktaş for giving us time for the particle size analysis and letting us use the analyzer. I also would like to thank Kerime Güney for the chemical analysis, and all the Ch.E. Workshop members for their continuous help throughout the thesis.

I would like to express my sincere gratitude to my friends Anıl Erdoğan, Deniz Gürhan and Işık Aşar for their helps during the continuous boric acid production experiments and Salih Obut for the Mat Lab Programming. I also would like to thank my room mates Barış Ünal and Ceren Oktar for the valuable discussions and listening to me whenever I need.

Furthermore, I would like to express my deepest gratefulness to my family. Without their support, tolerance and encouragement, this thesis could not have come to an end.

Finally, I am thankful to my husband for his understanding and unlimited support.

To My Dearest Husband Teoman

and Beloved Son Emre ...

TABLE OF CONTENTS

	<u>Page</u>
ABSTRACT	iv
ÖZ	vii
ACKNOWLEDGEMENT	x
TABLE OF CONTENTS	xii
LIST OF TABLES	xvii
LIST OF FIGURES	xxii
LIST OF SYMBOLS AND ABBREVIATIONS	xxviii
CHAPTER	
1. INTRODUCTION	1
1.1. Borate Minerals	1
1.2. Boric Acid Production in the World	4
1.3. Boric Acid Production in Turkey	6
2. LITERATURE SURVEY	10
2.1. Dissolution of Colemanite and Its Kinetics	10
2.2. Crystal Growth of Calcium Sulfate Dihydrate and Its Kinetics	12
2.3. Heterogeneous Solid Fluid Reaction Modeling	15
2.4. The Studies On The Residence Time Distribution In Fluid-Solid Reactors.....	18
2.5. Reactor Modeling with Residence Time Distribution.....	20
2.6. Objective of the Present Study.....	21
3. MODELING	23
3.1. Gypsum Crystal Growth Model	24

3.2. Terminology of Mixing	24
3.3. Simulation of Continuous Flow Reactors	27
3.3.1. Macrofluid Model for n-CSTR's in Series	28
3.3.2. Microfluid Model for n-CSTR's in Series	31
3.3.3. Plug Flow Model	32
4. EXPERIMENTAL	34
4.1. Materials	34
4.2. Batch Reactor Experiments	34
4.2.1. Experimental Setup	34
4.2.2. Experimental Procedure	37
4.2.3. Scope of the Experiments	37
4.3. Continuous Flow Stirred Slurry Reactors in Series Experiments....	37
4.3.1. Experimental Setup	38
4.3.2. Dynamic Behavior Experiments	43
4.3.2.1. Experimental Procedure	43
4.3.2.2. Scope of the Experiments	44
4.3.3. Boric Acid Production Experiments	45
4.3.3.1. Experimental Procedure	45
4.3.3.2. Scope of the Experiments	46
4.4. Analytical Procedures	49
4.4.1. Determination of Boric Acid Concentration	49
4.4.2. Determination of Calcium Ion Concentration	49
4.4.3. Determination of Sulfate Ion Concentration	49
4.4.4. Determination of Magnesium Ion Concentration	50
4.4.5. Crystal Size Determination	50
4.4.5.1. Particle Size Distribution of Gypsum Crystals	50
4.4.5.2. Light Microscope Images of Gypsum Crystals	51

5. RESULTS AND DISCUSSION	52
5.1. Results of Colemanite Analysis	52
5.1.1. Screen Analysis of Colemanite	52
5.1.2. Chemical Analysis of Colemanite	57
5.1.3. Particle Size Distribution of Colemanite	59
5.2. Dynamic Behavior Experiments on Continuous Flow Stirred Slurry Reactors	61
5.2.1. Liquid Residence Time Experiments	62
5.2.1.1. Effect of Stirring Rate on Liquid Residence Time	62
5.2.1.2. Check of Different Tracers on Liquid Residence Time	66
5.2.2. Solid Residence Time Experiments	69
5.2.3. Liquid Residence Time Experiments in a Solid/Liquid System	71
5.2.3.1. Effect of Stirring Rate on Liquid Residence Time	71
5.2.3.2. Effect of Solid to Liquid Ratio on Liquid Residence Time	73
5.3. Batch Reactor Experiments	78
5.4. Boric Acid Production Experiments on Continuous Flow Stirred Slurry Reactors in Series	83
5.4.1. Parameters Affecting the Performance of CFSSR's in Series	84
5.4.2. Variation of the Concentration of Boric Acid in Solution at Steady State	84
5.4.3. Variation of the Concentration of Calcium Ion in Solution at Steady State	88
5.4.4. pH and Temperature Variation of the Experiments at Steady State	93
5.4.5. Variation of the Concentrations of Sulfate and Magnesium Ions in Solution at Steady State	95
5.4.6. Comparison of Variation of Calcium and Sulfate Ion Molar Flow Rate	97
5.4.7. Conversion Expressions Used During the Study	98
5.4.8. Effect of Solid Hold-Up on the Residence Time of Liquid and Solid Components	99
5.5. Particle Size Distribution of Gypsum Crystals	101
5.5.1. Particle Size Distribution of Gypsum Crystals in a Batch Reactor	101
5.5.2. Particle Size Distribution of Gypsum Crystals in	102

Continuous Flow Stirred Slurry Reactors	112
5.6. Light Microscope Images of Gypsum Crystals	112
5.6.1. Light Microscope Images of Gypsum Crystals in a Batch Reactor	113
5.6.2. Light Microscope Images of Gypsum Crystals in Continuous Flow Stirred Slurry Reactors	113
5.7. Simulation of Boric Acid Reactors	116
5.7.1. Gypsum Crystal Growth Model	116
5.7.2. Simulation of Continuous Reactors	122
5.7.2.1. Macrofluid model for n-CSTR's in Series	122
5.7.2.2. Microfluid model for n-CSTR's in Series	126
5.7.2.3. Plug Flow Model	130
5.7.2.4. Comparison of the Model Results	133
5.8. Comparison of the Results	136
5.8.1. Batch Reactor versus Continuous Reactor Experiments	136
5.8.2. Verification of the Experimental Data with the Model Results	140
6. CONCLUSIONS	143
7. RECOMMENDATIONS.....	147
REFERENCES	149
APPENDICES	
A. Chemical Analysis of Colemanite	155
A.1. Determination of B₂O₃ Content	155
A.2. Determination of SiO₂ Content	156
A.3. Determination of Na₂O and K₂O Content	157
A.4. Determination of CaO, MgO, Al₂O₃, Fe₂O₃, SrO and TiO₂ Content	157
B. Raw Data of Dynamic Behavior Experiments	158
B.1. Data of Liquid Residence Time Experiments	159
B.2. Data of Solid Residence Time Experiments	163
B.3. Data of Liquid Residence Time Experiments in a Solid / Liquid System	164

C.	Raw Data of the Batch Reactor Experiments	167
C.1.	Data of Experiment HB2.1& HB2.2	168
C.2.	Data of Experiment HB2.3	170
C.3.	Data of Experiment HB3.1	171
D.	Raw Data of Boric Acid Production Experiments in Continuously Stirred Slurry Reactors	172
D.1.	Data of Experiment HC2.1	173
D.2.	Data of Experiment HC2.2	175
D.3.	Data of Experiment HC2.3	177
D.4.	Data of Experiment HC2.4	179
D.5.	Data of Experiment HC2.5	182
D.6.	Data of Experiment HC2.6	184
D.7.	Data of Experiment HC2.7	186
D.8.	Data of Experiment HC2.8	188
D.9.	Data of Experiment HC3.1	190
D.10.	Data of Experiment HC3.2	192
E.	Raw Data of Solid Hold-up Experiments	194
F.	Sample Calculations	197
F.1.	CaO/SO ₄ ²⁻ Molar Ratio Calculation	198
F.2.	Solid Hold-up, Calculation	199
F.3.	Residence Time of Solid and Liquid Components in the Reactor ..	199
F.4.	Material Balances	201
F.5.	Conversion Calculations	202
F.6.	Unit Conversions	203
G.	Modeling	205
G.1.	Macrofluid Model Mat Lab Program	206
G.2.	Microfluid Model Mat Lab Program	207
G.3.	Mat Lab Program Outputs for the Verification of Experimental Data	208
VITA	213

LIST OF TABLES

TABLE	<u>Page</u>
1.1. Commercially important borate minerals (Roskill, 2002)	2
1.2. Distribution of borate minerals (Kirk Othmer, 1992)	3
1.3. Reserves of boron minerals in Turkey (Roskill, 2002)	3
1.4. Boric acid producers and their capacities (Roskill, 2002).....	5
3.1. Comparison of macrofluid and microfluid behavior in a reactor	27
3.2. Comparison of batch, plug flow and mixed flow reactors in terms of the behaviors of micro and macrofluids	27
4.1. The Batch Reactor Experiments Performed during the Study	37
4.2. Dynamic Behavior Experiments Performed	44
4.3a. Performed Experiments in Grouped Style in Continuous Flow Stirred Slurry Reactors in Series	47
4.3b. Performed Experiments in Continuous Flow Stirred Slurry Reactors in Series	48
5.1.1. The screen analysis of Hisarcık 1 colemanite	53
5.1.2. The screen analysis of Hisarcık 2 colemanite	54
5.1.3. The screen analysis of Hisarcık 3 colemanite	56
5.1.4. Chemical analysis of Hisarcık 1 colemanite (dry basis, wt%) (METU, Chemical Eng. Dept.)	58
5.1.5. Chemical analysis of Hisarcık colemanites (dry basis, wt%) (METU, Chemical Eng. Dept.)	59
5.1.6. Volume weighted mean diameters of the colemanites	61
5.2.1. Comparison of the two experimental values with the theoretical ones (volumetric flow rate = 42.5 ml/min, tracer= nickel)	66
5.2.2. Comparison of different tracers with the theoretical ones (volumetric slow rate = 42.5 ml/min, stirring rate = 500 rpm)	68
5.2.3. Comparison of the residence time and the variance per square of residence time for step input experiments	70
5.2.4. Comparison of the residence time of liquid and solid and the variance per square of liquid residence time for different stirring rates	72

5.2.5.	Comparison of the residence time of liquid and the variance per square of residence time for different solid to liquid ratios (g solid/ml liquid)	74
5.2.6.	The residence time of liquid evaluated from Figure 5.2.11 and Equation 5.2.17 at different solid to liquid ratios (g solid/ml liquid)	76
5.4.1.	Steady state values of produced boric acid concentrations and molar flow rates in the experiments	84
5.4.2.	Steady state values of calcium ion concentrations and molar flow rates in the experiments	88
5.4.3.	Steady state values of pH and temperature in the experiments	93
5.4.4.	Steady state values of the magnesium and sulfate ion concentrations in the fourth reactor in the experiments	94
5.4.5.	Conversion calculated in terms of colemanite and sulfate ion entering the system	98
5.4.6.	Solid hold-up and residence time of the solid and liquid components in each of the reactors in series	99
5.5.1.	Volume weighted mean diameter (μm) of the particles obtained from the software of the laser diffraction particle size analyzer for the experiments performed by using Hisarcik 2 colemanite, 0-250 μm	108
5.7.1.	The model parameters of the batch reactor experiments	119
5.7.2.	Gypsum Crystal Growth Model Obtained from Different Batch Reactor Experiments	120
5.7.3.	The calcium ion concentration evaluated at the exit of the n^{th} CSTR, estimated by macrofluid model using the rate expression in Eq. 5.7.1 ($C_o = 0.053 \text{ mol/l}$, $C_{\text{sat}} = 0.013 \text{ mol/l}$)	123
5.7.4.	The calcium ion concentration evaluated at the exit of the n^{th} CSTR, estimated by macrofluid model using the rate expression in Eq. 5.7.2 ($C_o = 0.043 \text{ mol/l}$, $C_{\text{sat}} = 0.011 \text{ mol/l}$)	124
5.7.5.	The calcium ion concentration evaluated at the exit of the n^{th} CSTR, estimated by macrofluid model using the rate expression in Eq. 5.7.3 ($C_o = 0.0299 \text{ mol/l}$, $C_{\text{sat}} = 0.0056 \text{ mol/l}$)	124
5.7.6.	The calcium ion concentration evaluated at the exit of the n^{th} CSTR, estimated by microfluid model using the rate expression in Eq. 5.7.1 ($C_o = 0.053 \text{ mol/l}$, $C_{\text{sat}} = 0.013 \text{ mol/l}$)	127
5.7.7.	The calcium ion concentration evaluated at the exit of the n^{th} CSTR, estimated by microfluid model using the rate expression in Eq. 5.7.2 ($C_o = 0.043 \text{ mol/l}$, $C_{\text{sat}} = 0.011 \text{ mol/l}$)	127
5.7.8.	The calcium ion concentration evaluated at the exit of the n^{th} CSTR, estimated by microfluid model using the rate expression in Eq. 5.7.3 ($C_o = 0.0299 \text{ mol/l}$, $C_{\text{sat}} = 0.0056 \text{ mol/l}$)	128
5.7.9.	Plug Flow Model Expressions	131
5.7.10.	The calcium ion concentration evaluated at the exit of the PFR with the plug flow models given in Table 5.7.9	132

5.8.1.	Comparison of batch reactor and continuous reactor results performed by Hisarcık 2, 0-250 μm , colemanite in terms of boric acid, calcium ion concentrations, pH and volume weighted mean diameter (μm) of the gypsum crystals obtained at initial $\text{CaO}/\text{SO}_4^{2-}$ molar ratio of 1.00, Stirring Rate = 500 rpm (batch), 400 rpm (continuous), temperature = 85°C	138
5.8.2.	Comparison of batch reactor and continuous reactor results performed by Hisarcık 3, 0-150 μm , colemanite in terms of boric acid, calcium ion concentrations, pH and volume weighted mean diameter (μm) of the gypsum crystals obtained at initial $\text{CaO}/\text{SO}_4^{2-}$ molar ratio of 1.00, stirring rate =400 rpm, temperature = 85°C	139
5.8.3.	Calcium ion concentrations at the exit of the CSTR's obtained by macrofluid, microfluid models and the experimental data	141
B.1.	Variation in nickel concentrations in liquid residence time experiments at different stirring rates	159
B.2.	Comparison of E(t) and F(t) values of the liquid residence time experiments and the ideal reactor (Pulse tracer=Nickel)	160
B.3.	Variation in the concentrations of different tracers on the liquid residence time at 500 rpm	161
B.4.	Comparison of E(t) and F(t) values of different tracers (stirring rate=500 rpm) and the ideal reactor	162
B.5.	Variation in colemanite weight during positive and negative step tracer experiments (Stirring Rate=500 rpm)	163
B.6.	Variation in nickel concentrations in liquid residence time experiments at different stirring rates	164
B.7.	Variation in lithium concentrations of liquid at different solid to liquid ratios (g solid/ml liquid)	165
B.8.	The $-\ln(C/C_0)$ vs t/τ values for different S/L ratios (g solid/ml liquid).....	166
C.1.	Boric acid and calcium ion concentrations during the Experiment HB2.1, Hisarcık 2 colemanite, 0-250 μm , $\text{CaO}/\text{SO}_4^{2-} = 0.95$, stirring rate = 500 rpm, T= 80°C	168
C.2.	Boric acid and calcium ion concentrations during the Experiment HB2.2, Hisarcık 2 colemanite, 250-1000 μm , $\text{CaO}/\text{SO}_4^{2-} = 0.95$, stirring rate = 500 rpm, T= 80°C	169
C.3.	Boric acid and calcium ion concentrations during the Experiment HB2.3, Hisarcık 2 colemanite, 0-250 μm , $\text{CaO}/\text{SO}_4^{2-} = 1$, stirring rate = 500 rpm, T= 85°C	170
C.4.	Variation in pH during the Experiment HB2.3, Hisarcık 2 colemanite, 0-250 μm , $\text{CaO}/\text{SO}_4^{2-} = 1$, stirring rate = 500 rpm, T= 85°C	170
C.5.	Boric acid and calcium ion concentrations during the Experiment HB3.1, Hisarcık 3 colemanite, 0-150 μm , $\text{CaO}/\text{SO}_4^{2-} = 1$, stirring rate = 400 rpm, T= 85°C	171
C.6.	Variation in pH during the Experiment HB3.1, Hisarcık 3 colemanite, 0-150 μm , $\text{CaO}/\text{SO}_4^{2-} = 1$, stirring rate = 400 rpm, T= 85°C	171

D.1.	Calcium ion concentrations of the effluent streams during the Experiment HC2.1, Hisarcık 2 colemanite, 0-250 μm , $\text{CaO}/\text{SO}_4^{2-} = 1$, stirring rate = 400 rpm, $T = 85^\circ\text{C}$, colemanite feed rate = 5 g/min	173
D.2.	Temperature and pH values during the Experiment HC2.1, Hisarcık 2 colemanite, 0-250 μm , $\text{CaO}/\text{SO}_4^{2-} = 1$, stirring rate = 400 rpm, $T = 85^\circ\text{C}$, colemanite feed rate = 5 g/min	174
D.3.	Calcium ion concentrations of the effluent streams during the Experiment HC2.2, Hisarcık 2 colemanite, 0-250 μm , $\text{CaO}/\text{SO}_4^{2-} = 1$, stirring rate = 400 rpm, $T = 85^\circ\text{C}$, colemanite feed rate = 7.5 g/min	175
D.4.	Temperature and pH values during the Experiment HC2.2, Hisarcık 2 colemanite, 0-250 μm , $\text{CaO}/\text{SO}_4^{2-} = 1$, stirring rate = 400 rpm, $T = 85^\circ\text{C}$, colemanite feed rate = 7.5 g/min	176
D.5.	calcium ion concentrations of the effluent streams during the Experiment HC2.3, Hisarcık 2 colemanite, 0-250 μm , $\text{CaO}/\text{SO}_4^{2-} = 1$, stirring rate = 400 rpm, $T = 85^\circ\text{C}$, colemanite feed rate = 10 g/min	177
D.6.	Temperature and pH values during the Experiment HC2.3, Hisarcık 2 colemanite, 0-250 μm , $\text{CaO}/\text{SO}_4^{2-} = 1$, stirring rate = 400 rpm, $T = 85^\circ\text{C}$, colemanite feed rate = 10 g/min	178
D.7.	Calcium ion concentrations of the effluent streams during the Experiment HC2.4, Hisarcık 2 colemanite, 0-250 μm , $\text{CaO}/\text{SO}_4^{2-} = 1.37$, stirring rate = 400 rpm, $T = 85^\circ\text{C}$, colemanite feed rate = 5 g/min.....	179
D.8.	Temperature and pH values during the Experiment HC2.4, Hisarcık 2 colemanite, 0-250 μm , $\text{CaO}/\text{SO}_4^{2-} = 1.37$, stirring rate = 400 rpm, $T = 85^\circ\text{C}$, colemanite feed rate = 5 g/min	180
D.9.	Calcium ion concentrations of the effluent streams during the Experiment HC2.5, Hisarcık 2 colemanite, 0-250 μm , $\text{CaO}/\text{SO}_4^{2-} = 1.37$, stirring rate = 400 rpm, $T = 85^\circ\text{C}$, colemanite feed rate = 10 g/min	182
D.10.	Temperature and pH values during the Experiment HC2.5, Hisarcık 2 colemanite, 0-250 μm , $\text{CaO}/\text{SO}_4^{2-} = 1.37$, stirring rate = 400 rpm, $T = 85^\circ\text{C}$, colemanite feed rate = 10 g/min	183
D.11.	Boric acid and calcium ion concentrations of the effluent streams during the Experiment HC2.6, Hisarcık 2 colemanite, 0-250 μm , $\text{CaO}/\text{SO}_4^{2-} = 1.37$, stirring rate = 400 rpm, $T = 85^\circ\text{C}$, colemanite feed rate = 10 g/min	184
D.12.	Temperature and pH values during the Experiment HC2.6, Hisarcık 2 colemanite, 0-250 μm , $\text{CaO}/\text{SO}_4^{2-} = 1.37$, stirring rate = 400 rpm, $T = 85^\circ\text{C}$, colemanite feed rate = 10 g/min	185
D.13.	Calcium ion concentrations of the effluent streams during the Experiment HC2.7, Hisarcık 2 colemanite, 0-250 μm , $\text{CaO}/\text{SO}_4^{2-} = 1.37$, stirring rate = 400 rpm, $T = 85^\circ\text{C}$, colemanite feed rate = 15 g/min	186
D.14.	Temperature and pH values of the effluent streams during the Experiment HC2.7, Hisarcık 2 colemanite, 0-250 μm , $\text{CaO}/\text{SO}_4^{2-} = 1.37$, stirring rate = 400 rpm, $T = 85^\circ\text{C}$, colemanite feed rate = 15 g/min	187

D.15.	Calcium ion concentrations of the effluent streams during the Experiment HC2.8, Hisarcık 2 colemanite, 0-250 μm , $\text{CaO}/\text{SO}_4^{2-} = 2.17$, stirring rate = 400 rpm, $T = 85^\circ\text{C}$, colemanite feed rate = 10 g/min	188
D.16.	Temperature and pH values during the Experiment HC2.8, Hisarcık 2 colemanite, 0-250 μm , $\text{CaO}/\text{SO}_4^{2-} = 2.17$, stirring rate = 400 rpm, $T = 85^\circ\text{C}$, colemanite feed rate = 10 g/min	189
D.17.	Boric acid and calcium ion concentrations of the effluent streams during the Experiment HC3.1, Hisarcık 3 colemanite, 0-150 μm , $\text{CaO}/\text{SO}_4^{2-} = 1.00$, stirring rate = 400 rpm, $T = 85^\circ\text{C}$, colemanite feed rate = 3.5 g/min	190
D.18.	Temperature and pH values during the Experiment HC3.1, Hisarcık 3 colemanite, 0-150 μm , $\text{CaO}/\text{SO}_4^{2-} = 1.00$, stirring rate = 400 rpm, $T = 85^\circ\text{C}$, colemanite feed rate = 3.5 g/min	191
D.19.	Boric acid and calcium ion concentrations of the effluent streams during the Experiment HC3.2, Hisarcık 3 colemanite, 0-150 μm , $\text{CaO}/\text{SO}_4^{2-} = 1.00$, stirring rate = 400 rpm, $T = 85^\circ\text{C}$, colemanite feed rate = 10 g/min.....	192
D.20.	Temperature and pH values during the Experiment HC3.2, Hisarcık 3 colemanite, 0-150 μm , $\text{CaO}/\text{SO}_4^{2-} = 1.00$, stirring rate = 400 rpm, $T = 85^\circ\text{C}$, colemanite feed rate = 10 g/min	193
E.1.	Variation of solid hold-up during the Experiment HC3.1, Hisarcık 3 colemanite, 0-150 μm , $\text{CaO}/\text{SO}_4^{2-} = 1.00$, colemanite feed rate = 3.5 g/min	195
E.2.	Variation of solid hold-up during the Experiment HC3.2, Hisarcık 3 colemanite, 0-150 μm , $\text{CaO}/\text{SO}_4^{2-} = 1.00$, colemanite feed rate = 10 g/min	196
G.1.	Output of Mat Lab Program for microfluid model for the verification of Experiment HC3.1	208
G.2.	Output of Mat Lab Program for microfluid model for the verification of Experiment HC3.2	209
G.3.	Output of Mat Lab Program for macrofluid model for the verification of Experiment HC3.1	211
G.4.	Output of Mat Lab Program for macrofluid model for the verification of Experiment HC3.2	212

LIST OF FIGURES

FIGURE	<u>Page</u>
2.1. Macrokinetics of heterogeneous solid-liquid reaction crystallizations (Bechtloff, 2001)	16
2.2. Mechanism for sink type microphase	18
3.1. Schematic representation of macrofluid behavior	26
3.2. Schematic representation of microfluid behavior	26
3.3. Schematic representation of inlet of the reactor, in which a microfluid or a macrofluid is entering the reactor	26
3.4. Change of E(t) function with CSTR number	30
3.5. Change of F(t) function with CSTR number	30
4.1. Schematic diagram of the set-up used for the batch reactor experiments	35
4.2. Photograph of the set-up used for the batch reactor experiments ...	36
4.3. Schematic diagram of the set-up used for the continuous flow stirred slurry reactor experiments	40
4.4. Technical drawing of the continuous flow stirred slurry reactor	41
4.5. Photograph of the set-up used for the continuous flow stirred slurry reactor experiments	42
5.1.1. Particle size distribution curve (differential analysis) for Hisarcık 1 colemanite	53
5.1.2. Particle size distribution curve (cumulative analysis) for Hisarcık 1 colemanite	54
5.1.3. Particle size distribution curve (differential analysis) for Hisarcık 1 colemanite	55
5.1.4. Particle size distribution curve (cumulative analysis) for Hisarcık 2 colemanite	55
5.1.5. Particle size distribution curve (differential analysis) for Hisarcık 3 colemanite.....	56
5.1.6. Particle size distribution curve (cumulative analysis) for Hisarcık 3 colemanite	57
5.1.7. Particle size distribution of Hisarcık 1 colemanite	60
5.1.8. Particle size distribution of Hisarcık 2 colemanite	60

5.1.9.	Particle size distribution of Hisarcık 3 colemanite	60
5.2.1.	Variation in nickel concentration depending on the stirring rate during the liquid residence time experiments (Volumetric flow rate = 42.5 ml/min)	63
5.2.2.	Comparison of the E(t) curves for two different stirring rates and the ideal reactor	64
5.2.3.	Comparison of the F(t) curves for two different stirring rates and the ideal reactor	65
5.2.4.	Comparison of concentrations of different tracers	66
5.2.5.	Comparison of the E(t) curves for different tracers and the ideal reactor	67
5.2.6.	Comparison of the F(t) curves for different tracers and the ideal reactor	67
5.2.7.	Responses to a negative and a positive step input given to the feed rate of colemanite	69
5.2.8.	Variation in lithium concentration depending on the stirring rate during the liquid residence time experiments (Liquid feed rate = 42.5 ml/min, colemanite feed rate=7.2 g/min)	71
5.2.9.	Variation in lithium concentration depending on the solid to liquid ratio (g solid/ml liquid) during the liquid/solid residence time experiments (Colemanite feed rate = 7.2 g/min)	73
5.2.10.	Normalized lithium concentrations with respect to the initial tracer concentration as a function of time depending on the solid to liquid ratio (g solid/ml liquid) (Colemanite feed rate = 7.2 g/min)	75
5.2.11.	Normalized lithium concentrations with respect to the initial tracer concentration, as given in Equation 5.2.14, as a function of time depending on the solid to liquid ratio (g solid/ml liquid) (Colemanite feed rate = 7.2 g/min)	76
5.3.1.	Variations in the boric acid concentration depending on the colemanite particle size during the dissolution of colemanite in aqueous sulfuric acid at 80°C and a stirring rate of 500 rpm. The initial CaO/SO ₄ ²⁻ molar ratio is 0.95	78
5.3.2.	Variations in the calcium ion concentration depending on the colemanite particle size during the dissolution of colemanite in aqueous sulfuric acid at 80°C and a stirring rate of 500 rpm. The initial CaO/SO ₄ ²⁻ molar ratio is 0.95	79
5.3.3.	Variations in the boric acid concentration during the dissolution of Hisarcık 2 colemanite, -250µm, in aqueous sulfuric acid at 85°C and a stirring rate of 500 rpm. The initial CaO/SO ₄ ²⁻ molar ratio is 1.....	80
5.3.4.	Variations in the boric acid concentration during the dissolution of Hisarcık 3 colemanite, -150µm, in aqueous sulfuric acid at 85°C and a stirring rate of 400 rpm. The initial CaO/SO ₄ ²⁻ molar ratio is 1	80
5.3.5.	Variations in the calcium ion concentration during the dissolution of Hisarcık 2 colemanite, -250µm, in aqueous sulfuric acid at 85°C and a stirring rate of 500 rpm. The initial CaO/SO ₄ ²⁻ molar ratio is 1.....	81

5.3.6.	Variations in the calcium ion concentration during the dissolution of Hisarcık 3 colemanite, -150µm, in aqueous sulfuric acid at 85°C and a stirring rate of 400 rpm. The initial CaO/SO ₄ ²⁻ molar ratio is 1.....	82
5.4.1.	Molar flow rate of boric acid produced with Hisarcık 2, 0-250 µm, and Hisarcık 3, 0-150 µm, colemanites, at initial CaO/ SO ₄ ²⁻ molar ratios of 1.00 and 1.37, where the experiment names are showed on each bar	85
5.4.2.	Molar flow rate of boric acid produced with Hisarcık 2, 0-250 µm, and Hisarcık 3, 0-150 µm, colemanites having a flow rate of 10 g/min, where the experiment names are showed on each bar	86
5.4.3.	Molar flow rate of calcium ion in solution depending on the colemanite feed rate obtained by using Hisarcık 2 colemanite, 0-250 µm, at initial CaO/ SO ₄ ²⁻ molar ratio of 1.00	89
5.4.4.	Molar flow rate of calcium ion in solution depending on the colemanite feed rate obtained by using Hisarcık 2 colemanite, 0-250 µm, at initial CaO/ SO ₄ ²⁻ molar ratio of 1.37	90
5.4.5.	Molar flow rate of calcium ion in solution depending on the colemanite feed rate obtained by using Hisarcık 3 colemanite, 0-150 µm, at initial CaO/ SO ₄ ²⁻ molar ratio of 1.00	91
5.4.6.	Molar flow rate of calcium ion in solution depending on the initial CaO/ SO ₄ ²⁻ molar ratio obtained by using Hisarcık 2, 0-250 µm, and Hisarcık 3, 0-150 µm, colemanites having a flow rate of 10 g/min	92
5.4.7.	Molar flow rate of magnesium ion obtained at steady state by using Hisarcık 2, 0-250 µm, colemanite, at initial CaO/ SO ₄ ²⁻ molar ratios of 1.00 and 1.37, where the experiment names are showed on each bar.....	95
5.4.8.	Molar flow rate of sulfate ion obtained at steady state by using Hisarcık 2, 0-250 µm, colemanite, at initial CaO/ SO ₄ ²⁻ molar ratios of 1.00 and 1.37, where the experiment names are showed on each bar.....	96
5.4.9.	Variation of molar flow rates of calcium and sulfate ion obtained at steady state by using Hisarcık 2, 0-250 µm, colemanite, at initial CaO/ SO ₄ ²⁻ molar ratios of 1.00 and 1.37 depending on the colemanite feed rate	97
5.5.1.	The particle size distribution of gypsum crystals during the dissolution of Hisarcık 2, 0-250 µm, colemanite in aqueous sulfuric acid at initial CaO/SO ₄ ²⁻ molar ratio of 1at 85°C and a stirring rate of 500 rpm	101
5.5.2.	The particle size distribution of gypsum crystals during the dissolution of Hisarcık 3, 0-150 µm, colemanite in aqueous sulfuric acid at initial CaO/SO ₄ ²⁻ molar ratio of 1at 85°C and a stirring rate of 400 rpm	102
5.5.3.	The particle size distribution of gypsum crystals obtained from the effluent streams of the reactors from Experiment HC 2.1, performed by using Hisarcık 2, 0-250 µm, colemanite at the initial CaO/SO ₄ ²⁻ molar ratio of 1.00, and colemanite feed rate of 5 g/min	103

5.5.4.	The particle size distribution of gypsum crystals obtained from the effluent streams of the reactors from Experiment HC 2.2, performed by using Hisarcık 2, 0-250 μm , colemanite at the initial $\text{CaO}/\text{SO}_4^{2-}$ molar ratio of 1.00, and colemanite feed rate of 7.5 g/min	103
5.5.5.	The particle size distribution of gypsum crystals obtained from the effluent streams of the reactors from Experiment HC 2.3, performed by using Hisarcık 2, 0-250 μm , colemanite at the initial $\text{CaO}/\text{SO}_4^{2-}$ molar ratio of 1.00, and colemanite feed rate of 10 g/min	104
5.5.6.	The particle size distribution of gypsum crystals obtained from the effluent streams of the reactors from Experiment HC 2.4, performed by using Hisarcık 2, 0-250 μm , colemanite at the initial $\text{CaO}/\text{SO}_4^{2-}$ molar ratio of 1.37, and colemanite feed rate of 5 g/min	104
5.5.7.	The particle size distribution of gypsum crystals obtained from the effluent streams of the reactors from Experiment HC 2.5, performed by using Hisarcık 2, 0-250 μm , colemanite at the initial $\text{CaO}/\text{SO}_4^{2-}$ molar ratio of 1.37, and colemanite feed rate of 10 g/min	105
5.5.8.	The particle size distribution of gypsum crystals obtained from the effluent streams of the reactors from Experiment HC 2.7, performed by using Hisarcık 2, 0-250 μm , colemanite at the initial $\text{CaO}/\text{SO}_4^{2-}$ molar ratio of 1.37, and colemanite feed rate of 15 g/min	105
5.5.9.	The particle size distribution of gypsum crystals obtained from the effluent streams of the reactors from Experiment HC 2.8, performed by using Hisarcık 2, 0-250 μm , colemanite at the initial $\text{CaO}/\text{SO}_4^{2-}$ molar ratio of 2.17, and colemanite feed rate of 10 g/min	106
5.5.10.	The particle size distribution of gypsum crystals obtained from the effluent streams of the reactors from Experiment HC 3.1, performed by using Hisarcık 3, 0-150 μm , colemanite at the initial $\text{CaO}/\text{SO}_4^{2-}$ molar ratio of 1.00, and colemanite feed rate of 3.5 g/min	106
5.5.11.	The particle size distribution of gypsum crystals obtained from the effluent streams of the reactors from Experiment HC 3.2, performed by using Hisarcık 3, 0-150 μm , colemanite at the initial $\text{CaO}/\text{SO}_4^{2-}$ molar ratio of 1.00, and colemanite feed rate of 10 g/min	107
5.5.12.	Variation of volume weighted mean diameters of gypsum crystals depending on the solid residence times during the dissolution of Hisarcık 2 colemanite, 0-250 μm , at initial $\text{CaO}/\text{SO}_4^{2-}$ molar ratio of 1.00 and solid hold-up of 0.04	109
5.5.13.	Variation of volume weighted mean diameters of gypsum crystals depending on the solid residence times during the dissolution of Hisarcık 2 colemanite, 0-250 μm , at initial $\text{CaO}/\text{SO}_4^{2-}$ molar ratio of 1.37 and solid hold-up of 0.06	110
5.5.14.	Variation of volume weighted mean diameters of gypsum crystals depending on the solid hold-up and residence times of solid during the dissolution of Hisarcık 2 colemanite, 0-250 μm . The colemanite feed rate is 10 g/min	111
5.5.15.	Variation of volume weighted mean diameters of gypsum crystals depending on the solid residence times during the dissolution of Hisarcık 3 colemanite, 0-150 μm , at initial $\text{CaO}/\text{SO}_4^{2-}$ molar ratio of 1.00 and solid hold-up of 0.05	112

5.6.1.	Light microscope images of gypsum crystals obtained by the batch reactor experiment, HB3.1. The residence time of the crystals is 210 min	113
5.6.2.	Light microscope images of gypsum crystals obtained by the continuous reactor experiment, HC3.1. The residence time of the crystals in each reactor is 60 min. The reactor number, n, is shown on top of each figure	114
5.6.3.	Light microscope images of gypsum crystals obtained by the continuous reactor experiment, HC3.2. The residence time of the crystals in each reactor is 20 min. The reactor number, n, is shown on top of each figure	115
5.7.1.	Reciprocal concentration of calcium ion as a function of time plot Experiments HB2.1 and HB2.2, at different particle sizes and initial $\text{CaO}/\text{SO}_4^{2-}$ molar ratio of 0.95, at 80°C and a stirring rate of 500 rpm.....	116
5.7.2.	Reciprocal concentration of calcium ion as a function of time plot for Experiment HB2.3, Hisarcık 2, 0-250 μm , experiment at initial $\text{CaO}/\text{SO}_4^{2-}$ molar ratio of 1, at 85°C and a stirring rate of 500 rpm	117
5.7.3.	Reciprocal concentration of calcium ion as a function of time plot for Experiment HB3.1, Hisarcık 3, 0-150 μm , experiment at initial $\text{CaO}/\text{SO}_4^{2-}$ molar ratio of 1, at 85°C and a stirring rate of 400 rpm.....	118
5.7.4.	Variations in the calcium ion concentration depending on the colemanite particle size during the dissolution of colemanite in aqueous sulfuric acid at 80°C and a stirring rate of 500 rpm. The initial $\text{CaO}/\text{SO}_4^{2-}$ molar ratio is 0.95. Experimental data were compared with the rate expression given in Eq 5.7.1	121
5.7.5.	Variations in the calcium ion concentration during the dissolution of Hisarcık 2, 0-250 μm , colemanite in aqueous sulfuric acid at 85°C and a stirring rate of 500 rpm. The initial $\text{CaO}/\text{SO}_4^{2-}$ molar ratio is 1. Experimental data were compared with the rate expression given in Eq 5.7.2	121
5.7.6.	Variations in the calcium ion concentration during the dissolution of Hisarcık 3, 0-150 μm , colemanite in aqueous sulfuric acid at 85°C and a stirring rate of 400 rpm. The initial $\text{CaO}/\text{SO}_4^{2-}$ molar ratio is 1. Experimental data were compared with the rate expression given in Eq 5.7.3	122
5.7.7.	The calcium ion concentration evaluated at the exit of the n^{th} CSTR, estimated by macrofluid model using the rate expression in Eq. 5.7.1	125
5.7.8.	The calcium ion concentration evaluated at the exit of the n^{th} CSTR, estimated by macrofluid model using the rate expression in Eq. 5.7.2	125
5.7.9.	The calcium ion concentration evaluated at the exit of the n^{th} CSTR, estimated by macrofluid model using the rate expression in Eq. 5.7.3	126
5.7.10.	The calcium ion concentration evaluated at the exit of the n^{th} CSTR, estimated by microfluid model using the rate expression in Eq. 5.7.1	128

5.7.11.	The calcium ion concentration evaluated at the exit of the n^{th} CSTR, estimated by microfluid model using the rate expression in Eq. 5.7.2	129
5.7.12.	The calcium ion concentration evaluated at the exit of the n^{th} CSTR, estimated by microfluid model using the rate expression in Eq. 5.7.3	129
5.7.13.	The calcium ion concentrations evaluated at the exit of the PFR depending on the model expressions in Eq. 5.7.5-5.7.7	133
5.7.14.	Comparison of calcium ion concentration at the exit of the n -CSTR's estimated by macrofluid and microfluid models and PFR by using the rate expression in Eq. 5.7.1 for total space time of 40 min	134
5.7.15.	Comparison of calcium ion concentration at the exit of the n -CSTR's estimated by macrofluid and microfluid models and PFR by using the rate expression in Eq. 5.7.2 for total space time of 40 min	134
5.7.16.	Comparison of calcium ion concentration at the exit of the n -CSTR's estimated by macrofluid and microfluid models and PFR by using the rate expression in Eq. 5.7.3 for total space time of 40 min.....	135

LIST OF SYMBOLS AND ABBREVIATIONS

A	: area under the C_{pulse} curve
C	: concentration of calcium ion, mol/l
\bar{C}	: average calcium ion concentration, mol/l
$C(t)$: concentration of calcium ion at time t , mol/l
C_{exp}	: calcium ion concentration found experimentally, mol/l
C_0	: maximum concentration of calcium ion, mol/l
C_o	: calcium ion concentration at the inlet of first CSTR, mol/l
C_1	: calcium ion concentration at the outlet of first CSTR, mol/l
C_{macro}	: calcium ion concentration evaluated by macrofluid model, mol/l
C_{micro}	: calcium ion concentration evaluated by microfluid model, mol/l
C_{n-1}	: calcium ion concentration at the inlet of n^{th} CSTR, mol/l
C_n	: calcium ion concentration at the outlet of n^{th} CSTR, mol/l
C_{pulse}	: concentration of pulse tracer, ppm
C_{sat}	: saturation concentration of calcium ion, mol/l
C_{step}	: concentration of step tracer, ppm
\bar{C}_n	: average calcium ion concentration at the outlet of n^{th} reactor, mol/l
CFSSR	: continuous flow stirred slurry reactor
$E(t)$: residence time distribution function
$F(t)$: dimensionless form of C_{step} curve, integral of $E(t)$
F_{NaOH}	: factor of the NaOH
h_L	: liquid hold-up, volume of liquid/total volume
h_s	: solid hold-up, volume of solid/total volume
k	: crystal growth rate constant, $\text{l mol}^{-1} \text{s}^{-1}$
M	: amount of tracer, kg or moles
\dot{m}_g	: mass flow rate of globules, g/min
\dot{m}_L	: mass flow rate of liquid, g/min

\dot{m}_s : mass flow rate of solid, g/min
 n : number of CSTR's
 N_{NaOH} : normality of NaOH, N
RTD : residence time distribution
 V : vessel volume, m^3
 V_g : globule volume, m^3
 V_L : volume occupied by liquid, m^3
 V_R : reactor volume, m^3
 V_s : volume occupied by solid, m^3
 V_{NaOH} : volume of the NaOH, ml
 V_{sample} : volume of the sample, ml
 V_S : volume occupied by solid, m^3
 t : real time, s
 t_0 : time which is very close to 0
 \bar{t} : mean of the C_{pulse} curve, s
 \bar{t}_L : mean residence time of liquid, s
 \bar{t}_S : mean residence time of solid, s

Greek letters

δ : dirac delta function
 ρ : density, g/ml
 ρ_g : density of globules, g/ml
 ρ_L : density of liquid, g/ml
 ρ_s : density of solid, g/ml
 τ : residence time at PFR, sec
 τ : total residence time at the n-CSTR, s
 τ_i : residence time at each CSTR, s
 υ : volumetric flow rate of liquid, m^3/s
 υ_g : volumetric flow rate of globules, m^3/s
 σ^2 : variance, s^2

CHAPTER 1

INTRODUCTION

Boron is one of the most important elements in the world, whose compounds are used in all the manufacturing applications, except food, in highly industrialized countries. More than one half of the boron compounds are consumed in the manufacture of various kinds of glasses such as pyrex, frits and insulation-grade and textile grade fibers. The other important uses include soaps, detergents and bleaches. Metallurgical demand for boron is consumed as fluxing material in welding and soldering as a refining material and as a hardening material. Boron is also used as a neutron absorber, as a fire retardant in cellulosic insulation. The borates in agriculture are consumed as herbicides, fertilizers, and a soil sterilant (Roskill, 2002).

1.1. BORATE MINERALS

Boron does not occur in nature as a free element, but it always combined with oxygen to form borates. There are more than 230 borate minerals, of which the most common are shown in Table 1.1 (Roskill, 2002). Borax (tincal), kernite, colemanite, ulexite, probertite, hydroboracite, inderite, datolite, and szaibelyite (ascharite) are the only borate minerals of commercial importance. Borax and colemanite are the most important. Borate production comes mostly from seven countries: the United States, Turkey, Russia, Kazakhstan, Argentina, China, Peru, and Chile. Deposit areas and reserves in these countries are shown in Table 1.2 (Kirk Othmer, 1992)

Table 1.1. Commercially important borate minerals (Roskill, 2002)

TYPE	MINERAL	COMPOSITION	%B ₂ O ₃	NOTES
Hydrogen borates	Sassolite	B(OH) ₃	56.4	Natural boric acid. Once extracted in Italy
Sodium borates	Tincal (borax)	Na ₂ O.2B ₂ O ₃ .10H ₂ O	36.5	Major ore mineral; produced in Turkey/USA Intermediate or accessory mineral only Major ore mineral; converted to borax by weathering
	Tincalconite	Na ₂ O.2B ₂ O ₃ .5H ₂ O	48.8	
	Kernite (rasorite)	Na ₂ O.2B ₂ O ₃ .4H ₂ O	51	
Sodium-calcium borates	Ulexite (boronatocalcite)	Na ₂ O.2CaO.5B ₂ O ₃ .16H ₂ O	43	Major ore mineral, particularly in South America Secondary/accessory mineral
	Probertite (kramerite)	Na ₂ O.2CaO.5B ₂ O ₃ .10H ₂ O	49.6	
Calcium borates	Inyoite	2CaO.3B ₂ O ₃ .13H ₂ O	37.6	Minor ore mineral Intermediate mineral, rarely survives in quality Major ore mineral, particularly in Turkey; often secondary after inyoite Ore mineral at Bigadiç Turkey; minor elsewhere
	Meyerhoffite	2CaO.3B ₂ O ₃ .7H ₂ O	46.7	
	Colemanite	2CaO.3B ₂ O ₃ .5H ₂ O	50.8	
	Priceite (pandermite)	5CaO.6B ₂ O ₃ .9H ₂ O	49.8	
Calcium borosilicates	Howlite	4CaO.5B ₂ O ₃ .2SiO ₂ .5H ₂ O	44.5	Accessory mineral
	Datolite	2CaO.B ₂ O ₃ .SiO ₂ .H ₂ O	21.8	
	Danburite	CaO.B ₂ O ₃ .2SiO ₂	28.3	
Magnesium borates	Hydroboracite	CaO.MgO.3B ₂ O ₃ .6H ₂ O	50.5	Major ore mineral in Kazakhstan Accessory mineral Accessory with potash deposits
	Inderite	2MgO.3B ₂ O ₃ .15H ₂ O	37.3	
	Szaibelyite (ascharite)	2MgO.B ₂ O ₃ .H ₂ O	41.4	
	Kurnakovite	2MgO.3B ₂ O ₃ .15H ₂ O	37.3	
	Boracite	Mg ₃ B ₇ O ₁₃ .Cl	62.2	
	Suanite	Mg ₃ B ₂ O ₅	46.3	
	Kotoite	Mg ₃ B ₂ O ₆	36.5	
Pinnoite	MgO.B ₂ O ₃ .3H ₂ O	42.5		
Other borates	Cahnite	Ca ₂ AsBO ₆ .2H ₂ O	11.7	
	Vonsenite (paigeite)	(FeMg) ₂ FeBO ₅	10.3	
	Ludwigite	(FeMg)4Fe ₂ B ₂ O ₇	17.8	
	Tunellite	SrB ₆ O ₁₀ .4H ₂ O	52.9	

Table 1.2. Distribution of Borate Minerals (Kirk Othmer, 1992)

Country	Area	Principal Minerals	Reserves, 10 ⁶ t of B ₂ O ₃
United States	Boron, Calif.	tincal, kernite	41-50
	Searles Lake, Calif.	brine	15
	Death Valley, Calif.	colemanite, ulexite, probertite	several
Turkey	Bigadic	colemanite, priceite, ulexite	
	Emet	colemanite	23
	Kırka	tincal, colemanite, ulexite	122
Kazakhstan	Inder	szaibelyite	54
Russia	Dal'negorsk	datolite	
Argentina	Tincalayu	tincal, kernite, ulexite	23
China	Liaoning	szaibelyite	27

From the distribution of borate minerals, Table 1.2, it is seen that the largest reserves, in terms of boron content, are located in Turkey. The distribution of the reserves of boron minerals in Turkey are given in Table 1.3.

Table 1.3. Reserves of boron minerals in Turkey (Roskill, 2002)

BORON MINERAL	GROSS WEIGHT (MT)	B ₂ O ₃ , CONTENT (MT)
Colemanite	1.418	394
Tincal	604	156
Ulexite	49	14
Total	2.071	564

It is observed that the boron mineral that Turkey has in the largest amount, having a reserve of 394 Mt. Colemanite, like other borates, is a complex mineral, that is found in desert borax deposits and Tertiary clays in old lake beds. Colemanite is a secondary mineral, meaning that it occurs after the original deposition of other minerals. The mineral borax is directly deposited in arid regions from the evaporation of water due to runoff from nearby mountain ranges. The runoff is rich in the element boron and is highly concentrated by evaporation in the arid climate. Ground water flowing through the borax sediments is believed to react with the borax and form other minerals such as ulexite. It is believed that colemanite may

have formed from ulexite. Colemanite is found in geodes within the borax sediment. Its exact means of formation are still not well understood (Amethyst Galleries, 1997). It is also used in the manufacture of heat resistant glass, and has other industrial, medicinal and cosmetical uses (Friedman, 1999).

1.2. BORIC ACID PRODUCTION IN THE WORLD

The majority of boric acid is produced by the reaction of inorganic borates with sulfuric acid in an aqueous medium. Sodium borates are the principal raw material in the United States. European manufacturers have generally used partially refined calcium borates, mainly colemanite from Turkey. Turkey uses colemanite to produce boric acid.

In the United States boric acid is produced by United States Borax & Chemical Corp. in a 103,000 B_2O_3 metric ton per year plant by reacting crushed kernite ore with sulfuric acid. Coarse gangue is removed in rake classifiers and fine gangue is removed in thickeners. Boric acid is crystallized from strong liquor, nearly saturated in sodium sulfate, in continuous evaporative crystallizers, and the crystals are washed in a multistage countercurrent wash circuit.

When boric acid is made from colemanite, the ore is ground to a fine powder and stirred vigorously with diluted mother liquor and sulfuric acid at about 90°C. The by-product calcium sulfate is removed by settling and filtration, and the boric acid is crystallized by cooling the filtrate.

Boric acid crystals are usually separated from aqueous slurries by centrifugation and dried in rotary driers heated indirectly by warm air. To avoid overdrying, the product temperature should not exceed 50°C. Powdered and impalpable boric acid is produced by milling the crystalline material.

The principal impurities in technical-grade boric acid are the by-product sulfates, and various minor metallic impurities present in the borate ores (Kirk Othmer, 1992). The world producers of boric acid are given in Table 1.4.

Table 1.4. Boric Acid Producers and Their Capacities (Roskill, 2002)

COUNTRY	COMPANY	CAPACITY (T/Y)/10 ³
Argentina	Norquimica SA	5.4
	Industrials Quimicas Baradero	9.5
	Others	15.1
Bolivia	Tierra SA	15
Chile	Quiborax	36
	SQM	16
China	Ji'an City Boron Ore	30
	Zibo Yanxiang Rolling Steel Product Company Limited	13
	Dangdong Kuandian Boron Ore	6
	Dashiqiao City Huaxin Chemical Company Limited	5
	Yingkou City Xingdong Chemical Plant	5
	Mudanjiang Number 2 Chemical Factory	4
	Others	29.3
France	Borax Francais SA	- *
India	Borax Morarji	4.18
Italy	Societa Chimica di Larderello	55-60
Japan	Nippon Denko	4
Peru	JSC Inkobor	25
Russia	JSC Energomash-Bor	100
Spain	Borax Espana	*
Turkey	Eti Bor	185
USA	IMC Chemical	25
	US Borax	255-260

* Not known

Boric acid has a surprising variety of applications in both industrial and consumer products. It serves as a source of B₂O₃ in many fused products, including textile fiber glass, optical and sealing glasses, heat-resistant borosilicate glass, ceramic glazes, and porcelain enamels. It also serves as a component of fluxes for welding and brazing. A number of boron chemicals are prepared directly from boric acid. These include synthetic inorganic borate salts, boron phosphate, fluoborates, boron trihalides, borate esters, boron carbide, and metal alloys such as ferroboron.

Boric acid catalyzes the air oxidation of hydrocarbons and increases the yield of alcohols by forming esters that prevent further oxidation of hydroxyl groups to ketones and carboxylic acids.

The bacteriostatic and fungicidal properties of boric acid have led to its use as a preservative in natural products such as lumber, rubber latex emulsions, leather, and starch products.

NF-grade boric acid serves as a mild, nonirritating antiseptic in mouthwashes, hair rinse, talcum powder, eyewashes, and protective ointments. Although relatively nontoxic to mammals, boric acid powders are quite poisonous to some insects. With the addition of an anticaking agent, they have been used to control cockroaches and to protect wood against insect damage.

Inorganic boron compounds are generally good fire retardants. Boric acid, alone or in mixtures with sodium borates, is particularly effective in reducing the flammability of cellulosic materials. Applications include treatment of wood products, cellulose insulation, and cotton batting used in mattresses.

Because boron compounds are good absorbers of thermal neutrons, owing to isotope ^{10}B , the nuclear industry has developed many applications. High purity boric acid is added to the cooling water used in high pressure water reactors (Kirk Othmer, 1992).

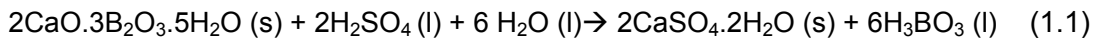
1.3. BORIC ACID PRODUCTION IN TURKEY

Boric acid is produced in Turkey via a batch and a continuous process by the factories located in Bandırma, Balıkesir and Emet, Kütahya, respectively. The annual production capacity of the Bandırma Plant is 85,000 tons. However, the Emet Plant's production capacity is 100,000 tons.

The production of boric acid in Turkey includes the following steps: size reduction of the ore, the reaction of colemanite with sulfuric acid, filtration of the by-product, gypsum (calcium sulphate dihydrate), crystallization of the cooled **boric acid**,

filtration of the crystals from the main solution, drying the product and storage (Gürbüz *et.al.*, 1998; Kalafatoğlu *et. al.*, 2000, Balkan and Tolun, 1985).

The overall reaction in a boric acid reactor is as follows:



Bandırma Plant operates in a batch model until the filtration unit. It has twelve batches operating. Colemanite undergoes primary and secondary crushing. Prior to the addition of sulfuric acid, further size reduction is affected by employing a ball mill. The ground material is taken to the batch reactors where returning mother liquor and sulfuric acid are mixed at 85 to 95 °C. The steam is used for heating purpose and it is given directly to the slurry. The slurry is stirred. The reaction time is between 45-60 minutes. The formed gypsum particles and other insolubles are filtered and the clear filtrate is sent to the crystallizer where it cooled down to 40 °C. The formed boric acid crystals are then centrifuged and dried to obtain a product of 99.5% purity (Özbayoğlu *et.al*, 1992).

Emet Plant operating in a continuous mode has six slurry reactors in series. In the production five of them are taken into production operation. The reactors are continuously stirred and the temperature in the reactors is kept constant at 85-88°C. The reactors are jacketed and heated by steam circulating around the jackets. The pH and the temperatures of the reactors are measured continuously. The sulfuric acid, 93 wt%, is first mixed with the weak boric acid solution; ~5-6% in the static mixer and fed continuously to the first reactor. The colemanite, on the other hand, is crushed until having a particle size of -150 µm, and fed also to the first reactor. The reaction is given in Equation 1.1.

The by-product calcium sulphate dihydrate (gypsum, $\text{CaSO}_4 \cdot 2\text{H}_2\text{O}$) crystallizes in the reactors. Filtration of gypsum crystals after the reaction is a crucial process in the production of boric acid in high purity and with high efficiency, as a subsequent crystallization of boric acid from the supernatant solution is affected by contaminations. For this reason, before the filtration process in the plant, a polyelectrolyte is added to the slurry to make the filtration easier. The slurry is sent

to the horizontal vacuum belt filters to get rid of the gypsum crystals and the other insolubles.

The obtained clear filtrate is sent to the polish filters and then to the crystallizers operating in series. The formed boric acid crystals are washed with demineralized water to remove the sulfate ions. After that, it is sent to the centrifugation and drying unit.

The production of boric acid in continuous flow stirred slurry reactors is a new developing technology. There is lack of data to improve this technology. Data should be generated in laboratory scale or in pilot scale to overcome the unexpected problems. In this thesis it is tried to provide data and know-how to the boric acid production technology with continuous flow stirred slurry reactors.

This chapter, Chapter 1, gives information on borate minerals, especially colemanite, distribution of them in the world, boric acid production in the world and in Turkey.

Chapter 2 deals with the literature survey on the dissolution of colemanite, crystallization of gypsum, solid-fluid reaction modeling and the residence time distribution studies done by researchers.

Chapter 3 gives brief information on the solid-liquid systems and discusses modeling of slurry reactors with different residence times using different approaches. In other words, macrofluid model and microfluid models are applied to the n-CSTR's and they are compared with the PFR approach.

In Chapter 4, the set-ups of the batch and continuous reactor systems are given together with the experimental procedures and the scopes. The analytical procedures performed to the samples are also explained in this chapter.

The results of the dynamic behavior experiments, batch reactor and continuous reactor boric acid production experiments are presented in Chapter 5. Also, the experiments performed are compared and the model results are verified with the experimental data.

Chapter 6, the last chapter, concludes on the achieved important results and reveals beneficial information to the boric acid industry.

CHAPTER 2

LITERATURE SURVEY

Literature survey is examined in six parts. The first one is the dissolution of colemanite and its kinetics. The second one is the crystal growth of calcium sulfate dihydrate, followed by the heterogeneous solid fluid reaction modeling. The fourth part deals with the studies on residence time distribution in fluid-solid reactors and the other part gives the studies on the reactor modeling. In the last section, the objective of the present study is explained.

2.1. DISSOLUTION OF COLEMANITE AND ITS KINETICS

Turkey has the largest colemanite reserves in the world, the reserves of which are placed in the western part of Turkey (eg. Emet, Bigadiç, Kestelek, Hisarcık). Researchers in Turkey mainly focus their studies on the dissolution of colemanite and the kinetics of it.

Gürbüz et. al. (1998) found that the dissolution of colemanite in dilute water and boric acid solutions were very fast. Besides this, the dissolution of colemanite in dilute water increased the pH value considerably. The pH value increased from 6.5-7 to 9 in the first 5 minutes. In the boric acid solutions, the pH change is less and the solution remained to have a constant value.

Gürbüz et.al (1998) also stated that the dissolution of colemanite in distilled water was low compared to the boric acid solutions. The solubility of colemanite in distilled water at 90 °C was found as 1.7 g col/1000 g solution. The solubility of

colemanite in 7.5%, 10% and 20% boric acid solutions at 90 °C were found as 4.3, 8.13 and 19.6 g col /1000 g sol, respectively.

Bechtloff et.al (2001) studied the citric acid production from the reaction of calcium citrate and sulfuric acid. The by-product of the reaction was gypsum, which resembles the boric acid production from the reaction of colemanite and sulfuric acid. The dissolution of calcium citrate was found to be enhanced by the initially added citric acid. This was due to the increased solubility which was the same conclusion obtained from Gürbüz et. al. for the production of boric acid.

Kalafatoğlu et. al. (2000) stated that if in the reaction of colemanite and sulfuric acid the concentration of sulfuric acid was more, besides the colemanite, some other impurities also dissolved. So, in this study, the most suitable concentration for sulfuric acid was searched and it was shown that if the acid concentration is hold around %5, the dissolution of clay and the other impurities was less.

Kocakerim and Alkan (1988) studied the kinetics of dissolution of colemanite in water saturated with SO₂. The effects of particle size, temperature and stirring rate were determined. It was found that the rate of dissolution increases with decreasing particle size and with increasing temperature, but is unaffected by stirring rate. The dissolution rate was chemically controlled. The activation energy and the pre-exponential factor were calculated as 53.97 kJ/mol and 26.1 km/s, respectively.

Özmetin et. al. (1996) investigated the dissolution of colemanite in aqueous acetic acid solutions. It was also found that the dissolution rate increases with increasing temperature and decreasing solid-to-liquid ratio and particle size. No important effect of stirring rate was observed. The activation energy of the process was determined to be 51.49 kJ/mol. It was determined by graphical and statistical methods that the reaction fits a model in the form of $-\ln(1-X)=kt$, where X is the conversion.

Dissolution kinetics of colemanite in sulfuric acid in the absence and presence of ultrasound was studied by Okur et.al (2002). An Avrami-type equation was used

successfully to explain kinetic data. Activation energy was 30 kJ/mol in both situations. Ultrasound affected the pre-exponential factor in rate constant.

Tunç and Kocakerim (1998) studied the dissolution kinetics of colemanite in sulfuric acid. It was found that the conversion rate increased with the particle size and solid-to-liquid ratio. As temperature and stirring rate increased, the conversion rate also increased. Conversion rate increased with the acid concentration upto 1 M and decreased with the concentrations above 1 M. By using statistical and graphical methods, a reaction model was determined.

Bilal et.al (2003) studied the dissolution of colemanite in sulfuric acid in a batch reactor at different temperatures, initial concentration of sulfuric acid and the amounts of boric acid initially added to the system. It was found that the reaction of colemanite with sulfuric acid was very fast and complete conversion was obtained in nearly 15 minutes. Initial boric acid concentration had insignificant effect on dissolution rate of colemanite. Increasing temperature and increasing sulfuric acid concentration up to 0.5 wt % increased the dissolution rate.

2.2. CRYSTAL GROWTH OF CALCIUM SULFATE DIHYDRATE AND ITS KINETICS

It is believed that three phases of crystalline calcium sulfate exists: calcium sulfate dihydrate (gypsum, $\text{CaSO}_4 \cdot 2\text{H}_2\text{O}$), calcium sulfate hemihydrate ($\text{CaSO}_4 \cdot 1/2\text{H}_2\text{O}$) and calcium sulfate anhydrate (CaSO_4) (Hand, 1997). Calcium sulfate dihydrate is either found in the nature as a mineral or precipitated from aqueous solutions (Packter, 1974), as well as from the hydration of calcium sulfate hemihydrate (Badens et.al., 1999; Boisvert et.al., 2000).

Calcium sulfate dihydrate forms small needle-like crystals having a monoclinic, prismatic structure with water molecules between the calcium and sulfate ions in the unit cell. The crystal structures of calcium sulfate dihydrate and calcium sulfate hemihydrate differ from each other because of the amount of the lattice water (Klepetsanis and Koutsoukos, 1998).

The formation of calcium sulfate dihydrate from aqueous solution has been investigated by using different structural techniques such as scanning electron

microscope, optical microscope (Liu et.al, 1976; Liu and Nancollas, 1975b; Klepetsanis and Koutsoukos, 1989), X-ray diffraction (Nancollas et.al, 1973; Smith and Sweett, 1971), radioactive tracer (Brandse et.al, 1977).

The crystal growth kinetics of calcium sulfate dihydrate in aqueous solutions has been studied under various conditions; in supersaturated solutions over a wide temperature range (Klepetsanis et.al., 1999), at heated metal surfaces (Gill and Nancollas, 1980), in the presence of additives (Smith and Alexander, 1970; Liu and Nancollas, 1975a, 1975b), polymers (Amjad, 1988), organophosphorus compounds (Klepetsanis and Koutsoukos, 1998), sodium chloride (Brandse et.al, 1977), polyelectrolytes (Öner et.al, 1998), phosphates (Rinaudo et.al, 1996) and in low supersaturation (Christoffersen et.al, 1982).

Smith and Sweett (1971) studied the crystallization of calcium sulfate dihydrate from aqueous solutions at 30°C in the absence of added seeded crystals, which indicated that nucleation was heterogenous. The growth rate was proportional to the crystal surface area and to the square of supersaturation. It was shown in this study that the rate-controlling step was dehydration of calcium ions. The growth rate was found to increase with increasing pH.

Balkan and Tolun (1985) investigated the factors affecting the formation of gypsum in the production of boric acid from colemanite. The parameters used in this study were the process conditions and impurity effects. Optimum process conditions for the formation of easily filterable gypsum were determined as, for the reaction temperature, 80°C; for the reaction time, 1 hour; in the presence of sufficient seed surface area. The surface area of the seed was calculated from the crystal growth rate of gypsum in the reaction medium.

Nancollas et. al. (1973) had shown the growth of calcium sulfate dihydrate seed crystals from supersaturated solutions at temperatures where the phase was thermodynamically stable to involve a surface controlled rate determining step. The data indicated that the rate determining step in $\text{CaSO}_4 \cdot 2\text{H}_2\text{O}$ crystal growth involved a surface reaction. Seeded crystal growth experiments near the dihydrate-hemihydrate phase transition temperature (103°C in salt free solutions at 4 atm)

showed that phase transformation accompanies the seeded growth of the less stable modification.

Klepetsanis and Koutsoukos (1998) investigated the spontaneous precipitation of equimolar calcium sulfate supersaturated solutions at conditions of sustained supersaturation over the temperature range 20-60°C. In all the cases, the only phase forming was identified as calcium sulfate dihydrate. Kinetic analysis of the rates, which depended strongly on the solution supersaturation, suggested a polynuclear mechanism, and yielded activation energy of 44 kcal/mole, indicative of a surface controlled mechanism.

Klepetsanis et.al. (1999) investigated the spontaneous precipitation of calcium sulfate in supersaturated solutions over the temperature range between 25-80°C. From measurements of the induction times preceding the onset of precipitation the surface energy of the forming solid, identified as gypsum, was found between ca. 12 and 25 mJ/m² for the temperature range between 80 and 25°C, respectively. Kinetic analysis showed that over 50°C it was possible that the anhydrous calcium sulfate was forming as a transient phase converting into the more stable calcium sulfate dihydrate.

Çetin et. al. (2001) studied the formation and growth kinetics of gypsum during the dissolution of colemanite in aqueous sulfuric acid in a batch reactor by varying the temperature (60-90°C), stirring rate (150-400 rpm), and the initial concentrations of the reactants. The stirring rate was found to have no significant effect on the dissolution. The minimum saturation concentration of the calcium ion was obtained at 80°C when the initial CaO/H₂SO₄ molar ratio was 0.85. The boric acid concentration in the solution decreased with the decreasing initial concentration of sulfuric acid.

Recent studies also performed in batch reactors, have shown that the crystal growth of calcium sulfate dihydrate on seed crystals follows a second order kinetics from the solution supersaturated in calcium and sulfate ions (Nancollas et.al, 1973; Gill and Nancollas, 1980; Smith and Swett, 1971; Brandse et.al., 1977; Çetin et.al, 2001). The crystallization of gypsum from the supersaturated solution obtained by the dissolution of colemanite in aqueous sulfuric acid also obeyed a second order

rate law by assuming that the initial concentrations of calcium and sulfate ions were equal.

The effect of particle size of colemanite on gypsum crystallization in batch reactor was investigated by Erdoğan et. al (2003). As the colemanite particle size decreased, the faster the dissolution was observed. Also, formation rate of gypsum crystals were faster if particle size of colemanite was small. It was concluded that the particle size of gypsum crystals formed during the reaction increased with increasing particle size of reacted colemanite in given ranges.

Anderson et.al. (1998a, 1998b) described the “autocatalytic” microphase action by developing a model which simultaneously considers reaction, crystallization, and microphase processes. The chief conclusion is that the growth kinetics and initial crystal size distribution of the precipitating solids had a profound influence on the reaction rate. In the second part of the study, the theoretical conclusions were validated by using an industrially important system, e.g. the reaction of calcium citrate (solid) with sulfuric acid (aqueous) to produce citric acid (desired product) and calcium sulfate dihydrate (solid by-product). It was found that enhancements as high as 2.81 could indeed be obtained as a result of “autocatalysis” microphase action of the product calcium sulfate.

2.3 HETEROGENOUS SOLID FLUID REACTION MODELING

Heterogeneous reactions involve solid-fluid, liquid-liquid, and gas-liquid system. Here, the heterogeneous reaction systems involving only solid-fluid reactions are considered. Heterogeneous solid-liquid reaction crystallizations are widely used in practice but information on modeling, analysis and optimization is hardly discussed in literature.

Different sorts of behavior of reacting solid particles (macro kinetics) can be found as shown in Figure 2.1.

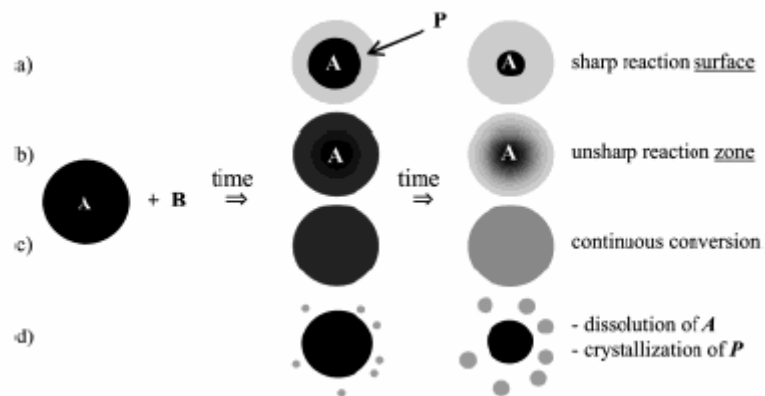


Figure 2.1. Macrokinetics of Heterogeneous solid-liquid Reaction Crystallizations (Bechtloff, 2001)

Different type of behavior of reacting solid particles can be seen in Figure 2.1. In Figure 2.1(a-c), an insoluble solid reactant A in the reaction medium is seen, where only a solid phase reaction on the surface of A can occur. The shrinking core model developed by Yagi and Kunii (1955, 1961) explains this type of behavior of reacting solid particles. According to this model, the reaction occurs first at the outer skin of the particles. Then, the zone of the reaction moves into the solid leaving behind a solid product layer called as ash. (Levenspiel, 1999)

If the reacting solid has a slight or a high solubility, a liquid phase reaction may dominate the process, as seen in Figure 2.1 (d). So, the dissolution of solid reactant and the crystallization of the product happen simultaneously. When the fluid becomes supersaturated, the solid product precipitates. However, the solid product may cover solid reactant. It may lead to a reduced reaction rate or incomplete conversion of solid reactant (Bechtloff et al., 2001)

Multiphase reactions involving a sparingly soluble solid in a liquid are quite common in the chemical and pharmaceutical industries. These reactions can be chemically controlled; diffusion controlled, or is controlled simultaneously by diffusion and reaction. A recent trend in the design and analysis of such reactions is to enhance the rates of diffusion by various means. One method is to use a microphase. When one of the products of the reaction is a solid, enhancements can be achieved by using this solid in microphase form. Since the enhancement occurs only after the

reaction product nucleates and the product itself is involved in the enhancement, this process is regarded as “autocatalytic” microphase behavior (Anderson, 1996; Doraiswamy, 2001).

It should be noted that researchers have also studied the effect of microphase on the phase transfer catalysts, use of microphase in multiphase reactions and the enhancement in the rate of a solid-liquid reaction due to microphase action (Hagenson et.al, 1994; Glatzer and Doraiswamy, 2000; Mehra 1988; Mehra et.al., 1998).

A microphase is described as a dispersed phase with particles, droplets, or bubbles that are smaller than the diffusion length of the solute. The diffusion film thickness is usually between 50 and 100 μm , whereas the microphase constituent size is less than 10 μm . Microphases can be composed of many different materials, such as microemulsions, catalysts, slurries, reactants, reaction products, and others. Due to this wide variety of compositions, microphases are classified as: sinks, catalysts and sources. Each of these acts differently. A sink may be chemically or physically active, but it does not aid in the reaction or emit any extrinsic species. The mechanism of sink and catalyst type microphase is given in Figure 2.2. The solute A will absorb onto the sink type microphase. The reactant B will also absorb onto the microphase if it has an affinity for the microparticles, and the reaction between A and B will ensue on the microphase. The product will then be released.

The mechanism of a catalyst type microphase is similar to that of a sink, except it provides for the reactive interaction between A and B. The solute A does not diffuse onto a source type microphase. The source type microphase transports B into the vicinity of the macrointerphase to react with A.

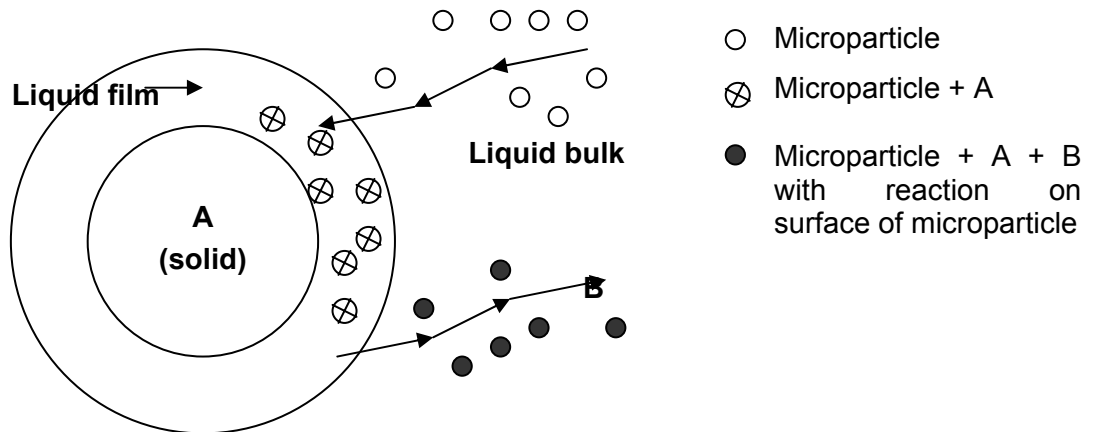
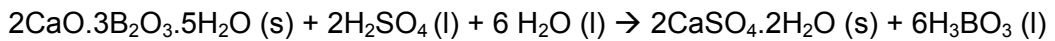


Figure 2.2. The mechanism for sink type microphase

When heterogeneous reactions are accompanied by crystallization of a product in the same liquid phase, the microcrystalline product will act as a microphase, as long as it has an affinity for the solute. An “autocatalytic” microphase is usually a sink (Anderson, 1996; Doraiswamy, 2001).

Recall equation 1.1,



In this reaction, the microparticles resemble to the initially formed gypsum crystals (~10 μm), solid A is colemanite (Ca⁺²) and B is the sulfuric acid solution (SO₄⁻²). The reaction between calcium cations and the sulfate anions occur on the microparticle, which helps the crystal to grow.

2.4. THE STUDIES ON THE RESIDENCE TIME DISTRIBUTION IN FLUID-SOLID REACTORS

In all the above studies given in literature a batch type reactor was used where liquid and the solids involved in the reaction(s) all have the same residence time. That is equal to the operating time of the batch reactor. When a continuous reactor is used, the residence time of the fluid and the solid(s) may differ from each other.

Residence time distribution (RTD, age distribution) is defined as the fraction of the material in the outlet stream that has been in the times between t and $t + dt$. In other words RTD is defined as the length of time different elements spend in a particular system under consideration. RTD depends on several factors which may also be interdependent: rheological properties, flow rate, temperature, and density of the carrier fluid, shape, density and concentration of the solid particles (Ramaswamy et.al., 1995; Baptista et.al., 1996).

The distribution of residence time in continuous flow systems is first studied by Danckwerts (1953). There have been numerous techniques for studying and investigating the residence time distribution of solid / liquid two-phase flow. These methods include visual observation, photography, laser beam, play-back videotaping, radioactive tracer and magnetic response. These different techniques require the use of different experimental set-ups and various types of particles and liquid media (Ramaswamy et.al., 1995). Many researchers had chosen the tracer method in their investigations (Baptista et.al., 1996; Abouzeid et.al., 1980; Kiared et.al., 1997; Alkhaddar et.al., 2001).

To describe the continuous flow processes in particulate systems, Abouzeid et.al. (1980) used the axial dispersion model and Alkaddar et.al. (2001) used both the axial dispersion model and the tanks in series model, where it was stated that axial dispersion model gave closer representation of the experimental data. For modeling the residence time distribution, Kiared et.al. (1997) used the one-dimensional cross-flow multistage stirred reactors (CFMSR) model.

Stokes and Nauman (1970) studied on the residence time distribution functions for stirred tanks in series. Many physical systems were modeled as a number, N , of the stirred tank reactors in series. In fitting experimental data, it was necessary to consider the case where N is not an integer. Two non-integer extensions to the tanks in series model were discussed. Methods for data reduction were represented and compared for a set of experimental measurements on a single stirred tank reactor.

Smolders and Baeyens (2000) stated that the residence time distribution (RTD) of solids for the design of CFB reactors, where conversion increases proceeded with

time, was essential. The residence time distribution for the solids was measured at different working conditions. The resulting average residence times were correlated as a function of gas velocity and solids circulation rate and were compared with the literature data. In order to predict the RTD of the solids, the solids/gas flow was firstly described by a plug flow with dispersion.

Wes et.al. (1976) explained that for the design of a rotary drum reactor, knowledge of the mechanism of both heat transfer and the dispersion of the solids was important. In that contribution the movement of solids in a horizontal rotary drum was investigated. Residence time distribution measurements were performed in an industrial scale reactor. Also, in model sections of this reactor, the behavior of solids was studied. In model sections the rotational speed of the drum, the number and the height of the strips on the reactor wall and the angle between the strip and wall, as well as the degree of filling, were varied.

Abouzied and Fuerstenau (1979) stated that the behavior of particulate materials being transported through the rotary drums was strongly affected by the addition of mixing aids to the system. This effect was reflected in three main dependent parameters: holdup, variance of the residence time distribution, and the extent of particulate segregation in the drum. In addition, the discharge rate of material fluctuated widely due to the presence of mixing aids. The holdup decreased to a limiting value with increasing volume of mixing aids. The dimensionless variance of the residence time distribution increased with increasing volume of mixing aids up to a certain limit, beyond which it remained constant.

2.5 REACTOR MODELING WITH RESIDENCE TIME DISTRIBUTION

The flows of reacting fluids through agitated vessels used in industrial production can be very complex. For practical purposes, idealized models are necessary in order to describe the interaction of the resulting flow pattern with a chemical reaction or precipitation purposes. Once the residence time distribution is determined the conversion that will be achieved in the real reactor can be predicted provided that the specific reaction rate is known, together with the degree of mixing of molecules.

The problem associated with the mixing of fluids during the reaction is important for extremely fast reactions in homogenous systems, as well as for all heterogeneous systems. This problem has two overlapping aspects: first, the *degree of segregation* of the fluid, or whether the mixing occurs on the microscopic level (mixing of individual molecules) or the macroscopic level (mixing of clumps, groups, or aggregates of molecules); and second, the *earliness of mixing* or whether fluid mixes early or late as it flows through the vessel. For a given state of macromixing (i.e., a given RTD), these two extremes of micromixing will give the upper and lower limits on conversion in a non-ideal reactor. These models were first studied by Danckwerts (1958) and Zwietering (1959). Chai and Valderrama (1982), studied on a new approach by using the RTD of real systems basing on these researches.

Macrofluid (segregation) and microfluid models have different applications. Researchers have represented the behavior of the liquid-solid mixtures with these models (Di Felice, 1993; Izumi, 1997; Tavaré, 1994, Zauner and Jones, 2002). On the basis of a reactor model, CSTR, the experimental data was used to evaluate the degree of segregation within the reaction mixture (Method and Roy, 1973).

2.6. OBJECTIVE OF THE PRESENT STUDY

In this study, the reaction of colemanite with sulfuric acid will be studied in a series of continuous flow stirred tank reactors. The overall reaction is given in Equation 1.1. However, it consists of two steps. In the dissolution reaction, boric acid is produced (in solution) and the second step is the crystallization of calcium sulfate dihydrate (gypsum). Calcium sulfate dihydrate crystals are in the shape of thin needles. It is very difficult to filter these thin crystals from the solution. A considerable amount of boric acid is kept in the cake, which is discharged after the filtration. The calcium sulfate dihydrate crystals must grow to an appropriate size in the reactor. The crystal growth process should be synchronized with the dissolution reaction.

In the production of boric acid from colemanite and sulfuric acid, there are at least three phases, a liquid and two solid phases (colemanite and gypsum). In a batch reactor all phases have the same operating time (residence time). In a continuous

reactor, they may have different residence time distributions. The residence times of both the reactant and the product solid particles are very important because they affect the dissolution conversion of the colemanite and the growth of the calcium sulfate dihydrate crystals.

The main aim of this study is to investigate the dynamic behavior of the continuous flow stirred slurry reactors. Slurry reactors are very difficult to work with, and by performing this study, the problems that can occur in the reactors can be seen easily and these problems can be solved to increase the performance of reactors.

The second aim is to study the steady state performance of the continuous flow stirred slurry reactors (CFSSR) in series during the boric acid production. Also it is intended to examine the dissolution and crystal growth reactions in continuous flow stirred slurry and batch reactors.

The colemanite is a heterogeneous mineral; its composition may vary from sample to sample. Either with changing compositions or particle sizes of the colemanite, the boric acid quality may change. It is focused on finding the conditions and controls that do not vary the quality of the boric acid significantly.

In the present doctoral work, the crystal growth model obtained from the batch reactor data, together with the residence time distribution of the continuous reactor is applied to the macrofluid and microfluid models to find the calcium ion concentration in the each exit of continuous flow boric acid slurry reactor and to validate the results with the experimental data. The second informative part of the study is to compare the particle size distribution and the volume weighted mean diameters of the gypsum crystals obtained in a batch reactor and each continuous reactor in series.

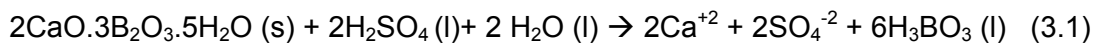
The experimental conditions were selected according to the ones in the Emet Boric Acid Plant. This study aimed to provide beneficial information to Turkish Boric Acid Industry. The other intension of the thesis is to simulate the industrial continuous boric acid reactors for non ideal conditions.

CHAPTER 3

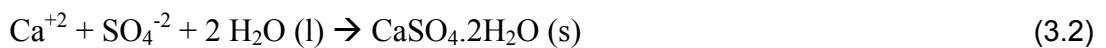
MODELING

During the dissolution of colemanite in aqueous sulfuric acid, boric acid is produced (in solution) and the calcium sulfate dihydrate (gypsum) is crystallized. By monitoring the calcium ion concentration in solution the supersaturation level of calcium ion concentration can be figured out. The reactions occurring can be written in two steps:

Dissolution of colemanite:



Calcium sulfate dihydrate (gypsum) crystal growth:



The boric acid slurry reactors consist of solid-liquid-solid components. The solids in the reactor are colemanite and gypsum. Colemanite dissolves to produce boric acid and at the same time gypsum is formed. In this consecutive reaction system, solid and liquid hold-up of the reactors may vary.

In the modeling section it is aimed to simulate the continuous boric acid reactors by using of the macrofluid or microfluid models together with the gypsum crystal growth model obtained from the batch reactor data.

3.1. GYPSUM CRYSTAL GROWTH MODEL

The crystal growth of gypsum on seed crystals follows a second order kinetics from the solution supersaturated in calcium and sulfate ions as shown in the recent studies. The crystallization kinetics of calcium sulfate dihydrate was studied during the dissolution of colemanite in aqueous sulfuric acid in a previous study by using a batch reactor (Çetin et.al,2001) and the kinetics found is

$$-\frac{dC}{dt} = k (C - C_{\text{sat}})^2 \quad (3.3)$$

where the crystal growth rate constant, k , is in $\text{l.mol}^{-1}.\text{s}^{-1}$. It is assumed to be constant during the growth process and C_{sat} is the saturation concentration of calcium ion in solution.

Colemanite is almost completely dissolved in the first few minutes. The concentration of calcium ion, C_0 , corresponds to maximum Ca^{2+} concentration attained in the very first minute, t_0 . Therefore, t_0 is very close to zero. Eq. 3.3 is integrated between t_0 and t as follows:

$$\frac{1}{C - C_{\text{sat}}} - \frac{1}{C_0 - C_{\text{sat}}} = k (t - t_0) \quad (3.4)$$

where t is in seconds. The plot of the reciprocal concentration of calcium ion versus time gives a straight line, from the slope of which the crystal growth rate constant, k , is evaluated. Maximum and saturation calcium ion concentrations are found experimentally from the batch reactor experiments.

The next step is to write the calcium ion concentration as a function of time, $C(t)$. From the variation of calcium ion concentration in solution, amount of gypsum that will be formed can be deduced.

3.2. TERMINOLOGY OF MIXING

The problem associated with the mixing of fluids during the reaction is important for extremely fast reactions in homogenous systems, as well as for all heterogeneous systems. This problem has two overlapping aspects: first, the *degree of segregation*

of the fluid, or whether the mixing occurs on the microscopic level (mixing of individual molecules) or the macroscopic level (mixing of clumps, groups, or aggregates of molecules); and second, the *earliness of mixing* or whether fluid mixes early or late as it flows through the vessel. The terminology used in this chapter is listed below:

- macrofluid = segregated fluid
- microfluid = totally molecular dispersed fluid
- micromixing = mixing that produces a microfluid
- macromixing = mixing that produces a segregated = a macrofluid

The more complex models of non-ideal reactors necessary to describe reactions other than first order must contain information about micromixing in addition to that of macromixing. Macromixing produces a distribution of residence times without, however, specifying how molecules of different ages encountering one another in the reactor. Micromixing, on the other hand, describes how molecules of different ages encounter one another in the reactor. There are two extremes of micromixing: (1) all molecules of the same age group remain together as they travel through the reactor and are not mixed until they exit the reactor (i.e., complete segregation) (2) molecules of different age groups are completely mixed at the molecular level as soon as they enter the reactor (complete micromixing). For a given state of macromixing (i.e., a given residence time distribution, RTD), these two extremes of micromixing will give the upper and lower limits on conversion in a non-ideal reactor. For reaction orders greater than one, the segregation will give the highest conversion while for reaction order less than one the complete mixing model will give the highest conversion. A fluid in which the globules of a given age do not mix with other globules is called a macrofluid, while a fluid in which molecules are free to move everywhere is called a microfluid. The extremes of early and late mixing are referred to as complete segregation and maximum mixedness, respectively (Fogler, 1992).

The views of macrofluid and microfluid behavior are presented in Figures 3.1 - 3.3, respectively (Bratz, 2001).

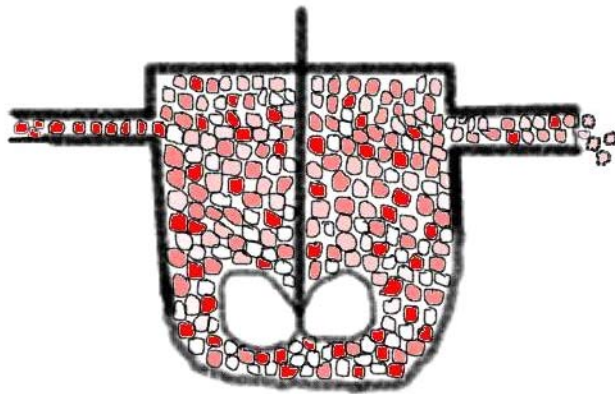


Figure 3.1. Schematic representation of macrofluid behavior

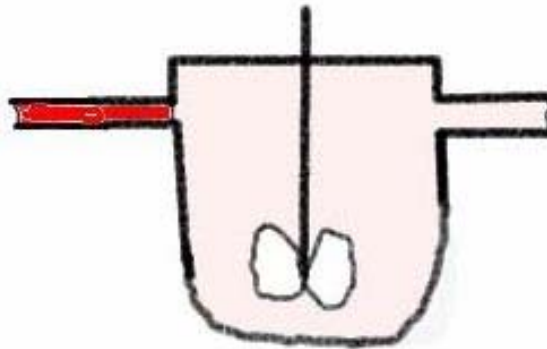


Figure 3.2. Schematic representation of microfluid behavior

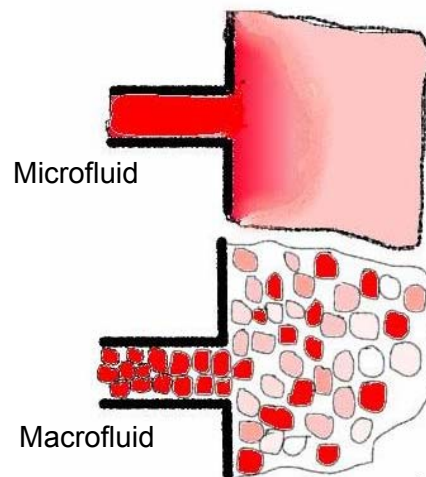


Figure 3.3. Schematic representation of inlet of the reactor, in which a microfluid or a macrofluid is entering the reactor

From Figures 3.1-3.3, it can be seen that in macrofluid behavior the molecules moves in clumps and each clump behaves as a batch reactor, but in a microfluid, the fluid is said to be molecularly dispersed. The comparison of the two types can be found in Table 3.1.

Table 3.1. Comparison of macrofluid and microfluid behavior in a reactor

Macrofluid	Microfluid
Molecules moves about in clumps, and each clump is uniform in composition.	Individual molecules have no attachment to or for their neighbors, each moves independently.
The molecules does not lose its identity, its past history is not known, and its age can be estimated by examining its neighboring molecules.	Each molecule loses its identity, its past history can not be told whether a molecule is a newcomer or an old-timer in the reactor.

3.3. SIMULATION OF CONTINUOUS FLOW REACTORS

Before explaining the simulation of the continuous reactors, the behavior of fluids in the two types of reactors is compared in Table 3.2.

Table 3.2. Comparison of batch, plug flow and mixed flow reactors in terms of the behaviors of microfluid and macrofluid

Batch and Plug Flow Reactor	Mixed Flow Reactor (CSTR)
Micro and macrofluids act alike	Micro and macrofluids act differently
Degree of segregation does not affect conversion or product distribution	Degree of segregation affects conversion or the product distribution

Because there is no molecular interchange between globules, each acts essentially as its own batch reactor. The reaction time in any one of these tiny batch reactors is equal to the time that the particular globule spends in the reaction environment. The

distribution of residence times among the globules is given by the RTD of the particular reactor.

Gypsum growth model parameters were used to evaluate the concentration of calcium ion at the exit of the continuous flow reactors; plug flow reactor model (PFR) and continuous flow stirred tank reactors (CSTR) in series model by either macrofluid or microfluid approach.

The following assumptions have been made during the modeling:

- CSTR's, having equal volumes, are at steady state.
- There is a uniform temperature distribution in the reactors, and each reactor had the same uniform temperature.
- Colemanite is almost completely dissolved in the first few minutes.
- The volumetric flow rates of the solid and liquid are constant.
- The solid hold up, i.e. solid to liquid ratio, in each reactor does not differ at steady state and each reactor had equal liquid volumes.
- Distribution of the solid particles in the reactors is uniform.

3.3.1. MACROFLUID MODEL FOR N-CSTR'S IN SERIES

When a macrofluid enters a mixed flow reactor, the reactant concentration in an aggregate does not drop immediately to a low value but decreases in the same way as it would in a batch reactor. In this model, the flow through the reactor is visualized to consist of a continuous series of globules (little batch reactors). These globules retain their identity; that is, they do not interchange material with other globules in the fluid during their period of residence in the reaction environment. In addition, each globule spends a different amount of time in the reactor. In essence, all the molecules that have the same residence time in the reactor are lumped into the same globule.

In macrofluid model, gypsum crystals with the surrounding fluid can be considered as a series of globules. Each globule acts like a little batch reactor having a residence time τ . The residence time distribution function, $E(t)$, for this multiphase system is defined for globules. In general it is defined for single phase systems. $E(t)$ expression of the ideal CSTR's is given below:

$$E(t) = \frac{t^{n-1}}{(n-1)! \tau_i^n} e^{-t/\tau_i} \quad (3.5)$$

where n is the number of reactors, τ_i is the space time of the globules in each CSTR that is estimated by dividing the volume of globules in CSTR by the volumetric flow rate of the globules. To clarify, the volume of the globules can be taken as the summation of liquid and solid volumes. Volumetric flow rate of the globules are found by dividing the total flow rate to the density of the globules. Each globule has the same solid to liquid ratio and during these suppositions, the density of the globules in the reactors is assumed to be constant. The calculation of the volume and volumetric flow rate of the globules are given in the following equations.

$$\tau_g = \frac{V_g}{v_g} \quad (3.6)$$

$$V_g = V_s + V_L \quad (3.7)$$

$$v_g = \frac{\dot{m}_g}{\rho_g} \quad (3.8)$$

$$\dot{m}_g = \dot{m}_s + \dot{m}_L \quad (3.9)$$

$$\rho_g = \rho_L h_L + \rho_s (1 - h_L) \quad (3.10)$$

$$h_L = \dot{m}_L / \dot{m}_g \quad (3.11)$$

By using equations 3.6 -3.11, the residence time of the globules, τ_g , can be calculated. The residence times of the solid and liquid are taken as equal, which is also equal to the residence time of the globules. So, the E(t) function of the slurry reactor can be estimated by using equation 3.5, by inserting the residence time of the globules calculated from equation 3.6.

The E(t) function for the slurry reactors is drawn in Figure 3.4 for a total residence time of 240 min by changing the number of CSTR's from 1 to 40. Here, the residence time in each CSTR is found by dividing the total residence time to the number of reactors.

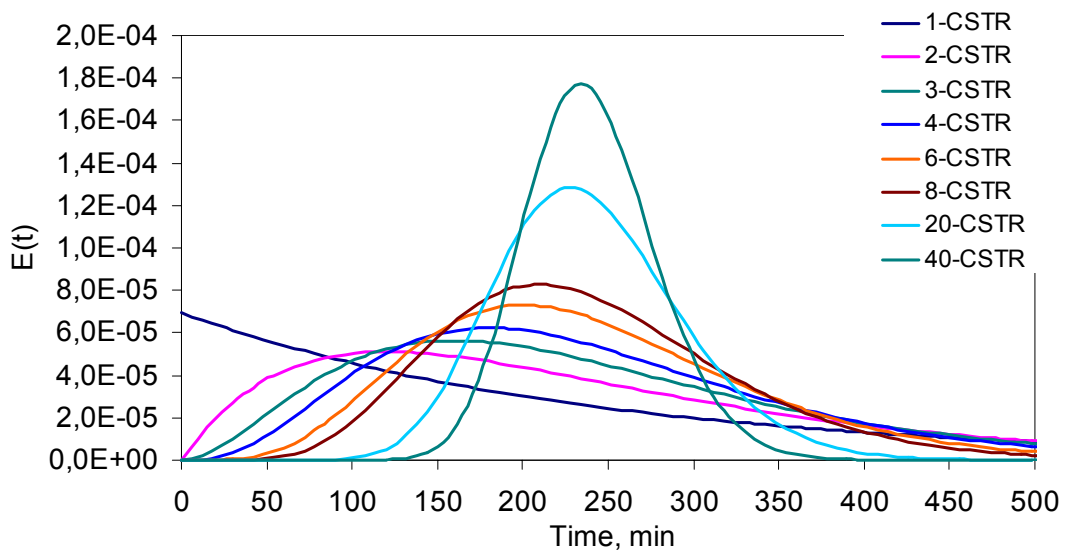


Figure 3.4. Change of E(t) function with CSTR number

As seen from Figure 3.4 as the reactor number increases, the E(t) expression comes close to the PFR's E(t) expression, which will be explained in the coming parts of this chapter.

From E(t) function, F(t) function can easily be found by the following definition:

$$F(t) = \int_0^t E(t) dt \quad (3.12)$$

Figure 3.5 shows the F(t) as a function time depending on the number of CSTR's.

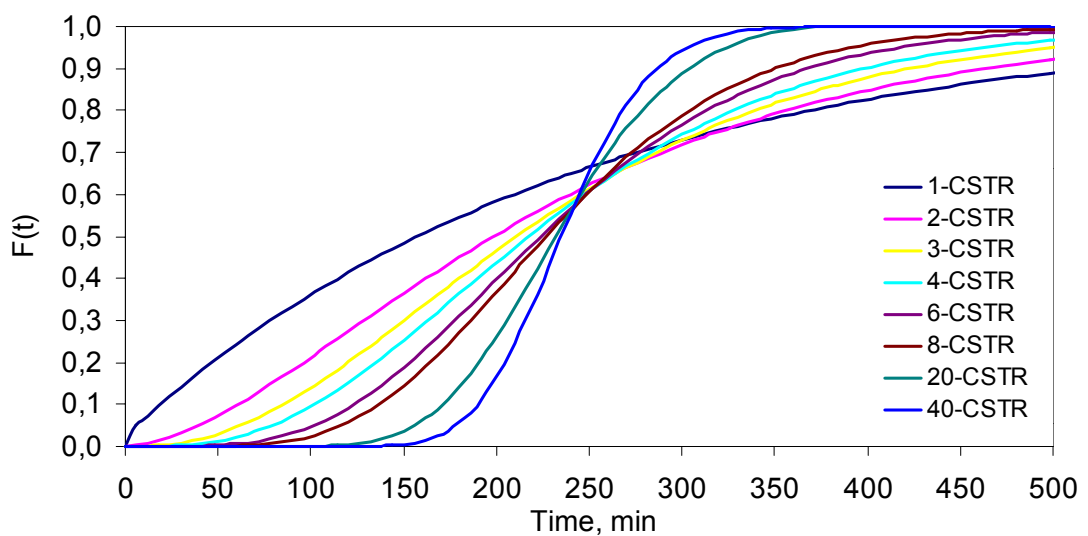


Figure 3.5. Change of F(t) function with CSTR number

In macrofluid model, each of the globules in the reactor is considered to have different concentrations of reactants, $[Ca^{2+}]$, and products. These globules are mixed together immediately upon exiting to yield the exit concentration of Ca^{2+} , \bar{C} , which is the average concentration at the exit of the stirred slurry reactors:

$$\bar{C} = \int_0^{\infty} C(t) \cdot E(t) dt \quad (3.13)$$

The concentrations of the individual species in the different globules are determined from batch reactor calculations. For a constant volume batch reactor, the calcium ion concentrations as a function of time, $C(t)$, was found from Equations. 3.4. This equation is solved together with the residence time distribution function, $E(t)$ given in Eq. 3.5, to give the average exit calcium ion concentration. For the n-CSTR, the calcium ion concentrations at the outlet of the n^{th} reactor, \bar{C}_n , is obtained by combining $C(t)$ and Eqn 3.5. The calcium ion concentration at the exit of the reactors can be estimated by using the computer program utilizing numerical integration techniques.

3.3.2. MICROFLUID MODEL FOR N-CSTR'S IN SERIES

A fluid in which the globules of a given age do not mix with other globules is called a macrofluid, while a fluid in which molecules are free to move everywhere is called a microfluid. In the microfluid model, the liquid reactant is assumed to be completely or perfectly mixed.

When a microfluid containing reactant A is put into a mixed flow reactor (CSTR), the reactant concentration everywhere drops to the low value prevailing in the reactor. No clump of molecules retains its high initial concentration of A.

For one CSTR the design equation is

$$\frac{C_0 - C_1}{\tau_j} = k (C_1 - C_{\text{sat}})^2 \quad (3.14)$$

For the other CSTR's in series, the design equation is solved around each reactor. For n-CSTR's in series, the design equation for the n^{th} reactor is

$$\frac{C_{n-1} - C_n}{\tau_i} = k(C_n - C_{sat})^2 \quad (3.15)$$

While doing the microfluid model calculations, the space time is calculated in the same way as in the calculations of the macrofluid model, i.e. it is total space time in the n-CSTR's is the multiplication of τ_i with the number of CSTR's. A computer program can also be written for the solution of the microfluid model.

3.3.3. PLUG FLOW MODEL

Another way of looking at the continuous flow system is the PFR. Because the fluid flows down the reactor in plug flow, each exit stream corresponds to a specific residence time in the reactor. In macrofluid model, batches of molecules are removed from the reactor at different locations along the reactor in such a manner so as to duplicate the RTD function, $E(t)$. The molecules removed near the entrance to the reactor correspond to those molecules having short residence times in the reactor. Physically this effluent would correspond to the molecules that rapidly channel through the reactor. The further the molecules travel along the reactor before being removed, the longer their residence time. The points at which the various groups or batches of molecules are removed correspond to the RTD function of the reactor (Levenspiel, 1999).

For the plug flow reactor the calcium ion concentration at the exit of the reactor is also estimated from the $E(t)$ expression of the PFR. $E(t)$ function is represented by Dirac Delta function as follows:

$$E(t) = \delta(t - \tau) \quad (3.16)$$

The Dirac delta function has the following properties:

$$\delta(x) = 0 \text{ when } x \neq 0$$

$$\delta(x) = \infty \text{ when } x = 0 \quad (3.17)$$

$$\int_{-\infty}^{\infty} \delta(x) dx = 1.0 \quad (3.18)$$

$$\int_{-\infty}^{\infty} g(x) \delta(x - \tau) dx = g(\tau) \quad (3.19)$$

By using the property of the Dirac Delta Function, the calcium ion concentration at the exit of the PFR by using Eq. 3.13 becomes equal to Eq. 3.20:

$$\bar{C} = \int_0^{\infty} C(t) \cdot \delta(t - \tau) dt = C(\tau) \quad (3.20)$$

where $C(\tau)$ is the concentration of calcium ion as a function of the space time.

When the plug flow reactor is considered from the microfluid point of view, the design equation for plug flow reactor with the given gypsum crystal growth kinetics is analogous to batch reactor design equation since the change in the density of liquid is neglected and liquid flow rate is assumed to be constant.

$$\tau = \frac{1}{k} \int_{C_0}^C \frac{dC}{(C - C_{sat})^2} \quad (3.21)$$

By taking the integral of equation 3.21, equation 3.22 is obtained.

$$\frac{1}{C - C_{sat}} - \frac{1}{C_0 - C_{sat}} = k\tau \quad (3.22)$$

The calcium ion concentration as a function of space time is found from Eq. 3.22 using the same kinetic parameters found from gypsum crystal growth model. The calcium ion concentration as a function of τ will give $C(\tau)$, where τ is the volume of the liquid divided by the volumetric flow rate of liquid. As observed, same concentration expression is obtained from the macrofluid and microfluid expressions. It is assumed that liquid to solid volume ratio does not change along the reactor. There is no mixing in axial direction and complete mixing in liquid in radial direction.

CHAPTER 4

EXPERIMENTAL

4.1. MATERIALS

Colemanite mineral (25-100 mm, Hisarcık, Turkey), sulfuric acid (93 wt%) and boric acid (99.9% b.w.) were supplied by Eti Holding A.Ş. (Ankara, Turkey). The size of the colemanite was first reduced by means of a jaw crusher then a hammer mill, and sieved. The colemanite mineral having different particle size ranges; namely 0-150 μm , 0-250 μm , and +250 μm ; was used in this study. The colemanite used in the study had different compositions. As the origins of the colemanite were the same, the colemanite used was named as Hisarcık 1, Hisarcık 2 and Hisarcık 3. The chemical compositions of the colemanite are given in Chapter 5. All other chemicals used in the analysis were purchased in reagent grade from Merck (Darmstadt, Germany) and J.T. Baker (Deventer, Holland).

4.2. BATCH REACTOR EXPERIMENTS

4.2.1. EXPERIMENTAL SETUP

The experimental setup consists of a reactor, a mechanical stirrer, a heating jacket, a thermocouple and a temperature control unit. The schematic diagram of the set-up for the batch reactor experiments is given in Figure 4.1. The photograph of the set-up can be seen in Figure 4.2. The reactor having an inside diameter of 12 cm and a height of 30 cm (the bottom section) is made up of borosilicate glass (İldam Kimya, Ankara, Turkey). The stirrer used in the experiments was designed to

achieve a homogeneous mixture. The stirrer had two stages and each stage had four blades.

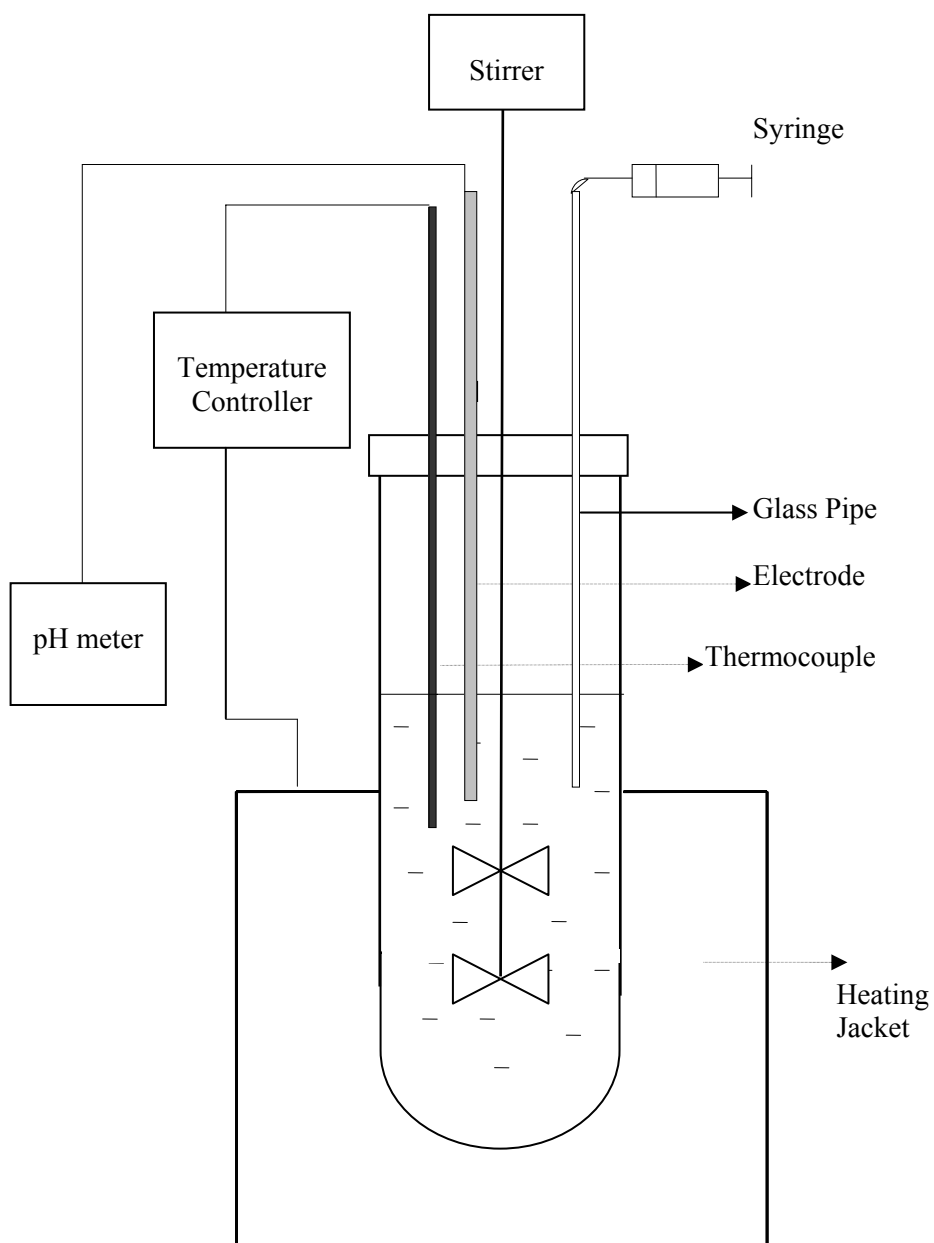


Fig. 4.1. Schematic diagram of the set-up used for the batch reactor experiments



Figure 4.2. Photograph of the set-up used for the batch reactor experiments

4.2.2. EXPERIMENTAL PROCEDURE

The sulfuric acid was added to distilled water in the reactor and the reactor was heated to the reaction temperature. The colemanite was fed to the reactor at one lot and this time was taken as the start of the reaction. At certain time intervals samples were taken from the reactor by means of a syringe and immediately filtered by the help of a vacuum pump. The B_2O_3 and calcium content of the solution was analyzed by means of titration and Atomic Absorption Spectrophotometer (Philips PU 9200 X), respectively.

4.2.3. SCOPE OF THE EXPERIMENTS

All the batch reactor experiments performed aimed to find the crystal growth kinetics of gypsum. The experimental conditions are given in Table 4.1.

Table 4.1. The Batch Reactor Experiments Performed during the Study

Experiment Name	Colemanite	Particle Size Of Colemanite	CaO/So_4^{2-} Molar Ratio	Temp. (°C)	Stirring Rate (Rpm)
HB2.1	Hisarcık 2	0-250 μm	0.95	80	500
HB2.2	Hisarcık 2	250-1000 μm	0.95	80	500
HB2.3	Hisarcık 2	0-250 μm	1.0	85	500
HB3.1	Hisarcık 3	0-150 μm	1.0	85	400

4.3. CONTINUOUS FLOW STIRRED SLURRY REACTORS IN SERIES (CFSSR'S) EXPERIMENTS

4.3.1. EXPERIMENTAL SETUP

Experimental set-up consists of a solid feeding unit, an acid feeding unit, and four continuously stirred reactors in series unit, followed by a filtration unit. The schematic diagram and the photograph of the set-up is given in Figures 4.3 and 4.5, respectively.

The solid feeding unit consisted of three parts. The first part was the funnel, where colemanite was put, the second part consisted of a mechanical stirrer (Heidolph RZR 2041) connected to a screw type feeder, and the last part was the vibratory feeder (Retsch DR 100). The colemanite falling from the funnel was first fed to the screw type feeder, which carried it to the vibratory feeder. Colemanite, which fell to the vibratory feeder, was then fed to the first reactor.

Acid feeding unit consisted of 100 l feed tank, a mechanical stirrer (Janke & Kunkel K.C. RW38), a porcelain diver heater placed inside the tank, a temperature controller (Elimko 200) and a thermocouple connected to the heater, and a peristaltic pump (Watson Marlow 505S). Heated acid was fed to the first reactor by means of the peristaltic pump.

The reactors are made up of glass (Çalışkan Cam, Ankara). The volume of each reactor was 1.8 l. Each reactor was heated and continuously stirred. First reactor had a silicone heating tape connected to a temperature controller (Isopad TD2000) and a thermocouple. The other three reactors were jacketed and hot water was circulated around each of them by means by a circulating water bath (Heto HWT 100, OBN 28). The technical drawing of one of the continuous flow stirred slurry reactor is given in Figure 4.4, having hot water circulation around it. The dimensions of the first reactor were the same, except the hot water circulation. In only difference in the dimensions of the batch reactor was the height of the reactor, 30 cm, whereas the volume used in the reactor was 1.5 lt.

The temperatures of the reactors were measured by use of digital thermometers. Stirring was done by means of mechanical stirrers and baffles were placed inside the reactors for homogenous stirring. There were level differences between the reactors and the outlet of one reactor was connected to the inlet of the next reactor by means of overflows. The pH's of the reactors were recorded by the help of a pH-meter (Mettler Toledo MP 200).

The outlet of the last reactor was connected to a filtration unit. The products, boric acid (aqueous) and gypsum (solid) were separated by use of vacuum filtration. This unit consisted of a vacuum pump (KNF NO22) connected to a 2 l nutsche flask and a buhner funnel, having a 15 cm diameter, on top of it. Filter paper was placed on

the funnel and gypsum particles were collected on the filter paper whereas, boric acid was collected in the flask.

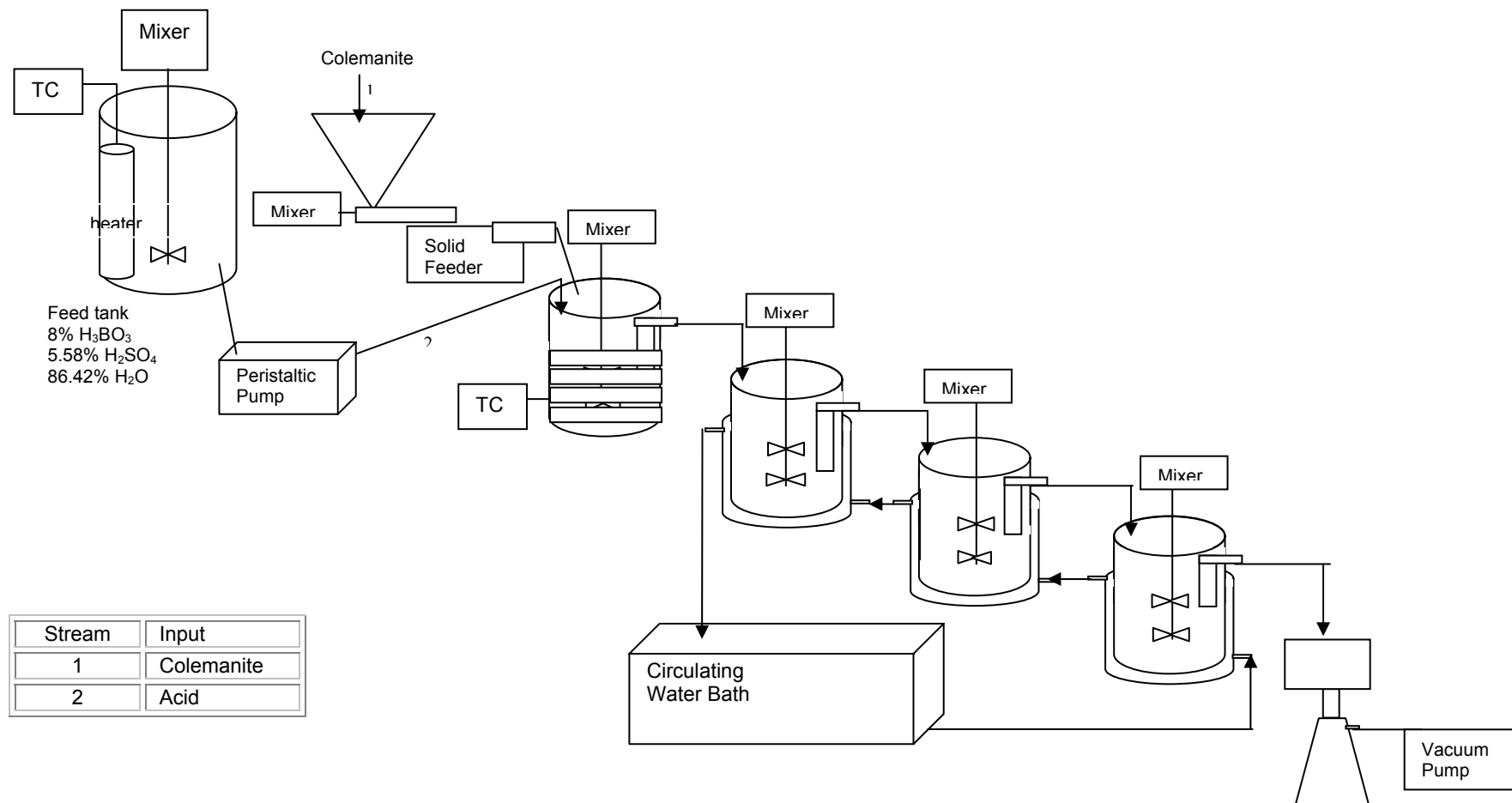


Figure 4.3. Schematic diagram of the set-up used for the continuous flow stirred slurry reactor experiments

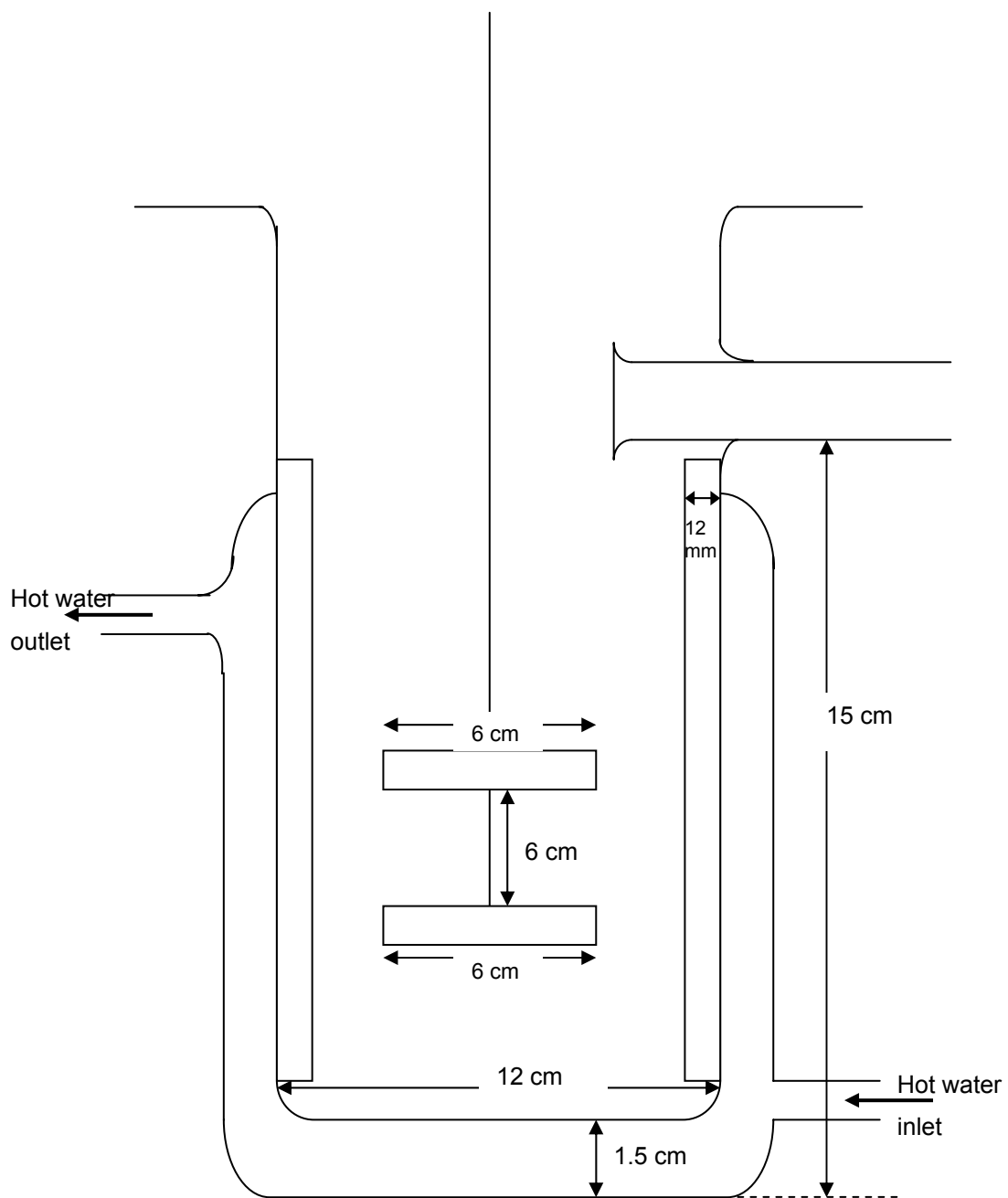


Figure 4.4. Technical drawing of the continuous flow stirred slurry reactor



Figure 4.5. Photograph of the set-up used for the continuous flow stirred slurry reactor experiments

4.3.2. DYNAMIC BEHAVIOR EXPERIMENTS

4.3.2.1. EXPERIMENTAL PROCEDURE

The experiments were all performed by using a single CSTR, the volume of which was 1840 ml. In all dynamic behavior experiments, in other words residence time distribution experiments, distilled water was used with a flow rate of 42.5 ml/min, i.e., there was no reaction in the reactor system (sulfuric acid has not been added).

First of all, in order to check if the CSTR that was used during the experiments approached an ideal one, the liquid residence time experiments were performed by injecting nickel to the inlet stream as a pulse tracer. In the experiments the data was taken by mixing cup readings, that is, the effluent of the reactor was collected in flasks for 10 min intervals and samples were taken from each flask. The nickel concentration of each sample was determined by means of Atomic Absorption Spectrophotometer (Philips PU 9200 X).

Two different stirring rates, namely 500 and 750 rpm, were applied to the same system to see the effect of the stirring rate on the residence time of the liquid. Also two different tracers, lithium and nickel were given to the system at a stirring rate of 500 rpm to check different tracers.

The behavior of a single CSTR to the step tracer of colemanite was studied at 500 rpm either giving 4.3 g/min colemanite to the system or preventing the colemanite flow and taking mixing cup readings, that is, the effluent of the reactor was filtered for 5 min intervals and waited to dry to see the amount of colemanite collected.

The behavior of a CSTR to a pulse tracer of lithium when both liquid and colemanite was flowing at steady state was searched at two different stirring rates (500, 750 rpm). The colemanite and water flow rates were 7.2 g/min and 42.5 ml/min, respectively. Mixing cup readings were taken, that is, the effluent of the reactor was collected in flasks for 10 min intervals and after the precipitation of the colemanite, and samples were taken from the liquid part of each flask. The colemanite used in the experiments was Hisarcık1 colemanite. The lithium amount of the Hisarcık1 colemanite was 0.028%.

Same procedure was repeated at 500 rpm with different solid to liquid ratios (0.085, 0.17, 0.34). For these cases, the flow rate of colemanite kept constant at 7.2 g/min, while the flow rate of water changed (84.7, 42.5, 21.2 g/min).

4.3.2.2. SCOPE OF THE EXPERIMENTS

The dynamic behavior experiments were performed as shown in Table 4.2.

Table 4.2. Dynamic Behavior Experiments Performed

Set 1: Liquid Residence Time Experiments				
Experiment Name	Tracer (Pulse)	Liquid Feed Rate (g/min)	Solid* Feed Rate (g/min)	Stirring Rate (rpm)
HC1.1	Nickel	42.5	-	500
HC1.2	Nickel	42.5	-	750
HC1.3	Lithium	42.5	-	500
SET 2: SOLID RESIDENCE TIME EXPERIMENTS				
Experiment Name	Tracer (Step)	Liquid Feed Rate (g/min)	Solid* Feed Rate (g/min)	Stirring Rate (rpm)
HC1.4	Colemanite (negative input)	-	4.3	500
HC1.5	Colemanite (positive input)	-	4.3	500
SET 3: LIQUID RESIDENCE TIME EXPERIMENTS IN A SOLID/LIQUID SYSTEM				
Experiment Name	Tracer (Pulse)	Liquid Feed Rate (g/min)	Solid* Feed Rate (g/min)	Stirring Rate (rpm)
HC1.6	Lithium	42.5	7.2	500
HC1.7	Lithium	42.5	7.2	750
HC1.8	Lithium	84.7	7.2	500
HC1.9	Lithium	21.2	7.2	500

* Solid used in the experiments is Hisarcık 1, 0-250 μm , colemanite.

4.3.3. BORIC ACID PRODUCTION EXPERIMENTS

4.3.3.1. EXPERIMENTAL PROCEDURE

The water bath and the feed tank were heated to the desired temperatures of 90°C and 85°C, respectively. While they were heating, 16% boric acid solutions were prepared and also heated to 85°C by the use of magnetic stirrers with heater (Heidolph MR 3001). Distilled water was used for this preparation. Tap water was distilled by the use of a water distillation apparatus (Nüve NS 108).

On the other hand, solid and acid feeding units were calibrated before the experiments. It was critical to use dry colemanite during the experiments, so colemanite was stored at 85°C in the oven (Nüve FN 500) till the rest of the experiments.

The hot water was circulated through the jackets of the last three reactors, where hot water inlet was from the last reactor. At the same time, the controller of the silicone heating tape was adjusted to 85°C in the first reactor. Then, hot 16% boric acid solutions were put into the first three reactors. The last reactor was left empty.

At the beginning of the experiment, the colemanite and acid feeders were operated at the same time and this time was accepted as the zero time, which describes the starting moment of the reaction. Samples were begun to be taken when the first product was taken from the last reactor. The samples are taken in time intervals.

Colemanite and acid feeding was checked continuously and feeding of colemanite to the solid feeder funnel and acid to the acid tank was done in appropriate intervals.

During the experiments, samples were withdrawn from all of the reactors by means of a 50 ml syringe attached to a 15 cm long glass pipe. The samples were immediately filtered by a filtration unit resembling the one described in the experimental set-up for product filtration. In this unit, analytical funnels were placed above 250 ml nutsche flasks and this apparatus was put into hot water, in order to prevent the boric acid solution to crystallize. Blue band filter papers were put on the

funnels and solid particles were collected on it. Samples for examining the boric acid and calcium ions in solution were taken from the flask by the help of 5 ml and 1 ml micropipettes (Finpipette, Thermo Labsystems), respectively.

The filtration process should be quick to prevent boric acid to crystallize on the filter paper. So, the procedure explained for filtration was not applicable to the systems having high solid hold-ups. For such systems, another filtration system, which was by using syringe filters, was adapted to the system to find the boric acid and calcium ion concentrations in the solution. The syringe filters were first put into the oven until they reach a temperature of 85°C, the same temperature with the slurry. Then, the slurry, taken by the syringe was filtered by inserting the tip of the syringe to the filter.

The temperatures of the reactors and the pH values were recorded during the experiments. The pH values of the reactors were used in determining if the reactor comes to steady state or not.

The samples of the boric acid solution were taken from the flask when the system comes to steady state. These samples were analyzed for the sulfate ion and magnesium ion concentrations.

4.3.3.2. SCOPE OF THE EXPERIMENTS

The parameters that were not changed during the experiments were listed below:

- The concentration of sulfuric acid (5.58%) and boric acid (8%) in the feed tank
- Stirring rate of the reactors (400 rpm)
- Temperature of the reactors and the feed tank (82°C– 85°C in reactors, 85°C in the feed tank)
- Initial boric acid concentration (16%) put in the first three reactors

Three sets of experiments were performed during the study. In two sets of the experiments, the changes in the flow rates of the colemanite and acid were used to observe the changes in the sizes of gypsum crystals. While changing the flow rates

of colemanite and acid, $\text{CaO}/\text{SO}_4^{2-}$ molar ratio and solid hold-up values, h_s , was constant.

In the last set of the experiments, $\text{CaO} / \text{SO}_4^{2-}$ molar ratio and solid hold-up values, h_s were changed. These two ratios were very critical in this study. So, the effect of these ratios was observed by changing the acid feed rates at constant colemanite feed rate. The performed experiments are tabulated in Table 4.3a and 4.3b.

Table 4.3a. Performed Experiments in Grouped Style in Continuous Flow Stirred Slurry Reactors in Series

COLEMANİTE USED	CONDITIONS	COLEMANİTE FEED RATE (G/MİN)	ACİD FEED RATE (G/MİN)
Hisarcık2 (0-250 μm)	$\text{CaO}/\text{SO}_4^{2-} : 1.00$ $h_s : 0.04$	5	48.5
		7.5	72.7
		10	97
	$\text{CaO}/\text{SO}_4^{2-} : 1.37$ $h_s : 0.06$	5	35
		10	70
		15	105
	$\text{CaO}/\text{SO}_4^{2-} : 2.17$ $h_s : 0.09$	10	45
Hisarcık 3 (0-150 μm)	$\text{CaO}/\text{SO}_4^{2-} : 1.00$ $h_s : 0.05$	3.5	30
		10	90

Table 4.3b. Performed Experiments in Continuous Flow Stirred Slurry Reactors in Series

EXPERIMENT NAME	COLEMANİTE	PARTICLE SIZE OF COLEMANİTE	CAO/SO ₄ ²⁻ MOLAR FLOW RATE	SOLID HOLD-UP, H _s	COLEMANİTE FEED RATE (G/MİN)	ACİD FEED RATE (G/MİN)
HC2.1	Hisarcık 2	0-250 µm	1.00	0.04	5	48.5
HC2.2	Hisarcık 2	0-250 µm	1.00	0.04	7.5	72.7
HC2.3	Hisarcık 2	0-250 µm	1.00	0.04	10	97
HC2.4	Hisarcık 2	0-250 µm	1.37	0.06	5	35
HC2.5	Hisarcık 2	0-250 µm	1.37	0.06	10	70
HC2.6*	Hisarcık 2	0-250 µm	1.37	0.06	10	70
HC2.7	Hisarcık 2	0-250 µm	1.37	0.06	15	105
HC2.8	Hisarcık 2	0-250 µm	2.17	0.09	10	45
HC3.1	Hisarcık 3	0-150 µm	1.00	0.05	3.5	30
HC3.2	Hisarcık 3	0-150 µm	1.00	0.05	10	90

* Experiment H2.6 was performed for the reproducibility analysis

4.4. ANALYTICAL PROCEDURES

4.4.1. DETERMINATION OF BORIC ACID CONCENTRATION

The boric acid concentration of the liquid phase was determined as follows: 5 ml of sample was taken from the solution, which was filtered by using blue band filter, and put into a bottle. Methyl red indicator was put on it and 1-2 drops of 1:3 (by vol.) H₂SO₄ was added to the solution. Then, 6 N NaOH was put until the color changes from pink to yellow. After this step, H₂SO₄ was again added to the solution until the color turns back to pink. This solution is titrated with 0.5 N NaOH until a pH of 4.5 is obtained. At this step a titrator involving a magnetic stirrer and pH-meter (TitroLine easy, Schott) was used to get accurate results. Then, phenolphthalein indicator was put into the bottle and 10-15 g mannitol was added to the solution. The solution was again titrated with 0.5 N NaOH until the pH of the solution becomes 8.5. The volume of the NaOH used in this step was recorded and used to calculate the boric acid concentration from the following formula:

$$H_3BO_3 \text{ (mol/l)} = V_{NaOH} F_{NaOH} N_{NaOH} / V_{sample}$$

where V_{NaOH} , F_{NaOH} , N_{NaOH} and V_{sample} are the volume of the NaOH used, factor of the NaOH, normality of NaOH, and the volume of the sample, respectively.

4.4.2. DETERMINATION OF CALCIUM ION CONCENTRATION

Calcium ion concentration of the samples was determined by Atomic Absorption Spectrophotometer (Philips PU 9200X) in METU Chemical Engineering Department. 1 ml samples were taken to the 100 ml plastic balloon georgette and deionized water was added on the sample. The liquid samples were directly measured at atomic absorption spectrophotometer after diluting the sample to a maximum of 15 ppm. Before each analysis the atomic absorption spectrophotometer was calibrated between 0 - 15 ppm calcium content.

4.4.3. DETERMINATION OF SULFATE ION CONCENTRATION

Sulfate ion in solution was determined gravimetrically. The procedure was as follows:

The solution was filtered and from the filtrate 25 ml was taken. 10 ml HCl, 1 ml 3% H₂O₂ and methyl red indicator was added to the solution. The solution was boiled to oxidize the R₂O₃ groups, which are iron, aluminum and titanium. It was continued to boil until a remaining red color was seen in the solution. The solution was precipitated by adding drop by drop 1:1 (by vol.) NH₄OH. The solution having a yellow color was boiled on hot plate for 5 minutes. The solution was filtered and the filtrate was taken. 10 ml HCl, 25 ml 10% hot BaCl₂ and methyl red indicator was added to the solution. The solution was precipitated as BaSO₄ by stirring. The solution was then left on hot plate for one hour. Then, the solution was taken and waited overnight. After that, the solution was filtered and washed with hot water. The solution was put into constant weight crucible and weighed. The crucible was then put into the oven and heated to 850°C. The crucible was left at 850°C for one hour and then weighed. The weight difference will give the amount of BaSO₄. The BaSO₄ amount was then converted to sulfate ion concentration.

4.4.4. DETERMINATION OF MAGNESIUM ION CONCENTRATION

Magnesium ion concentration of the samples was determined by Atomic Absorption Spectrophotometer (Philips PU 9200X) in METU Chemical Engineering Department. The liquid samples were directly measured at atomic absorption spectrophotometer after diluting the sample to a maximum of 0.9 ppm. Before each analysis the atomic absorption spectrophotometer was calibrated between 0.3 – 0.9 ppm magnesium content.

4.4.5. CRYSTAL SIZE DETERMINATION

4.4.5.1. PARTICLE SIZE DISTRIBUTION OF GYPSUM CRYSTALS

When the system comes to steady state, the pH of the slurry was constant; samples were taken from all of the reactors and filtered. These samples were washed during filtration to get rid of the boric acid in the filtrate. The solid collected from the reactors were further washed by putting a small amount of solid into a large volume of water and stirred. The solid was then again filtered and put into sample bottles. Water was also added to the bottles. Tap water used was used during the analysis.

The particle size distributions of the solid samples were determined by a particle size analyzer (Malvern Instruments, Mastersizer 2000), in Ankara University, Chemical Engineering Department, utilizing the principle of laser ensemble light scattering. This instrument can detect the particle range of 0.02-2000 μm . The analysis was done by using wet dispersion method with a repeatability of +/- 0.5%. The dispersant used in the analysis was tap water.

In the analysis, some amount of solid was taken from the sample bottles and put into 800 ml beaker filled with water. This beaker was put on its place in the analyzer. Solid was continued to be added until the laser obscuration value on the computer reaches 14-15%. Then the analyzer was ready to give the crystal size distribution of the sample. The analysis was repeated for three times to see if the same result was obtained or not. It was seen that reproducible results were obtained. Then, the volume weighted mean of the curves were calculated by the software of the analyzer.

4.4.5.2. LIGHT MICROSCOPE IMAGES OF GYPSUM CRYSTALS

The colemanite particles were examined under the light microscope. In the analysis, Prior Laboratory Microscope Model B 3000 was used. Microscope was connected online to a computer by Pro Series, high performance CCD camera. Images were seen live in monitor by an analytical imaging software called Image Pro Plus 3.0 for Windows. The views of the samples were snapped and saved into the computer.

CHAPTER 5

RESULTS AND DISCUSSION

5.1. RESULTS OF COLEMANITE ANALYSIS

5.1.1. SCREEN ANALYSIS OF COLEMANITE

Colemanite, named as Hisarcık 1, had average particle sizes of 2.5 cm. Colemanite is first crushed in the jaw crusher and then ground in a hammer mill. To get the size distribution, sieve analysis is performed. In previous experiments, performed by Çetin et. al (2001) particles smaller than 250 μm was used. So, the first sieve analysis is performed to see the amount of the colemanite left on the 60 mesh sieve (corresponding to 250 μm). It was seen that nearly 35 percent of the colemanite was left on this sieve. It is seen that the maximum particle diameter of the colemanite is between 1-2 mm (18-10 mesh, respectively). The screen analysis of the Hisarcık 1 colemanite is given in Table 5.1.1, in which the mass fractions of the colemanite on each sieve and the cumulative mass fractions of the colemanite under that sieve were given. The particle diameter is the maximum diameter of the particles that could pass the former sieve. The average particle diameter stands for the arithmetic mean of the minimum and maximum diameter of the particles on that sieve. Figure 5.1.1 presents the differential particle size distribution of the Hisarcık 1 colemanite particles sieved. The mass fraction of the colemanite particles on each sieve according to their average particle diameters were illustrated, whereas Figure 5.1.2 illustrates the particle size distribution of the Hisarcık 1 colemanite particles by the cumulative amount of the colemanite particles under the stated particle diameters. For each particle diameter, cumulative mass fraction of the colemanite smaller than that diameter is given.

Table 5.1.1. The screen analysis of Hisarcık 1 colemanite

Mesh No	Dp _i , μm	Mass Fraction	Avg. Dp _i , μm	Cum. Mass Fraction
25	710	0.056	-	0.944
35	500	0.070	605	0.874
45	355	0.140	428	0.734
60	250	0.074	303	0.660
70	212	0.053	231	0.607
100	150	0.152	181	0.455
120	125	0.013	138	0.441
pan	-	0.441	63	0.000

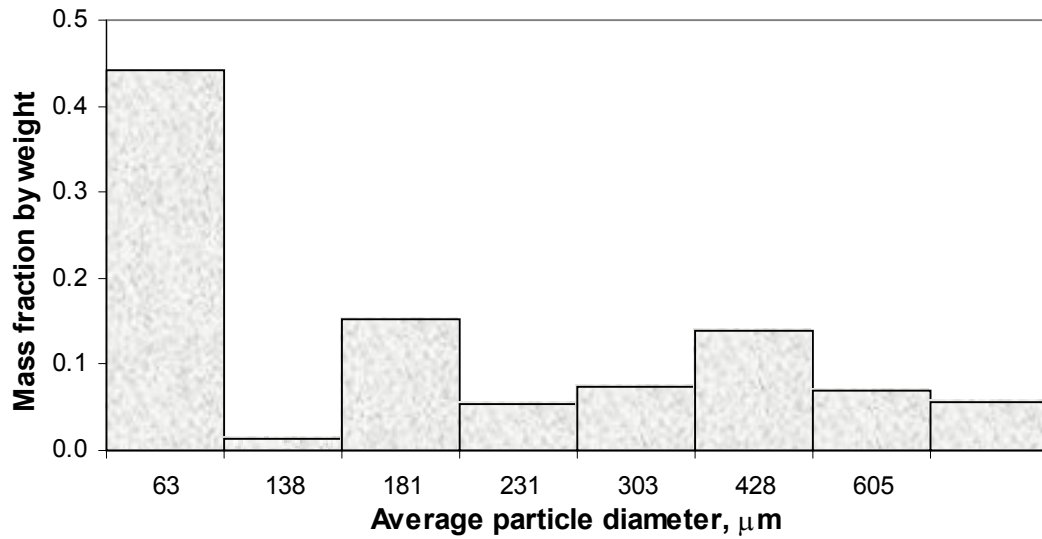


Figure 5.1.1. Particle size distribution curve (differential analysis) for Hisarcık 1 colemanite

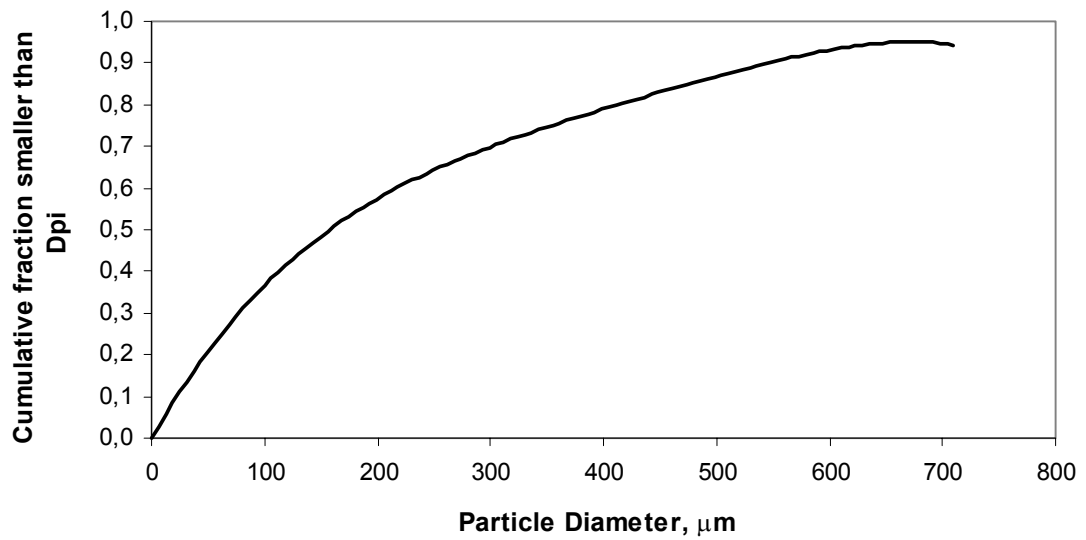


Figure 5.1.2. Particle size distribution curve (cumulative analysis) for Hisarcık 1 colemanite

The colemanite named as Hisarcık 2, arrived under the name of 25-100 mm, which denotes its size. The sieve analysis of it was also performed and given in Table 5.1.2. the differential and cumulative analysis are shown in Figures 5.1.3 and 5.1.4, respectively.

Table 5.1.2. The screen analysis of Hisarcık 2 colemanite

Mesh No	Dpi, μm	Mass Fraction	Avg. Dpi, μm	Cum. Mass Fraction
25	710	0.054	-	0.946
35	500	0.085	605	0.860
45	355	0.087	428	0.773
60	250	0.049	303	0.724
100	150	0.373	200	0.350
140	106	0.170	128	0.180
170	90	0.075	98	0.105
270	53	0.063	45	0.042
pan	-	0.042	27	0.000

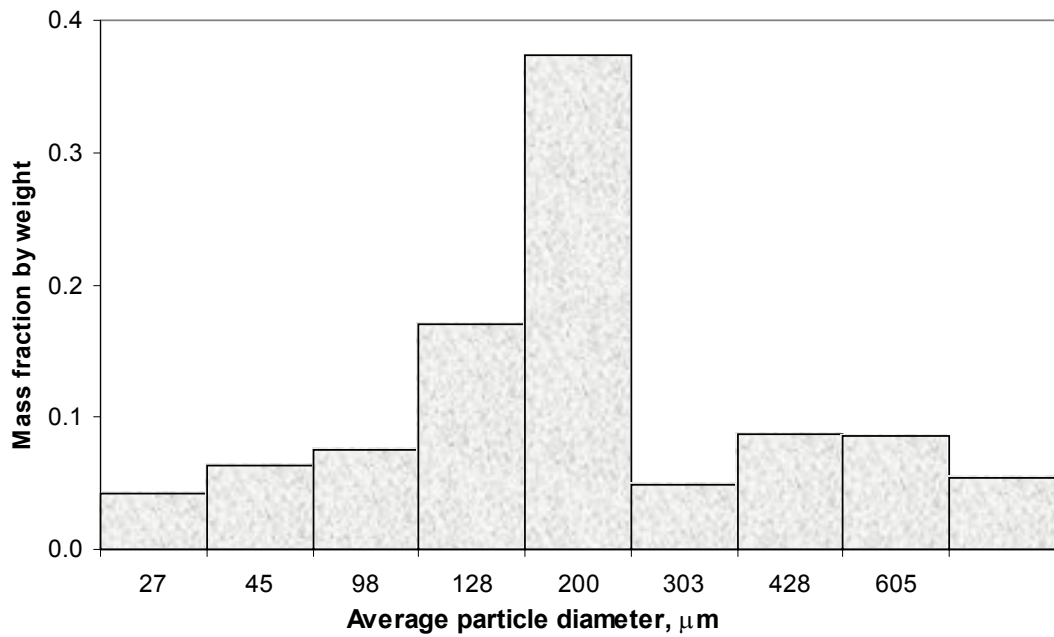


Figure 5.1.3. Particle size distribution curve (differential analysis) for Hisarcık 2 colemanite

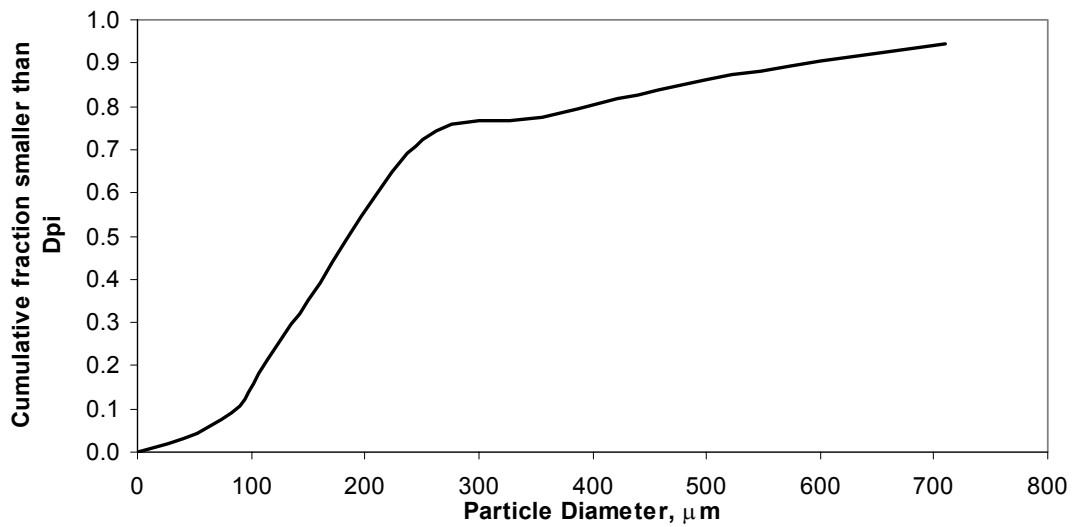


Figure 5.1.4. Particle size distribution curve (cumulative analysis) for Hisarcık 2 colemanite

Hisarcık 3 colemanite was brought from Emet Boric Acid Plant. The maximum diameter of the colemanite minerals was 150 μm . Therefore, no size reduction was necessary. The screen analysis of the Hisarcık 3 colemanite is given in Table 51.3.

Figure 5.1.5 and Figure 5.1.6 present the differential particle size distribution and the cumulative particle size distribution of the Hisarcık 3 colemanite respectively.

Table 5.1.3. The screen analysis of Hisarcık 3 colemanite

Mesh No	Dpi, μm	Mass Fraction	Avg. Dpi, μm	Cum. Mass Fraction
100	150	0.134	-	0.866
140	106	0.243	128	0.623
170	90	0.325	98	0.298
270	53	0.117	72	0.181
pan	-	0.181	26.5	0

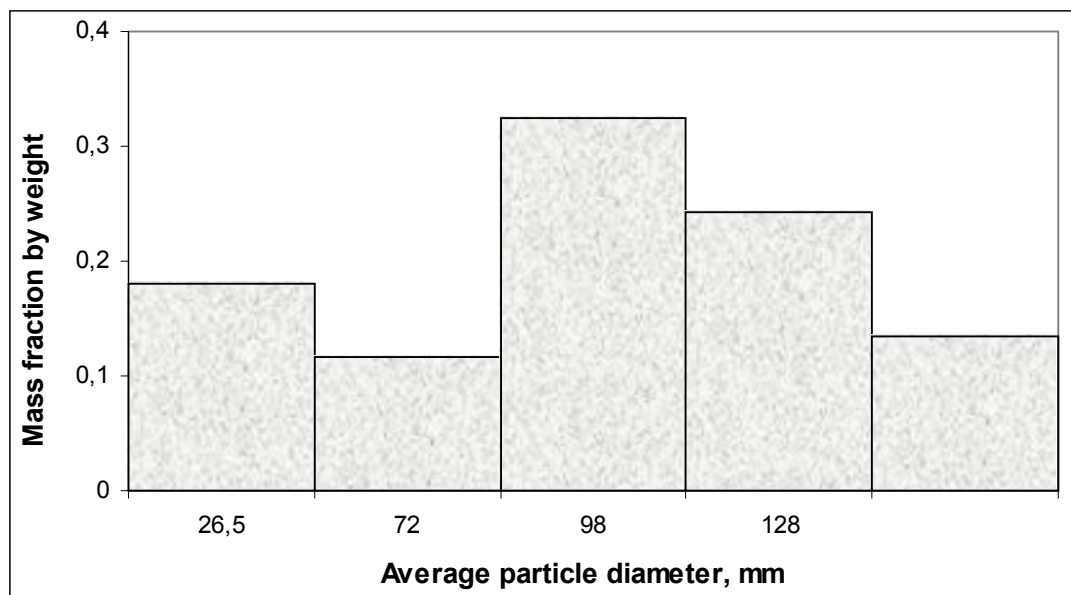


Figure 5.1.5. Particle size distribution curve (differential analysis) for Hisarcık 3 colemanite

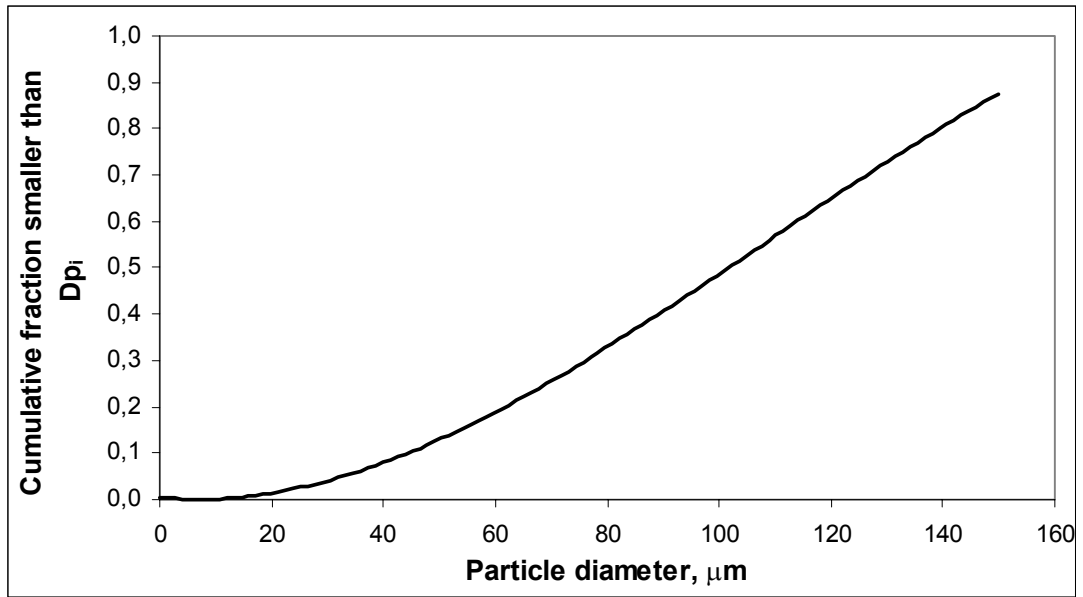


Figure 5.1.6 Particle size distribution curve (cumulative analysis) for Hisarcık 3 colemanite

5.1.2. CHEMICAL ANALYSIS OF COLEMANITE

To see if the size of the colemanite changes the chemical composition, the chemical analysis of Hisarcık 1 colemanite was done on different sizes, 250-1000 μm , 0 -250 μm and 0-1000 μm . The size named as 0-1000 μm is the hammer mill product consisting of 35% colemanite greater than 250 μm . The chemical analysis of the colemanites is given in Appendix A. The chemical composition of Hisarcık 1 colemanite is given in Table 5.1.3.

Table 5.1.4. Chemical analysis of Hisarcık 1 colemanite (dry basis, wt%) (METU, Chemical Eng. Dept.)

Component	250-1000 μm	0 - 250 μm	0-1000 μm
B ₂ O ₃	39.17	37.72	38.53
CaO	23.63	24.23	22.25
Na ₂ O	0.58	0.78	0.17
MgO	1.92	1.93	2.19
Al ₂ O ₃	1.77	1.48	1.69
SiO ₂	18.51	19.71	7.72
Fe ₂ O ₃	1.06	0.84	1.06
As ₂ O ₃	0.59	0.51	0.55
SrO	0.88	1.03	0.94
TiO ₂	0.13	0.11	0.11
K ₂ O	2.27	1.55	1.55
BaO	0.02	0.02	0.02
Others	9.47	10.09	23.22

As seen from this table, the change in the particle size did not change the analysis results significantly, especially the calcium oxide and boron trioxide results did not differ much, which are important values for the experiments. CaO/B₂O₃ ratio is a critical value for the case of the amount of sulfuric acid addition. As sulfuric acid amount changes the calcium ion concentration changes with respect to time (Çetin *et.al.*, 2001).

The chemical analysis of Hisarcık 2 and Hisarcık 3 colemanites were also done. The comparison of different colemanites, together with the published ones by Kalafatoğlu *et.al.*, 2000 and Özkan, 1999, is also given in Table 5.1.4.

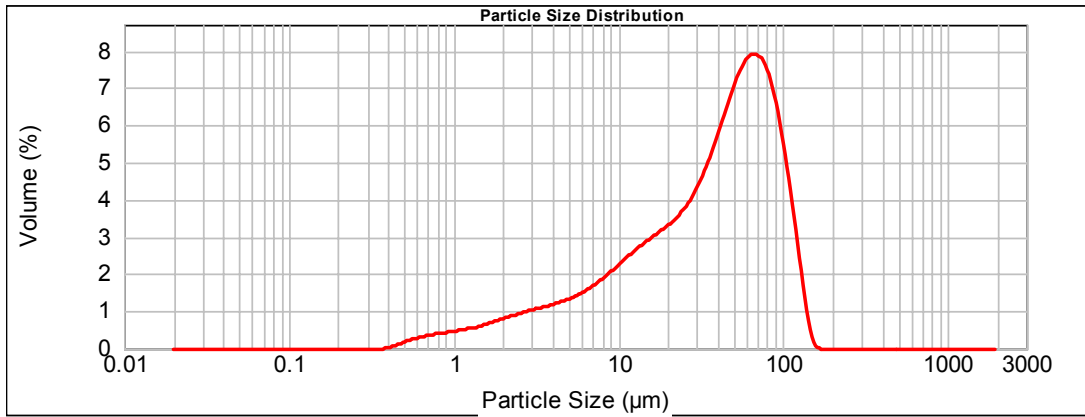
Table 5.1.5. Chemical analysis of Hisarcık colemanites (dry basis, wt%)
(METU, Chemical Eng. Dept.)

Component	Hisarcık 1 Colemanite	Hisarcık 2 Colemanite	Hisarcık 3 Colemanite	Kalafatoğlu et. al., 2000	Özkan, 1999
B ₂ O ₃	38.53	43.57	34.61	43.10	43.69
CaO	22.25	30.90	28.41	25.77	20.50
Na ₂ O	0.17	0.22	1.30	0.17	0.06
MgO	2.19	0.79	2.36	2.09	1.18
Al ₂ O ₃	1.69	0.22	1.49	1.27	0.86
SiO ₂	7.72	0.60	2.23	5.84	3.77
SO ₃		0.14	0.65	1.14	0.21
Fe ₂ O ₃	1.06	0.17	0.61	0.59	0.31
As ₂ O ₃	0.55	0.00	0.42	0.25	2.00
SrO	0.94	0.56	0.88	1.17	1.55
TiO ₂	0.11	0.20	0.14	0.02	
K ₂ O	1.55	0.08	0.74	0.42	0.19
BaO	0.02	0.005	0.017	0.01	
Li	0.028	0.045			
Others	23.22	22.50	26.13	18.16	25.68

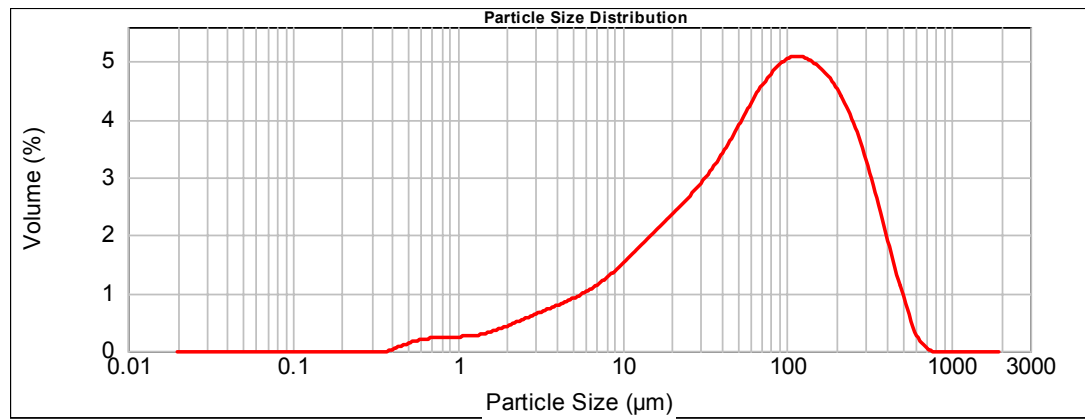
As seen from Table 5.1.4, Hisarcık 2 colemanite is the most valuable one among the three colemanites used in the study due to its boron trioxide content. The boron trioxide content of Hisarcık 3 colemanite, on the other hand, was the lowest among all other colemanites.

5.1.3. PARTICLE SIZE DISTRIBUTION OF COLEMANITE

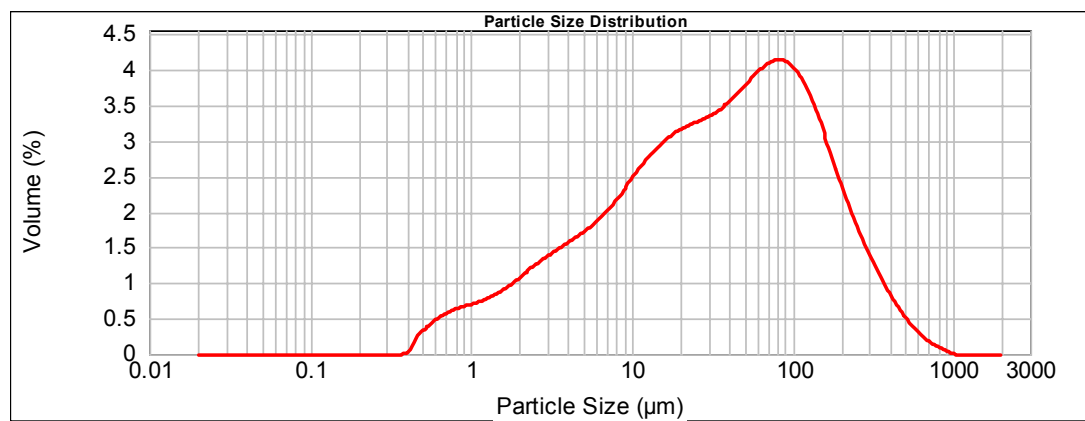
The particle size distribution of the colemanite was also examined with the laser diffraction particle size analyzer. The particle size distribution of the colemanites used in the study are given in the Figures 5.1.5 - 5.1.7 for Hisarcık 1, Hisarcık 2 and Hisarcık 3 colemanites, having particle sizes determined from the screen analysis as 0-250 µm, 0-250 µm and 0-150 µm, respectively.



Figures 5.1.7. Particle size distribution of Hisarcık 1 colemanite



Figures 5.1.8. Particle size distribution of Hisarcık 2 colemanite



Figures 5.1.9. Particle size distribution of Hisarcık 3 colemanite

The particle size distribution of the colemanites, Figures 5.1.5-5.1.7, did not give particle sizes similar to that of the screen analysis. In laser diffraction particle size analyzer, the shapes of the particles are taken as a sphere, and the volumes are calculated accordingly. The volume weighted mean diameter, also called as the De Broucker mean, was generated by the laser diffraction instrument, which was the arithmetic average of the diameters of the colemanites. The volume weighted mean diameters obtained from the software of the particle size analyzer are given in Table 5.1.5.

Table 5.1.6. Volume weighted mean diameters of the colemanites

Colemanite	Particle Size Obtained From Sieve Analysis	Mean Diameter Of Colemanite Obtained From Particle Size Analyzer
Hisarcık 1	0-250 μm	44.53 μm
Hisarcık 2	0-250 μm	113.13 μm
Hisarcık 3	0-150 μm	73.56 μm

Hisarcık 1 colemanite was used for the dynamic behavior experiments, Hisarcık 2 and Hisarcık 3 were used for the boric acid production in batch and continuous reactor experiments. The second column in Table 5.1.5 is the size obtained from the sieve analysis, and gives the diameter range of the colemanite particles. The last column is the volume weighted mean diameter of the colemanite particles. As seen, the mean diameters found from the analyzer are in the range of the diameters obtained from the sieve analysis.

5.2. DYNAMIC BEHAVIOR EXPERIMENTS ON CONTINUOUS FLOW STIRRED SLURRY REACTORS

There are two ideal patterns, plug flow and mixed flow. These can give very different behavior like the size of the reactor and distribution of the products. These two patterns are simple to treat and one or the other is often optimum no matter what we are designing for. But real equipment always deviates from these ideals. Deviation from these ideal patterns can be caused by channeling of fluid, by

recycling of fluid, or by creation of stagnant regions in the vessel. These behaviors can be found by performing residence time distribution, RTD, experiments. These non-idealities should be avoided since it always lowers the performance of the reactors. In order to check the performance of the slurry reactors residence time distribution experiments were performed in either a liquid or a solid-liquid system. During the RTD experiments a non reactive tracer was chosen and it is given as a pulse or a step input. After giving a tracer to the system, concentration of the tracer at the effluent stream was recorded with respect to time, and $C(t)$ curves were analyzed to detect the nonidealities in the reactor.

5.2.1. LIQUID RESIDENCE TIME EXPERIMENTS

Dynamic behavior studies were performed by using only one continuously stirred baffled tank reactor having a volume of 1840 ml. Various parameters were selected and applied to the experiments to see their effects on the residence time distribution.

5.2.1.1. EFFECT OF STIRRING RATE ON LIQUID RESIDENCE TIME

The tank reactor was stirred by means of a mechanical stirrer. The peristaltic pump was connected to the inlet fluid stream to have a constant liquid feed rate of 42.5 ml/min. For the fluid stream distilled water was used throughout the residence time experiments.

In the first experiment, nickel, 1000 ppm, was injected to the inlet stream, as an inert tracer with a volume of 10 ml. Two different stirring rates were applied to the system to see the effect of stirring rate on the residence time distribution. In both experiments the data was taken by mixing cup readings. The data is given in Appendix B, Table B.1. The results of the two experiments are given in Figure 5.2.1 for comparison. The plot was also named as C_{pulse} curve.

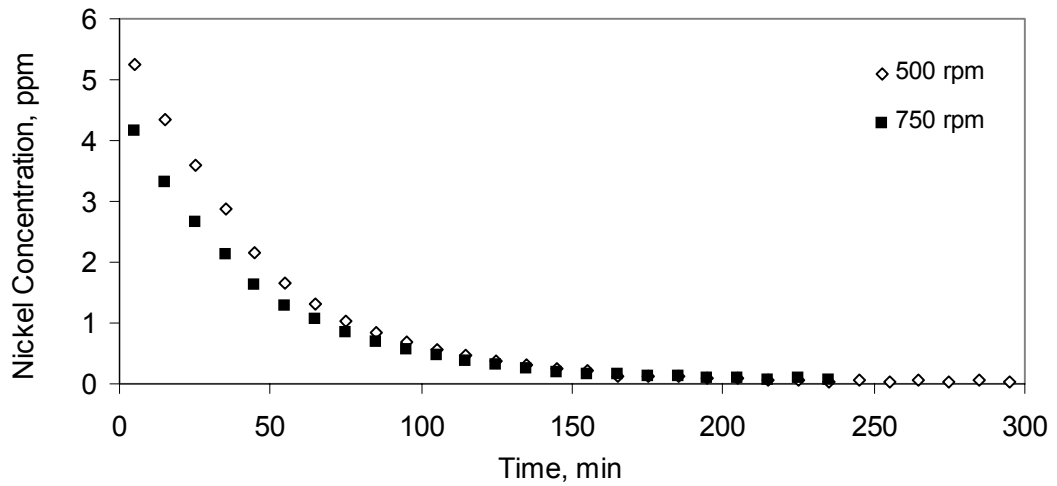


Figure 5.2.1. Variation in nickel concentration depending on the stirring rate during the liquid residence time experiments (Volumetric flow rate = 42.5 ml/min)

The area under the C_{pulse} curve is calculated as follows:

$$A = \int_0^{\infty} C \, dt \cong \sum_i C_i \Delta t_i = \frac{M}{\nu} \quad (5.2.1)$$

where A is the area under the C_{pulse} curve, M is the amount of tracer in kg and ν : volumetric flow rate of liquid in m^3/s . To find the residence time distribution, $E(t)$ from the C_{pulse} curve, the concentration scale was simply changed such that the area under the curve is unity.

$$E(t) = \frac{C_{\text{pulse}}}{M/\nu} \quad (5.2.2)$$

The normalization of the experimental data was done by the use of equations 5.2.1 and 5.2.2.

The $E(t)$ curves at two stirring rates, 500 rpm and 750 rpm are given in Figure 5.2.2. By using the $E(t)$ values, $F(t)$ values were also calculated from Equation 5.2.3.

$$F(t) = \int_0^t E(t) \, dt \quad (5.2.3)$$

The $F(t)$ curves are given in Figure 5.2.3. The $E(t)$ and $F(t)$ values for the experiments are given in Table B.2.

To see if the reactor approaches an ideal one or not, the E(t) and F(t) curves for an ideal CSTR reactor was drawn and compared with the experimentally found ones. During the calculation of E(t) and F(t) values for an ideal reactor, the equations used were

$$E(t) = \frac{e^{-t/\tau_i}}{\tau_i} \quad (5.2.4)$$

F(t) equation was found by using Equations 5.2.3, i.e., taking the integral of the E(t) equation, which is:

$$F(t) = 1 - e^{-t/\tau_i} \quad (5.2.5)$$

The ideal reactor's E(t) and F(t) curves are also drawn in Figure 5.2.2-5.2.3, respectively. The values for E(t) and F(t) are given in Table B.2.

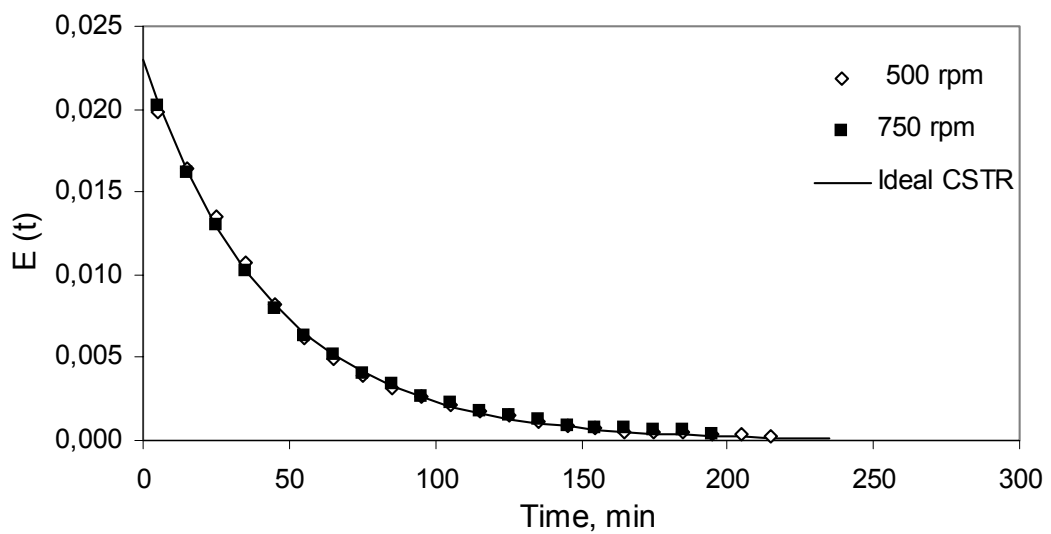


Figure 5.2.2. Comparison of the E(t) curves for two different stirring rates and the ideal reactor

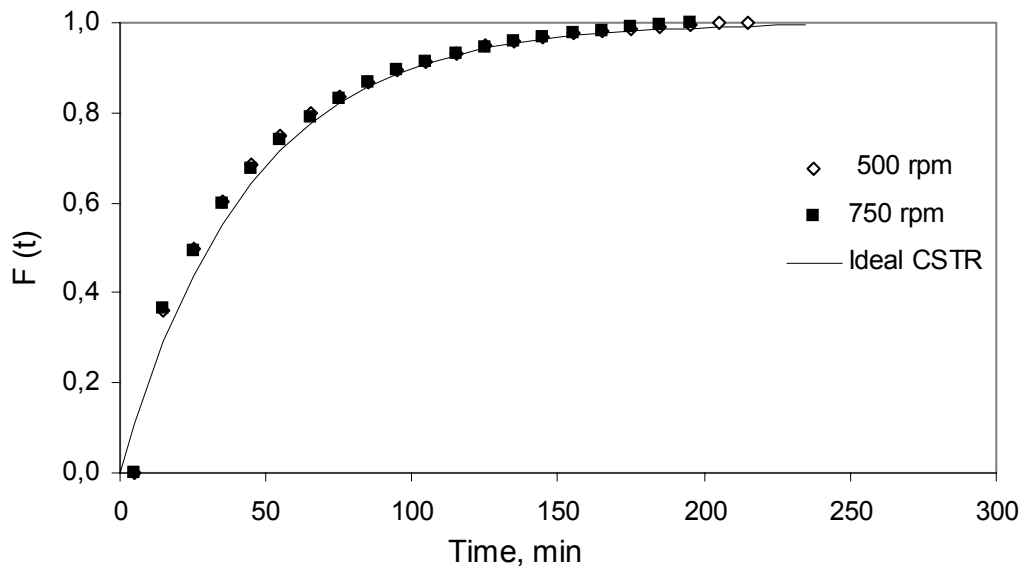


Figure 5.2.3. Comparison of the $F(t)$ curves for two different stirring rates and the ideal reactor

It can be seen from Figure 5.2.2 and 5.2.3 that the reactor used in the experiments was an ideal reactor and stirring rate studied had no effect on the liquid residence time.

The residence time, τ , was calculated by Equation 5.2.6 as $\tau = V/v$. The mean of the C_{pulse} curve was also calculated by Equation 5.2.6, but this time the experimental data was used. The two values should be equal to each other.

$$\bar{t} = \frac{\int_0^{\infty} t C dt}{\int_0^{\infty} C dt} \cong \frac{\sum_i t_i C_i \Delta t_i}{\sum_i C_i \Delta t_i} = \frac{V}{v} \quad (5.2.6)$$

The values calculated without the experimental data were called theoretical values. Variance, which shows the spread of the curves, was also calculated from Equation 5.2.7.

$$\sigma^2 = \frac{\int_0^{\infty} t^2 C dt}{\int_0^{\infty} C dt} - \bar{t}^2 \cong \frac{\sum_i t_i^2 C_i \Delta t_i}{\sum_i C_i \Delta t_i} - (\bar{t})^2 \quad (5.2.7)$$

The mean of the curve, area under the curve and the variance per square of the mean of the curves are compared in Table 5.2.1.

Table 5.2.1. Comparison of the two experimental values with the theoretical ones (volumetric flow rate = 42.5 ml/min, tracer= nickel)

	Experimental		Theoretical
	500 rpm	750 rpm	
A, g.min /l	0.265	0.205	0.235
\bar{t} , min	43.5	43.7	43.3
σ^2 / \bar{t}^2	0.91	0.88	

The data for the mean residence time for all the cases seemed to be close to each other. It can be stated that the experimentally evaluated data parallels with the theoretical ones.

5.2.1.2. CHECK OF DIFFERENT TRACERS ON LIQUID RESIDENCE TIME

In liquid residence time experiments where colemanite was used as a solid, lithium was used as an inert tracer. For this reason, the liquid residence time experiment was repeated by using lithium and the usage of different tracers were checked. Liquid residence time experiment HC1.1, stirring rate of 500 rpm, was repeated with the same amount of lithium instead of nickel to see the difference, if any, between the results. The concentration values of the tracers are compared in Figure 5.2.4, and the data is given in Table B.3.

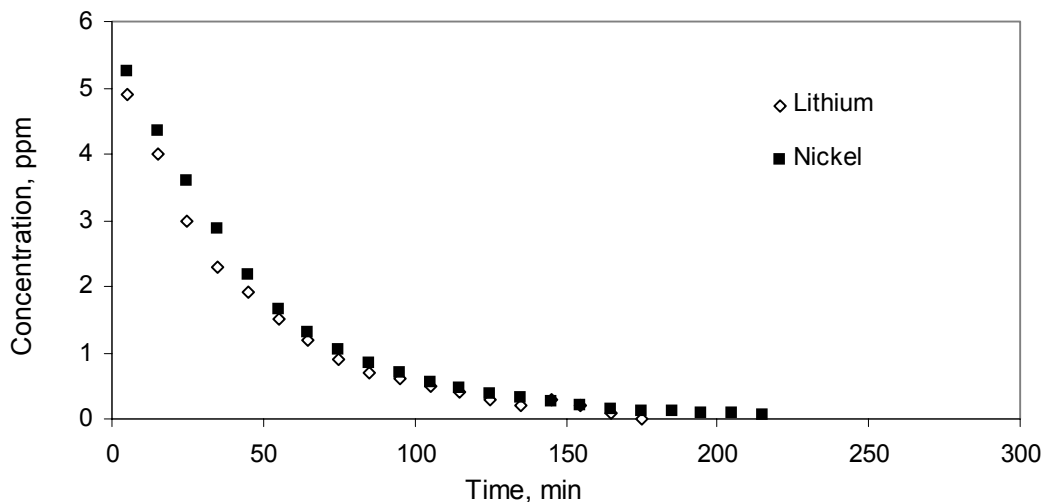


Figure 5.2.4. Comparison of concentrations of different tracers

To normalize the concentration values, $E(t)$ and $F(t)$ curves are drawn and compared with the ideal CSTR in Figures 5.2.5-5.2.6, respectively. $E(t)$ and $F(t)$ values are tabulated in Table B.4.

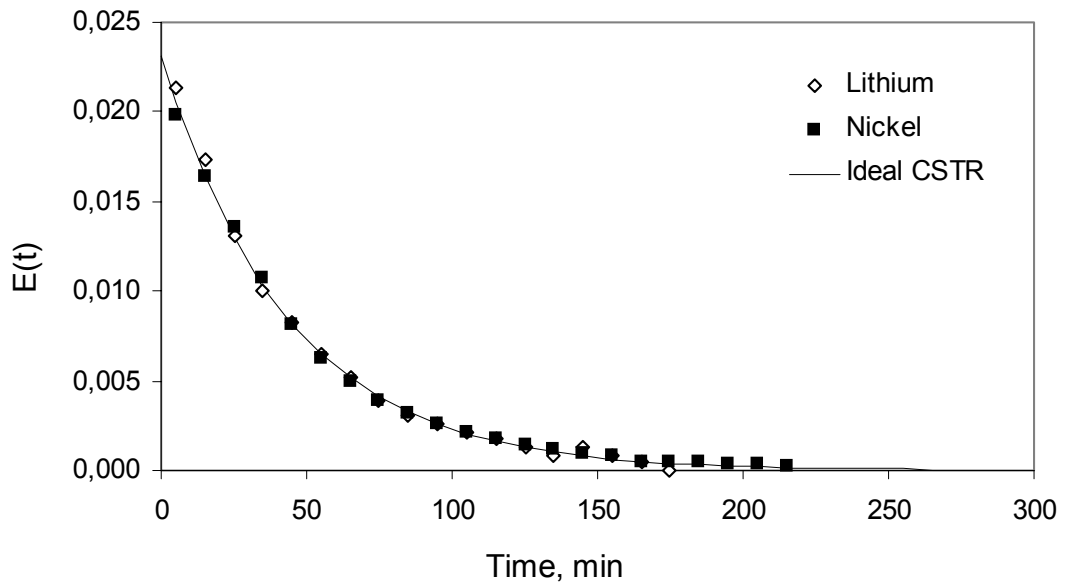


Figure 5.2.5. Comparison of the $E(t)$ curves for different tracers and the ideal reactor

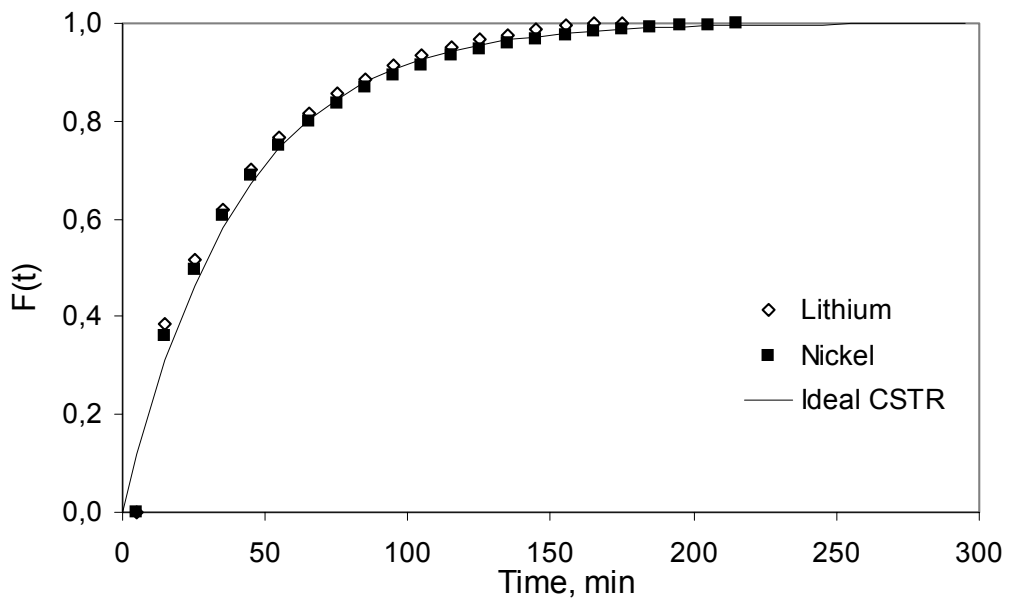


Figure 5.2.6. Comparison of the $F(t)$ curves for different tracers and the ideal reactor

As it can be seen from Figure 5.2.5-5.2.6, the change in the inert tracer gave the same results, and the reactor approached to the ideal one. This result, in a way, shows the reproducibility of the liquid residence time experiments. The mean of the curve, area under the curve and the variance per square of mean of the curves are compared in Table 5.2.2.

Table 5.2.2. Comparison of different tracers with the theoretical ones (Volumetric Flow rate = 42.5 ml/min, Stirring rate = 500 rpm)

	Experimental		Theoretical
Tracer	Nickel	Lithium	
A, g.min / l	0.265	0.230	0.235
\bar{t} , min	43.5	40.2	43.3
σ^2 / \bar{t}^2	0.91	0.82	

The data for the mean residence time seemed to be close to each other. It can be stated that the experimentally evaluated data was comparable with the theoretical ones.

5.2.2. SOLID RESIDENCE TIME EXPERIMENTS

The solid residence time experiments were performed to get familiar with the slurry reactors and to get prepared for the start-up of the boric acid production experiments in continuous flow stirred slurry reactors.

In all the dynamic behavior experiments where colemanite was used, Hisarcık 1 colemanite was used, the chemical analysis of which is given in Section 5.1.2. For the solid residence time study, the behavior of a single CSTR to the step tracer of colemanite, either negative or positive step input, was studied by giving 4.3 g/min colemanite to the reactor, when the system was at steady state, and taking mixing cup readings, that is, the effluent of the reactor was filtered for 5 min intervals and

dried to see the amount of colemanite collected. The stirring rate during the experiments was 500 rpm.

The data for two experiments are given in Appendix B, Table B.5. The comparison of negative and positive step inputs to the same system are given in Figure 5.2.7.

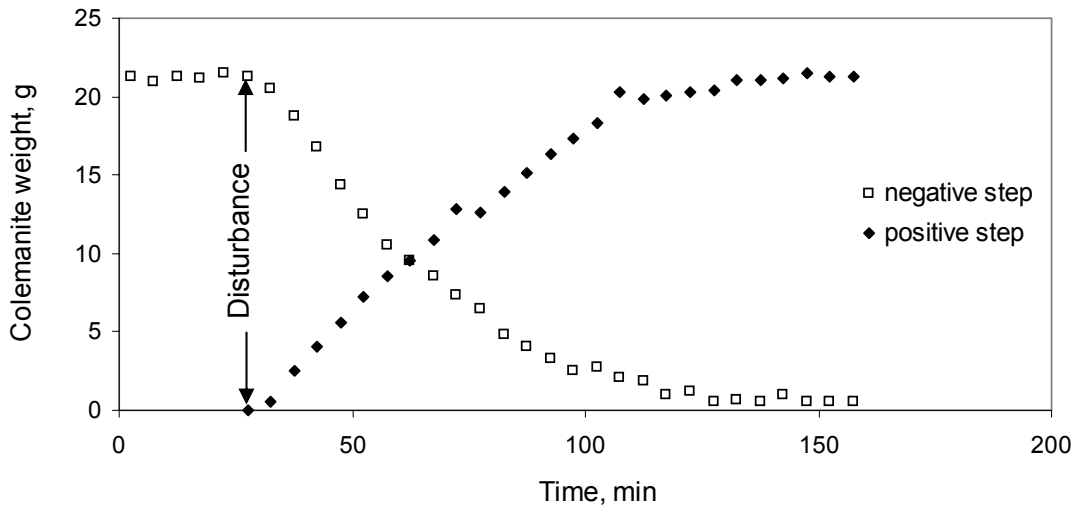


Figure 5.2.7. Responses to a negative and a positive step input given to the feed rate of colemanite

As seen from Figure 5.2.7, the data for negative and positive step input experiments resembled each other. The residence time, and the variance was calculated by using the equations 5.2.8-5.2.9, respectively.

$$\bar{t} = \frac{\int_0^{\infty} (C_{\max} - C) dt}{\Delta C_{\max}} = \frac{\sum_{i=1} (C_{\max} - C_i) \Delta t_i}{\Delta C_{\max}} \quad (5.2.8)$$

$$\sigma^2 = \frac{2 \cdot \int_0^{\infty} t(C_{\max} - C) dt}{\Delta C_{\max}} - \bar{t}^2 = \frac{\int_0^{C_{\max}} t^2 dC}{\Delta C_{\max}} - \bar{t}^2 \quad (5.2.9)$$

In equations 5.2.8-5.2.9, C_{\max} values for negative and positive step tracers were 21.3 g for each of the experiments, which was equal to the amount of colemanite

collected in five minutes. The theoretical calculation of C_{\max} and mean residence time is given in Equations 5.2.10 and 5.2.11, respectively.

$$C_{\max} = \frac{m}{v} \quad (5.2.10)$$

$$\text{Area} = C_{\max} \bar{t} = \frac{mV}{v^2} \quad (5.2.11)$$

The mean residence time was calculated from equations 5.2.10 and 5.2.11 as 43.8 min. The comparisons of the experimental and theoretical values are given in Table 5.2.3.

Table 5.2.3. Comparison of the residence time and the variance per square of residence time for step input experiments

	Experimental		Theoretical
Step Input	Negative	Positive	
\bar{t} , min	96.3	46.2	43.8
σ^2 / \bar{t}^2	0.12	0.12	

The mean residence times evaluated from the negative and positive step response experiments should give similar values but they were found different as seen from Table 5.2.3. The reason for this difference was that for the negative step experiment, as the amount of solid decreased in the reactor, the readings were still taken. During the calculations, the area was found greater than that of the positive step experiments, which makes the mean residence time higher. The mean residence time found for the positive step input experiment was close to the theoretical calculation. So, while studying solid residence time experimentally, giving a positive step input is recommended.

5.2.3. LIQUID RESIDENCE TIME EXPERIMENTS IN A SOLID/LIQUID SYSTEM

When distilled water was fed together with colemanite, a pulse tracer of nickel, 1000 ppm, was injected to the liquid stream. The atomic absorption spectrophotometer results of nickel analysis showed that, nickel was adsorbed on the colemanite. And all the nickel in the solution was completely adsorbed within 20 minutes. So, different tracers were searched for this type of an experiment. The tested tracers were cobalt, cadmium, copper, calcium, sodium, lithium and potassium. First, the amounts of tracers on the liquid-colemanite solution were observed. It was seen that colemanite delivered calcium, sodium and potassium to the solution. The tracer test results showed that colemanite adsorbed cobalt, cadmium, copper, whereas the concentrations of calcium, sodium and potassium increased as time passed in the solution. Lithium gave the best result, as the concentration of it did not change for the rest of the experiment. So, lithium was chosen as an inert tracer for the rest of the experiments.

5.2.3.1. EFFECT OF STIRRING RATE ON LIQUID RESIDENCE TIME

Distilled water and colemanite are fed to the reactor by means of a peristaltic pump and a solid feeder with flow rates of 42.5 ml/min and 7.2 g/min, respectively. Lithium, 1000 ppm, was injected as a pulse tracer to the inlet water stream with a volume of 10 ml. Mixing cup readings were taken, i.e., the effluent of the reactor was collected in flasks for 10 min intervals and waited for the colemanite to precipitate. Then samples were taken from the liquid part of the flasks and their lithium concentration was analyzed with Flame Spectrophotometer. The lithium concentrations at two different stirring rates are given in Table B.6. The graph of it is given in Figure 5.2.8.

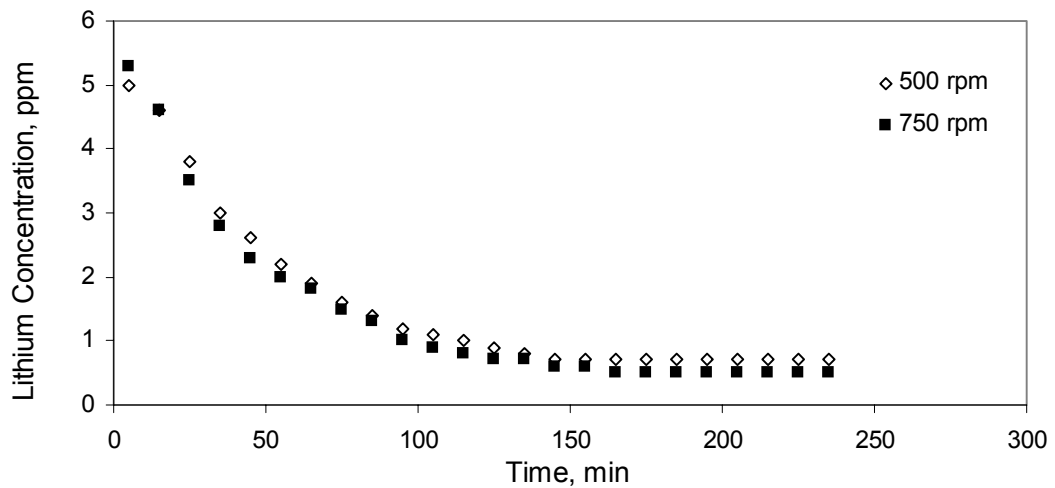


Figure 5.2.8. Variation in lithium concentration depending on the stirring rate during the liquid residence time experiments (Liquid feed rate = 42.5 ml/min, colemanite feed rate=7.2 g/min)

A similar calculation for a stirring rate of 750 rpm was also done, as the residence time of solid at this stirring rate was not known. The residence time and variance of the curves evaluated from the experimental data for different stirring rates are listed in Table 5.2.4.

Table 5.2.4. Comparison of the residence time of liquid and solid and the variance per square of liquid residence time for different stirring rates

Stirring Rate	500 rpm	750 rpm
\bar{t}_L , min	39.6	40.1
\bar{t}_S , min	52.3	45.2
σ^2 / \bar{t}_L^2	0.56	0.62

The residence time of liquid, which was calculated theoretically was 43.3 min. the ones found in a solid/liquid system was lower, which was considerable. From the residence time of the liquid, the residence time of solid was determined. The residence time of the liquid, \bar{t}_L and solid, \bar{t}_S was calculated from

$$\bar{t}_L = \frac{V_L}{v_L} = \tau_L \quad (5.2.12)$$

$$\bar{t}_S = \frac{V_S \cdot \rho_S}{v_S \cdot \rho_S} = \frac{V_S \cdot \rho_S}{\dot{m}_S} \quad (5.2.13)$$

The residence time of liquid at 500 rpm was determined by a pulse tracer of lithium. The residence time liquid found was given in Table 5.2.4 as 39.6 min. So the volume occupied by the liquid could be found from Equation 5.2.12 as 1683 ml. As the total volume of the reactor was 1840 ml, the volume occupied by the solid was found by subtracting the liquid volume from the total volume. The volume occupied by solid was calculated to be 157 ml. From Equation 5.2.13, the residence time of solid was calculated as the mass flow rate and the density of the colemanite were 7.2 g/min and 2.4 g/ml, respectively. The residence time of solids was found to be 52.3 min. The residence time of solid at 750 rpm was found in the same way as 45.2 min. The residence time of solids is also given in Table 5.2.4.

The ratio of solid volume to total volume should be equal to the solid flow rate to the total flow rate.

$$\frac{V_S}{V_L + V_S} = 0.085 \text{ for 500 rpm and } 0.074 \text{ for 750 rpm, where else,}$$

$$\frac{v_S}{v_L + v_S} = \frac{7.2 \text{ g/min} \div 2.4 \text{ g/ml}}{42.5 \text{ ml/min} + (7.2 \text{ g/min} \div 2.4 \text{ g/ml})} = 0.066$$

The solid and liquid hold-ups were calculated by dividing the solid and liquid volumes to the total volume. The liquid and solid hold-ups were found as 0.915 and 0.085 for 500 rpm, and 0.926 and 0.074 for 750 rpm, respectively.

5.2.3.2. EFFECT OF SOLID TO LIQUID RATIO ON LIQUID RESIDENCE TIME

The effects of different solid to liquid ratios on the residence time of liquid were examined by applying the same procedure explained above. The stirring rate was kept constant at 500 rpm. The flow rate of colemanite was kept at 7.2 g/min, but the flow rate of liquid was changed. The studied S/L ratios, expressed as mass flow rate of solid to the volumetric flow rate of liquid, were 0.085, 0.17, and 0.34. The lithium concentrations found in solution are tabulated in Table B.7. The effect of different S/L ratios on the residence time was given in Figure 5.2.9.

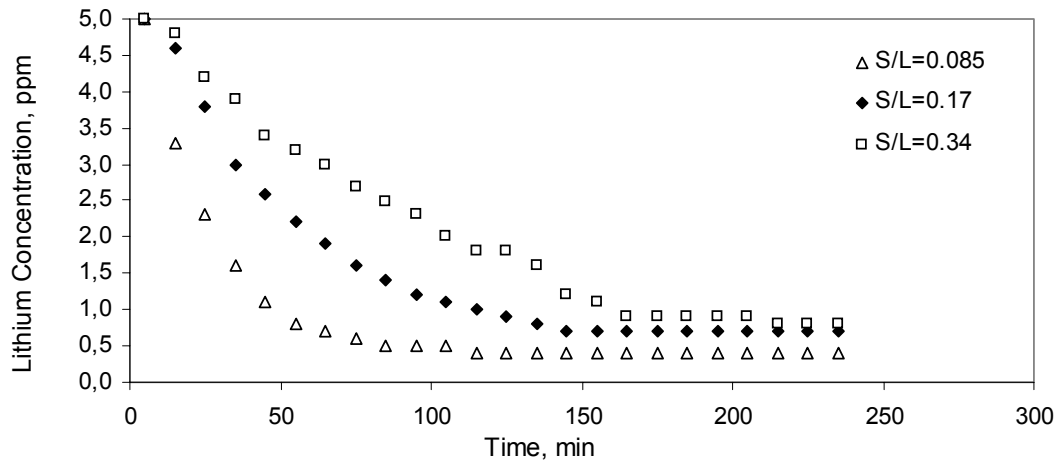


Figure 5.2.9 Variation in lithium concentration depending on the solid to liquid ratio (g solid/ml liquid) during the liquid/solid residence time experiments (Colemanite feed rate = 7.2 g/min)

The residence time and variance per square of the liquid residence time was evaluated from the experimental data by using Equations 5.2.6 and 5.2.7, respectively. These values for different solid to liquid ratios are given in Table 5.2.5.

Table 5.2.5. Comparison of the residence time of liquid and the variance per square of residence time for different solid to liquid ratios (g solid/ml liquid)

S/L ratio (g solid/ml liquid)	0.085	0.17	0.34
h_s (volume of solid / total volume)	0.034	0.066	0.124
\bar{t}_L , min	26.1	39.6	60.6
σ^2 / \bar{t}_L^2	0.74	0.56	0.51

To normalize the curves, first the design equation of a single CSTR was written. The material balance on a pulse tracer was given as

$$\frac{v_L C_1}{V_L} = -\frac{dC_1}{dt} \quad (5.2.14)$$

$$\int_{C_0}^C \frac{dC_1}{C_1} = -\frac{1}{\tau_L} \int_0^t dt \quad (5.2.15)$$

$$\frac{C}{C_0} = e^{-t/\tau_L} \quad \text{or} \quad -\ln\left(\frac{C}{C_0}\right) = \frac{1}{\tau_L} t \quad (5.2.16)$$

Residence time of liquid, τ_L , can be found from the following equation:

$$\tau_L = \frac{V_L}{v_L} = \left(\frac{V_L}{v_L}\right) \cdot \left(\frac{V_R}{V_L}\right) \cdot \left(\frac{V_L}{V_R}\right) = \frac{V_R}{v_L} \cdot h_L \quad (5.2.17)$$

$$h_L = 1 - h_S \quad (5.2.18)$$

where V_R is the reactor volume, v_L is the volumetric flow rate of liquid and h_L and h_S are the liquid and solid hold-ups, respectively.

C_0 , the pulse input given was 5 ppm. First the normalized tracer concentrations with respect to the initial concentration versus time was drawn, Figure 5.2.10. Then $-\ln(C/C_0)$ vs t graphs are drawn in Figure 5.2.11. As seen from Equation 5.2.16, $-\ln(C/C_0)$ vs t graphs should be linear, having a slope of $1/\tau_L$. The $-\ln(C/C_0)$ vs t values for different S/L ratios are given in Table B.8.

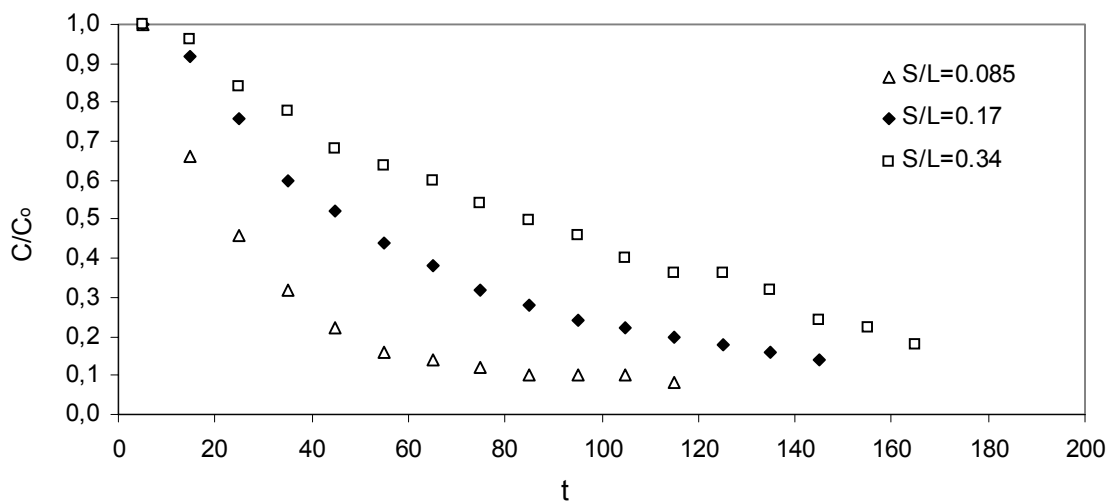


Figure 5.2.10. Normalized lithium concentrations with respect to the initial tracer concentration as a function of time depending on the solid to liquid ratio (g solid/ml liquid) (Colemanite feed rate = 7.2 g/min)

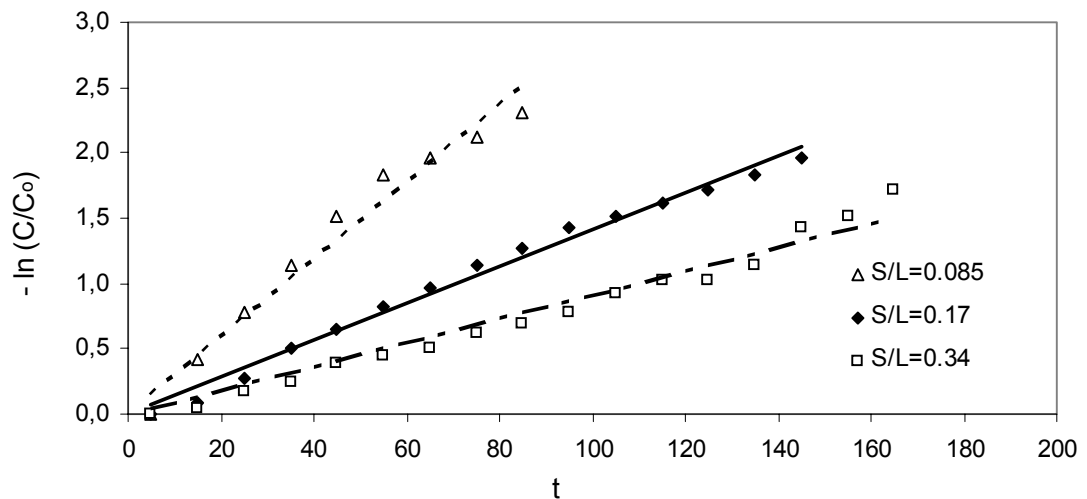


Figure 5.2.11. Normalized lithium concentrations with respect to the initial tracer concentration, as given in Equation 5.2.14, as a function of time depending on the solid to liquid ratio (g solid/ml liquid) (Colemanite feed rate = 7.2 g/min)

The $-\ln(C/C_0)$ vs t plot gave linear lines for different S/L ratios and the slopes of the lines were 0.0296 ($R^2 = 0.97$), 0.0141 ($R^2 = 0.99$) and 0.0091 ($R^2 = 0.97$) for the ratios of 0.085, 0.17 and 0.34, respectively. The slopes of the lines gave the $1/\tau_L$ values and from the τ_L values the liquid and solid hold-ups can be estimated from Equation 5.2.17, and 5.2.18, respectively. The liquid residence times estimated by this method are tabulated in Table 5.2.6.

Table 5.2.6. The residence time of liquid evaluated from Figure 5.2.11 and Equation 5.2.17 at different solid to liquid ratios (g solid/ml liquid)

S/L ratio (g solid/ml liquid)	0.085	0.17	0.34
Figure 5.2.11			
Slope of Figure 5.2.11, min^{-1}	0.0296	0.0141	0.0091
τ_L , min	33.8	70.9	109.9
Equation 5.2.17			
h_s (volume of solid / total volume)	0.034	0.066	0.124
v_L , ml/min	84.7	42.5	21.2
τ_L , min	21.0	40.4	76.0

The liquid residence time was found theoretically by using the solid hold-up values and equation 5.2.17. In this equation the volume of the reactor V_R was taken as 1840 ml. As seen from Table 5.2.6, the residence times evaluated by using the slopes of $-\ln(C/C_0)$ vs t plot, Figure 5.2.11, gave higher liquid residence times than the ones evaluated by using Equation 5.2.17. The residence times found by using area under the curve method, Table 5.2.5, gave closer values to the theoretical one, Equation 5.2.17. So, to find the mean residence time by using the area under the curve method was more consistent.

To conclude the dynamic behavior study performed in the boric acid slurry reactors, the inert tracer that should be selected was lithium. The area under the curve method was suitable to find the mean residence time of the liquid and solid components. Giving a positive step input to the system for finding the solid residence time gave accurate results. The reactor to be used for the continuous boric acid production experiments approached an ideal one under the conditions studied. The dynamic behavior study should be performed before going into the pilot or industrial scale. By this way beneficial information on the system was attained, problems, if any, would be solved which increased the performance of the reactors.

5.3. BATCH REACTOR EXPERIMENTS

During the dissolution of colemanite in aqueous sulfuric acid, boric acid is produced (in solution) and the calcium sulfate dihydrate (gypsum) is crystallized. By monitoring the calcium ion concentration in solution the supersaturation level of the calcium ion concentration can be figured out.

The first set of the experiments was performed with Hisarcık 2 colemanite. The particle size of the colemanite used was 0-250 μm and 250-1000 μm . The $\text{CaO}/\text{SO}_4^{2-}$ molar ratio was 0.95. The initial concentration of SO_4^{2-} was 0.623 mol/l. The temperature of the reaction system was kept constant at 80°C and the stirring rate was 500 rpm. During the experiments boric acid and calcium ion concentrations in solution were determined. The raw data of the batch reactor experiments are given in Appendix C.

The dissolution of colemanite mineral was observed from the variation of boric acid concentration with respect to time. Figure 5.3.1 gives the variation of boric acid concentration with respect to time for two different colemanite particle sizes.

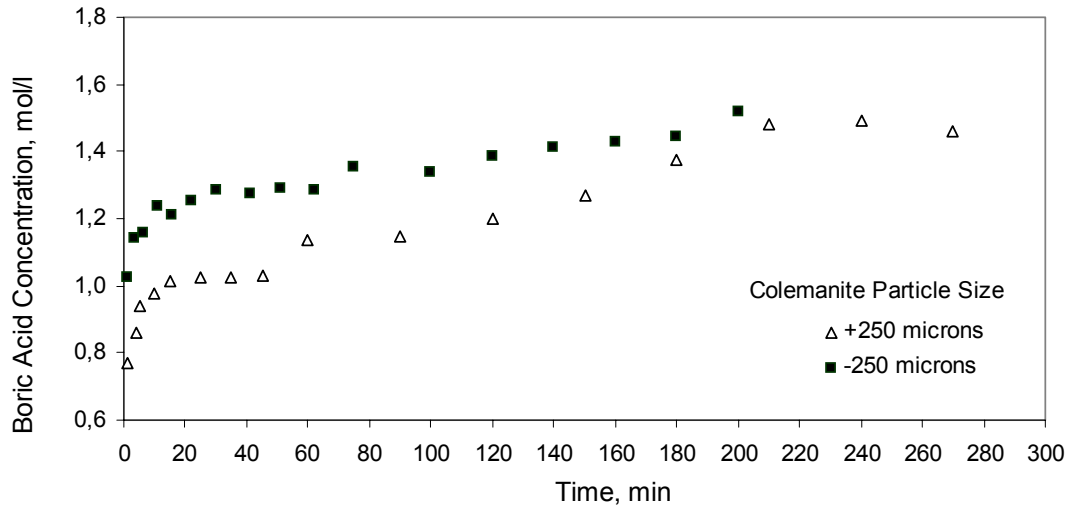


Figure 5.3.1. Variations in the boric acid concentration depending on the colemanite particle size during the dissolution of Hisarcık 2 colemanite in aqueous sulfuric acid at 80°C and a stirring rate of 500 rpm. The initial $\text{CaO}/\text{SO}_4^{2-}$ molar ratio is 0.95

As seen from Figure 5.3.1, dissolution rate of colemanite showed the same trend for two different colemanite particle sizes, but small particles dissolved faster than the others. A fast dissolution period was observed until 15 min, which was then followed by a plateau. The plateau formation can be explained by the coating of colemanite particles with gypsum (Imamutdinova et.al, 1978; Bilal et.al, 2003). After 45 min, the film of gypsum crystals dissolved and the thickness of the film decreases, some of the colemanite particles then were free to dissolve and produce boric acid. After this period, colemanite particles had a slower rate of dissolution. The dissolution of the colemanite particles finished at 210 min.

The second step was the crystallization reaction, which involves the nucleation and growth of calcium sulfate dihydrate crystals. This reaction might require longer time than that needed for the formation of boric acid. The crystallization of gypsum from the solution was followed by monitoring the calcium ion concentration, C , in the solution with respect to time as it is decreased by the formation of gypsum crystals.

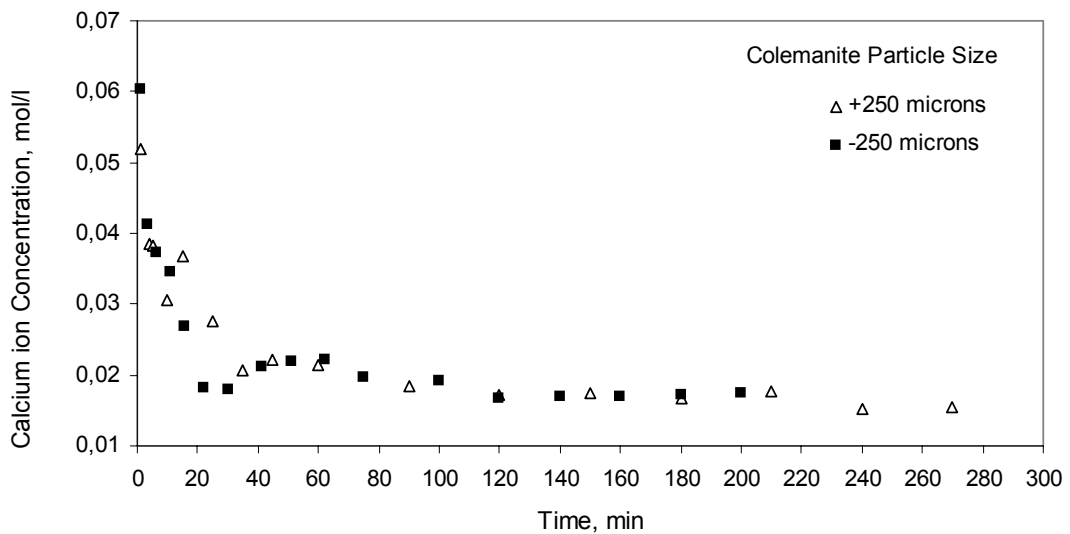


Figure 5.3.2. Variations in the calcium ion concentration depending on the colemanite particle size during the dissolution of Hisarcık 2 colemanite in aqueous sulfuric acid at 80°C and a stirring rate of 500 rpm. The initial $\text{CaO}/\text{SO}_4^{2-}$ molar ratio is 0.95.

As it is illustrated in Figure 5.3.2, the calcium ion concentration in the liquid phase showed a rapid increase in the first minute, and then it decayed. A slightly inclined plateau was observed between 30- 70 min. and then it reached to a saturation value. The inclined plateau can be explained due to the decreasing thickness of gypsum film and the dissolution of colemanite mineral. The calcium ions were then free to pass to the solution. The variation of Ca^{2+} concentration was almost the same for the experiments carried out at two different colemanite particle sizes.

The other two experiments were performed by taking $\text{CaO}/\text{SO}_4^{2-}$ molar ratio as 1.0. The temperature was kept constant at 85°C, and the stirring rate was 500 rpm and 400 rpm for Hisarcık 2 (0-250 μm), and Hisarcık 3 (0-150 μm) colemanites, respectively. These batch reactor experiment results will be compared with the continuously stirred slurry reactor experiments in terms of boric acid and calcium ion concentration and also in terms of the particle size of the gypsum produced.

The variations of boric acid concentration in the experiments with the Hisarcık 2 and Hisarcık 3 colemanites are given in Figures 5.3.3 and 5.3.4, respectively.

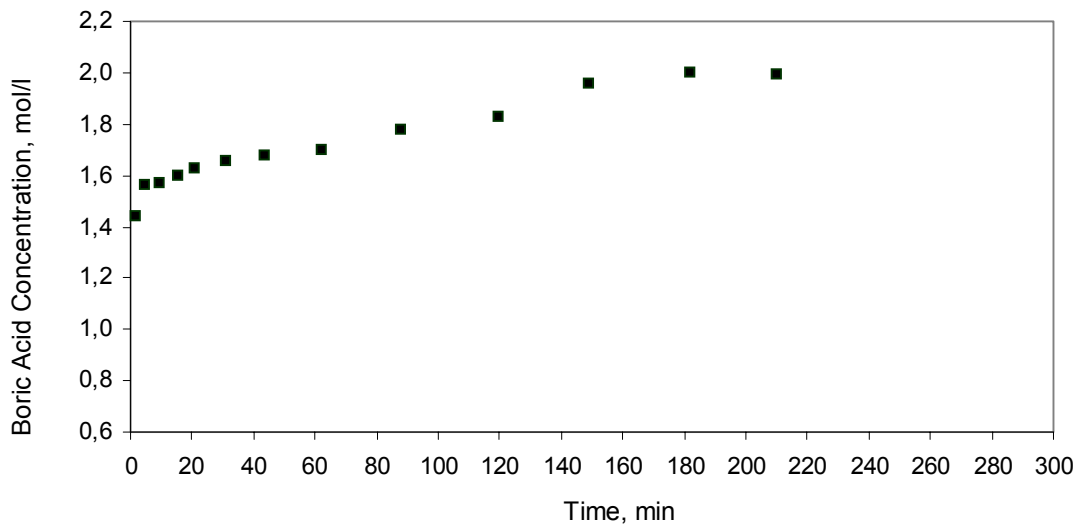


Figure 5.3.3. Variations in the boric acid concentration during the dissolution of Hisarcık 2 colemanite, -250 μ m, in aqueous sulfuric acid at 85°C and a stirring rate of 500 rpm. The initial CaO/SO₄²⁻ molar ratio is 1.0.

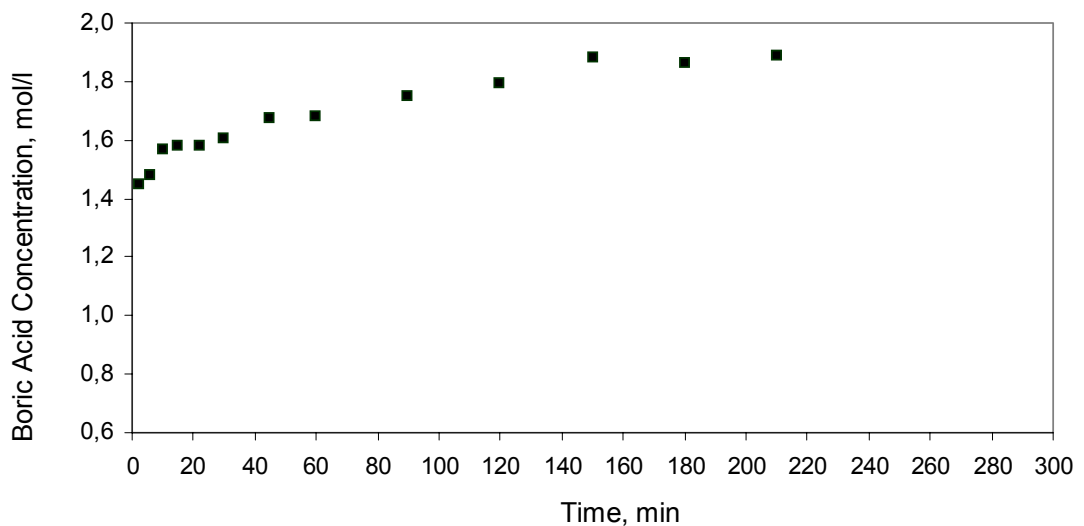


Figure 5.3.4. Variations in the boric acid concentration during the dissolution of Hisarcık 3 colemanite, -150 μ m, in aqueous sulfuric acid at 85°C and a stirring rate of 400 rpm. The initial CaO/SO₄²⁻ molar ratio is 1.

It can be seen from Figures 5.3.3 and 5.3.4 that the boric acid concentration did not follow the same trend as Figure 5.3.1. In Figures 5.3.3 and 5.3.4, the dissolution did not have a sharp plateau region. This can be attributed to the increased reaction temperature, which was 85°C, and in Figure 5.3.4 to the small particle size of colemanite. The boric acid concentration value reached in Figure 5.3.4 is lower as

the boron content of the Hisarcık 3 colemanite is lower than the Hisarcık 2 colemanite.

As observed from Figures 5.3.3 and 5.3.4, nearly 90% of the colemanite dissolved in the first ten minutes, which showed that the dissolution of the colemanite was very fast.

The calcium ion concentrations in the same experiments are given in Figures 5.3.5 and 5.3.6 for Hisarcık 2 and Hisarcık 3 colemanites, respectively.

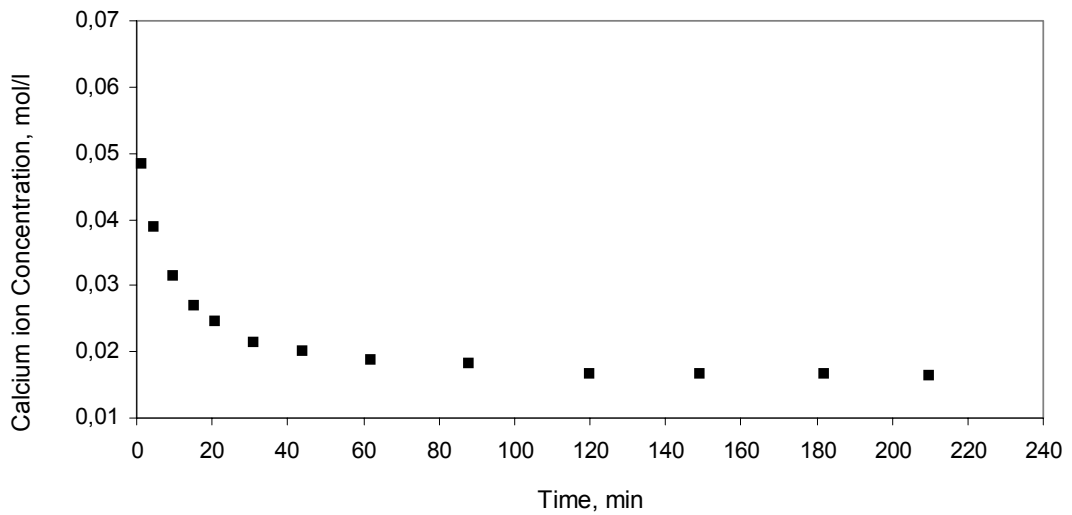


Figure 5.3.5. Variations in the calcium ion concentration during the dissolution of Hisarcık 2 colemanite, $-250\mu\text{m}$, in aqueous sulfuric acid at 85°C and a stirring rate of 500 rpm. The initial $\text{CaO}/\text{SO}_4^{2-}$ molar ratio is 1.

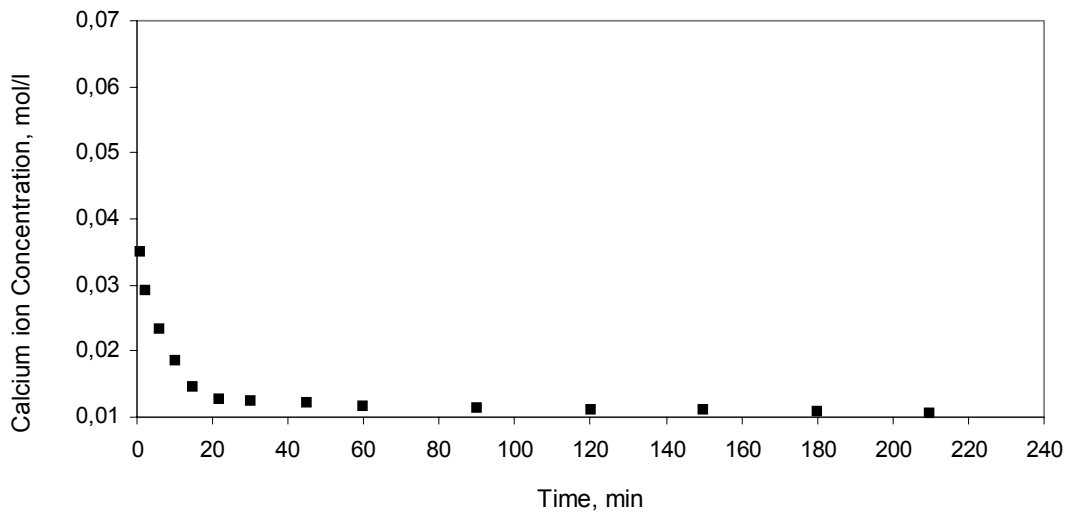


Figure 5.3.6. Variations in the calcium ion concentration during the dissolution of Hisarcık 3 colemanite, -150 μ m, in aqueous sulfuric acid at 85°C and a stirring rate of 400 rpm. The initial CaO/SO₄²⁻ molar ratio is 1.

The calcium ion concentrations in solution showed rapid decreases. In a way the calcium ion concentration trend agrees with the boric acid concentration variation. The trend in Figure 5.3.2 was not also observed in Figures 5.3.5 and 5.3.6. The calcium ion concentration in Hisarcık 3 colemanite, Figure 5.3.6, gives even a sharper decrease and lower saturation value, which can be attributed to the difference in the chemical compositions of the colemanites.

5.4. BORIC ACID PRODUCTION EXPERIMENTS ON CONTINUOUS FLOW STIRRED SLURRY REACTORS IN SERIES (CFSSR'S)

Colemanite mineral, named as Hisarcık 2 and Hisarcık 3 was used during the boric acid production experiments. Colemanite was fed with a constant flow rate to the first reactor. The particle size of the Hisarcık 2 and Hisarcık 3 colemanites were 0-250 μ m and 0-150 μ m, respectively. Acid having a composition of 8% H₃BO₃ and 5.58% H₂SO₄ was also fed to the first reactor. The first three tanks were initially full of 16% H₃BO₃. Feeding of acid and colemanite began at the same time, and this time was taken as the zero time, which denoted the beginning of the experiment.

5.4.1. PARAMETERS AFFECTING THE PERFORMANCE OF CFSSR'S IN SERIES

The parameters that were important in this reaction system can be listed as follows:

- stirring rate
- temperature of the reactors
- the flow rate of colemanite
- the flow rate of acid
- the concentration of boric acid and sulfuric acid in the feed tank
- the $\text{CaO}/\text{SO}_4^{2-}$ molar ratio
- the solid hold-up
- residence time of solid and liquid components in the reactors.

The parameters selected to be studied were all related to the residence time distribution of the components in the reactor. Only, the composition of the acid tank, although an important parameter, was not changed. Because, the composition of the acid did not have any influence on the residence time of the solid and liquid components in the reactors. The stirring rate and temperature of the reactors were also not changed.

The flow rates of the colemanite and the acid were changed as the changes occurring on these streams affect the residence time of the solid and liquid components in the reactors. The initial $\text{CaO}/\text{SO}_4^{2-}$ molar ratio and the solid hold-up values were also changed accordingly. A change in the solid hold-up alters the residence time of the solid and liquid components directly.

5.4.2. VARIATION OF THE CONCENTRATION OF BORIC ACID IN SOLUTION AT STEADY STATE

At the initial $\text{CaO}/\text{SO}_4^{2-}$ molar ratio of 1.00, three different sets of experiments were performed, one with Hisarcık 2, and two with Hisarcık 3. In these experiments, colemanite, and accordingly acid feed rates were changed. The solid hold-up was kept constant at a value of 0.04 for these. In the second set, three different experiments were performed with Hisarcık 2 colemanite, using an initial $\text{CaO}/\text{SO}_4^{2-}$ molar ratio of 1.37 and solid hold-up value of 0.06. The last set of the experiments,

using Hisarcık 2 and Hisarcık 3 colemanite, had the same colemanite feed rate, 10 g/min. In this set, the effect of acid feed rate was investigated.

These experiments are listed in Table 4.3a. The raw data of the experiments are given in Appendix D. The $\text{CaO}/\text{SO}_4^{2-}$ molar ratio and the solid hold-up value, and also the residence time calculations are given for a representative experiment in Appendix F.

During the experiments, pH of the solution in the reactors was recorded to examine if the reactors reached their steady state conditions or not. The steady state values of calcium ion and boric acid concentrations, temperature and pH values were found by taking the average of the last two or three values of the raw data. The steady state values of boric acid in the experiments are given in Table 5.4.1. The unit conversion of boric acid concentrations to the molar flow rates are shown in a representative experiment in Appendix F. The material balances are submitted in Appendix F.

Table 5.4.1. Steady state values of produced boric acid concentrations and molar flow rates in the experiments

COLEMANİTE USED	CONDITIONS	COLEMANİTE FEED RATE (G/MİN)	ACİD FEED RATE (G/MİN)	H ₃ BO ₃	
				mol/l	mol/min
Hisarcık2 (0-250 µm)	CaO/SO ₄ ²⁻ : 1.00 h _s : 0.04	5	48.5	2.66	0.1254
		7.5	72.7	2.66	0.1880
		10	97	2.66	0.2508
	CaO/SO ₄ ²⁻ : 1.37 h _s : 0.06	5	35	3.18	0.1079
		10	70	3.18	0.2158
		15	105	3.18	0.3237
	CaO/SO ₄ ²⁻ : 2.17 h _s : 0.09	10	45	3.32*	0.1411
Hisarcık 3 (0-150 µm)	CaO/SO ₄ ²⁻ : 1.00 h _s : 0.05	3.5	30	2.53	0.0736
		10	90	2.47	0.2159

*Theoretical value=4.20 mol/l

The colemanite was completely dissolved in the first reactor, so the same concentration of boric acid, Table 5.4.1, was attained in four of the reactors. 16% boric acid was put to the first three reactors before the start-up of the experiments. The system came to steady state faster.

There was 100% conversion in the experiments, except Experiment HC2.8, which stated that all the colemanite was converted to boric acid. In experiment HC2.8 where $\text{CaO}/\text{SO}_4^{2-}$ molar ratio was 2.17, the colemanite seemed not to be totally converted to boric acid, the conversion was 69% as can be seen from the low boric acid concentration. This can be due to the limiting sulfuric acid amount in solution.

In Table 5.4.1, although the boric acid concentration at the initial $\text{CaO}/\text{SO}_4^{2-}$ molar ratios of 1.00 and 1.37 was constant, the molar flow rate of boric acid increased with colemanite feed rate.

The change in boric acid molar flow rate with initial $\text{CaO}/\text{SO}_4^{2-}$ molar ratios of 1.00 and 1.37 are given for Hisarcık 2 and Hisarcık 3 colemanites in Figures 5.4.1 and the change in boric acid molar flow rate at constant colemanite feed rate of 10 g/min is shown in Figure 5.4.2.

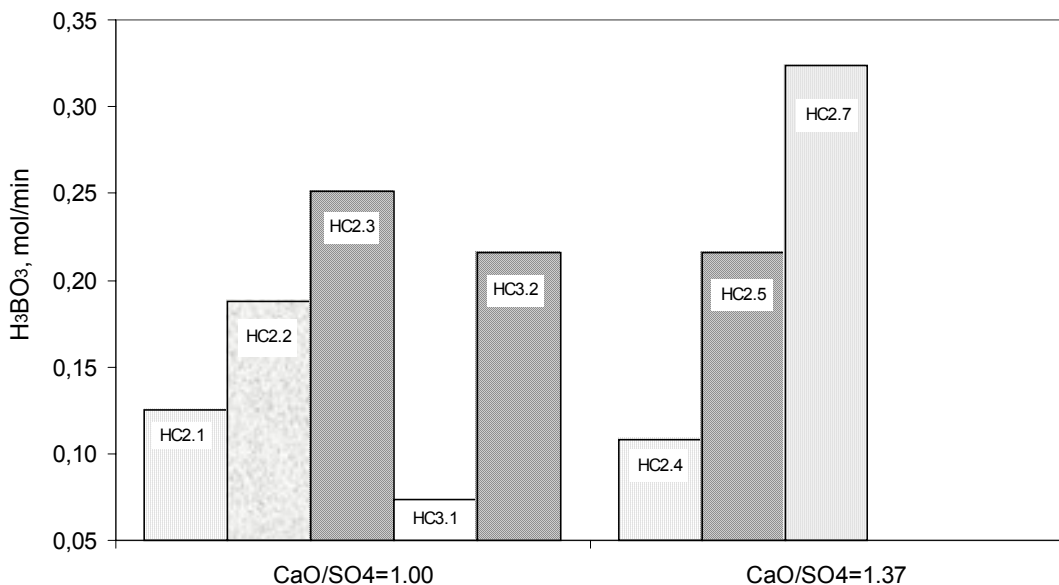


Figure 5.4.1. Molar flow rate of boric acid produced with Hisarcık 2, 0-250 μm , and Hisarcık 3, 0-150 μm , colemanites, at initial $\text{CaO}/\text{SO}_4^{2-}$ molar ratios of 1.00 and 1.37, where the experiment names are showed on each bar

As seen from Figure 5.4.1, at the same initial $\text{CaO}/\text{SO}_4^{2-}$ molar ratios, the molar flow rate of boric acid increased with colemanite feed rate, whereas at the same colemanite feed rate, the molar flow rate of boric acid decreased with the increase in molar ratio. In this figure, same texture of the bars represented the same colemanite feed rate.

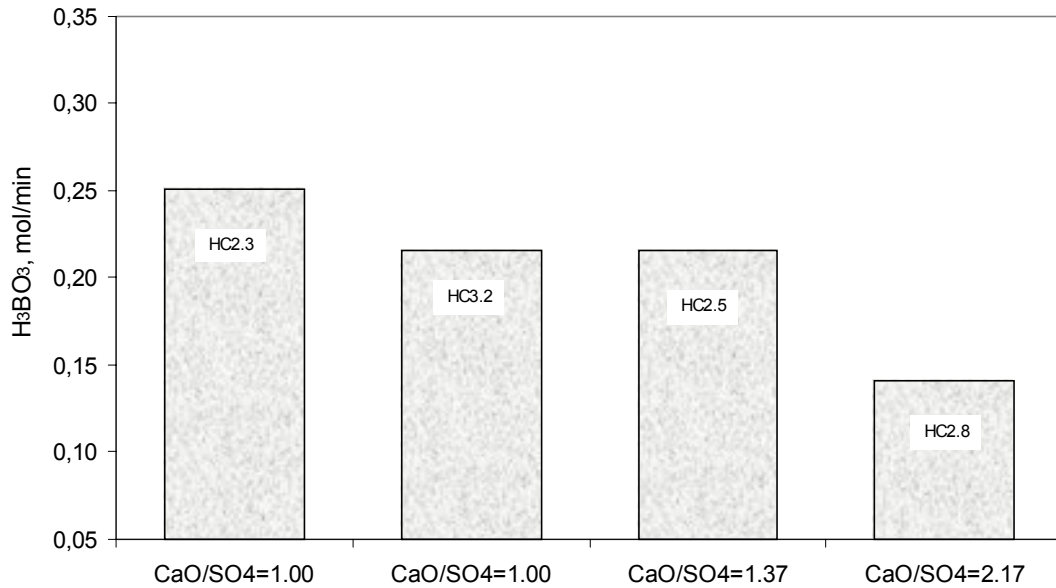


Figure 5.4.2. Molar flow rate of boric acid produced with Hisarcık 2, 0-250 μm , and Hisarcık 3, 0-150 μm , colemanites having a flow rate of 10 g/min, where the experiment names are showed on each bar

The change in boric acid molar flow rate with the initial molar ratio of $\text{CaO}/\text{SO}_4^{2-}$ was seen in Figure 5.4.2 for Hisarcık 2 and Hisarcık 3 colemanites. As noticed, the molar flow rate of boric acid decreased with the initial molar ratio. This decrease was due to the decrease of acid feed rate coming from acid tank, leading to decrease of boric acid feed rate and increase of molar ratio. The decrease of boric acid molar flow rate with the change of colemanite from Hisarcık 2 to Hisarcık 3 was also seen from Figure 5.4.2. This decrease was because of the decrease of B_2O_3 content of Hisarcık 3 colemanite.

5.4.3. VARIATION OF THE CONCENTRATION OF CALCIUM ION IN SOLUTION AT STEADY STATE

The steady state values of the calcium ion concentrations and molar flow rates are presented in Table 5.4.2. At the first glance, it was seen that at an initial $\text{CaO}/\text{SO}_4^{2-}$ molar ratio of 1.00, the calcium ion concentration decreased with the increase of reactor number; whereas the reverse was true for the higher molar ratios.

Table 5.4.2. Steady state values of calcium ion concentrations and molar flow rates in the experiments

Colemanite	HİSARCIK 2							HİSARCIK 3	
	CaO/SO ₄ ²⁻ =1.00			CaO/SO ₄ ²⁻ =1.37			CaO/SO ₄ ²⁻ =2.17	CaO/SO ₄ ²⁻ =1.00	
Experiment Name	HC2.1	HC2.2	HC2.3	HC2.4	HC2.5	HC2.7	HC2.8	HC3.1	HC3.2
Colemanite feed rate (g/min)	5	7.5	10	5	10	15	10	3.5	10
Calcium ion Concentration, ppm									
Reactor 1	500	1300	1000	2800	1600	1300	3300	420	550
Reactor 2	400	800	600	3100	2100	2500	3300	310	380
Reactor 3	300	700	600	3100	3100	2800	3300	270	330
Reactor 4	300	700	600	3500	3300	1900	3100	260	300
Molar Flow Rate of Calcium ion in Solution, mol/min									
Ca ²⁺ in colemanite, mol/min	0.0276	0.0414	0.0552	0.0276	0.0552	0.0828	0.0552	0.0178	0.0507
Reactor 1	0.00059	0.0023	0.0024	0.0024	0.0027	0.0033	0.0036	0.00031	0.00120
Reactor 2	0.00047	0.0014	0.0014	0.0026	0.0036	0.0064	0.0036	0.00023	0.00083
Reactor 3	0.00035	0.0012	0.0014	0.0026	0.0053	0.0071	0.0036	0.00020	0.00072
Reactor 4	0.00035	0.0012	0.0014	0.0030	0.0056	0.0048	0.0034	0.00019	0.00066

To examine the change of calcium ion molar flow rate in the sets of experiments, where their $\text{CaO}/\text{SO}_4^{2-}$ molar ratios were 1.00 and 1.37, Figures 5.4.3-5.4.5 are drawn.

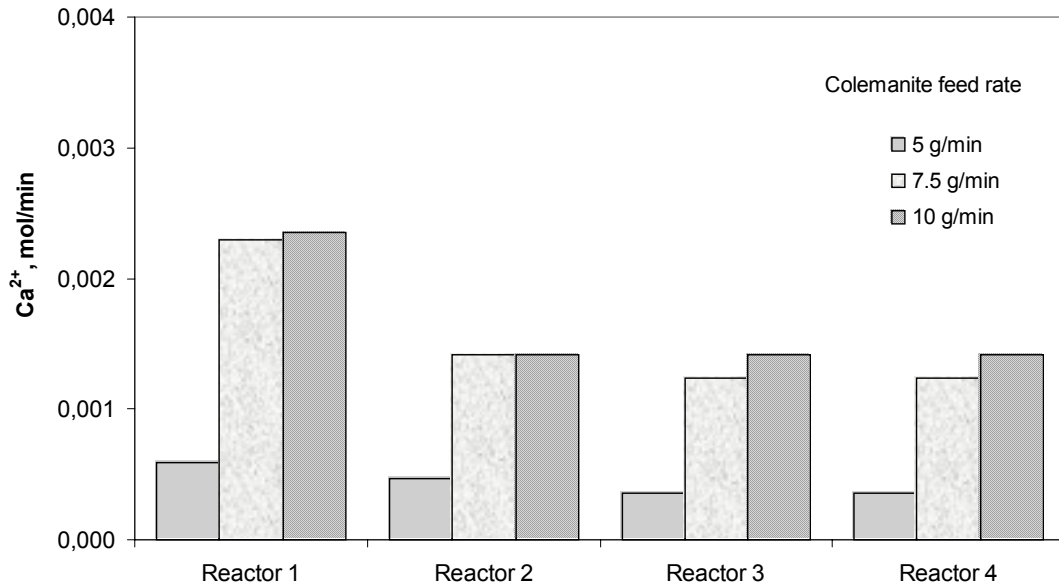


Figure 5.4.3. Molar flow rate of calcium ion in solution depending on the colemanite feed rate obtained by using Hisarcık 2 colemanite, 0-250 μm , at initial $\text{CaO}/\text{SO}_4^{2-}$ molar ratio of 1.00

It was observed from Figure 5.4.3 that, the calcium ion molar flow rates decreased with the increase in reactor number when the initial $\text{CaO}/\text{SO}_4^{2-}$ molar ratio was 1.00. In the first reactors the decrease was obvious, where as after the second reactor; there were minor changes in the molar flow rates of calcium ion in each of the three experiments. The decrease in the calcium ion concentration in the reactors showed that by the increase of the reactor number, the calcium ion concentration got closer to the saturation concentration.

It can be seen that at colemanite feed rate of 5 g/min, the calcium ion molar flow rate was less compared to the higher colemanite feed rates. This can be observed in each of the slurry reactors. The minimum attainable calcium ion concentrations were 0.00035, 0.0012 and 0.0014 mol/min for colemanite feed rates of 5, 7.5 and 10 g/min, respectively.

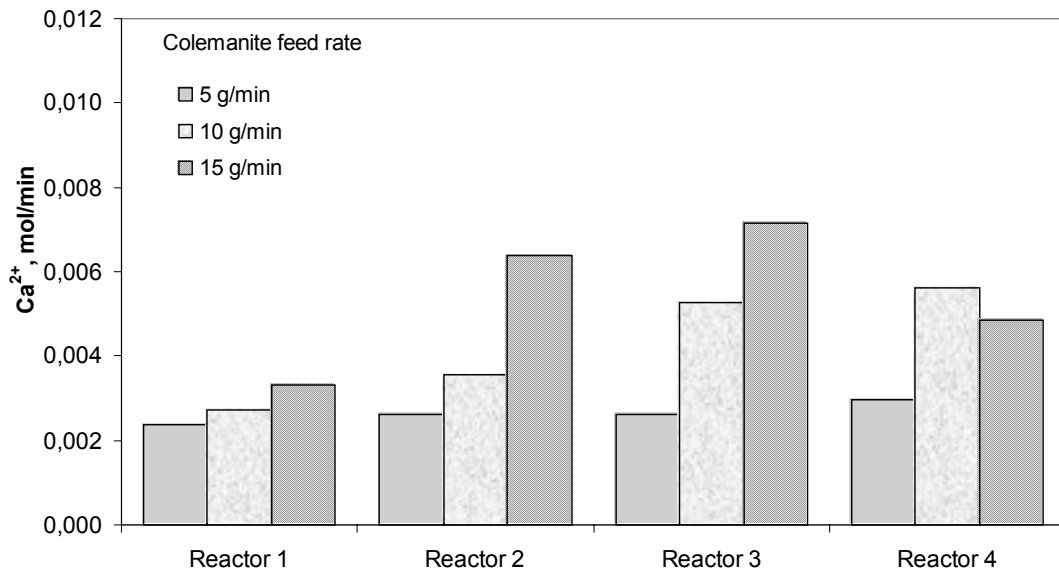


Figure 5.4.4. Molar flow rate of calcium ion in solution depending on the colemanite feed rate obtained by using Hisarcık 2 colemanite, 0-250 μm , at initial $\text{CaO}/\text{SO}_4^{2-}$ molar ratio of 1.37

It was seen from Figure 5.4.4 that, at the initial $\text{CaO}/\text{SO}_4^{2-}$ molar ratio of 1.37, the molar flow rate of calcium ion increased with the reactor number, which was the reverse for molar ratio of 1.00, Figure 5.4.3. There was increase of calcium ion molar flow rate with the increase of flow rates of colemanites in each of the reactors.

As the sulfate ion concentration in solution was not sufficient to bond the calcium ions in solution, the calcium ion concentration increased with the reactor number and therefore calcium ion molar flow rates increased in the following reactors. The maximum molar flow rates of calcium ion achieved were 0.0030, 0.0056, and 0.0071 mol/min for colemanite feed rates of 5, 10 and 15 g/min, respectively.

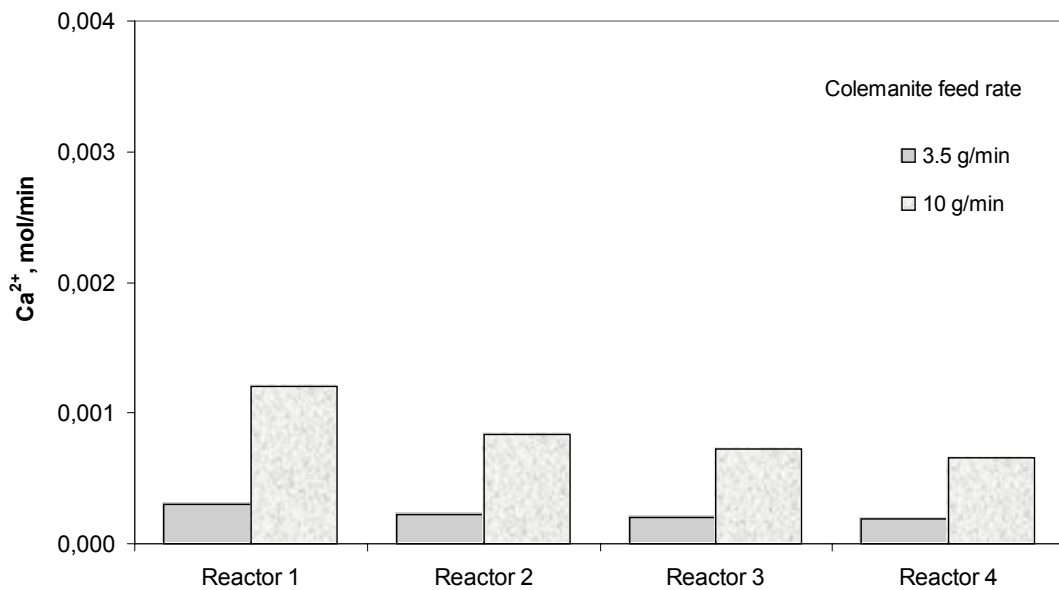


Figure 5.4.5. Molar flow rate of calcium ion in solution depending on the colemanite feed rate obtained by using Hisarcık 3 colemanite, 0-150 μm , at initial $\text{CaO}/\text{SO}_4^{2-}$ molar ratio of 1.00

The initial $\text{CaO}/\text{SO}_4^{2-}$ molar ratio was also 1.00 in Figure 5.4.5. The calcium ion molar flow rate increased with the colemanite feed rate, but the calcium ion molar flow rate decreased with the number of reactors. The same behavior was also observed in Figure 5.4.3, where initial $\text{CaO}/\text{SO}_4^{2-}$ molar ratio was 1.00. The only difference in the two sets was the differing colemanites.

In Figure 5.4.5 Hisarcık 3 colemanite with a calcium oxide content of 28.41% was used whereas, in Figure 5.4.3, Hisarcık 2 colemanite with a calcium oxide content of 30.90% was used. The minimum attainable calcium ion molar flow rates were 0.00019 and 0.00066 mol/min for colemanite feed rates of 3.5 and 10 g/min, respectively.

In order to compare the effect of $\text{CaO}/\text{SO}_4^{2-}$ molar ratio of 1.00 at constant colemanite feed rate Figure 5.4.6 is drawn. The difference in colemanites was denoted by H2 and H3 which represented Hisarcık 2 and Hisarcık 3 colemanites, respectively.

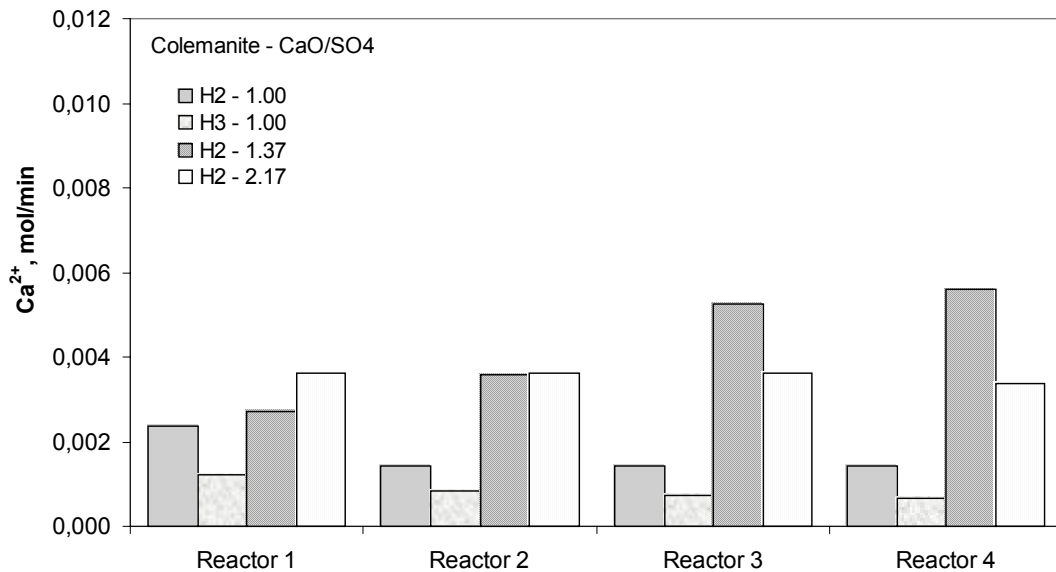


Figure 5.4.6. Molar flow rate of calcium ion in solution depending on the initial $\text{CaO}/\text{SO}_4^{2-}$ molar ratio obtained by using Hisarcık 2, 0-250 μm , and Hisarcık 3, 0-150 μm , colemanites having a flow rate of 10 g/min

In Figure 5.4.6, the $\text{CaO}/\text{SO}_4^{2-}$ molar ratios of the experiments, together with the colemanite name, at constant colemanite feed rate were shown. It can be investigated that for slow acid feed rates, where $\text{CaO}/\text{SO}_4^{2-}$ molar ratios was 1.00, the calcium ion molar flow rates showed a decreasing trend. But for medium acid feed rates, where $\text{CaO}/\text{SO}_4^{2-}$ molar ratios was 1.37, there seemed an increasing trend for the calcium ion molar flow rate. The change in calcium ion molar flow rate at $\text{CaO}/\text{SO}_4^{2-}$ molar ratio of 2.17 was actually not so remarkable. This can be due to the saturation of the reactor contents with calcium ion. In each of the reactors the molar flow rate of calcium ion showed a different behavior depending on the initial molar flow rate.

5.4.4. pH AND TEMPERATURE VARIATION OF THE EXPERIMENTS AT STEADY STATE

Temperature and pH were recorded continuously during the experiments. The temperature was recorded to control the heaters and pH was recorded to figure out the steady state of the system. The steady state values and the corresponding temperatures are given in Table 5.4.3.

Table 5.4.3. Steady state values of pH and temperature in the experiments

Colemanite	HİSARCIK 2							HİSARCIK 3	
	CaO/SO ₄ ²⁻ =1.00			CaO/SO ₄ ²⁻ =1.37			CaO/SO ₄ ²⁻ =2.17	CaO/SO ₄ ²⁻ =1.00	
Experiment Name	HC2.1	HC2.2	HC2.3	HC2.4	HC2.5	HC2.7	HC2.8	HC3.1	HC3.2
Colemanite feed rate (g/min)	5	7.5	10	5	10	15	10	3.5	10
pH values									
Reactor 1	0.47	0.16	0.49	3.80	3.20	3.50	4.00	0.65	0.30
Reactor 2	0.51	0.17	0.47	4.20	3.43	4.00	4.12	0.68	0.40
Reactor 3	0.51	0.15	0.45	4.07	3.60	4.09	4.20	0.71	0.46
Reactor 4	0.52	0.17	0.45	3.99	3.76	4.09	4.19	0.60	0.55
Temperature, °C									
Reactor 1	82	81	82	82	82	81	82	82	82
Reactor 2	84	83	84	84	83	82	82	84	83
Reactor 3	85	84	84	83	85	83	83	84	83
Reactor 4	85	84	84	85	85	83	84	85	84

It can be seen easily from the steady state data in Table 5.4.3 that as the $\text{CaO}/\text{SO}_4^{2-}$ molar ratio increased the pH values decreased drastically. At the molar ratio of $\text{CaO}/\text{SO}_4^{2-}$ of 1.00, the maximum value of achieved pH was 0.52, but at the molar ratios of $\text{CaO}/\text{SO}_4^{2-}$ to 1.37 and 2.17, the maximum achieved pH was 4.20. It can be concluded that as the concentration of boric acid increased, that led to an decrease in pH.

5.4.5. VARIATION OF THE CONCENTRATIONS OF SULFATE AND MAGNESIUM IONS IN SOLUTION AT STEADY STATE

The magnesium and sulfate ion concentrations were determined for the effluent of the fourth reactor in the experiments at steady state. The results of magnesium and sulfate ion concentrations in solution are given in Table 5.4.4. The conversion of the units of sulfate and magnesium ion concentrations to the molar flow rates are shown in a representative experiment in Appendix F.

Table 5.4.4. Steady state values of the magnesium and sulfate ion concentrations in the fourth reactor in the experiments

	Exp Name:	Colemanite feed rate (g/min)	Mg^{2+}		SO_4^{2-}	
			ppm	mol/min	ppm	mol/min
$\text{CaO}/\text{SO}_4^{2-}$ =1.00	HC2.1	5	350	0.00068	15000	0.0074
	HC2.2	7.5	300	0.00087	13500	0.0099
	HC2.3	10	240	0.00093	13000	0.0128
$\text{CaO}/\text{SO}_4^{2-}$ =1.37	HC2.4	5	70	0.00010	1040	0.0004
	HC2.5	10	50	0.00014	1040	0.0007
	HC2.7	15	40	0.00017	1060	0.0011

As examined from Table 5.4.4, the molar flow rates of the magnesium and sulfate ions showed similar behaviors. While magnesium ion molar flow rates were increasing, the sulfate ion molar flow rates were also increasing with the increase of flow rates of colemanites for the same $\text{CaO}/\text{SO}_4^{2-}$ molar ratio.

The change in the magnesium ion molar flow rates during the experiments is given in Figure 5.4.7.

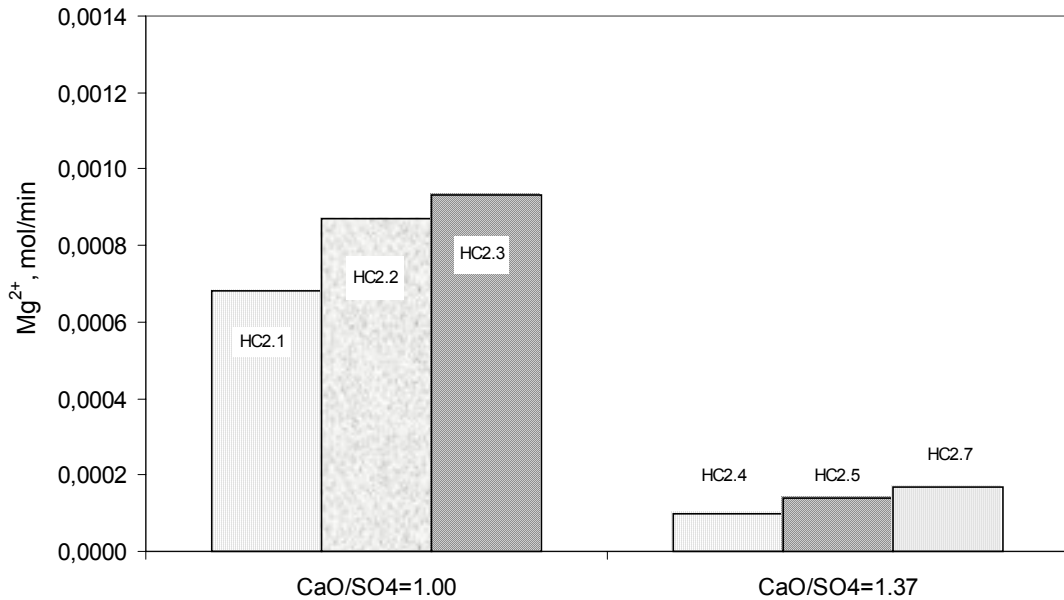


Figure 5.4.7. Molar flow rate of magnesium ion obtained at steady state by using Hisarcık 2, 0-250 μm , colemanite, at initial $\text{CaO}/\text{SO}_4^{2-}$ molar ratios of 1.00 and 1.37, where the experiment names are showed on each bar

It was observed from Figure 5.4.7 that the molar flow rate of magnesium ion increased with the increase of flow rates of colemanite in the $\text{CaO}/\text{SO}_4^{2-}$ molar ratios of 1.00 and 1.37. With the increase of $\text{CaO}/\text{SO}_4^{2-}$ molar ratio from 1.00 to 1.37, the magnesium ion molar flow rate decreased drastically.

The maximum magnesium ion molar flow rates obtained were for higher flow rates of colemanite, having values of 0.00093 and 0.00017 mol/min for $\text{CaO}/\text{SO}_4^{2-}$ molar ratio of 1.00 and 1.37, respectively.

The change in the sulfate ion molar flow rates during the experiments is given in Figure 5.4.8.

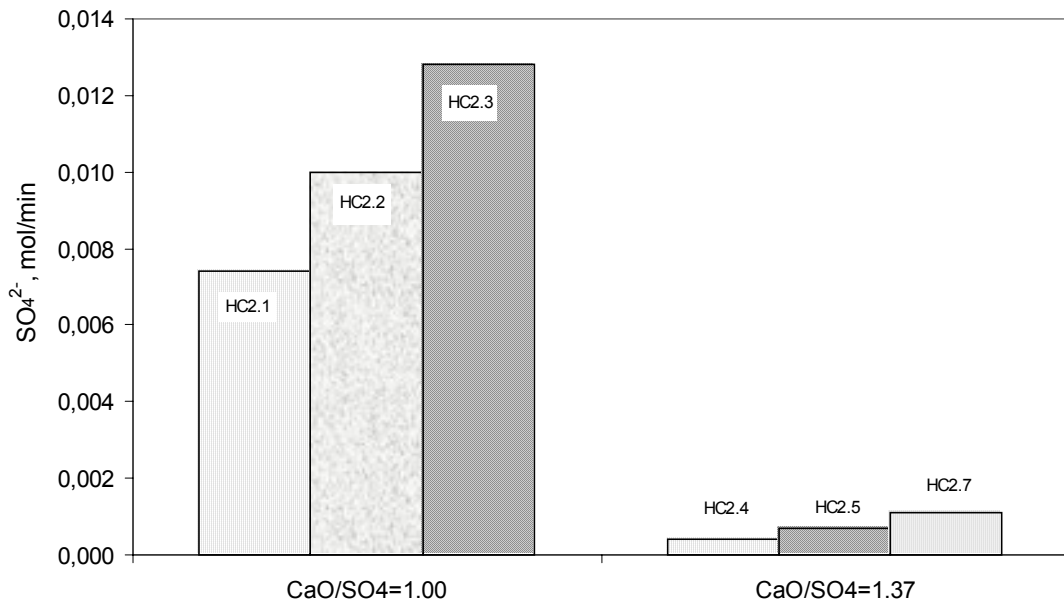


Figure 5.4.8. Molar flow rate of sulfate ion obtained at steady state by using Hisarcık 2, 0-250 μm , colemanite, at initial $\text{CaO}/\text{SO}_4^{2-}$ molar ratios of 1.00 and 1.37, where the experiment names are showed on each bar

Sulfate ion molar flow rates in Figure 5.4.8 also showed the same trend as Figure 5.4.7, which was drawn for the magnesium ion molar flow rate. Sulfate ion concentration increased with the increase of flow rates of colemanite in the $\text{CaO}/\text{SO}_4^{2-}$ molar ratios of 1.00 and 1.37. With the increase of $\text{CaO}/\text{SO}_4^{2-}$ molar ratio from 1.00 to 1.37, the sulfate ion concentration decreased drastically.

The maximum sulfate ion molar flow rates obtained were for higher flow rates of colemanite and acid, having values of 0.0128 and 0.0011 mol/min for $\text{CaO}/\text{SO}_4^{2-}$ molar ratio of 1.00 and 1.37, respectively.

5.4.6. COMPARISON OF VARIATION OF CALCIUM AND SULFATE ION MOLAR FLOW RATE

In order to compare the molar flow rates of calcium and sulfate ions in the experiments easily, the graphs of the calcium and sulfate ion molar flow rates for the fourth reactor are drawn together in Figure 5.4.9.

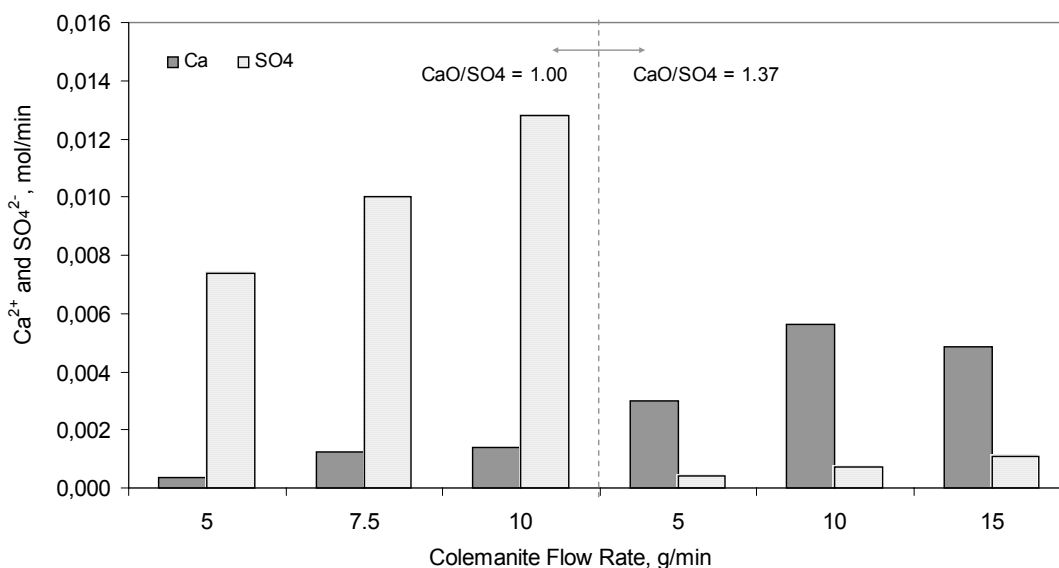


Figure 5.4.9. Variation of molar flow rates of calcium and sulfate ion obtained at steady state by using Hisarcık 2, 0-250 μm , colemanite, at initial $\text{CaO}/\text{SO}_4^{2-}$ molar ratios of 1.00 and 1.37 depending on the colemanite feed rate

It was investigated from Figure 5.4.9 that at $\text{CaO}/\text{SO}_4^{2-}$ molar ratio of 1.00, sulfate ion molar flow rate was higher than the calcium ion molar flow rate. In the case of $\text{CaO}/\text{SO}_4^{2-}$ molar ratio of 1.37, the reverse was true. This result was the expected one, as at $\text{CaO}/\text{SO}_4^{2-}$ molar ratio of 1.00, colemanite was limiting in the reaction system, whereas at $\text{CaO}/\text{SO}_4^{2-}$ molar ratios of 1.37, sulfuric acid was limiting in the reaction system. So, in $\text{CaO}/\text{SO}_4^{2-}$ molar ratio of 1.00, more sulfate ion was detected and in $\text{CaO}/\text{SO}_4^{2-}$ molar ratios of 1.37 more calcium ion and less sulfate ion could be detected in the reactors.

5.4.7. CONVERSION EXPRESSIONS USED DURING THE STUDY

In order to investigate the effect of $\text{CaO}/\text{SO}_4^{2-}$ molar ratio in terms of conversion, two conversion expressions were used. One of them was in terms of colemanite, which was the ratio of molar flow rate of boric acid produced from colemanite to the molar flow rate of boric acid if the entering colemanite totally reacted. The other was in terms of sulfuric acid entering the reactor, which can be explained by the ratio of the sulfate ion leaving the system in solid to the entering sulfate ion by sulfuric acid.

These expressions are explained in detail in a representative experiment in Appendix F. The calculated conversion values are given in Table 5.4.5.

Table 5.4.5. Conversion calculated in terms of colemanite and sulfate ion entering the system

	Exp Name:	Colemanite feed rate (g/min)	Conversion in terms of colemanite	Conversion in terms of sulfate
$\text{CaO}/\text{SO}_4^{2-} = 1.00$	HC2.1	5	1.00	0.73
	HC2.2	7.5	1.00	0.76
	HC2.3	10	1.00	0.77
$\text{CaO}/\text{SO}_4^{2-} = 1.37$	HC2.4	5	1.00	0.98
	HC2.5	10	1.00	0.98
	HC2.7	15	1.00	1.00
$\text{CaO}/\text{SO}_4^{2-} = 2.17$	HC2.8	10	0.69	
$\text{CaO}/\text{SO}_4^{2-} = 1.00$	HC3.1	3.5	1.00	
	HC3.2	10	1.00	

As determined from Table 5.4.5, the conversion calculated in terms of colemanite and sulfate ion gave higher conversions, except the experiment HC2.8, where $\text{CaO}/\text{SO}_4^{2-}$ was 2.17. The conversion calculated in terms of colemanite for that case was 0.69. The highest conversion was found for the conversion in terms of sulfate was for $\text{CaO}/\text{SO}_4^{2-}$ molar ratio of 1.37 as 1.00.

The solids at the outlet of each reactor were analyzed in terms of boron trioxide and it was found that there existed no unreacted colemanite in the solid, except Experiment HC2.8, and the solid was completely calcium sulfate. This showed that the colemanite was not totally converted to boric acid, i.e. there was excess colemanite given to the reactor, and the conversion of colemanite to the boric acid was 69%.

5.4.8. EFFECT OF SOLID HOLD-UP ON THE RESIDENCE TIME OF LIQUID AND SOLID COMPONENTS

Solid hold-up, h_s , was a very critical parameter in this study. It was defined as the ratio of volumetric flow rate of solid to the total volumetric flow rate. Knowing the solid hold-up of the system, the residence time of the solid and liquid components could be easily calculated. Two experiments were performed to see if there was a change in the solid hold-up of the system, mass of solid to the total volume, during the experiment. The raw data of the two experiments are given in Appendix E. It can be deduced from the steady state data that the solid hold-up of the reactors did not have a significant change.

The solid hold-up and residence time calculations are given in Appendix F. The solid hold-up values and the residence time of liquid and solid at each experiment are given in Table 5.4.6. The solid hold-up in each of the reactors did not differ at steady state, that's why the residence time calculations were done on a single reactor. For four reactors in series, the values in Table 5.4.6 should be multiplied by four to find the total residence time of 4 reactors in series.

Table 5.4.6. Solid hold-up and residence time of the solid and liquid components in each of the reactors in series

	Exp Name:	Colemanite feed rate (g/min)	Solid hold-up, h_s	Residence time of solid, τ_s (min)	Residence time of liquid, τ_L (min)
$\text{CaO}/\text{SO}_4^{2-} = 1.00$	HC2.1	5	0.04	35	37
	HC2.2	7.5	0.04	23	25
	HC2.3	10	0.04	17	18
$\text{CaO}/\text{SO}_4^{2-} = 1.37$	HC2.4	5	0.06	52	50
	HC2.5	10	0.06	26	25
	HC2.7	15	0.06	17	17
$\text{CaO}/\text{SO}_4^{2-} = 2.17$	HC2.8	10	0.09	39	38
$\text{CaO}/\text{SO}_4^{2-} = 1.00$	HC3.1	3.5	0.05	62	59
	HC3.2	10	0.05	22	20

It can be seen from Table 5.4.6 that as the molar ratio of $\text{CaO}/\text{SO}_4^{2-}$ increased, the solid hold-up also increased. For all of the experiments performed by using Hisarcık 2 and Hisarcık 3 colemanites, it was seen that the residence times of solid and liquid decreased with increased colemanite feed rate. It was seen that there was a 1 or 2 min difference between the solid and liquid residence times in each of the experiments. The closeness of the solid and liquid residence times implies on the establishment of steady state. The equal solid and liquid residence times was also observed for the single phase systems, which was also the approach made during the macrofluid modeling, Chapter 3.

5.5. PARTICLE SIZE DISTRIBUTION OF GYPSUM CRYSTALS

The samples from the batch reactor and continuous reactors were collected. The collected solid was washed out with hot water to get rid of the boric acid solution on it. Then samples were prepared for particle size distribution analysis. The sample preparation and the analysis of the samples were explained in detail in the experimental part. The aim was to compare the volume weighted mean diameters of the gypsum crystals and see if the crystals came to an easily filterable size in the continuous reactors or not.

5.5.1. PARTICLE SIZE DISTRIBUTION OF GYPSUM CRYSTALS IN A BATCH REACTOR

The solid samples were taken from the batch reactor experiments before ending the experiments, at about 210 min. The particle size distribution of the gypsum crystals are given for the batch reactor experiments performed by using Hisarcık 2, 0-250 μm , and Hisarcık 3, 0-150 μm are given in Figures 5.5.1 and 5.5.2, respectively.

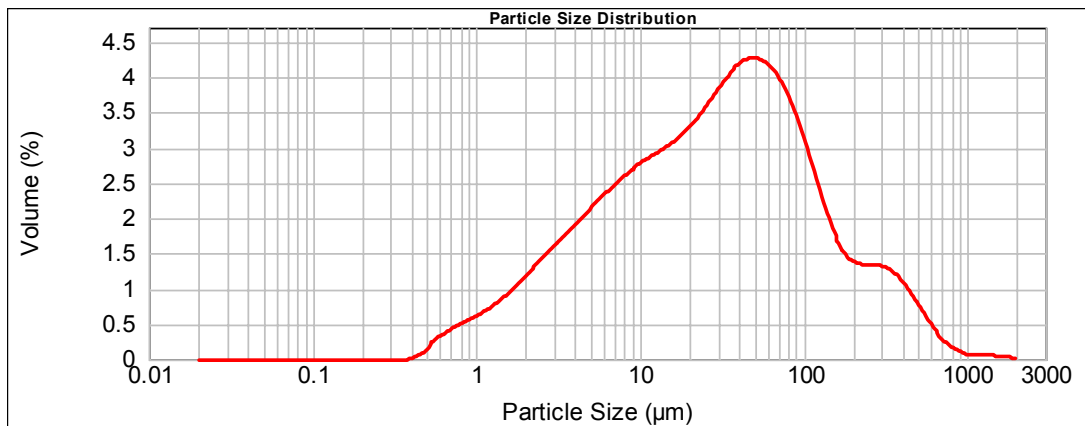


Figure 5.5.1. The particle size distribution of gypsum crystals during the dissolution of Hisarcık 2, 0-250 μm , colemanite in aqueous sulfuric acid at initial $\text{CaO}/\text{SO}_4^{2-}$ molar ratio of 1.0 at 85°C and a stirring rate of 500 rpm

The volume weighted mean diameter of the gypsum crystals were obtained from Figures 5.5.1, by the use of the software of the laser diffraction particle size analyzer,. The volume weighted mean diameter of the gypsum crystals obtained

from the dissolution of Hisarcık 2, 0-250 μm , colemanite in aqueous sulfuric acid at 85°C and 500 rpm was 72.1 μm .

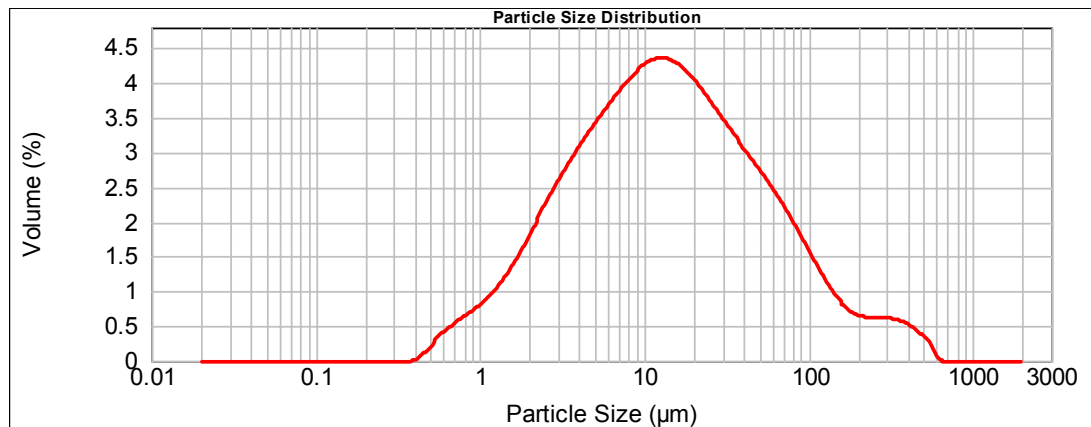


Figure 5.5.2. The particle size distribution of gypsum crystals during the dissolution of Hisarcık 3, 0-150 μm , colemanite in aqueous sulfuric acid at initial $\text{CaO}/\text{SO}_4^{2-}$ molar ratio of 1.0 at 85°C and a stirring rate of 400 rpm

The volume weighted mean diameter of the gypsum crystals, Figure 5.5.2, obtained from the dissolution of Hisarcık 3, 0-150 μm , colemanite in aqueous sulfuric acid at 85°C and 400 rpm was 36.9 μm . It can be seen easily from the comparison of the batch reactor experiments that the average diameter of the gypsum crystals increased when the particle size of the colemanite used increased.

When the particle size of the colemanite increased the dissolution rate decreased and less number of nuclei of gypsum was formed. During the growth period of the crystals, calcium and sulfate ions react on the nuclei and the crystals grew bigger. But when the particle size of colemanite decreased the number of gypsum nuclei increased as the dissolution rate of colemanite increased. That's why the crystals could not grew bigger.

5.5.2. PARTICLE SIZE DISTRIBUTION OF GYPSUM CRYSTALS IN CONTINUOUS FLOW STIRRED SLURRY REACTORS

When the system reached steady state, solid was collected by filtration, like taking samples but in great amounts, from each reactor in the system. These samples were then analyzed for their particle size distributions. The graphs obtained for the particle size distribution of gypsum crystals are given in Figures 5.5.3-5.5.9.

The laser diffraction instrument does not consider the shape of the particles. It considers them as a sphere and it initially calculates a distribution based around volume terms. While comparing the distributions taken from the particle size analyzer, it should be kept in mind that the gypsum crystals are rod-like. The volumes of the crystals are found by the analyzer and the volume weighted mean diameters were calculated by the software of the analyzer.

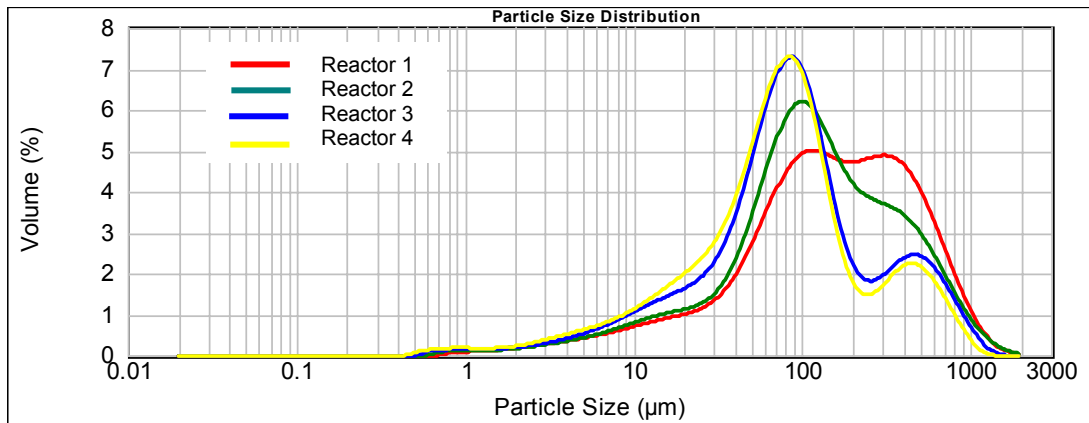


Figure 5.5.3. The particle size distribution of gypsum crystals obtained from the effluent streams of the reactors from Experiment HC 2.1, performed by using Hisarcık 2, 0-250 μm , colemanite at the initial $\text{CaO}/\text{SO}_4^{2-}$ molar ratio of 1.00, and colemanite feed rate of 5 g/min

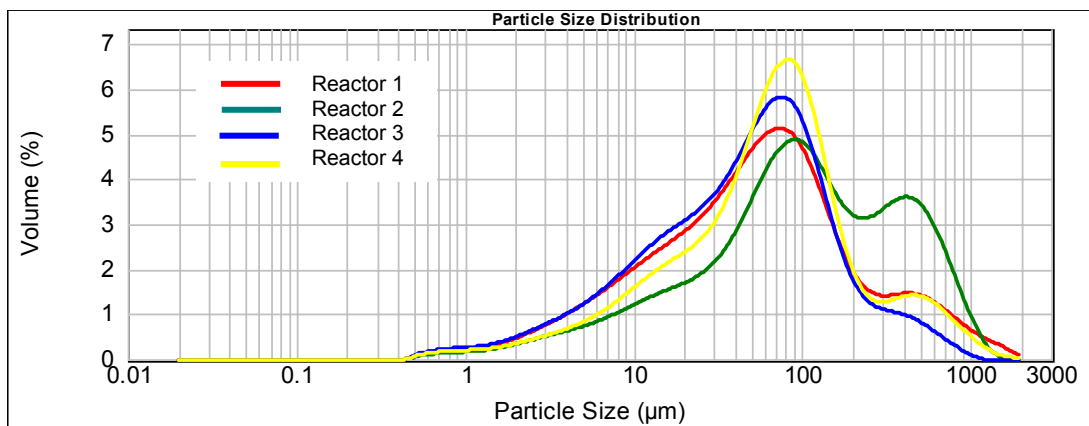


Figure 5.5.4. The particle size distribution of gypsum crystals obtained from the effluent streams of the reactors from Experiment HC 2.2, performed by using Hisarcık 2, 0-250 μm , colemanite at the initial $\text{CaO}/\text{SO}_4^{2-}$ molar ratio of 1.00, and colemanite feed rate of 7.5 g/min

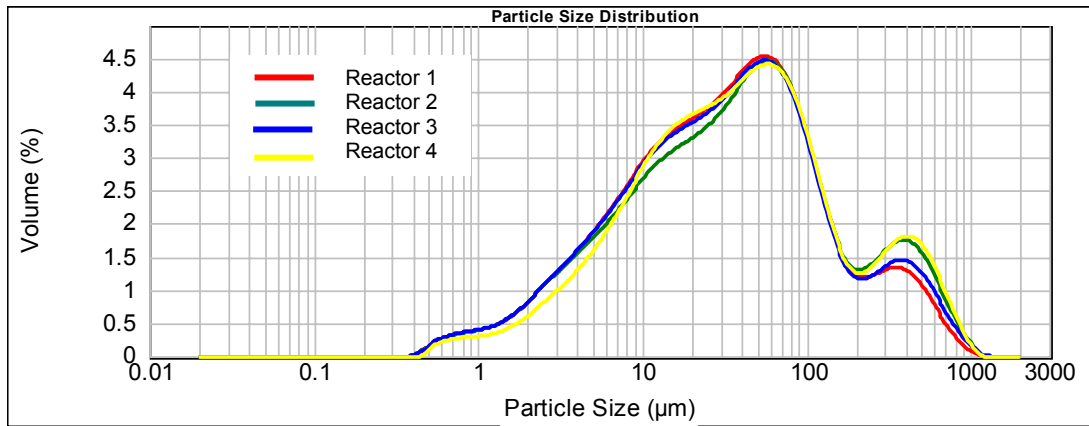


Figure 5.5.5. The particle size distribution of gypsum crystals obtained from the effluent streams of the reactors from Experiment HC 2.3, performed by using Hisarcık 2, 0-250 µm, colemanite at the initial $\text{CaO}/\text{SO}_4^{2-}$ molar ratio of 1.00, and colemanite feed rate of 10 g/min

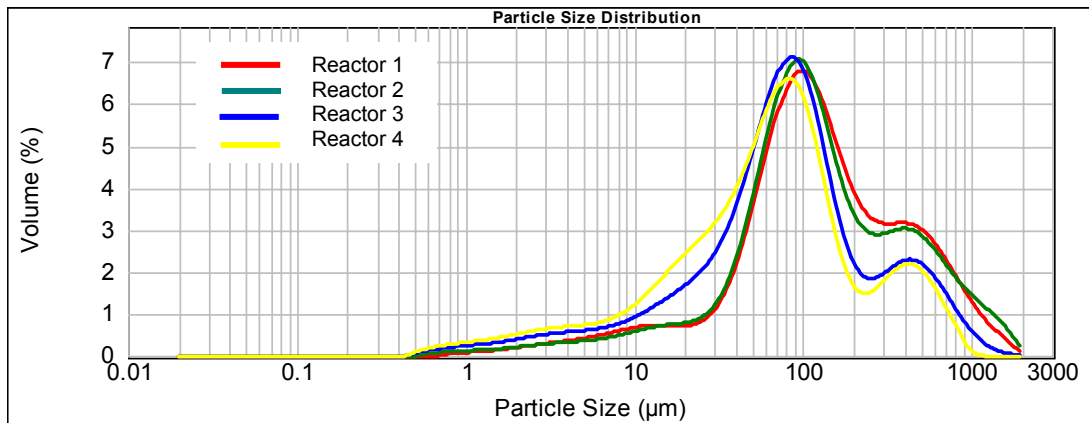


Figure 5.5.6. The particle size distribution of gypsum crystals obtained from the effluent streams of the reactors from Experiment HC 2.4, performed by using Hisarcık 2, 0-250 µm, colemanite at the initial $\text{CaO}/\text{SO}_4^{2-}$ molar ratio of 1.37, and colemanite feed rate of 5 g/min

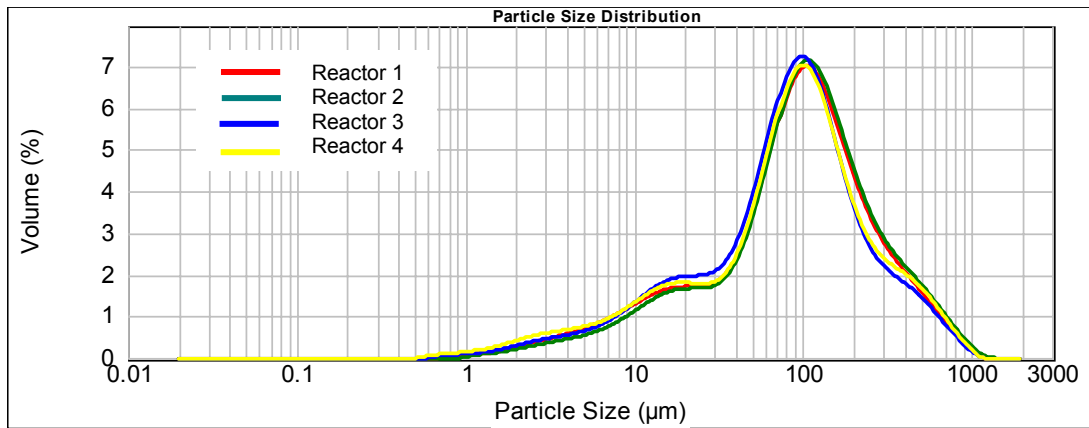


Figure 5.5.7. The particle size distribution of gypsum crystals obtained from the effluent streams of the reactors from Experiment HC 2.5, performed by using Hisarcık 2, 0-250 µm, colemanite at the initial $\text{CaO}/\text{SO}_4^{2-}$ molar ratio of 1.37, and colemanite feed rate of 10 g/min

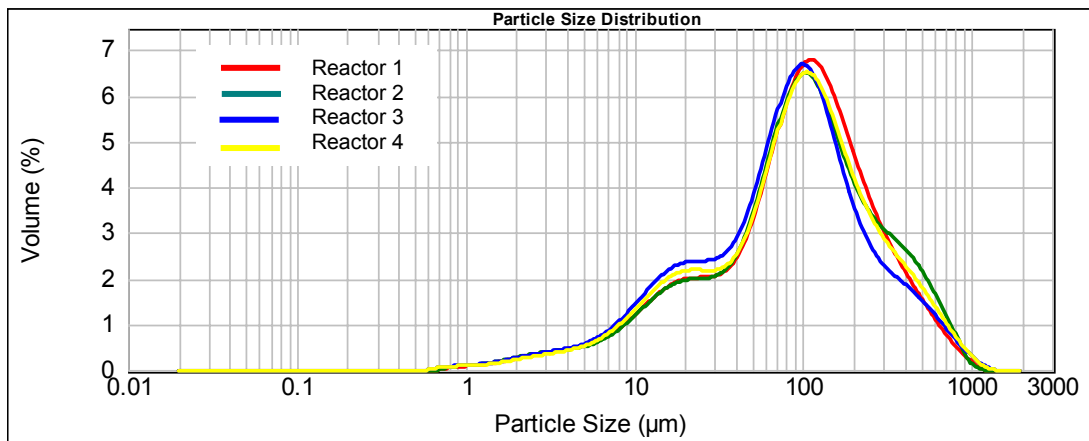


Figure 5.5.8. The particle size distribution of gypsum crystals obtained from the effluent streams of the reactors from Experiment HC 2.7, performed by using Hisarcık 2, 0-250 µm, colemanite at the initial $\text{CaO}/\text{SO}_4^{2-}$ molar ratio of 1.37, and colemanite feed rate of 15 g/min

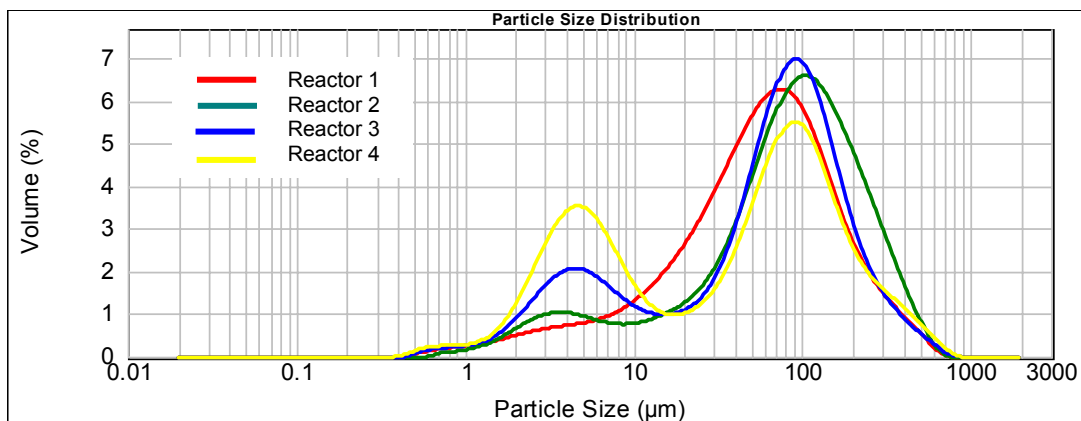


Figure 5.5.9. The particle size distribution of gypsum crystals obtained from the effluent streams of the reactors from Experiment HC 2.8, performed by using Hisarcık 2, 0-250 µm, colemanite at the initial $\text{CaO}/\text{SO}_4^{2-}$ molar ratio of 2.17, and colemanite feed rate of 10 g/min

As seen from Figures 5.5.5, 5.5.7 and 5.5.8, the particle size distribution curves at each reactor showed the same behavior. In these experiments the colemanite and acid feed rates were the highest, i.e. the residence time of colemanite at each reactor is the lowest.

The particle size distribution curves of the Hisarcık 3, 0-150 µm, colemanite is given in Figures 5.5.10 and 5.5.11.

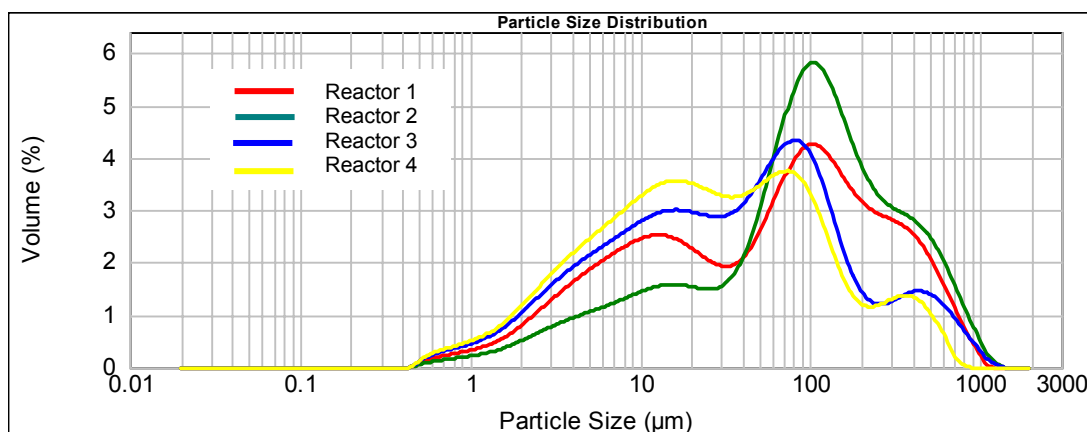


Figure 5.5.10. The particle size distribution of gypsum crystals obtained from the effluent streams of the reactors from Experiment HC 3.1, performed by using Hisarcık 3, 0-150 µm, colemanite at the initial $\text{CaO}/\text{SO}_4^{2-}$ molar ratio of 1.00, and colemanite feed rate of 3.5 g/min

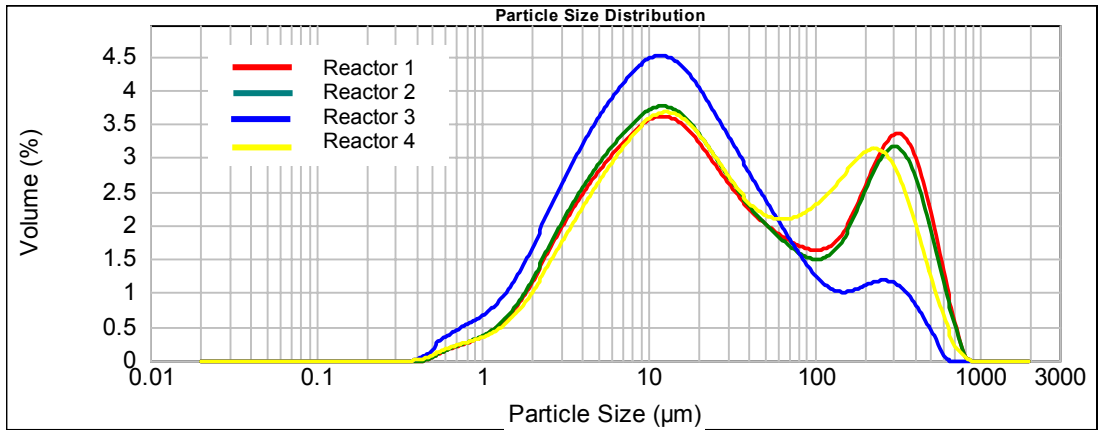


Figure 5.5.11. The particle size distribution of gypsum crystals obtained from the effluent streams of the reactors from Experiment HC 3.2, performed by using Hisarcık 3, 0-150 µm, colemanite at the initial $\text{CaO}/\text{SO}_4^{2-}$ molar ratio of 1.00, and colemanite feed rate of 10 g/min

The mean of the curves, that is the volume weighted mean diameter, was calculated by the software of the laser diffraction instrument. The mean of the curves are given in Table 5.5.1.

Table 5.5.1. Volume weighted mean diameter (μm) of the particles obtained from the software of the laser diffraction particle size analyzer for the experiments performed by using Hisarcık 2 colemanite, 0-250 μm

	Exp Name:	Solid Hold-up, h_s	Residence Time of Solid, τ_s (min)	Reactor 1	Reactor 2	Reactor 3	Reactor 4
$\text{CaO}/\text{SO}_4^{2-}=1.00$	HC2.1	0.04	35	240.1	204.8	159.8	137.1
	HC2.2	0.04	23	130.4	198.0	85.3	123.4
	HC2.3	0.04	17	79.1	95.1	84.4	98.2
$\text{CaO}/\text{SO}_4^{2-}=1.37$	HC2.4	0.06	52	227.6	237.0	152.1	122.4
	HC2.5	0.06	26	139.3	143.2	128.1	135.0
	HC2.7	0.06	17	141.1	151.5	133.2	146.5
$\text{CaO}/\text{SO}_4^{2-}=2.17$	HC2.8	0.09	39	86.1	116.9	90.9	83.2
$\text{CaO}/\text{SO}_4^{2-}=1.00$	HC3.1	0.05	60	130.7	163.1	96.3	69.4
	HC3.2	0.05	20	105.6	98.5	43.8	90.6

In order to observe the variation of the volume weighted mean diameters of the crystals, the values of which are given in Table 5.5.1, the graphs at the $\text{CaO}/\text{SO}_4^{2-}$ molar ratios of 1.00 and 1.37 are drawn in Figures 5.5.10 and 5.5.11, respectively.

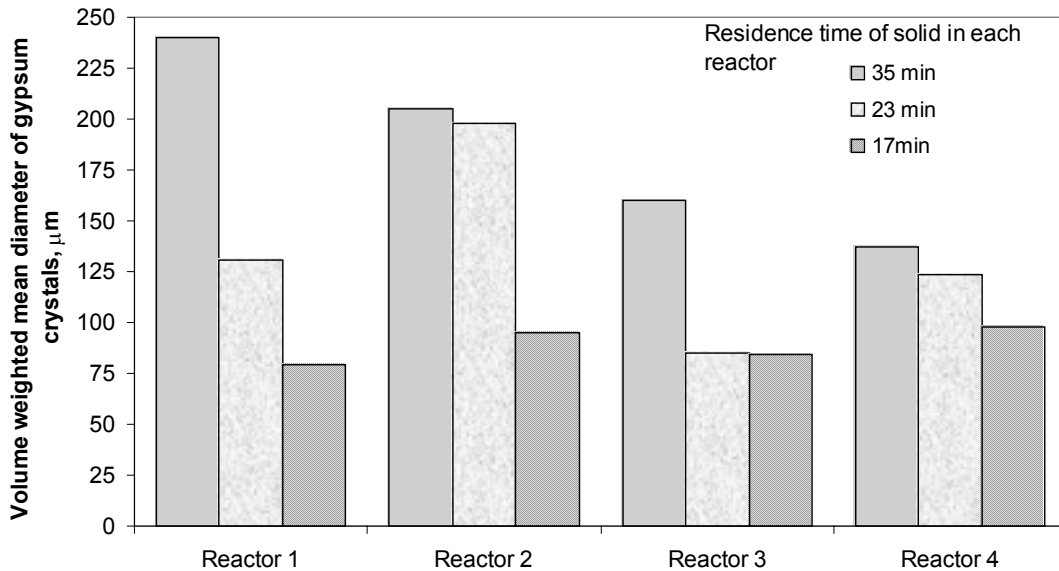


Figure 5.5.12 Variation of volume weighted mean diameters of gypsum crystals depending on the solid residence times during the dissolution of Hisarcık 2 colemanite, 0-250 μm , at initial $\text{CaO}/\text{SO}_4^{2-}$ molar ratio of 1.00 and solid hold-up of 0.04

As observed from Figure 5.5.12 at the same initial $\text{CaO}/\text{SO}_4^{2-}$ molar ratio of 1.00, as the flow rates of the colemanite was increased, i.e. the residence time of solid was decreased, the volume weighted mean diameter of the gypsum crystals decreased in each reactor. As the reactor number increased, the mean diameters of the crystals having a residence time of 35 min decreased, but the mean diameters of crystals having residence times of 23 and 17 min showed increasing and decreasing but similar trends. The decreasing trend of the mean diameters can be due to the high stirring rate of the reactors, 400 rpm, i.e. the crystals could break down at this stirring rate.

Maximum values of the mean diameters were seen in the first, second and fourth reactors, the values of which were 240.1, 198 and 98.2 μm for residence times of 35, 23 and 17 min, respectively.

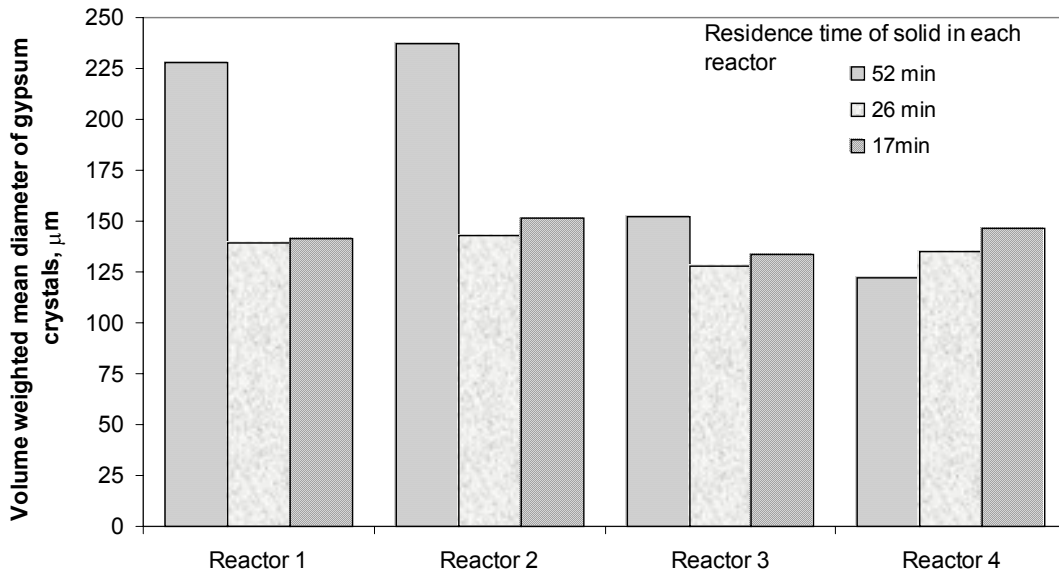


Figure 5.5.13 Variation of volume weighted mean diameters of gypsum crystals depending on the solid residence times during the dissolution of Hisarcik 2 colemanite, 0-250 μm , at initial $\text{CaO}/\text{SO}_4^{2-}$ molar ratio of 1.37 and solid hold-up of 0.06

As investigated from Figure 5.5.13 at the same initial $\text{CaO}/\text{SO}_4^{2-}$ molar ratio of 1.37, as the flow rates of colemanite increased, i.e. the residence time of solid decreased, the mean diameter of the crystals decreased as the reactor number increased. But at lower residence times, the mean diameter showed increasing and decreasing but similar trends as observed in Figure 5.5.12 when the molar ratio of $\text{CaO}/\text{SO}_4^{2-}$ was 1.00.

Maximum values of the mean diameters were seen in the second reactors, the values of which were 237.0, 143.2 and 151.5 μm for solid residence times of 52, 26 and 17 min, respectively. The drastic decrease of mean diameter at the third reactor at higher residence times can be attributed to the longer time spent in the reactor, which can cause breakage of the crystal at 400 rpm. Although the mean diameters can not reach so high values at lower residence times, they did not have a higher amount of breakage.

The variation of the mean diameters of the crystals at constant colemanite feed rate of 10 g/min is drawn in Figure 5.5.14

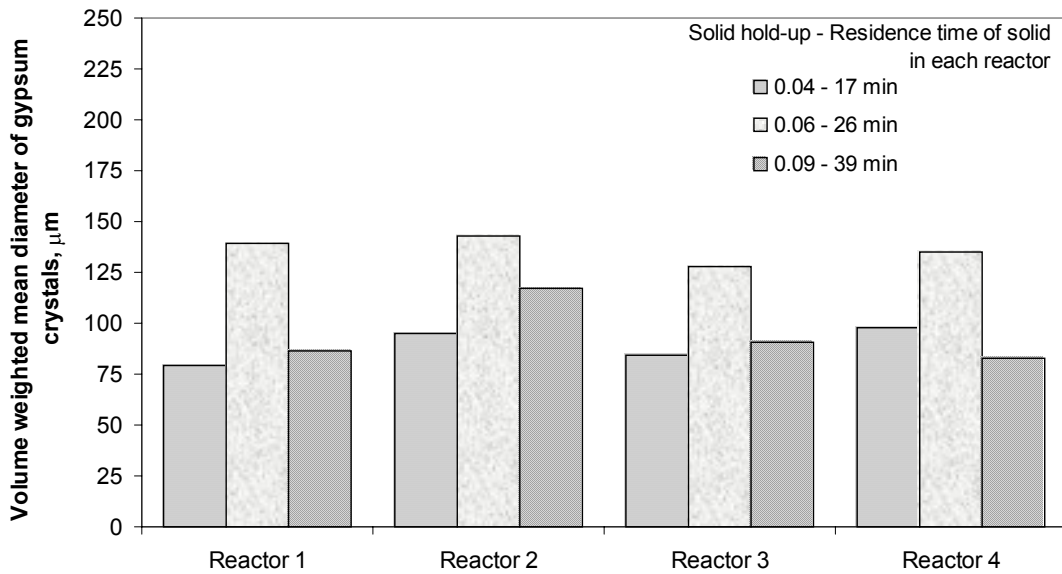


Figure 5.5.14 Variation of volume weighted mean diameters of gypsum crystals depending on the solid hold-up and residence times of solid during the dissolution of Hisarcık 2 colemanite, 0-250 μm . The colemanite feed rate is 10 g/min.

In Figure 5.5.14 the variations of mean diameters of the crystals at constant colemanite feed rates, but differing solid hold-ups were shown. As seen in this figure, when the reactor number increased, the mean diameters of the crystals increase and decrease. At a residence time of 17 min, the volume weighted mean diameters of the gypsum crystals increased till 98.2 μm , but at residence time of 26 min the mean diameter did not change much. Lastly, at a residence time of 39 min, the mean diameter decreased after the second reactor, same as the case for higher residence times in Figures 5.5.12 and 5.5.13. So, it can be stated that at higher stirring rates, 400 rpm for this case, high residence times were not preferable. In other words, if it is needed to work with higher residence times due to other reasons, the stirring rate should be decreased after the second reactor.

The volume weighted mean diameters of Hisarcık 3 colemanite obtained from the experiments HC3.1 and HC3.2 are compared in Figure 5.5.15.

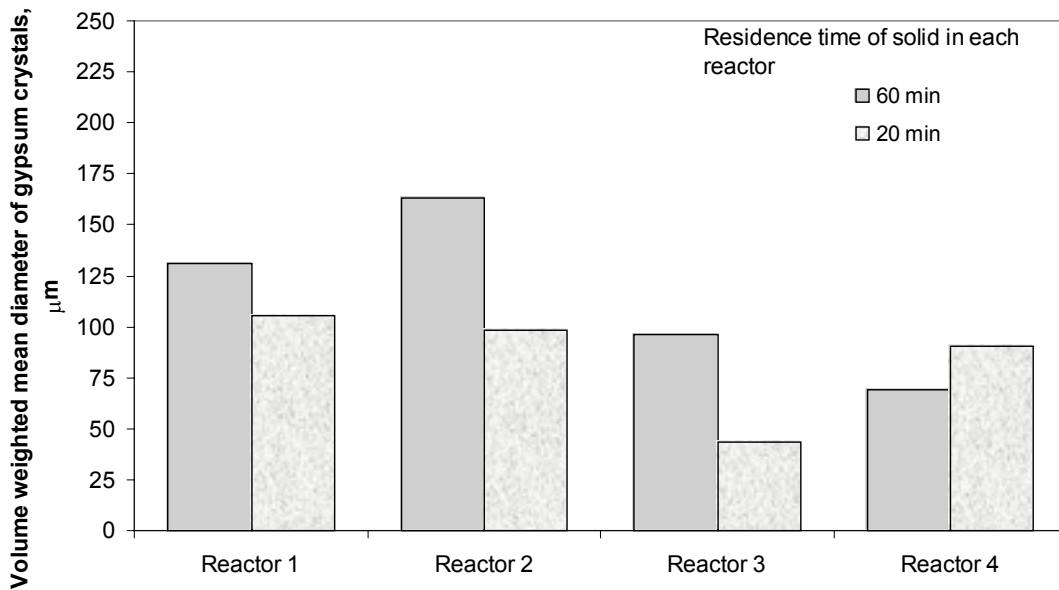


Figure 5.5.15. Variation of volume weighted mean diameters of gypsum crystals depending on the solid residence times during the dissolution of Hisarcık 3 colemanite, 0-150 μm , at initial $\text{CaO}/\text{SO}_4^{2-}$ molar ratio of 1.00 and solid hold-up of 0.05

As seen from Figure 5.5.15, the volume weighted mean diameter change of the gypsum crystals had the same trend as the one seen in Figure 5.5.12. When the residence time of the crystals in the reactor was high, the crystals had a tendency to break down easily after the second reactor, even though they have large diameters. When the residence time of the crystals in the reactor was low, they have smaller diameters and they also break down in the third reactor and could not even achieve the diameter obtained in the second reactor in the last one.

5.6. LIGHT MICROSCOPE IMAGES OF GYPSUM CRYSTALS

The images of the gypsum crystals, which are obtained by using the Hisarcık 3, 0-150 μm , colemanite, from the batch reactor and the continuous reactor experiments are given in this section.

5.6.1. LIGHT MICROSCOPE IMAGES OF GYPSUM CRYSTALS IN A BATCH REACTOR

The gypsum crystals obtained by the batch reactor experiments had a mean diameter of 36.9 μm , which was found by the particle size analyzer. The images of the gypsum crystals obtained by the batch reactor experiment are given in Figure 5.6.1. The crystals had a residence time of 210 min in the reactor, which was the total experiment time.

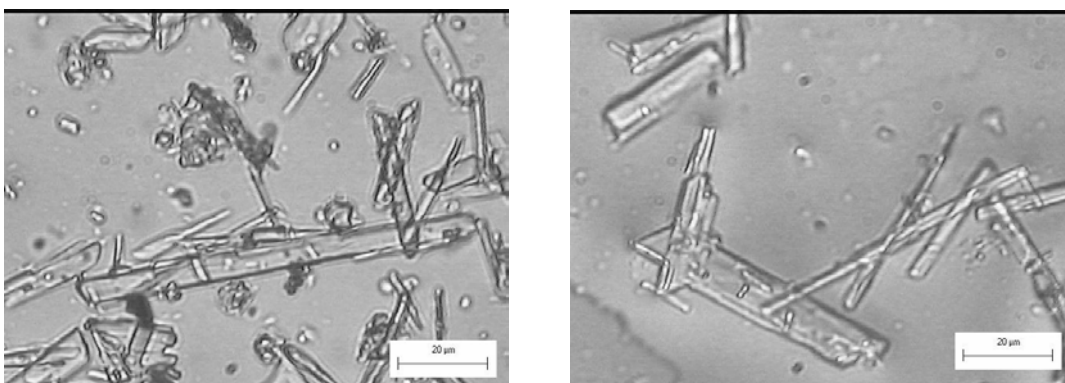


Figure 5.6.1. Light microscope images of gypsum crystals obtained by the batch reactor experiment, HB3.1. The residence time of the crystals is 210 min

As it can be seen from Figure 5.6.1, different sizes of gypsum crystals were present. The biggest dimension of the crystals is 60 μm . The width of the crystals seemed not to exceed 10 μm .

5.6.2. LIGHT MICROSCOPE IMAGES OF GYPSUM CRYSTALS IN CONTINUOUS FLOW STIRRED SLURRY REACTORS

The gypsum crystals obtained by using Hisarcık 3, 0-150 μm , colemanite in the two continuous reactor experiments are given in this section. The effect of the residence time on the growth of the gypsum crystals was discussed.

The gypsum crystal images of the experiment HC3.1 is given in Figure 5.6.2. In this continuous reactor experiment, the residence time in each reactor was 60 min. The biggest mean diameter of the crystals was obtained in the second reactor as 163.1 μm .

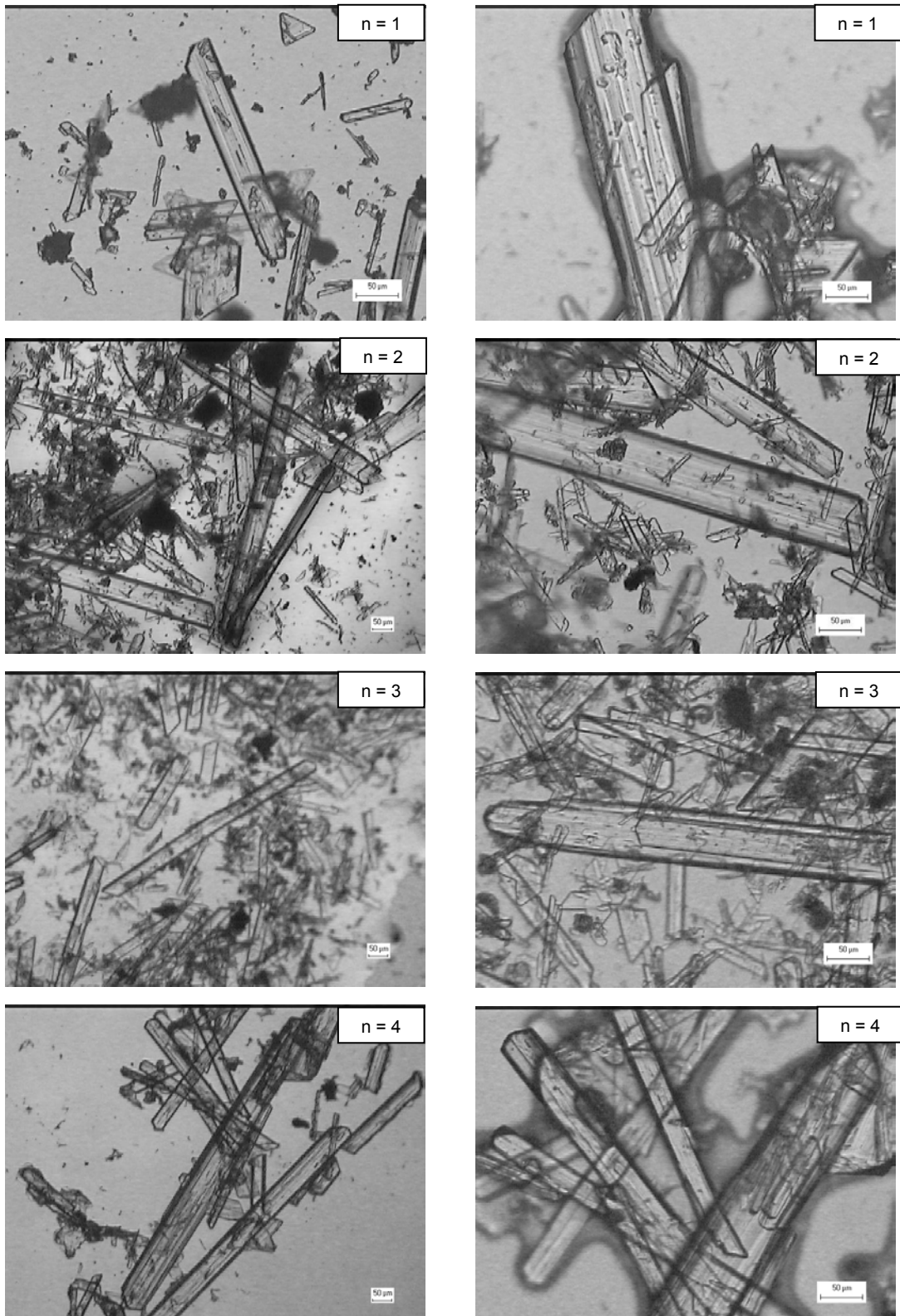


Figure 5.6.2. Light microscope images of gypsum crystals obtained by the continuous reactor experiment, HC3.1. The residence time of the crystals in each reactor is 60 min. The reactor number, n , is shown on top of each figure

In Figure 5.6.2, the views of the gypsum crystals were taken under different magnifications, to have detailed images. The views on the right hand side of the figure were closer views, when compared with the left hand side views. As seen from Figure 5.6.2, the crystals grew wider and taller. The crystals had dimensions even bigger than $250\ \mu\text{m}$ as seen in the images. The width of some crystals was even $100\ \mu\text{m}$. In order to compare the images with an another continuous reactor experiment, the crystal images of HC3.2 experiment, having a residence time of 20 min, is given in Figure 5.6.3.

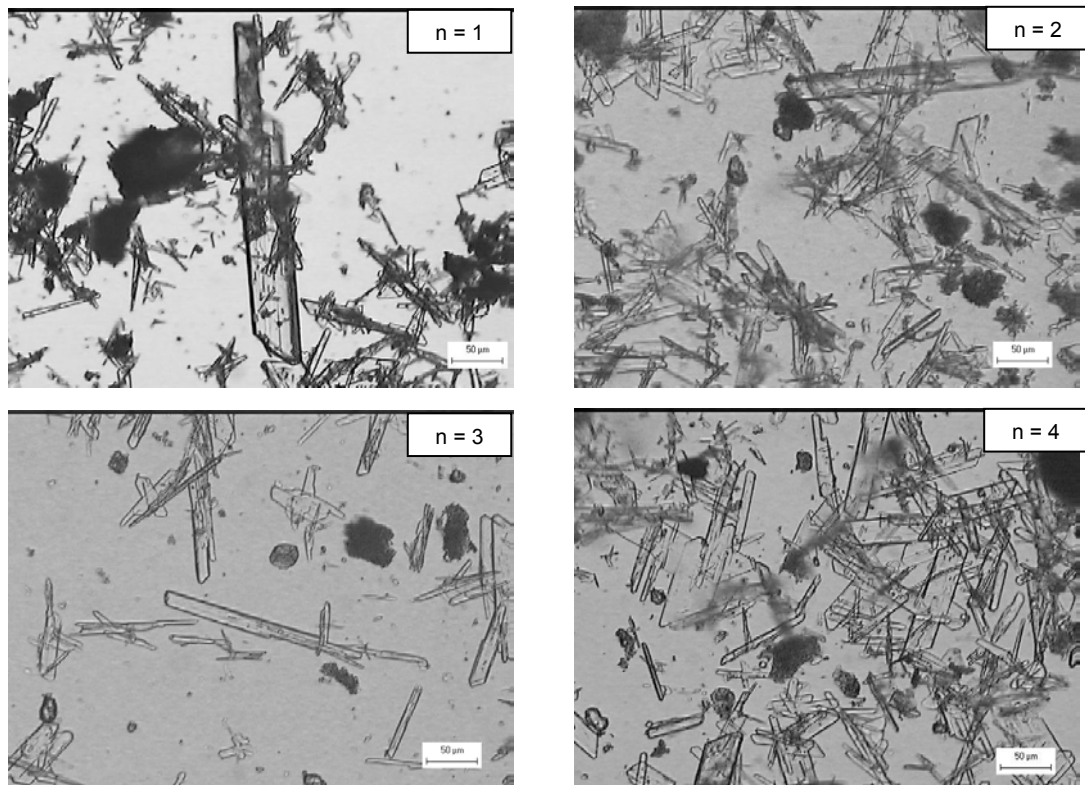


Figure 5.6.3. Light microscope images of gypsum crystals obtained by the continuous reactor experiment, HC3.2. The residence time of the crystals in each reactor is 20 min. The reactor number, n , is shown on top of each figure

Tall and wide crystals were also seen in Figure 5.6.3. But, the crystals width was seemed to be higher in the high residence time experiment. The images in Figures 5.6.2 and 5.6.3 showed the significance of working with continuous reactors when compared with the images of the batch reactor byproduct gypsum, Figure 5.6.1. The crystals obtained from the continuous reactors were also easily filterable, which was the main advantage of working with continuous reactors.

5.7. SIMULATION OF BORIC ACID REACTORS

By using the models explained in Chapter 3, the continuous boric acid reactors will be simulated by macrofluid and microfluid models together with the plug flow model by the use of the residence time of the continuous reactors and the gypsum crystal growth model obtained from batch reactor data.

5.7.1. GYPSUM CRYSTAL GROWTH MODEL

The gypsum crystal growth model was obtained by the use of batch reactor data, given in Section 5.3. The reciprocal concentration of calcium ion versus time plot, Equation 3.4, gave a straight line for the crystallization of gypsum from the solution obtained by the dissolution of colemanite in aqueous sulfuric acid at different particle sizes and initial $\text{CaO}/\text{SO}_4^{2-}$ molar ratio of 0.95, at 80°C and a stirring rate of 500 rpm, Figure 5.7.1.

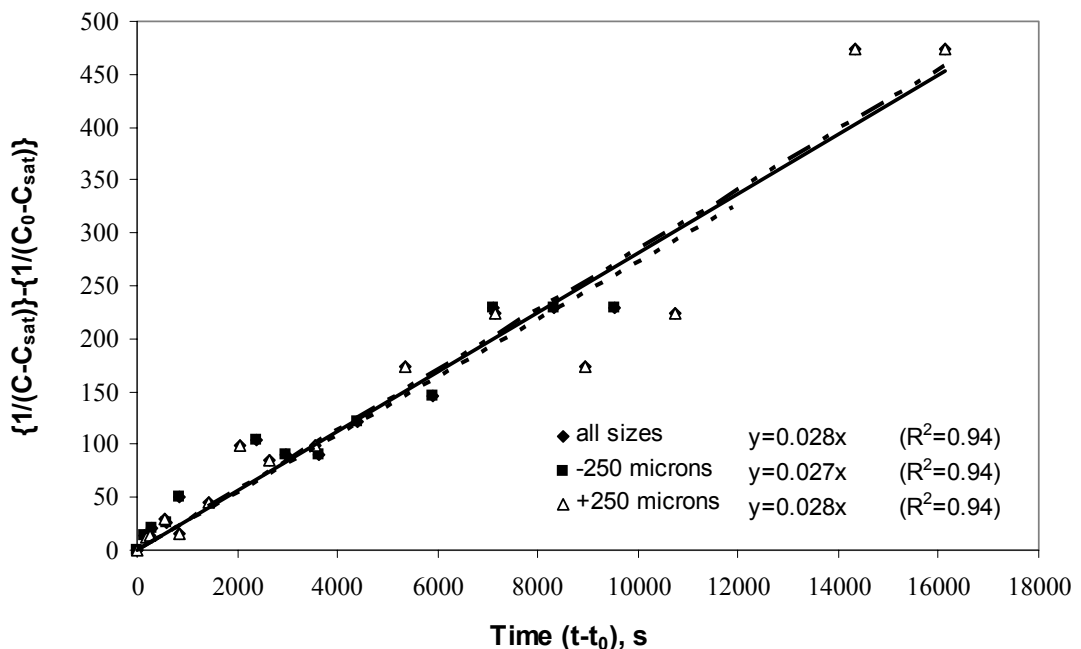


Fig. 5.7.1. Reciprocal concentration of calcium ion versus time plot Experiments HB2.1 and HB2.2, at different particle sizes and initial $\text{CaO}/\text{SO}_4^{2-}$ molar ratio of 0.95, at 80°C and a stirring rate of 500 rpm.

As seen from Figure 5.7.1, the fits for different particle size ranges showed the same trend, and their goodness of the fits were $R^2=0.94$. The slopes gave the reaction rate constant k' s as 0.027, 0.028 and 0.028 $\text{l mol}^{-1}\text{s}^{-1}$ for particle sizes of 0-250 μm , 250-1000 μm and 0-1000 μm , respectively. The reaction rate constant k is taken as 0.027 $\text{l mol}^{-1}\text{s}^{-1}$ for the rest of the calculations. Other parameters in Eq 3.4 were $C_0 = 0.053 \text{ mol/l}$ and $C_{\text{sat}} = 0.013 \text{ mol/l}$, which were found experimentally.

The model parameters found by Çetin et al (2001) for 80°C, 200 rpm were 0.146 $\text{l.mol}^{-1}\text{s}^{-1}$, 0.0193 mol/l, and 0.0031 mol/l for k , C_0 and C_{sat} , respectively. It should be remembered that colemanite used in this research had a different chemical composition, Hisarcık 1.

The other two experiments were analyzed in terms of finding the reaction rate constant, k , and the reciprocal concentration of calcium ion as a function of time plot is drawn in Figures 5.7.2 and 5.7.3 for Hisarcık 2 and Hisarcık 3 experiments respectively.

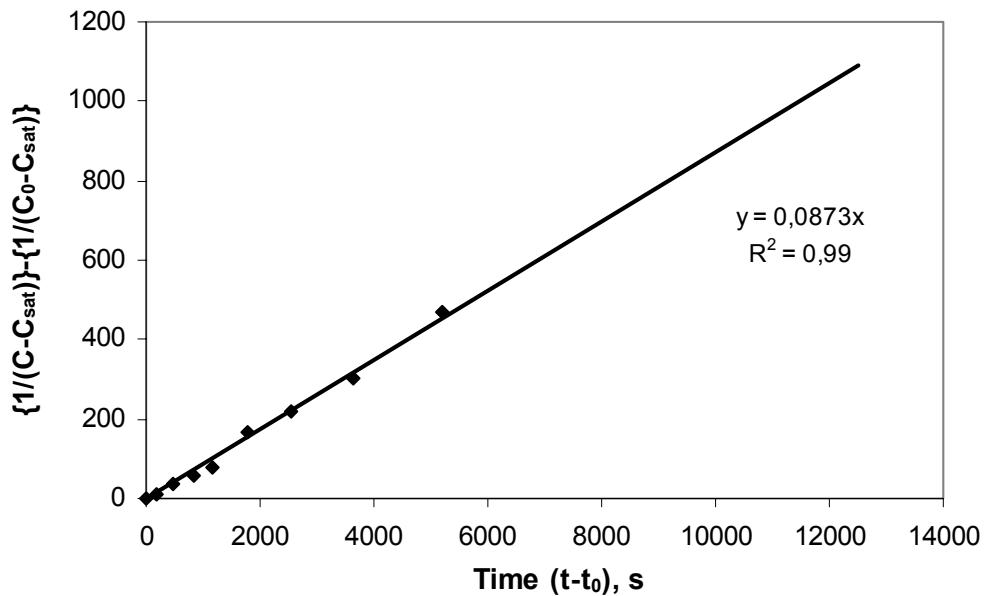


Fig. 5.7.2. Reciprocal concentration of calcium ion as a function of time plot for Experiment HB2.3, Hisarcık 2, 0-250 μm , experiment at initial $\text{CaO}/\text{SO}_4^{2-}$ molar ratio of 1, at 85°C and a stirring rate of 500 rpm.

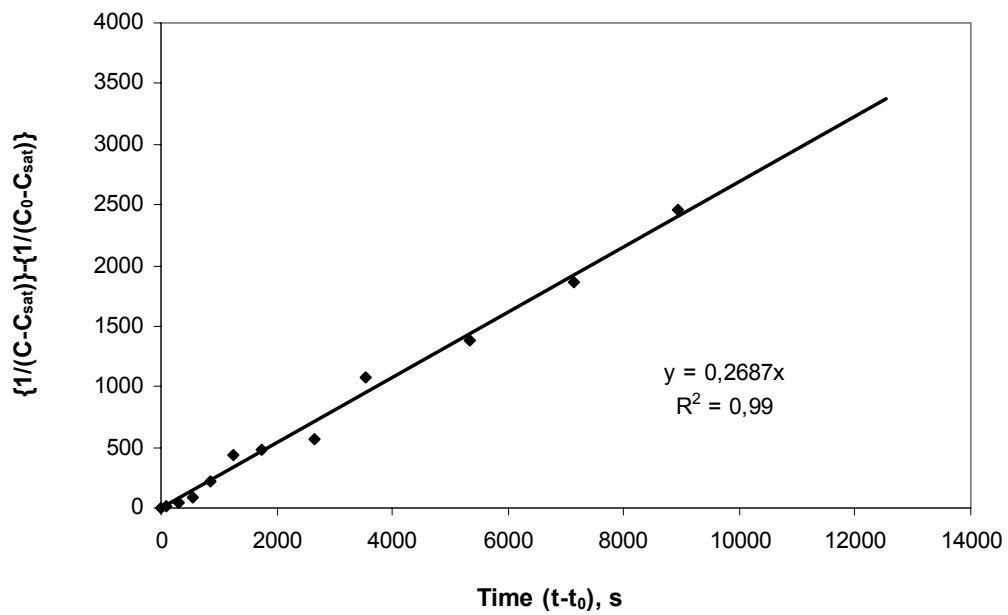


Fig. 5.7.3. Reciprocal concentration of calcium ion as a function of time plot for Experiment HB3.1, Hisarcık 3, 0-150 μm , experiment at initial $\text{CaO}/\text{SO}_4^{2-}$ molar ratio of 1, at 85°C and a stirring rate of 400 rpm.

The reaction rate constant, k' s, and the experimentally found concentration values are presented in Table 5.7.1 for all the batch experiments performed.

From the variation of calcium ion concentration in solution, amount of gypsum that will be formed can be deduced. Equation 3.4 can be rewritten, by inserting the model parameters in Table 5.7.1. The resulting equations, Equations 5.7.1-5.7.3, for each experiment is given in Table 5.7.2.

Table 5.7.1. The model parameters of the batch reactor experiments

Experiment Name	Colemanite	Particle Size	CaO/SO ₄ ²⁻ Molar Ratio	Temperature (°C)	Stirring Rate (Rpm)	K, L.Mol ⁻¹ .S ⁻¹	C ₀ , Mol/L	C _{sat} , Mol/L
HB2.1	Hisarcık 2	0-250 μm	0.95	80	500	0.027	0.053	0.013
HB2.2	Hisarcık 2	250-1000 μm	0.95	80	500			
HB2.3	Hisarcık 2	0-250 μm	1	85	500	0.087	0.043	0.011
HB3.1	Hisarcık 3	0-150 μm	1	85	400	0.269	0.0299	0.0056

Table 5.7.2. Gypsum Crystal Growth Model Obtained from Different Batch Reactor Experiments

Experiment Name	Particle Size, μM	$\text{CaO}/\text{So}_4^{2-}$ Molar Ratio	Temp. ($^{\circ}\text{C}$)	Stirring Rate (Rpm)	Gypsum Crystal Growth Model
HB2.1	0-250	0.95	80	500	$C(t) = \frac{49.1 + 0.013 t}{925.9 + t} \quad (5.7.1)$
HB2.2	250-1000	0.95	80	500	
HB2.3	0-250	1	85	500	$C(t) = \frac{14.46 + 0.011 t}{269.19 + t} \quad (5.7.2)$
HB3.1	0-150	1	85	400	$C(t) = \frac{4.24 + 0.0056 t}{93.15 + t} \quad (5.7.3)$

The calcium ion concentration variation graphs, Figures 5.2.2, 5.2.5 and 5.2.6 are redrawn in Figures 5.7.4-5.7.6 by inserting the models expressions in Eq. 5.7.1-5.7.3, respectively.

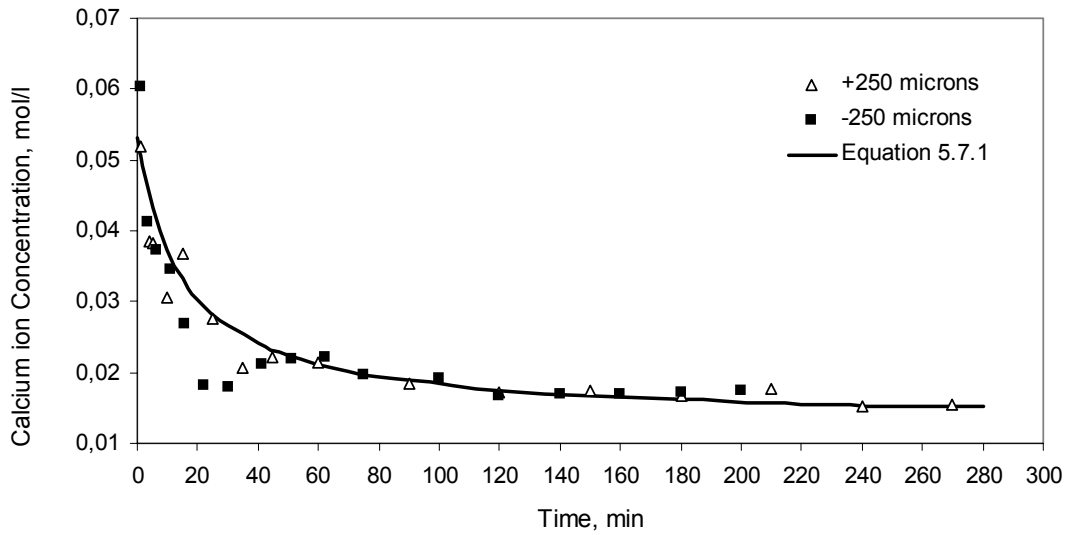


Fig. 5.7.4. Variations in the calcium ion concentration depending on the colemanite particle size during the dissolution of colemanite in aqueous sulfuric acid at 80°C and a stirring rate of 500 rpm. The initial $\text{CaO}/\text{SO}_4^{2-}$ molar ratio is 0.95. Experimental data were compared with the rate expression given in Eq 5.7.1

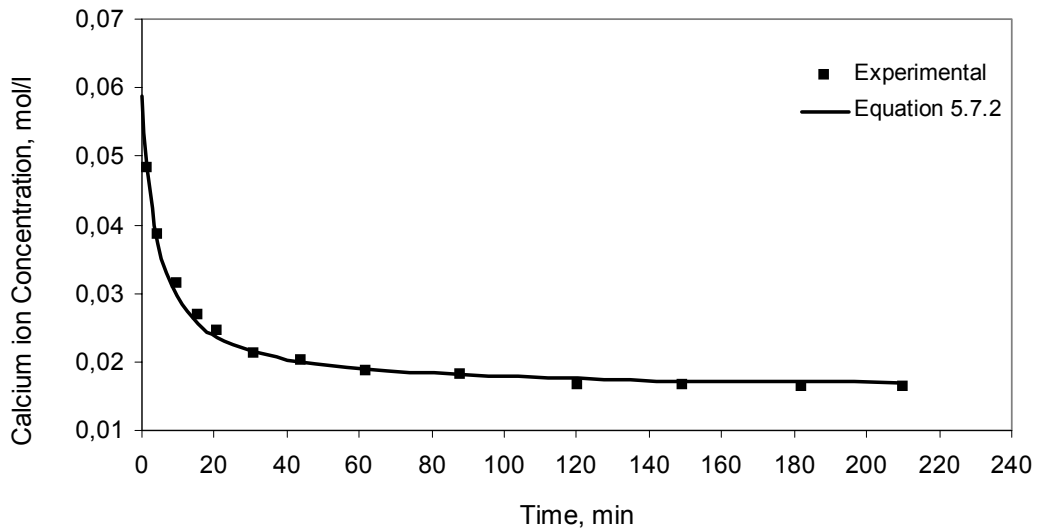


Fig. 5.7.5. Variations in the calcium ion concentration during the dissolution of Hisarcık 2, 0-250 μm , colemanite in aqueous sulfuric acid at 85°C and a stirring rate of 500 rpm. The initial $\text{CaO}/\text{SO}_4^{2-}$ molar ratio is 1.0. Experimental data were compared with the rate expression given in Eq 5.7.2

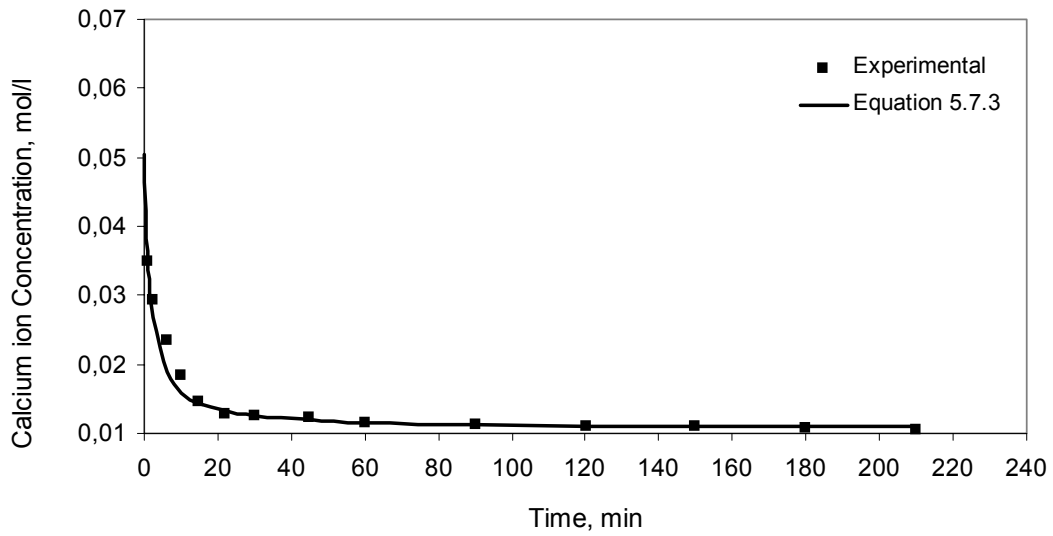


Fig. 5.7.6. Variations in the calcium ion concentration during the dissolution of Hisarcık 3, 0-150 μm , colemanite in aqueous sulfuric acid at 85°C and a stirring rate of 400 rpm. The initial $\text{CaO}/\text{SO}_4^{2-}$ molar ratio is 1. Experimental data were compared with the rate expression given in Eq 5.7.3

Although colemanite coating with gypsum is obviously seen in Figure 5.7.4, as explained in Section 5.3, it is not considered in this model. So, all the colemanite put into the reactor is said to dissolve in the very first minutes.

5.7.2. SIMULATION OF CONTINUOUS FLOW REACTORS

The gypsum growth model parameters were used to evaluate the concentration of calcium ion at the exit of the continuous flow reactors; plug flow reactor model (PFR) and continuous flow stirred tank reactors (CSTR) in series model by either macrofluid or microfluid approach.

5.7.2.1. MACROFLUID MODEL FOR N-CSTR'S IN SERIES

In macrofluid model, Equation 3.13 was used for the evaluation of exit concentration of Ca^{2+} , \bar{C} , which is the average concentration:

$$\bar{C} = \int_0^{\infty} C(t) \cdot E(t) dt \quad (3.13)$$

For a constant volume batch reactor, the calcium ion concentrations as a function of time, $C(t)$, was found in Equations. 5.7.1-5.7.3. These equations were solved together with the residence time distribution function, $E(t)$, to give the exit calcium ion concentration.

For the n-CSTR, the calcium ion concentrations at the outlet of the n^{th} reactor, \bar{C}_n , is obtained by combining Equations 3.5, 3.7 and 5.7.1-5.7.3. The resulting equation by using the model in Equation 5.7.1 can be written as:

$$\bar{C}_n = \int_0^{\infty} \frac{49.1 + 0.013 t}{925.9 + t} \cdot \frac{t^{n-1}}{(n-1)! \tau_i^n} e^{-t/\tau_i} dt \quad (5.7.4)$$

The calcium ion concentration at the exit of the reactors was estimated by using the Mat Lab program utilizing numerical integration techniques for 1 to 8 CSTR's in series. The program is given in Appendix G.1. The resulting values for the calcium ion concentrations are presented in Tables 5.7.3-5.7.5, for the models in Eqns 5.7.1-5.7.3, respectively. The space time in each CSTR can be found by dividing total space time to the number of reactors.

Table 5.7.3. The calcium ion concentration evaluated at the exit of the n^{th} CSTR, estimated by macrofluid model using the rate expression in Eq. 5.7.1 ($C_o = 0.053$ mol/l, $C_{\text{sat}} = 0.013$ mol/l)

Number of CSTR's	Total Space Time, τ				
	20 min	40 min	60 min	100 min	240 min
1-CSTR	0.0349	0.0295	0.0266	0.0234	0.0191
2-CSTR	0.0329	0.0270	0.0240	0.0208	0.0169
3-CSTR	0.0322	0.0261	0.0230	0.0199	0.0163
4-CSTR	0.0318	0.0256	0.0226	0.0195	0.0161
6-CSTR	0.0313	0.0251	0.0221	0.0191	0.0158
8-CSTR	0.0311	0.0249	0.0219	0.0189	0.0157

Table 5.7.4. The calcium ion concentration evaluated at the exit of the n^{th} CSTR, estimated by macrofluid model using the rate expression in Eq. 5.7.2 ($C_o = 0.043$ mol/l, $C_{\text{sat}} = 0.011$ mol/l)

Number of CSTR's	Total Space Time, τ				
	20 min	40 min	60 min	100 min	240 min
1-CSTR	0.0245	0.0202	0.0182	0.0162	0.0138
2-CSTR	0.0217	0.0175	0.0158	0.0141	0.0124
3-CSTR	0.0207	0.0167	0.0151	0.0136	0.0121
4-CSTR	0.0202	0.0163	0.0147	0.0134	0.0120
6-CSTR	0.0197	0.0159	0.0145	0.0132	0.0119
8-CSTR	0.0195	0.0158	0.0143	0.0131	0.0119

Table 5.7.5. The calcium ion concentration evaluated at the exit of the n^{th} CSTR, estimated by macrofluid model using the rate expression in Eq. 5.7.3 ($C_o = 0.0299$ mol/l, $C_{\text{sat}} = 0.0056$ mol/l)

Number of CSTR's	Total Space Time, τ				
	20 min	40 min	60 min	100 min	240 min
1-CSTR	0.0125	0.0100	0.0089	0.0079	0.0068
2-CSTR	0.0102	0.0082	0.0074	0.0067	0.0061
3-CSTR	0.0095	0.0077	0.0071	0.0065	0.0060
4-CSTR	0.0092	0.0075	0.0069	0.0064	0.0059
6-CSTR	0.0089	0.0074	0.0068	0.0063	0.0059
8-CSTR	0.0088	0.0073	0.0067	0.0063	0.0059

The calcium ion concentration at the exit of the n -CSTR's are shown in Figures 5.7.7-5.7.9, having different space time (τ) of 20 to 240 min for the macrofluid model results given in Tables 5.7.3-5.7.5, respectively.

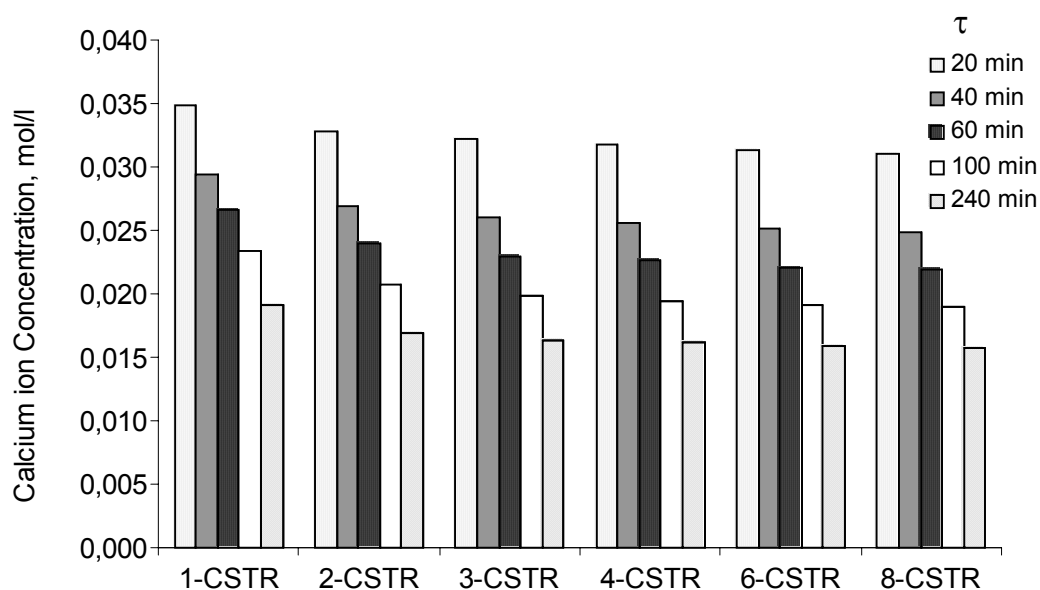


Fig. 5.7.7. The calcium ion concentration evaluated at the exit of the n^{th} CSTR, estimated by macrofluid model using the rate expression in Eq. 5.7.1

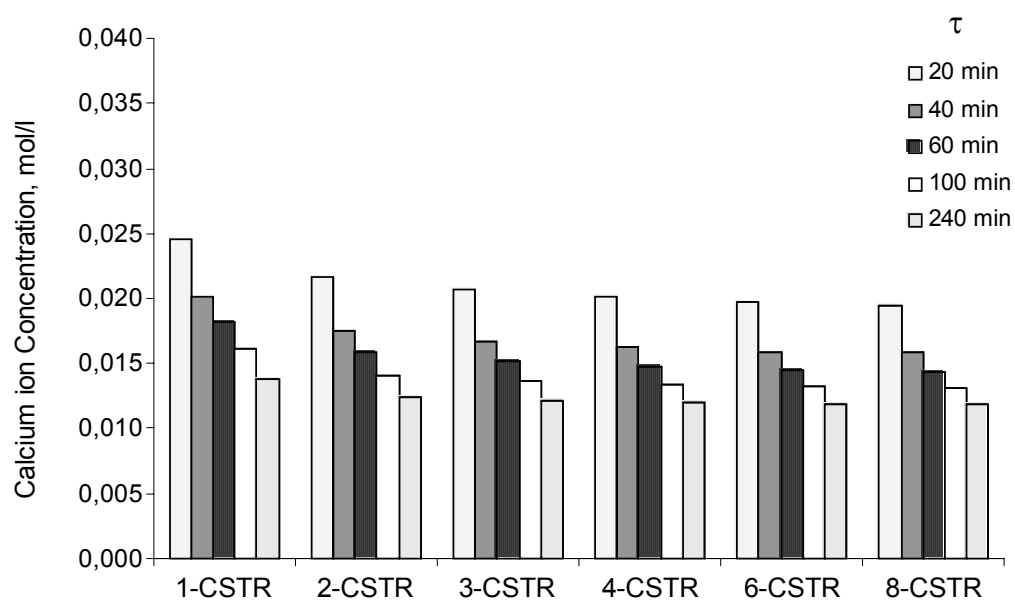


Fig. 5.7.8. The calcium ion concentration evaluated at the exit of the n^{th} CSTR, estimated by macrofluid model using the rate expression in Eq. 5.7.2

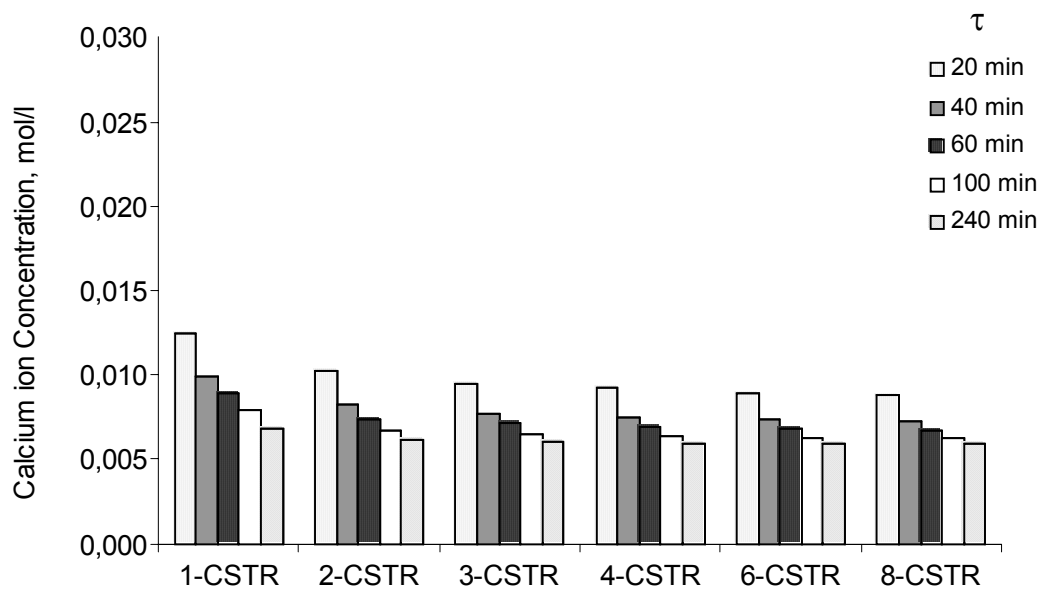


Fig. 5.7.9. The calcium ion concentration evaluated at the exit of the n^{th} CSTR, estimated by macrofluid model using the rate expression in Eq. 5.7.3

As examined from Figures 5.7.7-5.7.9, the average calcium ion concentrations at the exit of the CSTR's did not show significant decreases with the increase of CSTR number. On the other hand, the calcium ion concentration had a noteworthy decrease with the increase of residence time in each of the reactors.

5.7.2.2. MICROFLUID MODEL FOR N-CSTR'S IN SERIES

In the microfluid model, the liquid reactant is assumed to be completely or perfectly mixed. For n -CSTR's in series, the design equation for the n^{th} reactor was given in Equation 3.9 as

$$\frac{C_{n-1} - C_n}{\tau_j} = k(C_n - C_{\text{sat}})^2 \quad (3.15)$$

where the design equation was solved around each CSTR. While doing the microfluid model calculations, the space time is calculated in the same way as in the calculations of the macrofluid model, i.e. it is total space time in the n -CSTR's is the multiplication of τ_j with the number of CSTR's. A Mat Lab program was also written for the solution of the microfluid model and is given in Appendix G.2. Microfluid model results are presented for the total space times from 20 to 240 min

in Tables 5.7.6.-5.7.8 for the rate expressions in Equations 5.7.1-5.7.3, respectively, in the same way as macrofluid results to be easily comparable.

Table 5.7.6. The calcium ion concentration evaluated at the exit of the n^{th} CSTR, estimated by microfluid model using the rate expression in Eq. 5.7.1 ($C_o = 0.053$ mol/l, $C_{\text{sat}} = 0.013$ mol/l)

Number of CSTR's	Total Space Time, τ				
	20 min	40 min	60 min	100 min	240 min
1-CSTR	0.0359	0.0313	0.0288	0.0259	0.0219
2-CSTR	0.0337	0.0283	0.0255	0.0225	0.0187
3-CSTR	0.0328	0.0271	0.0242	0.0212	0.0176
4-CSTR	0.0322	0.0264	0.0235	0.0205	0.0170
6-CSTR	0.0317	0.0257	0.0228	0.0198	0.0165
8-CSTR	0.0314	0.0253	0.0224	0.0195	0.0162

Table 5.7.7. The calcium ion concentration evaluated at the exit of the n^{th} CSTR, estimated by microfluid model using the rate expression in Eq. 5.7.2 ($C_o = 0.043$ mol/l, $C_{\text{sat}} = 0.011$ mol/l)

Number of CSTR's	Total Space Time, τ				
	20 min	40 min	60 min	100 min	240 min
1-CSTR	0.0244	0.0212	0.0196	0.0179	0.0157
2-CSTR	0.0218	0.0185	0.0169	0.0154	0.0135
3-CSTR	0.0208	0.0175	0.0159	0.0145	0.0128
4-CSTR	0.0203	0.0169	0.0154	0.0140	0.0125
6-CSTR	0.0197	0.0163	0.0149	0.0136	0.0123
8-CSTR	0.0194	0.0161	0.0147	0.0134	0.0121

Table 5.7.8. The calcium ion concentration evaluated at the exit of the n^{th} CSTR, estimated by microfluid model using the rate expression in Eq. 5.7.3 ($C_o = 0.0299$ mol/l, $C_{\text{sat}} = 0.0056$ mol/l)

Number of CSTR's	Total Space Time, τ				
	20 min	40 min	60 min	100 min	240 min
1-CSTR	0.0129	0.0110	0.0101	0.0092	0.0080
2-CSTR	0.0108	0.0090	0.0083	0.0075	0.0067
3-CSTR	0.0100	0.0084	0.0077	0.0070	0.0063
4-CSTR	0.0096	0.0080	0.0074	0.0068	0.0062
6-CSTR	0.0092	0.0077	0.0071	0.0066	0.0061
8-CSTR	0.0090	0.0075	0.0070	0.0065	0.0060

The calcium ion concentration at the exit of the n -CSTR's are shown in Figures 5.7.10-5.7.12, having different space time (τ) of 20 to 240 min for the microfluid model results given in Tables 5.7.6-5.7.8, respectively.

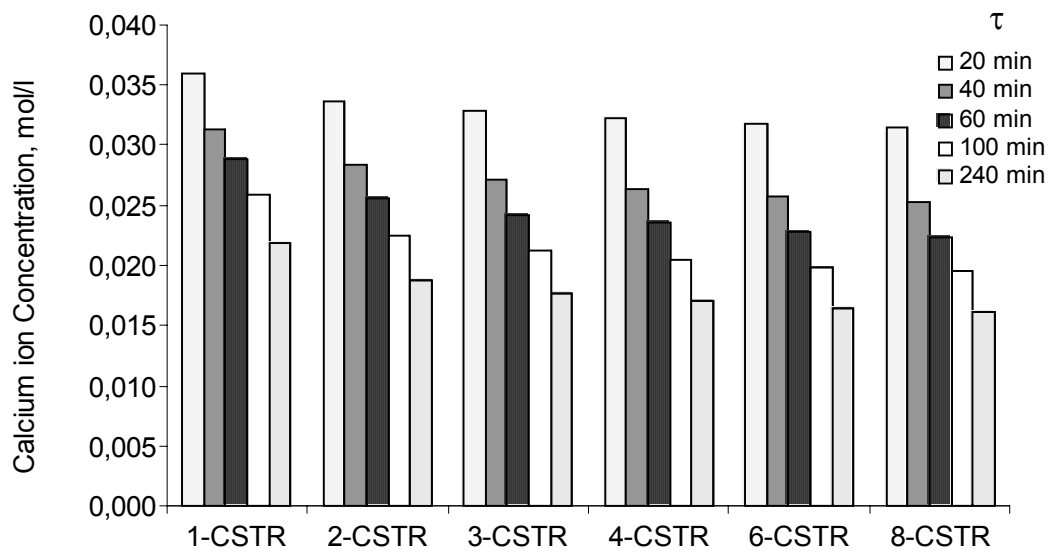


Figure 5.7.10. The calcium ion concentration evaluated at the exit of the n^{th} CSTR, estimated by microfluid model using the rate expression in Eq. 5.7.1

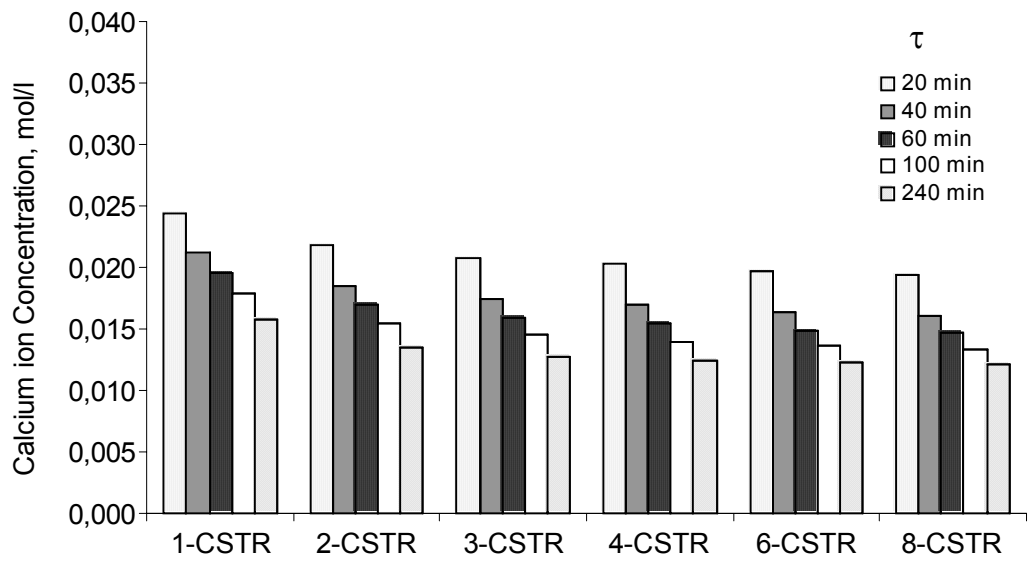


Fig. 5.7.11. The calcium ion concentration evaluated at the exit of the n^{th} CSTR, estimated by microfluid model using the rate expression in Eq. 5.7.2

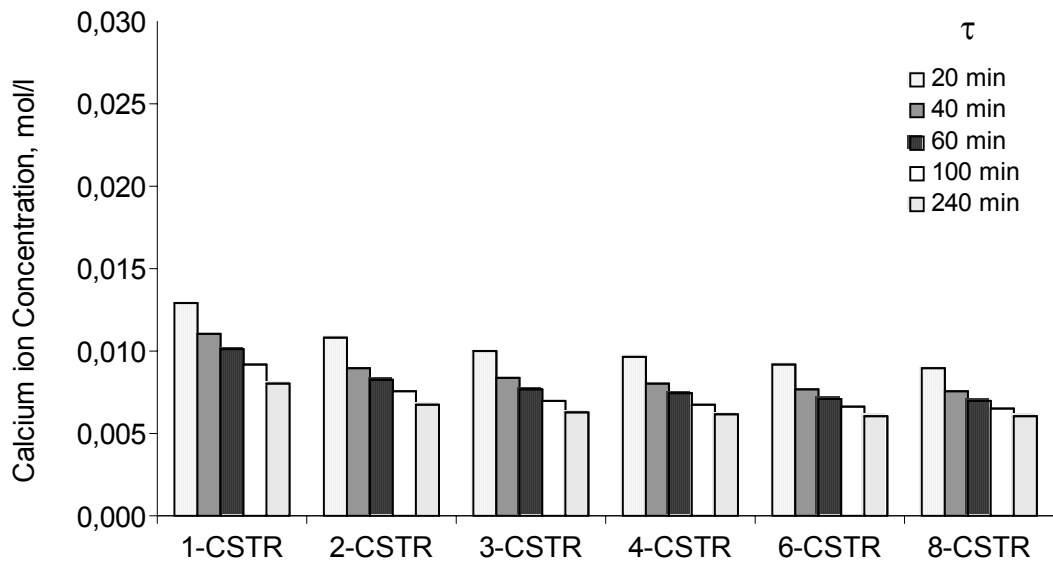


Fig. 5.7.12. The calcium ion concentration evaluated at the exit of the n^{th} CSTR, estimated by microfluid model using the rate expression in Eq. 5.7.3

The macrofluid and microfluid models seemed to give nearly the same results.

5.7.2.3. PLUG FLOW MODEL

The design equation for plug flow reactor was given in Equation 3.15. The calcium ion concentration as a function of space time is derived from Eq. 3.15 using the same kinetic parameters as in Table 5.7.1. The calcium ion concentration as a function of τ is given in Table 5.7.9.

Table 5.7.9. Plug Flow Model Expressions obtained with the model parameters in Table 5.7.1

Experiment Name	Particle Size, μM	$\text{CaO}/\text{So}_4^{2-}$ Molar Ratio	Temp. ($^{\circ}\text{C}$)	Stirring Rate (Rpm)	Gypsum Crystal Growth Model
HB2.1	-250	0.95	80	500	$C(\tau) = \frac{49.1 + 0.013 \tau}{925.9 + \tau} \quad (5.7.5)$
HB2.2	+250	0.95	80	500	
HB2.3	-250	1	85	500	$C(\tau) = \frac{14.46 + 0.011 \tau}{269.19 + \tau} \quad (5.7.6)$
HB3.1	-150	1	85	400	$C(\tau) = \frac{4.24 + 0.0056 \tau}{93.15 + \tau} \quad (5.7.7)$

where τ in Equations 5.7.5-5.7.7 was the volume of the liquid divided by the volumetric flow rate of liquid. It is assumed that liquid to solid volume ratio does not change along the reactor. There is no mixing in axial direction and complete mixing in liquid in radial direction. Eq. 5.7.5-5.7.7 were the same equations as Eq. 5.7.1-5.7.3, except t is the real time in a batch reactor whereas τ is the space time in PFR. The only difference in the equations was the usage of time, that was in a batch reactor t was used for time, as all the fluid spend the same amount of time in the reactor, whereas in a PFR, there was a residence time distribution, which led to the usage of τ .

The calcium ion concentration at the exit of the PFR was evaluated for different space times from 20 to 240 min for the expressions in Eq. 5.7.5-5.7.7 and the results are presented in Table 5.7.10.

Table 5.7.10. The calcium ion concentration evaluated at the exit of the PFR with the plug flow models given in Table 5.7.9

Experiment Name	Model Parameters	Space Time, τ				
		20 min	40 min	60 min	100 min	240 min
HB2.1 & HB2.2	$C_o=0.053$ mol/l $C_{sat}=0.013$ mol/l	0.0304	0.0241	0.0212	0.0184	0.0154
HB2.3	$C_o = 0.043$ mol/l $C_{sat} = 0.011$ mol/l	0.0188	0.0153	0.0140	0.0128	0.0118
HB3.1	$C_o = 0.0299$ mol/l $C_{sat} = 0.0056$ mol/l	0.0085	0.0071	0.0066	0.0062	0.0059

Plug Flow Model Results are drawn in Figure 5.7.13 with the model results in Table 5.7.10.

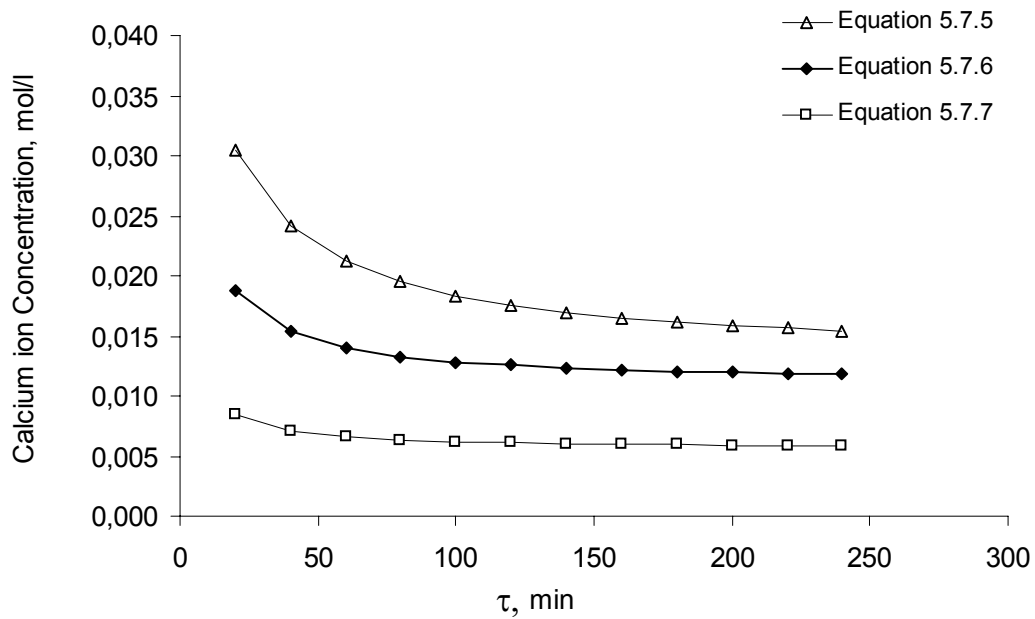


Figure 5.7.13. The calcium ion concentrations evaluated at the exit of the PFR depending on the model expressions in Eq. 5.7.5-5.7.7

The calcium ion concentrations at the exit of the PFR at different space times, τ , are given in Figure 5.7.13. As it can be observed, the model expression in Equation 5.7.7 gave the lowest calcium ion concentrations. The results of the n-CSTR's in series was comparable with that of the PFR, as the space time for PFR was taken as the total space time of the n-CSTR's.

5.7.2.4. COMPARISON OF MODEL RESULTS

The comparison of the calcium ion concentrations at the exit of the n-CSTR's by using macrofluid and microfluid approach and PFR are presented in Figures 5.7.14-5.7.16 at total space time of 40 min for the rate expressions in Eq. 5.7.1-5.7.3. (Eq. 5.7.5 - 5.7.7 for PFR).

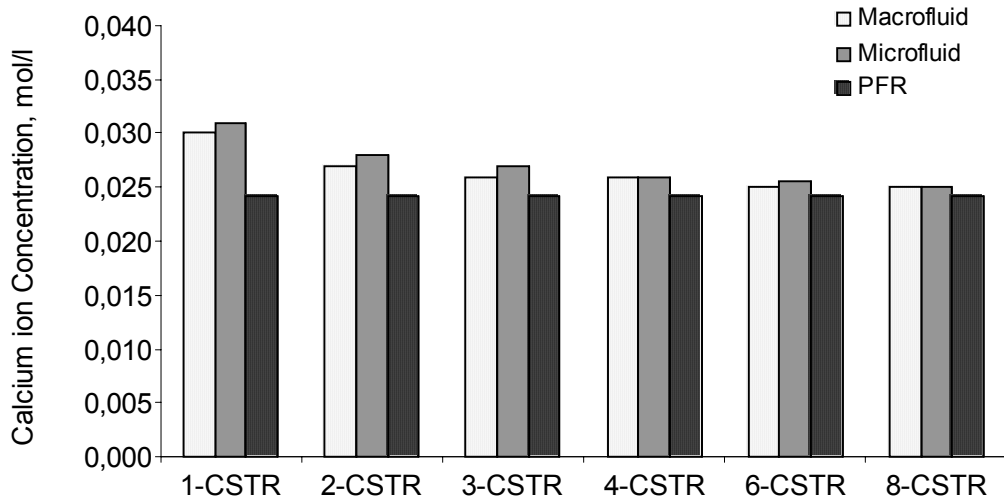


Figure 5.7.14. Comparison of calcium ion concentration at the exit of the n-CSTR's estimated by macrofluid and microfluid models and PFR by using the rate expression in Eq. 5.7.1 for total space time of 40 min.

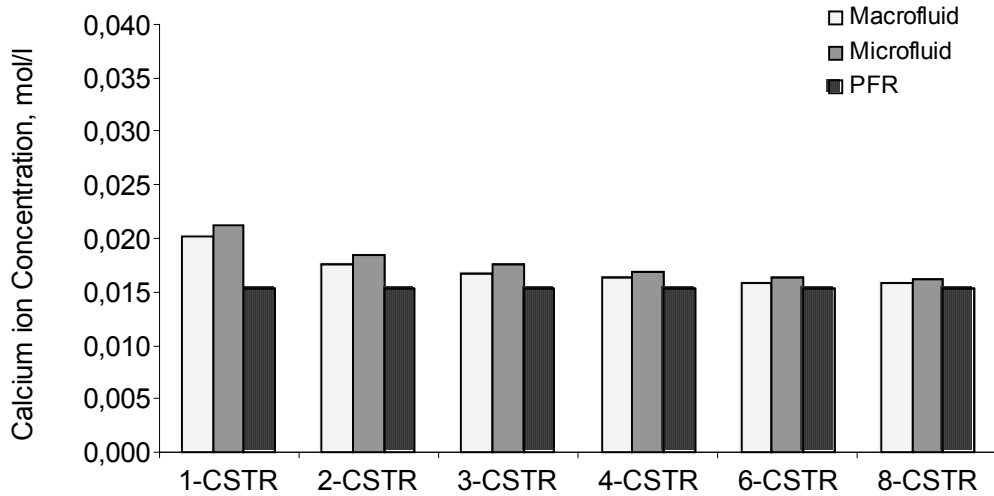


Fig. 5.7.15. Comparison of calcium ion concentration at the exit of the n-CSTR's estimated by macrofluid and microfluid models and PFR by using the rate expression in Eq. 5.7.2 for total space time of 40 min.

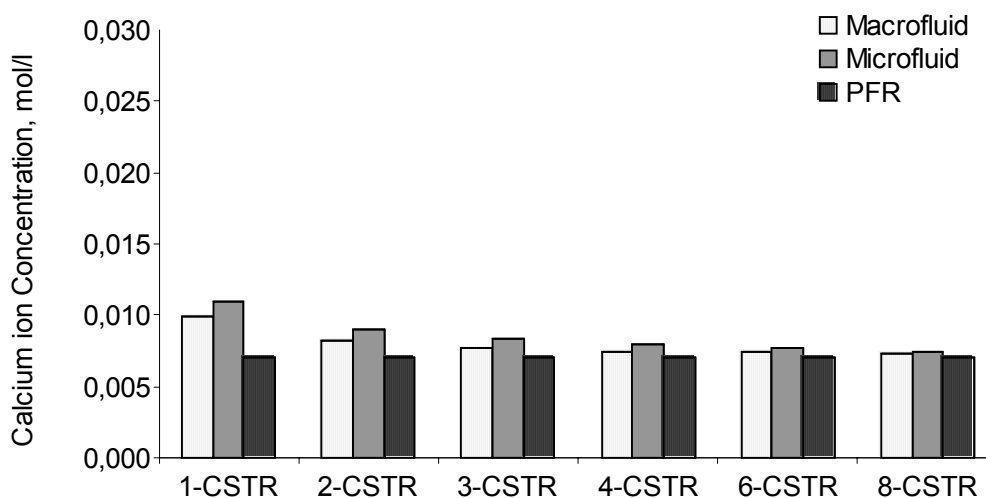


Figure 5.7.16. Comparison of calcium ion concentration at the exit of the n-CSTR's estimated by macrofluid and microfluid models and PFR by using the rate expression in Eq. 5.7.3 for total space time of 40 min.

The model results all gave the same behavior in Figures 5.7.14 - 5.7.16. The microfluid model gave higher calcium ion concentrations than the other two models as CSTR number decreases. If the number of CSTR's was increased, the model results come close to each other reaching the saturation concentration of calcium in each case.

The microfluid and macrofluid models were obtained by using the second order crystal growth model. The comparison of the microfluid, macrofluid models and PFR at $\tau = 40$ min was given in Figures 5.7.14-5.7.16. The same manner was also observed for the other residence times, namely, 20, 60, 100 and 240 min. It was seen at all the residence times that microfluid model gave higher calcium ion concentrations than the macrofluid model. The lowest concentration of calcium ion was found for the PFR, which approached to the saturation concentration of calcium. The difference in the models were significant in the first reactors, but as the reactor increased the difference decreased. Fogler (1992) also stated that for reaction orders greater than 1, the macrofluid model gives the highest conversion. In the models under study same conclusion can be drawn. As at lower calcium ion concentrations conversion was higher.

5.8. COMPARISON OF THE RESULTS

The results of the performed batch reactor and continuous reactor experiments were compared in terms of boric acid and calcium ion concentrations in solution. Also the volume weighted mean diameters of the gypsum crystals obtained from the particle size distribution curves were compared.

By using the gypsum crystal model the continuous boric acid reactors were simulated. The results of the models were verified with the experimental data.

5.8.1. BATCH REACTOR VERSUS CONTINUOUS REACTOR EXPERIMENTS

The compared batch and continuous reactor experiments were all performed at the same experimental conditions. Two sets of comparisons can be made by considering colemanites used. In the first set Hisarcık 2 colemanite with particle size of 0-250 μm was used, whereas in the second set Hisarcık 3 colemanite with particle size of 0-150 μm was used for the batch and continuous reactor experiments.

The experimental conditions were as follows: initial $\text{CaO}/\text{SO}_4^{2-}$ molar ratio was 1.00, temperature was 85°C and the stirring rate was 400 rpm. In one of the batch reactor experiments stirring rate was 500 rpm, but the stirring rate effect was shown to have a negligible effect on the boric acid and calcium ion concentrations obtained. It was also shown to have a negligible effect on the gypsum crystal growth rate constant. But stirring rate changed the particle size distribution of the gypsum crystal, and also the volume weighted mean diameters (Erdođdu, 2004).

The comparison of the batch and continuous reactors were given for Hisarcık 2 and Hisarcık 3 colemanites in Tables 5.8.1 and 5.8.2, respectively.

The boric acid concentrations obtained in the batch reactor experiments were not comparable with the continuous reactor experiments, as there was no initial addition of boric acid to the batch reactor. As seen from Tables 5.8.1 and 5.8.2, the calcium ion concentrations obtained from batch reactor experiments were reached

at higher residence times and increased reactor numbers. The pH values attained at the continuous reactor and the batch reactor were comparable.

The particle size of the gypsum crystals obtained in the batch and continuous reactors were also compared. It can be understood that even at lower residence times in a continuous reactor, the mean diameters of the gypsum crystals were higher than the one obtained in a batch reactor. At higher residence times the obtained gypsum crystals had the largest diameters.

Table 5.8.1. Comparison of batch reactor and continuous reactor results performed by Hisarcık 2, 0-250 μm , colemanite in terms of boric acid, calcium ion concentrations, pH and volume weighted mean diameter (μm) of the gypsum crystals obtained at initial $\text{CaO}/\text{SO}_4^{2-}$ molar ratio of 1.00, Stirring Rate = 500 rpm (batch), 400 rpm (continuous), temperature = 85°C

	Exp Name:		Residence Time of Solid, min	H_3BO_3 , mol/l	Ca^{2+} , mol/l	pH	Mean Diameter of Gypsum, μm
Batch Reactor	HB2.3		210	2.00	<i>0.0110*</i>	0.72	72.1
Continuous Reactor	HC2.1	Reactor 1	35	2.66	0.0125	0.47	240.1
		Reactor 2	35		0.0100	0.51	204.8
		Reactor 3	35		0.0075	0.51	159.8
		Reactor 4	35		0.0075	0.52	137.1
	HC2.2	Reactor 1	23	2.66	0.0325	0.16	130.4
		Reactor 2	23		0.0200	0.17	198.0
		Reactor 3	23		0.0175	0.15	85.3
		Reactor 4	23		0.0175	0.17	123.4
	HC2.3	Reactor 1	17	2.66	0.0250	0.49	79.1
		Reactor 2	17		0.0150	0.47	95.1
		Reactor 3	17		0.0150	0.45	84.4
		Reactor 4	17		0.0150	0.45	98.2

* Saturation concentration

Table 5.8.2. Comparison of batch reactor and continuous reactor results performed by Hisarcık 3, 0-150 μm , colemanite in terms of boric acid, calcium ion concentrations, pH and volume weighted mean diameter (μm) of the gypsum crystals obtained at initial $\text{CaO}/\text{SO}_4^{2-}$ molar ratio of 1.00, stirring rate =400 rpm, temperature = 85°C

	Exp Name:		Residence Time of Solid, min	H_3BO_3 , mol/l	Ca^{2+} , mol/l	pH	Mean Diameter of Gypsum, μm
	HB3.1		210	1.89	<i>0.0056*</i>	0.95	36.9
Continuous Reactor	HC3.1	Reactor 1	60	2.53	0.0105	0.65	130.7
		Reactor 2	60		0.0078	0.68	163.1
		Reactor 3	60		0.0068	0.71	96.3
		Reactor 4	60		0.0065	0.60	69.4
	HC3.2	Reactor 1	20	2.47	0.0138	0.30	105.6
		Reactor 2	20		0.0095	0.40	98.5
		Reactor 3	20		0.0083	0.46	43.8
		Reactor 4	20		0.0075	0.55	90.6

* Saturation concentration

5.8.2. VERIFICATION OF THE EXPERIMENTAL DATA WITH THE MODEL RESULTS

The results of experiments named as HC3.1 and HC3.2 were tried to be verified with the simulated models, namely the macrofluid and microfluid models. In these models model parameters found for the batch reactor experiment HB3.1 were used. In the batch and the continuous reactor experiments, the same conditions were supplied, where the initial $\text{CaO}/\text{SO}_4^{2-}$ molar ratio was 1.00, temperature was 85°C and the stirring rate was 400 rpm.

In order to verify the experimental data with the simulated models, first the Mat Lab program was executed for residence times of 20 and 60 min at each reactor. The output of the program was given in Appendix G.3.

The calcium ion concentrations obtained from the macrofluid, microfluid models and the experiments at each reactor having a residence time of 20 and 60 min, for Experiments HC3.2 and HC3.1, respectively, are given in Table 5.8.1.

It was observed from Table 5.8.1 that the experimentally found calcium ion concentrations were close to the microfluid model results. The deviation of the experimental results from the model results were also calculated and named as %error in Equations 5.8.1 and 5.8.2 for microfluid and macrofluid model results, respectively.

$$\% \text{ error} = \frac{C_{\text{micro}} - C_{\text{exp}}}{C_{\text{micro}}} \cdot 100 \quad (5.8.1)$$

$$\% \text{ error} = \frac{C_{\text{macro}} - C_{\text{exp}}}{C_{\text{macro}}} \cdot 100 \quad (5.8.2)$$

It was calculated that % error with Equation 5.8.1 was between 4 – 7%, i.e. the calcium ion concentrations obtained by experiments were that much higher than the microfluid model results. If the % error was calculated with Equation 5.8.2, it was seen that the experimental values were 10-19% higher than the macrofluid model results.

Table 5.8.3. Calcium ion concentrations at the exit of the CSTR's obtained by macrofluid, microfluid models and the experimental data

Ca²⁺, ppm					Ca²⁺, mol/l			
Residence Time = 20 min								
	Reactor 1	Reactor 2	Reactor 3	Reactor 4	Reactor 1	Reactor 2	Reactor 3	Reactor 4
Macrofluid Model	500	328	284	264	0.0125	0.0082	0.0071	0.0066
Microfluid Model	516	360	308	280	0.0129	0.0090	0.0077	0.0070
Experiment HC3.2	550	380	330	300	0.0138	0.0095	0.0083	0.0075
Residence Time = 60 min								
	Reactor 1	Reactor 2	Reactor 3	Reactor 4	Reactor 1	Reactor 2	Reactor 3	Reactor 4
Macrofluid Model	356	260	244	236	0.0089	0.0065	0.0061	0.0059
Microfluid Model	404	292	260	248	0.0101	0.0073	0.0065	0.0062
Experiment HC3.1	420	310	270	260	0.0105	0.0078	0.0068	0.0065

The experimental data was found to be closer to the microfluid model, which stated that the reaction occurs in the solution, not on the globules. To remind ourselves, globules were the formed gypsum crystals with the surrounding liquid. This concept was explained in Chapter 3, macrofluid modeling section.

The residence times of the solid and the liquid were taken equal to each other during the modeling and the $E(t)$ expression was defined for globules. In general $E(t)$ was defined for single phase systems. By doing the above assumption, $E(t)$ was possible to be used in this multiphase system. The residence times of the solid and the liquid were also found to be equal to each other, supporting the assumption. Also, the experimental data verified the microfluid model, which reveals the information that this multiphase system can be regarded as a single phase during modeling.

CHAPTER 6

CONCLUSIONS

One of the most important boron minerals, colemanite is reacted with sulfuric acid to produce boric acid. During this reaction, gypsum is formed as byproduct. The gypsum crystals formed in the reaction are in the shape of thin needles. These crystals, mixed with the insolubles coming from the mineral, are removed from the boric acid slurry by filtration. Filtration of gypsum crystals has an important role in boric acid production reaction because it affects the efficiency, purity and crystallization of boric acid. These crystals must grow to an appropriate size in the reactor. The growth process of gypsum crystals should be synchronized with the dissolution reaction. From the experiments performed on the batch and continuous flow stirred slurry reactor systems with three different colemanites having different particle sizes, the following conclusions were reached:

1. Although the colemanite used in the experiments had the same origin, the compositions and particle sizes were different. That is, the B_2O_3/CaO ratio of the colemanite could change during the experiments. This affects the amount of sulfuric acid addition to the reactor. The quality of boric acid produced was directly changed.
2. The dynamic behavior study was important in a solid-liquid system. This study was used for the detection of non-ideality in the reactors. This study showed that the reactors used in the experiments approached an ideal CSTR.

3. The selection of the tracer was also important in the dynamic behavior studies. The tracer that should be used during the experiments of the colemanite-water system was chosen as lithium. The other tracers either adsorbed on the colemanite or colemanite received some ions to the solution.
4. The solid hold-up in the colemanite-water system was changed from 0.085-0.034 g solid/ml liquid and the effect of solid hold-up on the residence time of the liquid was studied. It was seen that at low solid hold-ups, the residence time of the liquid was low, but the reverse was true for the high solid hold-ups.
5. It should be emphasized that a study on the dynamic behavior of continuous flow stirred slurry reactors gave valuable information on the product quality and the yield of the solid-liquid reactors.
6. The batch reactor experiments showed that during the dissolution of colemanite, the colemanite could be coated with gypsum, which slowed down the dissolution reaction.
7. As the particle size of colemanite decreased, the dissolution rate of colemanite increased. On the other hand, the number of nuclei of gypsum crystals increased with decreasing diameters.
8. The gypsum crystal growth kinetics, attained from the batch reactor data, differed with the change of colemanite, but for the same colemanite with differing particle sizes (0-250 μm , 250-1000 μm) the following kinetic model was obtained.

$$C(\tau) = \frac{49.1 + 0.013 \tau}{925.9 + \tau} \quad (5.7.5)$$

9. At the initial $\text{CaO}/\text{SO}_4^{2-}$ molar ratio of 1.00 and 1.37, the colemanite entering the reactor was totally converted to boric acid. There existed no unconverted colemanite in the solid, except at the initial $\text{CaO}/\text{SO}_4^{2-}$ molar ratio of 2.17.
10. The magnesium and sulfate ion concentrations were the selected impurities to be examined. It was seen that at initial $\text{CaO}/\text{SO}_4^{2-}$ molar ratios of 1.37 the sulfate and magnesium ion concentrations were lower than the values observed at the ratio of 1.00.
11. The decrease of the impurity concentrations with the increase of colemanite flow rate was also observed at constant initial $\text{CaO}/\text{SO}_4^{2-}$ molar ratio. The boric acid and calcium ion concentrations, on the other hand, increased with increasing initial $\text{CaO}/\text{SO}_4^{2-}$ molar ratios.
12. It was seen that at high residence times the L/D ratio of the crystals increased in the first reactors, but they were broken due to the high stirring rate in the 3rd reactor. It was observed that the gypsum crystals grew wider and taller in a continuous reactor. The crystals had volume weighted mean diameters of even 240 μm .
13. In the batch reactor the slurry had a residence time of 210 min. The residence times of continuous reactors, on the other hand, were varied by altering the colemanite feed rates. From the comparison of the two types of reactors, it can be seen that the calcium ion concentrations obtained in continuous reactors were close to the saturation concentration obtained in the batch reactor, especially for the cases of high residence time.
14. The mean diameters of the crystals obtained in the continuous reactors, especially at high residence times, were bigger than the ones obtained in a batch reactor.
15. It was seen that the average calcium ion concentration at the exit of the continuous reactors evaluated with the microfluid model were higher than

the macrofluid model, which stated that higher conversions were achieved with a macrofluid model.

16. As the residence time at each reactor increased, the calcium ion concentration decreased reaching to the saturation concentration of calcium. The increase of reactor number did not have a considerable effect on the calcium ion concentration.
17. The simulated models were verified with the experimental data. The experimentally found calcium ion concentrations checked with the concentrations found from the microfluid model. It was also calculated that the experimental data obeyed the microfluid model with a deviation of 4-7%.
18. The microfluid model states that the reaction was done in solution, not on the globules, the formed gypsum crystals with the surrounding fluid. With this behavior, boric acid that was produced was not hidden in the clumps but found in solution. That shows no segregation occurred under the processing conditions. In fact, segregation or formation of clumps is not wanted. Since they hinder valuable boric acid solution inside of them, they will be lost in filtration unit. It will decrease the yield of the process.

CHAPTER 7

RECOMMENDATIONS

From the studies done on the batch and continuous flow stirred slurry reactors in series system, the following points are recommended:

1. As the B_2O_3/CaO ratio of the colemanite can change during the experiments, sulfuric acid addition to the reactor changes, accordingly. There should be a pH control in the tank for the controlled sulfuric acid addition to avoid the variation of the colemanite.
2. For the industrial and future applications, scale up of the reactors and process control of the n-CFSSR's in series it is recommended to do the dynamic behavior study as it shows the way information was taken from the system.
3. As it is possible to have deviations from the ideal patterns, especially working with slurry reactors, the dynamic behavior study should be performed before the start-up of the industrial reactors. The tracer can even be given to the first reactor while the reaction is occurring in the reactors. The tracer then will be detected from each of the reactors effluent streams.
4. The tracer tests are also recommended to be repeated from time to time to find out if there is an increased solid hold-up or not in the reactor. It is critical to avoid the overflow.
5. The laboratory scale experiments lead to some recommendations. From the results of the calcium ion concentration and the mean diameters of the gypsum crystals it was recommended to have up to three continuous flow

stirred slurry reactors in series. The residence time of the slurry should be high and it was better to use the initial $\text{CaO}/\text{SO}_4^{2-}$ molar ratio of 1.37.

6. By the use of the laboratory scale data, it is not possible to work on the industrial scale. In between on a pilot plant should be constructed and the studies should be done on pilot scale.
7. By taking samples from the industrial plant, analysis should be performed on the samples to check the laboratory scale data.
8. The industrial reactors can be simulated by the use of the dynamic behavior study done on the industrial reactors and by the use of the kinetic parameters obtained from the batch reactor experiments. These batch reactor experiments should be performed with the conditions of the industrial reactors.
9. In this study, the ideal pattern of mixed flow was obtained in the studied conditions. The non-ideal conditions can also be studied. The simulation of the continuous reactors can be done for these cases.

REFERENCES

Abouzeid A.-Z.M. and Fuerstenau D.W., "Effect of Mixing Aids on the Transport Behavior of Particulate Solids", *Powder Technology*, Vol. 23, pp. 261-271, 1979

Abouzeid A.-Z.M., Fuerstenau D.W. and Sastry K.V.S., "Transport Behavior of Particulate Solids in Rotary Drums: Scale-Up of Residence Time Distribution Using the Axial Dispersion Model", *Powder Technology*, Vol. 27, pp. 241-250, 1980

Alkhaddar R.M., Higgins P.R., Philips D.A. and Andoh R.Y.G., "Residence Time Distribution of a Model Hydrodynamic Vortex Separator", *Urban Water*, Vol. 3, pp. 17-24, 2001

Amethyst Galleries, 1997

URL: <http://mineral.galleies.com/minerals/carbonat/colemani/colemani.htm>

Anderson J., "Microphase Assisted Autocatalysis", Ph.D. Thesis, Iowa State University, Ames, Iowa, 1996

Anderson J.G., Doraiswamy L.K. and Larson M.A., "Microphase-Assisted 'Autocatalysis' in a Solid-Liquid Reaction with a Precipitating Product - I. Theory", *Chemical Engineering Science*, Vol. 53, No. 13, pp. 2451-2458, 1998a

Anderson J.G., Doraiswamy L.K. and Larson M.A., "Microphase-Assisted 'Autocatalysis' in a Solid-Liquid Reaction with a Precipitating Product - II. Experimental", *Chemical Engineering Science*, Vol. 53, No. 13, pp. 2459-2468, 1998b

Amjad Z., "Kinetics of Crystal Growth of Calcium Sulfate Dihydrate. The Influence of Polymer Composition, Molecular Weight, and Solution pH", *Can. J. Chem.*, Vol. 66, pp. 1529-1536, 1988

Balkan A. and Tolun R., "Factors Affecting the Formation of Gypsum in the Production of Boric Acid from Colemanite", *Bull. Tech. Univ. İstanbul*, Vol. 38, pp. 207-231, 1985

Badens E., Veessler S. and Boistelle R., "Crystallization of Gypsum from Hemihydrate in Presence of Additives", *Journal of Crystal Growth*, Vol. 198/199, pp. 704-709, 1999

Baptista P.N., Oliveira F.A.R., Sannervik J. and Oliveira J.C., "The Effect of Mixing Particles with Different Characteristics on the Residence Time Distribution of

Particles in Two-Phase Flow in a Tubular System”, Journal of Food Engineering, Vol. 29, pp. 361-373, 1996

Bechtloff B., Jüsten P., Ulrich J., “The Kinetics of Heterogenous Solid-liquid Reaction Crystallizations-An Overview and Examples”, Chemie Ingenieur Technik, Vol.73, pp.453-460, 2001

Bilal C., Taylan N., Gürbüz H., Bulutcu A.N., “Effect of H₂SO₄, H₃BO₃ and Gypsum on the Dissolution of Colemanite in Sulfuric Acid Solution” ,Workshop on Advance In Sensoring In Industrial Crystallization, 18-20 June, pp.65-72, 2003

Bratz E., 2001

URL: <http://thor.tech.chemie.tu-munchen.de/~bratz/faqce/answ9a.htm>

Boisvert J.P., Domenech M.,Foissy A., Persello J. and Mutin J.C., “Hydration of Calcium Sulfate Hemihydrate (CaSO₄.1/2H₂O) into Gypsum (CaSO₄.2H₂O). The Influence of the Sodium Poly(acrylate)/Surface Interaction and Molecular Weight”, Journal of Crystal Growth, Vol. 220, pp. 579-591, 2000

Brandse W.P., van Rosmalen G.M. and Brouwer G., “The Influence of Sodium Chloride on the Crystallization Rate of Gypsum”, J. Inorg. Nucl. Chem., Vol. 39, pp. 2007-2010, 1977

Chai C-P, Valderrama J.O.,”A New Approach to View Partial Segregation Model in Chemical Reactors”, Chemical Engineering Science, Vol. 37, No. 3, pp. 494-496, 1982

Christoffersen M.R., Christoffersen J., Weijnen M.P.C. and van Rosmalen G.M., “Crystal Growth of Calcium Sulfate Dihydrate at Low Supersaturation”, Journal of Crystal Growth, Vol. 58, pp. 585-595, 1982

Çetin E., “Investigation on the Kinetics of Gypsum Formation in the Reaction of Boric Acid Production from the Colemanite and Sulphuric Acid”, M.Sc. Thesis, Middle East Technical University, Ankara, Turkey, 2000

Çetin E., Eroğlu İ. and Özkar S., “Kinetics of Gypsum Formation and Growth during the Dissolution of Colemanite in Sulfuric Acid”, Journal of Crystal Growth, Vol. 231, pp. 559-567, 2001

Danckwerts P.V., “Continuous Flow Systems Distribution of Residence times”, Chemical Engineering Science, Vol. 2, pp 1-13, 1953

Danckwerts P.V., “The Efect of Incomplete Mixing on Homogenous Reactions “, Chemical Engineering Science, Vol. 8, pp. 93-102 , 1958

Di Felice R.,”Mixing in Segregated, Binary-Solid Liquid-Fluidized Beds”, Chemical Engineering Science, Vol. 48, No. 5, pp. 881-888, 1993

Doraiswamy L.K., “Microphase-Assisted Reaction Engineering” in: Organic Synthesis Engineering, Oxford University Press Inc, New York, Chapter 23, pp. 744-764, 2001

Easton A.J., "Chemical Analysis of Silicate Rocks", Elsevier Publishing Company, London, 1972

Erdoğan Y., Aksu M., Demirbaş A. and Abalı Y., "Analyses of Boronic Ores and Sludges and Solubilities of Boron Minerals in CO₂-Saturated Water", Resources, Conservation and Recycling, Vol. 24, pp. 275-283, 1998

Erdođdu A., M.Sc. Thesis, Middle East Technical University, Ankara, Turker, 2004

Erdođdu A., Çakal G.Ö., Özkar N., Özkar S., Erođlu İ., "Effect of Particle Size of Colemanite on Gypsum Formation During Boric Acid Production", Workshop on Advance In Sensoring In Industrial Crystallization, 18-20 June, pp.41-48, 2003

Fogler, F.S., "The Elements of Chemical Reaction Engineering", 3rd Ed., Prentice Hall PTR, NJ, 1999

Friedman H., "The Mineral and Gemstone Kingdom", 1999
URL: <http://www.minerals.net/mineral/borates/colemani/colemani.htm>

Glatzer H.J. and Doraiswamy L.K., "Rate Enhancements Due To Autocatalysis and Heterogenization in Phase Transfer Catalysis: A Comparative Study", Chemical Engineering Science, Vol. 55, pp. 5149-5160, 2000

Gill J.S. and Nancollas G.H., "Kinetics of Growth of Calcium Sulfate Crystals at Heated Metal Surfaces", Journal of Crystal Growth, Vol. 48, pp. 34-40, 1980

Gürbüz H., Öçgüder S., Yavaşođlu-Taylan N., Sayan P. and Bulutcu A.N., "Kolemanitin Borik Asit Çözeltisinde Çözünürlüğü", UKMK 3, Erzurum, 2-4 Eylül, pp. 1259-1264, 1998

Hagenson L.C., Naik S.D. and Doraiswamy L.K., "Rate Enhancements in a Solid-Liquid Reaction Using PTC, Microphase, Ultrasound and Combinations Thereof", Chemical Engineering Science, Vol. 49, No. 24A, pp. 4787-4800, 1994

Hand R.J., "Calcium Sulfate Hydrates: A Review", British Ceramic Transactions, Vol. 96, No.3, pp. 116-120, 1997

Helvacı C. and Firman R.J., "Geological Setting and Mineralogy of Emet Borate Deposits, Turkey", Inst. Mining Metall Section B85, pp. 142-152, 1976

Imamutdinova V.M., Kol'tsov S.I., Zhurnal Priladno Kmimii, Vol. 51, No. 2, pp.249, 1978

Izumi T., "Model Analysis of Segregation Phenomena for Silicon Single Crystal Growth from Melt", Journal of Crystal Growth, Vol. 181, pp. 210-217, 1997

Kalafatođlu İ.E., Örs N. and Özdemir S.S., "Hisarcık Kolemanitinin Sülfürik Asitle Çözünme Davranışı", UKMK 4, İstanbul, 4-7 Eylül, 2000

Kiared K., Larachi F., Guy C. and Chaouki J., "Trajectory Length and Residence-Time Distributions of the Solids in Three-Phase Fluidized Beds", Chemical Engineering Science, Vol. 52, Nos. 21/22, pp. 3931-3939, 1997

Kirk Othmer Encyclopedia of Chemical Technology, 4th Ed., John-Wiley and Sons Inc., N.Y., 1992

Klepetsanis P.G. and Koutsoukos P.G., "Precipitation of Calcium Sulfate Dihydrate at Constant Calcium Activity", Journal of Crystal Growth, Vol. 98, pp. 480-486, 1989

Klepetsanis P.G. and Koutsoukos P.G., "Spontaneous Precipitation of Calcium Sulfate at Conditions of Sustained Supersaturation", Journal of Colloid and Interface Science, Vol. 143, pp. 299-308, 1991

Klepetsanis P.G. and Koutsoukos P.G., "Kinetics of Calcium Sulfate Formation in Aqueous Media: Effect of Organophosphorus Compounds", Journal of Crystal Growth, Vol. 193, pp. 156-163, 1998

Klepetsanis P.G., Dalas E. and Koutsoukos P.G., "Role of Temperature in the Spontaneous Precipitation of Calcium Sulfate Dihydrate", Langmuir, Vol. 15, pp. 1534-1540, 1999

Kocakerim M.M. and Alkan M., "Dissolution Kinetics of Colemanite in SO₂-Saturated Water", Hydrometallurgy, Vol. 19, pp. 385-392, 1988

Levenspiel O., "Chemical Reaction Engineering", 3rd Ed., John Wiley & Sons, NY, 1999

Liu S.T. and Nancollas G.H., "The Crystal Growth and Dissolution of Barium Sulfate in the Presence of Additives", Journal of Colloid and Interface Science, Vol. 52, pp. 582-592, 1975a

Liu S.T. and Nancollas G.H., "A Kinetic and Morphological Study of the Seeded Growth of Calcium Sulfate Dihydrate in the Presence of Additives", Journal of Colloid and Interface Science, Vol. 52, pp. 593-601, 1975b

Liu S.T., Nancollas G.H. and Gasiiecki E.A., "Scanning Electron Microscopic and Kinetic Studies of the Crystallization and Dissolution of Barium Sulfate Crystals", Journal of Crystal Growth, Vol. 33, pp. 11-20, 1976

Mehra A., "Intensification of Multiphase Reactions Through the Use of a Microphase – I. Theoretical", Chemical Engineering Science, Vol. 43, No. 4, pp. 899-912, 1988

Mehra A., "Intensification of Multiphase Reactions Through the Use of a Microphase – II. Experimental", Chemical Engineering Science, Vol. 43, No. 4, pp. 913-927, 1988

Method J.C., Roy P.H., "Experimental Evaluation of a Model-Based Degree of Segregation in a CSTR", Chemical Engineering Science, Vol. 28, pp. 1961-1966, 1973

Nancollas G. H., Reddy M.M. and Tsai F., "Calcium Sulfate Dihydrate Crystal Growth in Aqueous Solution at Elevated Temperatures", Journal of Crystal Growth, Vol. 20, pp. 125-134, 1973

Okur H., Tekin T., Ozer A.K., Bayramoğlu M., "Effect of Ultrasound on Dissolution of Colemanite in H_2SO_4 ", Hydrometallurgy, Vol. 67 pp. 79-86, 2002

Öner M., Doğan Ö. and Öner G., "The Influence of Polyelectrolytes Architecture on Calcium Sulfate Dihydrate Growth Retardation", Journal of Crystal Growth, Vol. 186, pp. 427-437, 1998

Özbayoğlu G. and Poslu K., "Mining and Processing of Borates in Turkey", Mineral Processing and Extractive Metallurgy Review, Vol. 9, pp. 245-254, 1992

Özmetin C., Kocakerim M.M., Yapıcı S. and Yartaşı A., "A Semiempirical Kinetic Model for Dissolution of Colemanite in Aqueous CH_3COOH Solutions", Ind. Eng. Chem. Res., Vol. 35, No. 7, pp. 2355-2359, 1996

Packter A., "The Precipitation of Calcium Sulfate Dihydrate from Aqueous Solution: Induction Periods, Crystal Numbers and Final Size", Journal of Crystal Growth, Vol. 21, pp. 191-194, 1974

Rinaudo C., Lanfranco A.M. and Boistelle R., "The Gypsum-Brushite System: Crystallization from Solutions Poisoned by Phosphate Ions", Journal of Crystal Growth, Vol. 158, pp. 316-321, 1996

Ramaswamy H.S., Abdelrahim K.A., Simpson B.K. and Smith J.P., "Residence Time Distribution (RTD) in a Aseptic Processing of Particulate Foods: A Review", Food Research International, Vol. 28, No. 3, pp. 291-310, 1995

Smith B.R. and Alexander A.E., "The Effect of Additives on the Process of Crystallization II. Further Studies on Calcium Sulfate (1)", Journal of Colloid and Interface Science, Vol. 34, No.1, pp. 81-90, 1970

Smith B.R. and Sweett F., "The Crystallization of Calcium Sulfate Dihydrate", Journal of Colloid and Interface Science, Vol. 37, No.3, pp. 612-618, 1971

Smolders K. and Baeyens J., "Overall Solids Movement and Solids Residence Time Distribution in a CFB-Riser", Chemical Engineering Science, Vol. 55, pp. 4101-4116, 2000

Stokes R.L. and Nauman E.B., "Residence Time Distribution Functions for Stirred Tanks in Series", The Canadian Journal of Chemical Engineering, Vol. 48, pp. 723-725, 1970

Tavare N.S., "Mixing, Reaction and Precipitation: An Interplay in continuous Crystallizers", Chemical Engineering Science, Vol. 49, No. 24B, pp. 5193-5201, 1994

Tunç M. and Kocakerim M.M., "Kolemanitin H_2SO_4 Çözeltisinde Çözünme Kinetiği", UKMK 3, Erzurum, 2-4 Eylül, pp. 1235-1240, 1998

Wes G.W.J., Drinkenburg A.A.H. and Stermerding S., "Solids Mixing and Residence Time Distribution in a Horizontal Rotary Drum Reactor", Powder Technology, Vol. 13, pp. 177-184, 1976

Woods G.W., "An Introduction to Boron: History, Sources, Uses, and Chemistry", Environmental Health Perspectives, Vol. 102, No. 7, pp. 5-11, 1994

Zauner R., Jones A.G., "On the Influence of Mixing on Crystal Precipitation Processes – Application of Segregated Feed Model", Chemical Engineering Science, Vol. 57, pp. 821-831, 2002

Zwietering T.N., "the Degree of Mixing in Continuous Flow Systems", Chemical Engineering Science, Vol. 11, pp. 1-15, 1959

APPENDIX A

CHEMICAL ANALYSIS OF COLEMANITE

A.1. DETERMINATION OF B₂O₃ CONTENT

1 g of grinded colemanite is weighed and put into a 250 ml flask. Then, 10 ml of H₂SO₄ (1/3 by volume) and 75 ml of distilled water are added. Condenser is attached to the flask. The obtaining slurry is heated until the boiling point of the slurry. After that, 10 drops of methyl-red indicator are added and the slurry is neutralized with dehydrated Na₂CO₃ by adding it slowly. Condenser is again attached to the flask and the slurry is heated until it boils. After that step, the slurry is filtered by using blue band filter paper. The cake and flask are washed with hot distilled water until the volume of the filtrate reaches a final volume of about 150 ml. 1:3 (by vol.) H₂SO₄ is added to the solution until the color of the solution changes from yellow to pink. After obtaining the pink color, 1ml of H₂SO₄ is added as excess. The solution in the flask is heated until it boils. Condenser is attached to the flask at the heating procedure. If the color of the solution turns back to yellow, a small amount of sulfuric acid is added. The solution in the flask is cooled to the room temperature. Water bath can be used for cooling. Then, 6 N NaOH is put into the flask until the color changes from pink to yellow. After this step, H₂SO₄ is again added to the solution until the color turns back to pink. This solution is titrated with 0.1 N NaOH until a pH of 4.5 is obtained. At this step a titrator involving a magnetic stirrer and pH-meter may be used to get accurate results. Then, phenolphthaleyn indicator and 10-15 g mannitol are added to the solution. The solution is again titrated with 0.1 N NaOH until the pH of the solution becomes 8.5. The volume of the NaOH used in the second step of titration is recorded and used to calculate the percentage of boron trioxide, B₂O₃, from the following formula:

$$\begin{aligned} \% \text{ B}_2\text{O}_3 &= (V_{\text{NaOH}} * F_{\text{NaOH}} * 0.1) / n * (69.6202/2) * (100/1000) \\ &= 0.348101 * (V_{\text{NaOH}} * F_{\text{NaOH}}) / n \end{aligned}$$

where

V_{NaOH} = Volume of NaOH required for titration after adding the mannitol to the solution, ml

F_{NaOH} = Factor of the 0.1 N NaOH solution

n = Amount of sample, g

A.2. DETERMINATION OF SiO₂ CONTENT

One gram sample is put into a platinum crucible and mixed with 4-6 grams of Na₂CO₃. The mixture is covered with 2 g Na₂CO₃. Temperature of the oven is increased to 1000 °C. The mixture is put into oven and it is waited for an hour. The mixture melts and the crucible is taken out the oven. The mixture is cooled and put inside 50 ml HCl (1+1) into a beaker. The solution is vaporized in an hot-plate until it becomes dry. This process is repeated twice. Then, 10 ml HCl and 100 ml hot water is added to the dry and cold solid mixture.

The solution is filtered through Whatman 42 filter paper. The inside of the beaker is washed with hot HCl (1+99). The filtrate is washed 10 times with hot HCl (1+99) and 5 times with hot water. After this process, the liquid portion of the last washing process is analyzed if chlorine ions remain in the cake. Therefore, three drops of liquid are mixed with 2 ml 0.1 N AgNO₃ and 1 drop 4N HNO₃. If white precipitation occurs, it means the filtrate contains chlorine ions. The filtrate is washed until the removal of chlorine ions.

The filter cake is burned in an 1000 °C oven and weighed. Then, into the crucible, a few drops of H₂SO₄ (1+1) and 10 ml HF are added. The mixture is vaporized in hote-plate gradually until white fume comes. The crucible is kept at 1000 °C for 2 minutes. Then weighed again. The difference of two values is the weight of SO₂ (Easton, 1972).

A.3 DETERMINATION OF Na₂O AND K₂O CONTENT

Into a platinum crucible, 0.5-1 g of sample is put. 5 ml of H₂SO₄ is added and the solution is mixed. Then, 5 ml of hydrofluoric acid is added and the solution is heated until sulfuric acid evaporates. When the solution is cooled, the procedure is repeated until the solid particles disappear. The solution is cooled; the wet sample is solved in water. The solution is heated until it becomes clear. After the solution is cooled, it is put inside a 200-ml flask and water is added. Then Na₂O and K₂O content of the solution are determined by Flame Photometer (Jenway PFP7 Flame Photometer) (Easton, 1972).

A.4. DETERMINATION OF CaO, MgO, Al₂O₃, Fe₂O₃, SrO AND TiO₂ CONTENT

One gram of sample is put into a platinum crucible and mixed with 4-6 grams of Na₂CO₃. The mixture is covered with 2 g Na₂CO₃. Temperature of the oven is increased to 1000 °C. The mixture is put into oven and it is waited for an hour. The mixture melts and the crucible is taken out the oven. The mixture is cooled and put inside 50 ml HCl (1+1) into an beaker. The solution is vaporized in an hot-plate until it becomes dry. This process is repeated twice. Then, 10 ml HCl and 100 ml hot water is added to the dry and cold solid mixture. The solution is filtered through Whatman 42 filter paper. The liquid is analyzed in Atomic Absorbtion Spectrophotometer for CaO, MgO, Al₂O₃, Fe₂O₃, SrO and TiO₂ content (Easton, 1972).

APPENDIX B

RAW DATA OF DYNAMIC BEHAVIOR EXPERIMENTS

Dynamic behavior experimental data of the solid / liquid system was given in three sections;

B.1. Data of Liquid Residence Time Experiments

B.2. Data of Solid Residence Time Experiments

B.3. Data of Liquid Residence Time Experiments in a Solid / Liquid System

B.1: DATA OF LIQUID RESIDENCE TIME EXPERIMENTS

Table B.1. Variation in nickel concentrations, ppm, in liquid residence time experiments at different stirring rates

Time interval Δt (min)	Average time in interval t	Stirring Rate	
		500 rpm	750 rpm
0-10	5	5.24	4.16
10-20	15	4.35	3.32
20-30	25	3.58	2.67
30-40	35	2.86	2.11
40-50	45	2.17	1.64
50-60	55	1.65	1.29
60-70	65	1.31	1.07
70-80	75	1.03	0.84
80-90	85	0.83	0.69
90-100	95	0.69	0.55
100-110	105	0.56	0.46
110-120	115	0.46	0.36
120-130	125	0.39	0.3
130-140	135	0.31	0.25
140-150	145	0.25	0.19
150-160	155	0.21	0.16
160-170	165	0.14	0.15
170-180	175	0.12	0.12
180-190	185	0.12	0.12
190-200	195	0.09	0.09
200-210	205	0.09	
210-220	215	0.06	
220-230	225	0.05	
230-240	235	0.04	

Table B.2. Comparison of E(t) and F(t) values of the liquid residence time experiments and the ideal reactor (Pulse tracer=Nickel)

Time	<i>E(t) values</i>			<i>F(t) values</i>		
	500 rpm	750 rpm	Ideal	500 rpm	750 rpm	Ideal
0			0.02294			0.000
5	0.0198	0.0203	0.02045	0	0	0.108
15	0.0164	0.0162	0.01626	0.362	0.364	0.291
25	0.0135	0.0130	0.01293	0.497	0.494	0.436
35	0.0108	0.0103	0.01028	0.605	0.597	0.552
45	0.0082	0.0080	0.00817	0.687	0.677	0.644
55	0.0062	0.0063	0.00650	0.749	0.740	0.717
65	0.0049	0.0052	0.00516	0.798	0.792	0.775
75	0.0039	0.0041	0.00411	0.837	0.833	0.821
85	0.0031	0.0034	0.00326	0.868	0.866	0.858
95	0.0026	0.0027	0.00260	0.894	0.893	0.887
105	0.0021	0.0022	0.00206	0.916	0.915	0.910
115	0.0017	0.0018	0.00164	0.933	0.933	0.928
125	0.0015	0.0015	0.00130	0.948	0.947	0.943
135	0.0012	0.0012	0.00104	0.959	0.960	0.955
145	0.0009	0.0009	0.00082	0.969	0.969	0.964
155	0.0008	0.0008	0.00066	0.977	0.977	0.971
165	0.0005	0.0007	0.00052	0.982	0.984	0.977
175	0.0005	0.0006	0.00041	0.986	0.990	0.982
185	0.0005	0.0006	0.00033	0.991	0.996	0.986
195	0.0003	0.0004	0.00026	0.994	1.000	0.989
205	0.0003		0.00021	0.998		0.991
215	0.0002		0.00017	1.000		0.993
225			0.00013			0.994
235			0.00010			0.995

Table B.3. Variation in the concentrations, ppm, of different tracers on the liquid residence time at 500 rpm

Time interval Δt (min)	Average time in interval t	Lithium Conc. (ppm)	Nickel Conc. (ppm)
0-10	5	4.9	5.24
10-20	15	4	4.35
20-30	25	3	3.58
30-40	35	2.3	2.86
40-50	45	1.9	2.17
50-60	55	1.5	1.65
60-70	65	1.2	1.31
70-80	75	0.9	1.03
80-90	85	0.7	0.83
90-100	95	0.6	0.69
100-110	105	0.5	0.56
110-120	115	0.4	0.46
120-130	125	0.3	0.39
130-140	135	0.2	0.31
140-150	145	0.3	0.25
150-160	155	0.2	0.21
160-170	165	0.1	0.14
170-180	175	0	0.12
180-190	185		0.12
190-200	195		0.09
200-210	205		0.09
210-220	215		0.06

Table B.4. Comparison of E(t) and F(t) values of different tracers (stirring rate=500 rpm) and the ideal reactor

Time	E(t) values			F(t) values		
	Lithium	Nickel	Ideal	Lithium	Nickel	Ideal
			0.02309			0.000
5	0.0213	0.0198	0.02058	0.000	0.000	0.117
15	0.0174	0.0164	0.01633	0.387	0.362	0.311
25	0.0130	0.0135	0.01296	0.517	0.497	0.463
35	0.0100	0.0108	0.01029	0.617	0.605	0.581
45	0.0083	0.0082	0.00817	0.700	0.687	0.674
55	0.0065	0.0062	0.00648	0.765	0.749	0.745
65	0.0052	0.0049	0.00515	0.817	0.798	0.801
75	0.0039	0.0039	0.00409	0.857	0.837	0.845
85	0.0030	0.0031	0.00324	0.887	0.868	0.879
95	0.0026	0.0026	0.00257	0.913	0.894	0.906
105	0.0022	0.0021	0.00204	0.935	0.916	0.927
115	0.0017	0.0017	0.00162	0.952	0.933	0.943
125	0.0013	0.0015	0.00129	0.965	0.948	0.955
135	0.0009	0.0012	0.00102	0.974	0.959	0.965
145	0.0013	0.0009	0.00081	0.987	0.969	0.973
155	0.0009	0.0008	0.00064	0.996	0.977	0.979
165	0.0004	0.0005	0.00051	1.000	0.982	0.984
175	0.0000	0.0005	0.00041	1.000	0.986	0.987
185		0.0005	0.00032		0.991	0.990
195		0.0003	0.00026		0.994	0.992
205		0.0003	0.00020		0.998	0.994
215		0.0002	0.00016		1.000	0.995

B.2: DATA OF SOLID RESIDENCE TIME EXPERIMENTS

Table B.5. Variation in colemanite weight during positive and negative step tracer experiments (Stirring Rate=500 rpm)

Time interval Δt (min)	Average time in interval t	Colemanite Weight (g)	
		Positive Step	Negative Step
0-5	2.5		21.3
5-10	7.5		20.9
10-15	12.5		21.3
15-20	17.5		21.2
20-25	22.5		21.5
25-30	27.5	0	21.3**
30-35	32.5	0.6	20.5
35-40	37.5	2.5	18.7
40-45	42.5	4.1	16.8
45-50	47.5	5.6	14.4
50-55	52.5	7.2	12.5
55-60	57.5	8.6	10.5
60-65	62.5	9.5	9.5
65-70	67.5	10.9	8.5
70-75	72.5	12.8	7.4
75-80	77.5	12.6	6.5
80-85	82.5	13.9	4.8
85-90	87.5	15.1	4.1
90-95	92.5	16.3	3.3
95-100	97.5	17.3	2.5
100-105	102.5	18.3	2.7
105-110	107.5	20.3	2.1
110-115	112.5	19.9	1.9
115-120	117.5	20.1	1
120-125	122,5	20.3	1.2
125-130	127,5	20.4	0.5
130-135	132,5	21.1	0.7
135-141	137,5	21.1	0.6
141-145	142,5	21.2	1
145-150	147,5	21.5	0.6
150-155	152,5	21.3	0.5
155-160	157,5	21.3	0.6

** Colemanite flow is stopped.

B.3: DATA OF LIQUID RESIDENCE TIME EXPERIMENTS IN A SOLID/LIQUID SYSTEM

Table B.6. Variation in nickel concentrations in liquid residence time experiments at different stirring rates

Time interval Δt (min)	Average time in interval t	Stirring Rate	
		500 rpm	750 rpm
0-10	5	5	5.3
10-20	15	4.6	4.6
20-30	25	3.8	3.5
30-40	35	3	2.8
40-50	45	2.6	2.3
50-60	55	2.2	2
60-70	65	1.9	1.8
70-80	75	1.6	1.5
80-90	85	1.4	1.3
90-100	95	1.2	1
100-110	105	1.1	0.9
110-120	115	1	0.8
120-130	125	0.9	0.7
130-140	135		0.7

Table B.7. Variation in lithium concentrations of liquid at different solid to liquid ratios (g solid/ml liquid)

Time interval Δt (min)	Average time in interval t	Solid to Liquid Ratio		
		S/L=0.085	S/L=0.17	S/L=0.34
0-10	5	5.0	5.0	5.0
10-20	15	3.3	4.6	4.8
20-30	25	2.3	3.8	4.2
30-40	35	1.6	3.0	3.9
40-50	45	1.1	2.6	3.4
50-60	55	0.8	2.2	3.2
60-70	65	0.7	1.9	3.0
70-80	75	0.6	1.6	2.7
80-90	85	0.5	1.4	2.5
90-100	95	0.5	1.2	2.3
100-110	105	0.5	1.1	2.0
110-120	115	0.4	1.0	1.8
120-130	125	0.4	0.9	1.8
130-140	135	0.4	0.9	1.6
140-150	145	0.4	0.9	1.2
150-160	155	0.4	0.9	1.1
160-170	165	0.4	0.9	0.9
170-180	175	0.4	0.9	0.9

Table B.8. The $-\ln(C/C_0)$ vs t values for different S/L ratios (g solid/ml liquid)

Average time in interval, t , min			$-\ln(C/C_0)$		
S/L=0.085	S/L=0.17	S/L=0.34	S/L=0.085	S/L=0.17	S/L=0.34
5	5	5	0.00	0.00	0.00
15	15	15	0.42	0.08	0.04
25	25	25	0.78	0.27	0.17
35	35	35	1.14	0.51	0.25
45	45	45	1.51	0.65	0.39
55	55	55	1.83	0.82	0.45
65	65	65	1.97	0.97	0.51
75	75	75	2.12	1.14	0.62
85	85	85	2.30	1.27	0.69
95	95	95	2.30	1.43	0.78
105	105	105	2.30	1.51	0.92
115	115	115	2.53	1.61	1.02
	125	125		1.71	1.02
	135	135		1.83	1.14
	145	145		1.97	1.43
		155			1.51
		165			1.71

APPENDIX C

RAW DATA OF BATCH REACTOR EXPERIMENTS

Four batch reactor experiments were performed. Raw data of them are submitted in this section.

C.1. Experiment HB2.1& HB2.2:

Hisarcık 2 Colemanite, 0-250 μm & 250-1000 μm , $\text{CaO}/\text{SO}_4^{2-} = 0.95$,
Stirring Rate = 500 rpm, T= 80°C

C.2. Experiment HB2.3:

Hisarcık 2 Colemanite, 0-250 μm , $\text{CaO}/\text{SO}_4^{2-} = 1$,
Stirring Rate = 500 rpm, T= 85°C

C.3. Experiment HB3.1:

Hisarcık 3 Colemanite, 0-150 μm , $\text{CaO}/\text{SO}_4^{2-} = 1$,
Stirring Rate = 400 rpm, T= 80°C

C.1: DATA OF EXPERIMENT HB2.1& HB2.2

Table C.1. Boric acid and calcium ion concentrations during the Experiment HB2.1, Hisarcık 2 colemanite, 0-250 μm , $\text{CaO}/\text{SO}_4^{2-} = 0.95$, stirring rate = 500 rpm, T= 80°C

Time, min	H_3BO_3 , mol/l	Ca^{2+} , mol/l
1	1.02	0.0603
4	1.14	0.0412
7	1.16	0.0372
11	1.24	0.0344
16	1.21	0.0268
22	1.26	0.0182
30	1.29	0.0180
41	1.28	0.0212
51	1.29	0.0219
62	1.29	0.0221
75	1.35	0.0197
100	1.34	0.0192
120	1.38	0.0167
140	1.41	0.0169
160	1.43	0.0170
180	1.45	0.0173
200	1.52	0.0174

Table C.2. Boric acid and calcium ion concentrations during the Experiment HB2.2, Hisarcık 2 colemanite, 250-1000 μm , $\text{CaO}/\text{SO}_4^{2-} = 0.95$, stirring rate = 500 rpm, T= 80°C

Time, min	H_3BO_3 , mol/l	Ca^{2+} , mol/l
1	0.77	0.0518
4	0.86	0.0386
5	0.94	0.0382
10	0.98	0.0306
15	1.02	0.0368
25	1.02	0.0275
35	1.03	0.0205
45	1.03	0.0221
60	1.13	0.0214
90	1.15	0.0185
120	1.20	0.0171
150	1.27	0.0176
180	1.38	0.0166
210	1.48	0.0176
240	1.49	0.0153
270	1.46	0.0155

C.2: DATA OF EXPERIMENT HB2.3

Table C.3. Boric acid and calcium ion concentrations during the Experiment HB2.3, Hisarcık 2 colemanite, 0-250 μm , $\text{CaO}/\text{SO}_4^{2-} = 1$, stirring rate = 500 rpm, $T = 85^\circ\text{C}$

Time, min	H_3BO_3 , mol/l	Ca^{2+} , mol/l
1.5	1.44	0.043
4.5	1.56	0.034
9.5	1.57	0.026
15.5	1.60	0.022
21	1.63	0.020
31	1.65	0.016
44	1.67	0.015
62	1.69	0.014
88	1.78	0.013
120	1.83	0.012
149	1.95	0.012
182	2.00	0.011
210	2.00	0.011

Table C.4. Variation in pH during the Experiment HB2.3, Hisarcık 2 colemanite, 0-250 μm , $\text{CaO}/\text{SO}_4^{2-} = 1$, stirring rate = 500 rpm, $T = 85^\circ\text{C}$

Time, min	pH
4	0.67
7	0.71
13	0.77
23	0.79
35	0.81
47	0.82
66	0.82
90	0.82
122	0.81
157	0.78
185	0.75
210	0.72

C.3: DATA OF EXPERIMENT HB3.1

Table C.5. Boric acid and calcium ion concentrations during the Experiment HB3.1, Hisarcık 3 colemanite, 0-150 μm , $\text{CaO}/\text{SO}_4^{2-} = 1$, stirring rate = 400 rpm, $T = 85^\circ\text{C}$

Time, min	H_3BO_3 , mol/l	Ca^{2+} , mol/l
1		0.0299
2.3	1.45	0.0242
6	1.48	0.0184
10	1.57	0.0134
15	1.58	0.0095
22	1.58	0.0077
30	1.60	0.0075
45	1.67	0.0073
60	1.68	0.0065
90	1.75	0.0063
120	1.79	0.0061
150	1.88	0.0060
180	1.86	0.0059
210	1.89	0.0056

Table C.6. Variation in pH during the Experiment HB3.1, Hisarcık 3 colemanite, 0-150 μm , $\text{CaO}/\text{SO}_4^{2-} = 1$, stirring rate = 400 rpm, $T = 85^\circ\text{C}$

Time, min	pH
5	0.72
9	0.76
13	0.8
18	0.84
25	0.88
34	0.90
48	0.91
64	0.94
94	0.95
120	0.95
150	0.95
180	0.95

APPENDIX D

RAW DATA OF BORIC ACID PRODUCTION EXPERIMENTS IN CONTINUOUSLY STIRRED SLURRY REACTORS

All the experiments were performed at a stirring rate of 400 rpm and a temperature of 85°C. The raw data of ten experiments are presented in this section.

D.1. Experiment HC2.1:

Hisarcık 2 Colemanite, 0-250 μm , $\text{CaO}/\text{SO}_4^{2-} = 1.00$, colemanite feed rate = 5 g/min

D.2. Experiment HC2.2:

Hisarcık 2 Colemanite, 0-250 μm , $\text{CaO}/\text{SO}_4^{2-} = 1.00$, colemanite feed rate = 7.5 g/min

D.3. Experiment HC2.3:

Hisarcık 2 Colemanite, 0-250 μm , $\text{CaO}/\text{SO}_4^{2-} = 1.00$, colemanite feed rate = 10 g/min

D.4. Experiment HC2.4:

Hisarcık 2 Colemanite, 0-250 μm , $\text{CaO}/\text{SO}_4^{2-} = 1.37$, colemanite feed rate = 5 g/min

D.5. Experiment HC2.5:

Hisarcık 2 Colemanite, 0-250 μm , $\text{CaO}/\text{SO}_4^{2-} = 1.37$, colemanite feed rate = 10 g/min

D.6. Experiment HC2.6:

Hisarcık 2 Colemanite, 0-250 μm , $\text{CaO}/\text{SO}_4^{2-} = 1.37$, colemanite feed rate = 10 g/min

D.7. Experiment HC2.7:

Hisarcık 2 Colemanite, 0-250 μm , $\text{CaO}/\text{SO}_4^{2-} = 1.37$, colemanite feed rate = 15 g/min

D.8. Experiment HC2.8:

Hisarcık 2 Colemanite, 0-250 μm , $\text{CaO}/\text{SO}_4^{2-} = 2.17$, colemanite feed rate = 10 g/min

D.9. Experiment HC3.1:

Hisarcık 3 Colemanite, 0-150 μm , $\text{CaO}/\text{SO}_4^{2-} = 1.00$, colemanite feed rate = 3.5 g/min

D.10. Experiment HC3.2:

Hisarcık 3 Colemanite, 0-150 μm , $\text{CaO}/\text{SO}_4^{2-} = 1.00$, colemanite feed rate = 10 g/min

D.1. DATA OF EXPERIMENT HC2.1

Table D.1. Calcium ion concentrations of the effluent streams during the Experiment HC2.1, Hisarcık 2 colemanite, 0-250 μm , $\text{CaO}/\text{SO}_4^{2-} = 1$, stirring rate = 400 rpm, $T = 85^\circ\text{C}$, colemanite feed rate = 5 g/min

Reactor 1	Time (min)	Ca^{2+} (ppm)
	71	562
	129	483
	194	571
	254	549
	316	402
	382*	520
Reactor 2	Time (min)	Ca^{2+} (ppm)
	73	453
	131	342
	196	336
	257	373
	319	327
	384*	398
Reactor 3	Time (min)	Ca^{2+} (ppm)
	76	488
	133	299
	197	260
	259	312
	322	307
	386*	305
Reactor 4	Time (min)	Ca^{2+} (ppm)
	78	521
	136	367
	198	270
	261	274
	323	259
	379*	277

* No B_2O_3 was detected in the solid.

Table D.2. Temperature and pH values during the Experiment HC2.1, Hisarcık 2 colemanite, 0-250 μm , $\text{CaO}/\text{SO}_4^{2-} = 1$, stirring rate = 400 rpm, $T = 85^\circ\text{C}$, colemanite feed rate = 5 g/min

Reactor 1	Time (min)	Temperature ($^\circ\text{C}$)	pH
	54	81.8	0.69
	81	82.2	0.68
	122	82.1	0.70
	141	82.0	0.66
	195	81.7	0.39
	248	81.7	0.55
	263	82.2	0.49
	324	81.8	0.47
	379	82.3	0.45
Reactor 2	Time (min)	Temperature ($^\circ\text{C}$)	pH
	54	83.9	0.76
	81	83.9	0.71
	124	83.8	0.67
	142	83.7	0.72
	196	83.9	0.53
	265	83.9	0.50
	264	83.7	0.52
	325	83.6	0.52
	379	83.8	0.46
Reactor 3	Time (min)	Temperature ($^\circ\text{C}$)	pH
	54	84.6	1.09
	82	84.8	0.82
	124	84.6	0.73
	142	84.5	0.72
	197	84.5	0.62
	250	84.4	0.51
	265	84.5	0.49
	325	84.7	0.51
	379	85.0	0.51
Reactor 4	Time (min)	Temperature ($^\circ\text{C}$)	pH
	54	84.5	1.47
	82	84.9	0.98
	125	84.3	0.87
	143	84.5	0.77
	198	84.3	0.69
	250	84.4	0.60
	265	84.5	0.51
	326	84.5	0.53
	379	84.5	0.51

D.2. DATA OF EXPERIMENT HC2.2

Table D.3. Calcium ion concentrations of the effluent streams during the Experiment HC2.2, Hisarcık 2 colemanite, 0-250 μm , $\text{CaO}/\text{SO}_4^{2-} = 1$, stirring rate = 400 rpm, $T = 85^\circ\text{C}$, colemanite feed rate = 7.5 g/min

Reactor 1	Time (min)	Ca^{2+} (ppm)
	51	1512
	88	1243
	153	1302
	212	1363
	275	1213
	370*	1296
Reactor 2	Time (min)	Ca^{2+} (ppm)
	54	1093
	89	661
	154	796
	214	919
	301	782
	373*	746
Reactor 3	Time (min)	Ca^{2+} (ppm)
	57	841
	91	590
	155	738
	215	913
	302	656
	375*	657
Reactor 4	Time (min)	Ca^{2+} (ppm)
	60	793
	92	672
	181	573
	215	737
	303	726
	377*	675

* No B_2O_3 was detected in the solid.

Table D.4. Temperature and pH values during the Experiment HC2.2, Hisarcık 2 colemanite, 0-250 μm , $\text{CaO}/\text{SO}_4^{2-} = 1$, stirring rate = 400 rpm, $T = 85^\circ\text{C}$, colemanite feed rate = 7.5 g/min

Reactor 1	Time (min)	Temperature ($^\circ\text{C}$)	pH
	71	81.7	0.32
	92	81.7	0.15
	150	80.5	0.07
	193	80.6	0.05
	244	81.0	0.08
	263	80.9	0.10
	304	80.8	0.28
	320	81.7	0.23
	368	81.0	0.10
	385	81.0	0.10
Reactor 2	Time (min)	Temperature ($^\circ\text{C}$)	pH
	73	83.3	0.90
	94	83.3	0.34
	151	82.7	0.10
	194	82.7	0.08
	244	82.4	0.07
	263	82.1	0.09
	305	83.1	0.19
	320	83.5	0.21
	368	83.2	0.16
	385	83.3	0.11
Reactor 3	Time (min)	Temperature ($^\circ\text{C}$)	pH
	45	83.6	1.98
	73	83.8	2.01
	95	83.9	0.66
	152	83.8	0.15
	194	83.8	0.07
	263	83.7	0.07
	305	83.9	0.11
	321	83.7	0.15
	368	83.8	0.18
	385	83.8	0.13
Reactor 4	Time (min)	Temperature ($^\circ\text{C}$)	pH
	47	84.3	1.80
	74	84.3	1.33
	120	84.3	1.02
	153	84.2	0.33
	195	84.1	0.18
	246	84.2	0.08
	306	84.4	0.09
	322	84.4	0.09
	368	84.3	0.18
	386	84.4	0.16

D.3. DATA OF EXPERIMENT HC2.3

Table D.5 Calcium ion concentrations of the effluent streams during the Experiment HC2.3, Hisarcık 2 colemanite, 0-250 μm , $\text{CaO}/\text{SO}_4^{2-} = 1$, stirring rate = 400 rpm, T= 85°C, colemanite feed rate = 10 g/min

Reactor 1	Time (min)	Ca ²⁺ (ppm)
	36	1248
	80	1024
	182	1037
	242	1010
	270	964
	333	945
	383*	1003
Reactor 2	Time (min)	Ca ²⁺ (ppm)
	40	939
	83	736
	184	777
	244	590
	271	670
	334	617
	385*	672
Reactor 3	Time (min)	Ca ²⁺ (ppm)
	44	863
	85	653
	186	804
	245	493
	273	601
	362	546
	386*	530
Reactor 4	Time (min)	Ca ²⁺ (ppm)
	47	936
	87	602
	187	741
	247	525
	275	597
	363	474
	389*	591

* No B₂O₃ was detected in the solid.

Table D.6. Temperature and pH values during the Experiment HC2.3, Hisarcık 2 colemanite, 0-250 μm , $\text{CaO}/\text{SO}_4^{2-} = 1$, stirring rate = 400 rpm, $T = 85^\circ\text{C}$, colemanite feed rate = 10 g/min

Reactor 1	Time (min)	Temperature ($^\circ\text{C}$)	pH
	27	80.8	0.35
	53	80.3	0.31
	77	80.5	0.24
	184	81.8	0.22
	215	81.2	0.36
	252	82	0.26
	304	81.7	0.49
	317	82	0.48
	333	81.8	0.49
	371	82	0.49
Reactor 2	Time (min)	Temperature ($^\circ\text{C}$)	pH
	29	83.7	0.51
	54	83.8	0.38
	77	83.9	0.23
	184	83.9	0.19
	207	83.8	0.39
	253	83.6	0.32
	304	83.9	0.47
	318	83.9	0.49
	334	84	0.47
	371	84.1	0.45
Reactor 3	Time (min)	Temperature ($^\circ\text{C}$)	pH
	30	83.6	0.8
	55	83.5	0.48
	78	83.7	0.29
	190	83.5	0.27
	207	83.7	0.35
	253	83.5	0.36
	305	83.5	0.38
	319	83.6	0.46
	334	83.8	0.45
	373	83.2	0.45
Reactor 4	Time (min)	Temperature ($^\circ\text{C}$)	pH
	30	84	1.14
	56	84	0.67
	79	84.1	0.42
	191	84.1	0.33
	208	84.1	0.23
	253	84	0.32
	305	84	0.35
	319	84	0.42
	335	83.9	0.45
	374	83.9	0.44

D.4. DATA OF EXPERIMENT HC2.4

Table D.7. Calcium ion concentrations of the effluent streams during the Experiment HC2.4, Hisarcık 2 colemanite, 0-250 μm , $\text{CaO}/\text{SO}_4^{2-} = 1.37$, stirring rate = 400 rpm, $T = 85^\circ\text{C}$, colemanite feed rate = 5 g/min

Reactor 1	Time (min)	Ca ²⁺ (ppm)
	68	878
	127	763
	195	1691
	251	2795
	305	2473
	373	2763
	420**	2734
Reactor 2	Time (min)	Ca ²⁺ (ppm)
	70	655
	128	437
	196	1154
	253	2426
	308	3098
	375	3133
	423*	3053
Reactor 3	Time (min)	Ca ²⁺ (ppm)
	71	587
	133	478
	199	510
	256	1287
	311	2017
	344	3003
	377	3210
	442*	3107
Reactor 4	Time (min)	Ca ²⁺ (ppm)
	76	638
	136	545
	201	458
	263	655
	314	1382
	346	2937
	379	3496
	443*	3444

* No B₂O₃ was detected in the solid.

Table D.8. Temperature and pH values during the Experiment HC2.4, Hisarcık 2 colemanite, 0-250 μm , $\text{CaO}/\text{SO}_4^{2-} = 1.37$, stirring rate = 400 rpm, $T = 85^\circ\text{C}$, colemanite feed rate = 5 g/min

Reactor 1	Time (min)	Temperature ($^\circ\text{C}$)	pH
	63	82.1	3.7
	211	82.0	3.89
	241	82.2	3.94
	248	82.2	3.96
	256	82.2	3.98
	301	82.1	3.98
	325	82.3	3.92
	364	82.1	3.74
	382	82.2	3.84
Reactor 2	Time (min)	Temperature ($^\circ\text{C}$)	pH
	63	84.3	2.7
	78	83.6	2.8
	211	84.4	3.7
	242	84.5	3.7
	248	84.5	3.99
	257	84.3	4.1
	301	84.6	4.25
	327	84.8	4.25
	364	84.5	4.21
	382	84.2	4.13
Reactor 3	Time (min)	Temperature ($^\circ\text{C}$)	pH
	63	83.5	1.86
	78	83.4	2.18
	94	83.5	2.2
	155	82.9	2.38
	211	83.5	3.02
	243	83.5	3.31
	248	83.4	3.46
	257	83.4	3.66
	302	83.3	3.96
	327	83.3	4.09
	365	82.7	4.15
	383	83.2	4.12
	394	83.3	4.09
	425	82.8	4.04

Table D.8. Cont'd

Reactor 4	Time (min)	Temperature (°C)	pH
	63	84.5	1.87
	78	84.4	1.96
	94	84.3	2.01
	155	84.3	2.21
	211	84.4	2.5
	244	84.3	2.68
	248	84.3	2.85
	258	84.3	3.06
	302	84.3	3.49
	328	84.4	3.8
	365	84.4	3.89
	383	84.5	3.99
	395	84.5	3.89
	426	84.4	4.02

D.5. DATA OF EXPERIMENT HC2.5

Table D.9. Calcium ion concentrations of the effluent streams during the Experiment HC2.5, Hisarcık 2 colemanite, 0-250 μm , $\text{CaO}/\text{SO}_4^{2-} = 1.37$, stirring rate = 400 rpm, $T = 85^\circ\text{C}$, colemanite feed rate = 10 g/min

Reactor 1	Time (min)	Ca^{2+} (ppm)
	42	1035
	92	2334
	188	2808
	264	2463
	374	1687
	420*	1618
Reactor 2	Time (min)	Ca^{2+} (ppm)
	53	657
	123	3231
	194	4007
	270	3909
	376	2133
	421*	2103
Reactor 3	Time (min)	Ca^{2+} (ppm)
	78	529
	135	3298
	208	3896
	303	3621
	378	3302
	423*	2801
Reactor 4	Time (min)	Ca^{2+} (ppm)
	82	459
	138	2560
	215	3960
	308	3683
	380	3328
	431*	3167

* No B_2O_3 was detected in the solid.

Table D.10. Temperature and pH values during the Experiment HC2.5, Hisarcık 2 colemanite, 0-250 μm , $\text{CaO}/\text{SO}_4^{2-} = 1.37$, stirring rate = 400 rpm, $T = 85^\circ\text{C}$, colemanite feed rate = 10 g/min

Reactor 1	Time (min)	Temperature ($^\circ\text{C}$)	pH
	30	81.4	0.67
	84	82.3	3.22
	181	82.2	3.32
	240	82.4	3.56
	313	82.4	3.45
	360	82.2	3.10
	383	82.4	3.32
	393	82.2	3.51
Reactor 2	Time (min)	Temperature ($^\circ\text{C}$)	pH
	30	83.6	0.8
	84	83.6	3.63
	181	83.3	3.8
	240	83.8	3.82
	313	83.6	3.93
	360	83.4	3.84
	383	83.4	3.40
	393	83.3	3.46
Reactor 3	Time (min)	Temperature ($^\circ\text{C}$)	pH
	30	83.8	1.07
	84	83.9	3.34
	181	83.9	3.80
	240	84.3	3.87
	313	84.1	4.03
	360	84.0	3.95
	383	84.5	3.65
	393	84.5	3.75
Reactor 4	Time (min)	Temperature ($^\circ\text{C}$)	pH
	30	84.5	1.51
	84	84.5	2.19
	181	84.7	3.73
	240	84.7	3.84
	313	84.8	4.00
	360	84.7	4.00
	383	84.7	3.81
	393	84.8	3.91

D.6. DATA OF EXPERIMENT HC2.6

Table D.11. Calcium ion concentrations of the effluent streams during the Experiment HC2.6, Hisarcık 2 colemanite, 0-250 μm , $\text{CaO}/\text{SO}_4^{2-} = 1.37$, stirring rate = 400 rpm, $T = 85^\circ\text{C}$, colemanite feed rate = 10 g/min

Reactor 1	Time (min)	Ca^{2+} (ppm)
	47	989
	105	1895
	201	2305
	265	1956
	358	1710
	416*	1698
Reactor 2	Time (min)	Ca^{2+} (ppm)
	56	1598
	115	2865
	216	3564
	278	3853
	363	2896
	425*	2103
Reactor 3	Time (min)	Ca^{2+} (ppm)
	84	1416
	126	3003
	229	3568
	303	3708
	397	3100
	438*	2915
Reactor 4	Time (min)	Ca^{2+} (ppm)
	93	1349
	142	2301
	234	3652
	319	3412
	412	3369
	446*	3200

* No B_2O_3 was detected in the solid.

Table D.12. Temperature and pH values during the Experiment HC2.6, Hisarcık 2 colemanite, 0-250 μm , $\text{CaO}/\text{SO}_4^{2-} = 1.37$, stirring rate = 400 rpm, $T = 85^\circ\text{C}$, colemanite feed rate = 10 g/min

Reactor 1	Time (min)	Temperature ($^\circ\text{C}$)	pH
	45	81.4	0.57
	103	82.3	3.01
	198	82.2	3.18
	229	82.3	3.47
	335	82.5	3.46
	355	82.3	3.19
	390	82.4	3.40
	402	82.3	3.49
Reactor 2	Time (min)	Temperature ($^\circ\text{C}$)	pH
	45	83.3	0.78
	103	83.5	3.59
	198	83.4	3.75
	229	83.6	3.79
	335	83.6	3.91
	355	83.5	3.88
	390	83.3	3.45
	402	83.4	3.47
Reactor 3	Time (min)	Temperature ($^\circ\text{C}$)	pH
	46	83.7	1.05
	104	84.1	3.29
	199	83.9	3.75
	230	84.1	3.86
	336	84.2	3.98
	356	84.5	3.84
	391	84.4	3.71
	403	84.4	3.73
Reactor 4	Time (min)	Temperature ($^\circ\text{C}$)	pH
	46	84.3	1.49
	104	84.4	2.17
	199	84.6	3.67
	230	84.4	3.79
	336	84.5	4.00
	356	84.6	3.99
	391	84.6	3.85
	403	84.5	3.89

D.7. DATA OF EXPERIMENT HC2.7

Table D.13. Calcium ion concentrations of the effluent streams during the Experiment HC2.7, Hisarcık 2 colemanite, 0-250 μm , $\text{CaO}/\text{SO}_4^{2-} = 1.37$, stirring rate = 400 rpm, $T = 85^\circ\text{C}$, colemanite feed rate = 15 g/min

Reactor 1	Time (min)	Ca^{2+} (ppm)
	39	1318
	105	1095
	115	1231
	164	1310
	207	1343
	320	1069
	416*	1366
Reactor 2	Time (min)	Ca^{2+} (ppm)
	42	2358
	124	1960
	172	2398
	247	2330
	325	2363
	412*	2547
Reactor 3	Time (min)	Ca^{2+} (ppm)
	46	2560
	52	2648
	128	2409
	175	2360
	257	2822
	330	2714
	417*	2769
Reactor 4	Time (min)	Ca^{2+} (ppm)
	57	2464
	131	2848
	178	2112
	260	1568
	338	1957
	419*	1807

* No B_2O_3 was detected in the solid.

Table D.14. Temperature and pH values of the effluent streams during the Experiment HC2.7, Hisarcık 2 colemanite, 0-250 μm , $\text{CaO}/\text{SO}_4^{2-} = 1.37$, stirring rate = 400 rpm, $T = 85^\circ\text{C}$, colemanite feed rate = 15 g/min

Reactor 1	Time (min)	Temperature ($^\circ\text{C}$)	pH
	31	80.9	3.68
	64	81.3	2.69
	135	80.1	3.5
	164	81.1	3.36
	202	80.9	3.4
	267	81.1	2.12
	305	81.3	3.1
	375	79.6	3.43
	394	81.5	3.56
Reactor 2	Time (min)	Temperature ($^\circ\text{C}$)	pH
	31	83.5	4.19
	64	83.2	3.99
	129	82.9	3.93
	146	83.2	3.93
	202	82.5	3.94
	244	83.0	3.96
	267	83.1	3.74
	307	82.4	3.64
	375	82.3	3.95
	394	82.7	4.05
Reactor 3	Time (min)	Temperature ($^\circ\text{C}$)	pH
	31	83.5	4.02
	64	83.5	4.19
	129	83.3	4.02
	146	83.2	4.02
	203	83.1	4.03
	244	83.1	4.08
	269	83.1	3.97
	307	83	3.75
	377	82.9	4.05
	394	82.8	4.12
Reactor 4	Time (min)	Temperature ($^\circ\text{C}$)	pH
	31	83.1	3.63
	64	83.3	4.16
	129	83.3	4.04
	146	83.8	4.04
	205	83.8	4.04
	244	83.8	4.07
	269	83.7	4.07
	308	83.4	3.88
	377	83.4	4.05
	395	83.5	4.13

D.8. DATA OF EXPERIMENT HC2.8

Table D.15. Calcium ion concentrations of the effluent streams during the Experiment HC2.8, Hisarcık 2 colemanite, 0-250 μm , $\text{CaO}/\text{SO}_4^{2-} = 2.17$, stirring rate = 400 rpm, $T = 85^\circ\text{C}$, colemanite feed rate = 10 g/min

Reactor 1	Time (min)	Ca^{2+} (ppm)
	61	2948
	130	3085
	204	2872
	301	3355
	361*	3314
Reactor 2	Time (min)	Ca^{2+} (ppm)
	75	3627
	134	3191
	205	2876
	305	3183
	362*	3554
Reactor 3	Time (min)	Ca^{2+} (ppm)
	80	3390
	138	3976
	211	3692
	306	3362
	365*	3365
Reactor 4	Time (min)	Ca^{2+} (ppm)
	83	2584
	143	3014
	213	3784
	309	3037
	366*	3021

* B_2O_3 in the solid was detected as 0.10 mol/l.

Table D.16. Temperature and pH values during the Experiment HC2.8, Hisarcık 2 colemanite, 0-250 μm , $\text{CaO}/\text{SO}_4^{2-} = 2.17$, stirring rate = 400 rpm, $T = 85^\circ\text{C}$, colemanite feed rate = 10 g/min

Reactor 1	Time (min)	Temperature ($^\circ\text{C}$)	pH
	61	81.6	3.89
	89	82.1	3.97
	145	82.4	3.99
	196	82.2	3.98
	246	82.4	4.02
	270	82.4	4.02
	318	82.5	3.97
Reactor 2	Time (min)	Temperature ($^\circ\text{C}$)	pH
	61	83.1	3.99
	89	82.9	4.1
	145	82.8	4.09
	196	82.4	4.13
	270	82.2	4.12
	318	81.9	4.13
Reactor 3	Time (min)	Temperature ($^\circ\text{C}$)	pH
	61	83.7	3.48
	89	83.8	4.08
	145	83.5	4.12
	196	83.6	4.14
	246	83.4	4.12
	270	83.5	4.18
	318	83.3	4.22
Reactor 4	Time (min)	Temperature ($^\circ\text{C}$)	pH
	61	84.7	3.02
	89	84.3	3.6
	145	84.4	4.02
	196	84.4	4.03
	246	84.3	4.04
	270	84.3	4.18
	312	84.2	4.20

D.9. DATA OF EXPERIMENT HC3.1

Table D.17. Boric acid and calcium ion concentrations of the effluent streams during the Experiment HC3.1, Hisarcık 3 colemanite, 0-150 μm , $\text{CaO}/\text{SO}_4^{2-} = 1.00$, stirring rate = 400 rpm, $T = 85^\circ\text{C}$, colemanite feed rate = 3.5 g/min

Reactor 1	Time (min)	Ca^{2+} (ppm)	H_3BO_3 (mol/l)
	91		2.31
	241	370	
	242	399	
	248		2.39
	331		2.50
	361	418	
	423		2.54
Reactor 2	Time (min)	Ca^{2+} (ppm)	H_3BO_3 (mol/l)
	92		2.37
	242	412	
	242	376	
	252		2.26
	331		2.65
	362	319	
	424		2.50
	427	313	
Reactor 3	Time (min)	Ca^{2+} (ppm)	H_3BO_3 (mol/l)
	142	518	2.38
	244	368	
	266		2.42
	364	359	
	367		2.52
	425	353	
	427	271	
	432		2.53
Reactor 4	Time (min)	Ca^{2+} (ppm)	H_3BO_3 (mol/l)
	145	663	2.13
	245	569	
	268		2.27
	366	296	
	367		2.35
	427.8	263	
	432		2.50

Table D.18. Temperature and pH values during the Experiment HC3.1, Hisarcık 3 colemanite, 0-150 μm , $\text{CaO}/\text{SO}_4^{2-} = 1.00$, stirring rate = 400 rpm, $T = 85^\circ\text{C}$, colemanite feed rate = 3.5 g/min

Reactor 1	Time (min)	Temperature ($^\circ\text{C}$)	pH
	0	82.4	
	72	81.8	0.21
	131	81.1	0.41
	149	82	0.77
	196	82	0.66
	253	81.9	0.64
	274	81.9	0.69
	312	81.9	0.66
	381	82.2	0.65
	421	81.8	0.63
Reactor 2	Time (min)	Temperature ($^\circ\text{C}$)	pH
	0	83.5	
	73	83.5	0.22
	132	83.7	0.31
	150	83.9	0.37
	197	83.9	0.46
	254	83.9	0.6
	275	84	0.63
	312	84	0.67
	381	83.9	0.68
	421	84	0.7
Reactor 3	Time (min)	Temperature ($^\circ\text{C}$)	pH
	0		
	73	83.8	0.57
	132	83.2	0.33
	151	83.4	0.33
	194	83.6	0.38
	254	83.6	0.51
	274	83.7	0.54
	313	83.7	0.61
	382	83.4	0.71
	421	83.5	0.72
Reactor 4	Time (min)	Temperature ($^\circ\text{C}$)	pH
	74	84	1.01
	133	84	0.53
	151	84.5	0.44
	197	84.5	0.4
	255	84.6	0.47
	274	84.7	0.47
	313	84.8	0.53
	379.2	84.7	0.62
	421.2	84.7	0.58

D.10. DATA OF EXPERIMENT HC3.2

Table D.19. Boric acid and calcium ion concentrations of the effluent streams during the Experiment HC3.2, Hisarcık 3 colemanite, 0-150 μm , $\text{CaO}/\text{SO}_4^{2-} = 1.00$, stirring rate = 400 rpm, $T = 85^\circ\text{C}$, colemanite feed rate = 10 g/min

Reactor 1	Time (min)	Ca^{2+} (ppm)	H_3BO_3 (mol/l)
	48		2.66
	56	683	
	147		2.38
	172	643	
	274		2.47
	361		2.47
	364	625	
	396	554	
Reactor 2	Time (min)	Ca^{2+} (ppm)	H_3BO_3 (mol/l)
	50		2.78
	58	596	
	148		2.47
	173	437	
	300		2.53
	306	413	
	362		2.48
	368	384	
Reactor 3	Time (min)	Ca^{2+} (ppm)	H_3BO_3 (mol/l)
	59	456	
	62		2.55
	152	405	
	154		2.43
	305	405	
	307		2.55
	365	340	
	373		2.49
	383	327	
Reactor 4	Time (min)	Ca^{2+} (ppm)	H_3BO_3 (mol/l)
	61	567	
	153	347	
	155		2.66
	305	322	2.56
	307		2.33
	367	298	
	374		2.51

Table D.20. Temperature and pH values during the Experiment HC3.2, Hisarcık 3 colemanite, 0-150 μm , $\text{CaO}/\text{SO}_4^{2-} = 1.00$, stirring rate = 400 rpm, $T = 85^\circ\text{C}$, colemanite feed rate = 10 g/min

Reactor 1	Time (min)	Temperature ($^\circ\text{C}$)	pH
	0	82.5	
	28	79.5	0.47
	70	80.1	0.33
	92	81.5	0.56
	181	81.7	0.54
	202	82	0.19
	253	82.1	0.27
	314	82.3	0.28
	334	81.7	0.28
	391	82	0.3
Reactor 2	Time (min)	Temperature ($^\circ\text{C}$)	pH
	0	83.7	
	29	83.2	0.62
	69	83	0.45
	93	83.5	0.41
	181	83.3	0.52
	200	82.9	0.33
	252	83.3	0.35
	314	83.3	0.42
	334	83.1	0.4
	391	83.1	0.4
Reactor 3	Time (min)	Temperature ($^\circ\text{C}$)	pH
	0	83.5	
	30	84.1	0.91
	70	83.9	0.56
	94	83.4	0.49
	182	83	0.51
	199	82.7	0.48
	250	82.4	0.39
	310	82.7	0.46
	333	82.5	0.48
	391	82.3	0.45
Reactor 4	Time (min)	Temperature ($^\circ\text{C}$)	pH
	30	84.2	1.26
	70	84.1	0.68
	95	83.7	0.58
	182	83.7	0.54
	199	83.6	0.57
	248	83.7	0.55
	310	83.3	0.52
	333	83.3	0.57
	389	83.5	0.52

APPENDIX E

RAW DATA OF SOLID HOLD-UP EXPERIMENTS

In two of the experiments samples were taken to check if the solid hold-up was changing at steady state with respect to the reactor number or not. It was seen that the hold-up did not change considerably. The solid hold-up data of experiments performed are given in this section. The experimental conditions are as follows:

Experiment HC3.1:

Hisarcık 3 Colemanite, 0-150 μm , $\text{CaO}/\text{SO}_4^{2-} = 1.00$, Colemanite feed rate = 3.5 g/min

Experiment HC3.2:

Hisarcık 3 Colemanite, 0-150 μm , $\text{CaO}/\text{SO}_4^{2-} = 1.00$, Colemanite feed rate = 10 g/min

Table E.1. Variation of solid hold-up during the Experiment HC3.1, Hisarcık 3 colemanite, 0-150 μm , $\text{CaO}/\text{SO}_4^{2-} = 1.00$, colemanite feed rate = 3.5 g/min

Time, min	Filter number	Reactor number	Sample amount, g	Solid amount, g	Liquid amount, g	Solid/Total	Liquid/Total
258	1	1	19.52	1.86	17.66	0.10	0.90
260	2	2	18.64	1.74	16.90	0.09	0.91
263	3	3	21.27	1.35	19.92	0.06	0.94
266	4	4	21.35	0.93	20.42	0.04	0.96
358	5	1	16.9	1.81	15.09	0.11	0.89
360	6	2	20.55	2.39	18.16	0.12	0.88
362	7	3	18.96	1.77	17.19	0.09	0.91
408	8	4	14.38	1.07	13.31	0.07	0.93
442	10	1	17.18	2.14	15.04	0.12	0.88
448	11	2	16.92	2.09	14.83	0.12	0.88
447	9	3	14.95	1.47	13.48	0.10	0.90
450	12	4	19.75	1.70	18.05	0.09	0.91

195

Solid Hold-up at the inlet of the first CSTR was

Solid/Total	Liquid/Total
0.10	0.90

Table E.2. Variation of solid hold-up during the Experiment HC3.2, Hisarcık 3 colemanite, 0-150 μm , $\text{CaO}/\text{SO}_4^{2-} = 1.00$, colemanite feed rate = 10 g/min

Time, min	Filter number	Reactor number	Sample amount, g	Solid amount, g	Liquid amount, g	Solid/Total	Liquid/Total
215	1	1	15.24	1.56	13.68	0.10	0.90
240	2	2	18.07	1.55	16.52	0.09	0.91
242	3	3	15.50	2.41	13.09	0.16	0.84
244	4	4	16.13	1.35	14.78	0.08	0.92
322	5	1	13.24	1.55	11.69	0.12	0.88
326	6	2	19.06	1.78	17.28	0.09	0.91
329	7	3	23.07	2.22	20.85	0.10	0.90
332	8	4	21.51	1.91	19.60	0.09	0.91
387	9	1	13.60	1.42	12.18	0.10	0.90
389	10	2	13.4	1.11	12.29	0.08	0.92
391	11	3	16.43	1.51	14.92	0.09	0.91
394	12	4	13.34	1.17	12.17	0.09	0.91

196

Solid Hold-up at the inlet of the first CSTR was

Solid/Total	Liquid/Total
0.10	0.90

APPENDIX F

SAMPLE CALCULATIONS

In this part the sample calculations are given on a representative experiment, where $\text{CaO} / \text{SO}_4^{2-}$ molar ratio is 1.00 and the colemanite feed rate is 10 g/min. The following sample calculations are given:

F.1. $\text{CaO} / \text{SO}_4^{2-}$ Molar Ratio Calculation

F.2. Solid Hold-up Calculation

F.3. Residence Time of Solid and Liquid Components in the Reactor

F.4. Material Balances

F.5. Conversion Calculations

F.6. Unit Conversions

F.1. CAO / SO₄²⁻ MOLAR RATIO CALCULATION

For Continuous Reactors:

Flow rate of colemanite: 10 g/min

Flow rate of acid: 97 g/min

CaO and SO₄²⁻ come to the reactor from colemanite and sulfuric acid, respectively.

The molar flow rate can be calculated from the following relations.

$$\text{CaO} = \left(\frac{10 \text{ g. colemanite}}{\text{min}} \right) \cdot \left(\frac{0.3090 \text{ g. CaO}}{\text{g. colemanite}} \right) \cdot \left(\frac{1 \text{ mol CaO}}{56 \text{ g.}} \right) = 0.055 \text{ mol/min}$$

$$\begin{aligned} \text{SO}_4^{2-} &= \left(\frac{97 \text{ g. acid}}{\text{min}} \right) \cdot \left(\frac{0.0558 \text{ g. H}_2\text{SO}_4}{\text{g. acid fed}} \right) \cdot \left(\frac{1 \text{ mol H}_2\text{SO}_4}{98 \text{ g.}} \right) \cdot \left(\frac{1 \text{ mol SO}_4^{2-}}{1 \text{ mol H}_2\text{SO}_4} \right) \\ &= 0.055 \text{ mol/min} \end{aligned}$$

$$\frac{\text{CaO}}{\text{SO}_4^{2-}} = \frac{0.055 \text{ mol/min}}{0.055 \text{ mol/min}} = 1 \text{ mol / mol}$$

For batch Reactor:

Amount of Colemanite added to the reactor: 169 g

Amount of Sulphuric Acid (%93 by weight) added to the reactor: 97 g

CaO and SO₄²⁻ come to the reactor from colemanite and sulfuric acid, respectively.

$$\text{CaO} = (169 \text{ g. colemanite}) \cdot \left(\frac{0.3090 \text{ g. CaO}}{\text{g. colemanite}} \right) \cdot \left(\frac{1 \text{ mol CaO}}{56 \text{ g.}} \right) = 0.93 \text{ mol}$$

$$\begin{aligned} \text{SO}_4^{2-} &= (53.57 \text{ ml. acid}) \cdot \left(\frac{1.84 \text{ g. acid}}{1 \text{ ml acid}} \right) \cdot \left(\frac{93 \text{ g H}_2\text{SO}_4}{100 \text{ g. acid}} \right) \cdot \left(\frac{1 \text{ mol H}_2\text{SO}_4}{98 \text{ g. H}_2\text{SO}_4} \right) \cdot \left(\frac{1 \text{ mol SO}_4^{2-}}{1 \text{ mol H}_2\text{SO}_4} \right) \\ &= 0.93 \text{ mol} \end{aligned}$$

$$\frac{\text{CaO}}{\text{SO}_4^{2-}} = \frac{0.93 \text{ mol}}{0.93 \text{ mol}} = 1$$

F.2. SOLID HOLD-UP, h_s , CALCULATION

Flow rate of colemanite: 10 g/min Density of colemanite: 2.4 g/ml

Flow rate of acid: 97 g/min Density of acid: 1.06 g/ml

$$h_s = \frac{v_s}{v_T} = \frac{\text{Volumetric flow rate of solid}}{\text{Total Volumetric flow rate}}$$

By knowing the densities of the colemanite and acid fed to the reactor, volumetric flow rates of the streams can be found.

$$v_s = \frac{10 \text{ g / min}}{2.4 \text{ g / ml}} = 4.17 \text{ ml / min}$$

$$v_L = \frac{97 \text{ g / min}}{1.06 \text{ g / ml}} = 91.51 \text{ ml / min}$$

$$v_T = 4.17 + 91.51 = 95.68 \text{ ml / min}$$

$$h_s = \frac{v_s}{v_T} = \frac{4.17 \text{ ml / min}}{95.68 \text{ ml / min}} = 0.04$$

F.3. RESIDENCE TIME OF SOLID AND LIQUID COMPONENTS IN THE REACTORS

For a given solid hold-up and the total volume of the reactor, the residence time of solid and liquid can be calculated. The solid hold-up can also be calculated as:

$$h_s = \frac{V_s}{V_T} = \frac{\text{Volume of solid}}{\text{Total Volume}}$$

Residence time of solid and liquid can be written from its definitions as:

$$\tau_s = \frac{V_s}{v_s} = \frac{\text{Volume of solid}}{\text{Volumetric flow rate of solid}}$$

and

$$\tau_L = \frac{V_L}{v_L} = \frac{\text{Volume of liquid}}{\text{Volumetric flow rate of liquid}}$$

The calculation of the volumetric flow rates of the solid and liquid components is shown in Part F.2. The formula can be written as:

$$v_s = \frac{\dot{m}_s}{\rho_s} = \frac{\text{mass flow rate of solid}}{\text{density of solid}}$$

$$v_L = \frac{\dot{m}_L}{\rho_L} = \frac{\text{mass flow rate of liquid}}{\text{density of liquid}}$$

From the summation of the formulae, the residence time definitions can be written as:

$$\tau_s = \frac{V_s}{v_s} = \frac{h_s \cdot V_T}{\dot{m}_s / \rho_s}$$

$$V_L = V_T - V_s$$

$$\tau_L = \frac{V_L}{v_L} = \frac{V_T - V_s}{\dot{m}_L / \rho_L}$$

Total volume of reactor = 1800 ml

\dot{m}_s = flow rate of colemanite = 10 g/min ρ_s = density of colemanite = 2.4 g/ml

\dot{m}_L = flow rate of acid = 97 g/min ρ_L = density of acid = 1.06 g/ml

h_s = solid hold-up = 0.04

$$\tau_s = \frac{V_s}{v_s} = \frac{h_s \cdot V_T}{\dot{m}_s / \rho_s} = \frac{0.04 \cdot (1800 \text{ ml})}{(10 \text{ g/min}) / (2.4 \text{ g/ml})} = 17.28 \text{ min}$$

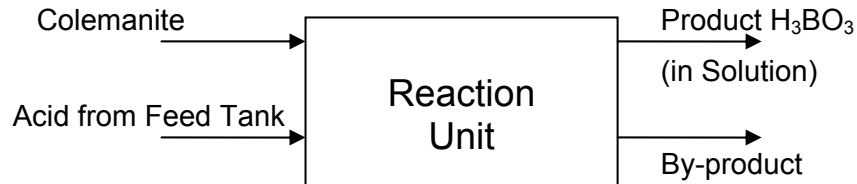
$$V_s = 0.04 \times 1800 = 72 \text{ ml}$$

$$V_L = V_T - V_s = 1800 - 72 = 1728 \text{ ml}$$

$$\tau_L = \frac{V_L}{v_L} = \frac{V_T - V_s}{\dot{m}_L / \rho_L} = \frac{1728 \text{ ml}}{(97 \text{ g/min}) / (1.03 \text{ g/ml})} = 18.35 \text{ min}$$

F.4. MATERIAL BALANCES

The flow chart of the reaction unit can be visualized as follows:



BORIC ACID BALANCE:

- Colemanite entering the reactor

B_2O_3 content of the Hisarcık 2 colemanite is 43.57%. So, the molar flow rate of the boric acid entering the reaction unit can be calculated.

Flow rate of colemanite: 10 g/min

Boric acid in by colemanite = BA_{col}

$$BA_{col} = \left(\frac{10 \text{ g. colemanite}}{\text{min}} \right) \cdot \left(\frac{0.4357 \text{ g. } B_2O_3}{\text{g. colemanite}} \right) \cdot \left(\frac{1 \text{ mol } B_2O_3}{69.6 \text{ g.}} \right) \cdot \left(\frac{2 \text{ mol B}}{1 \text{ mol } B_2O_3} \right) \cdot \left(\frac{1 \text{ mol } H_3BO_3}{1 \text{ mol B}} \right)$$

$$BA_{col} = 0.125 \text{ mol } H_3BO_3/\text{min}$$

- Acid from Feed tank

Acid tank contains 8% of boric acid.

Flow rate of acid: 97 g/min

Boric acid in by acid fed = BA_{tank}

$$BA_{tank} = \left(\frac{97 \text{ g. acid}}{\text{min}} \right) \cdot \left(\frac{0.08 \text{ g. } H_3BO_3}{\text{g. acid}} \right) \cdot \left(\frac{1 \text{ mol } H_3BO_3}{61.8 \text{ g.}} \right)$$

$$BA_{\text{tank}} = 0.125 \text{ mol H}_3\text{BO}_3/\text{min}$$

- H₃BO₃ as Product

The liquid at the outlet of the reaction unit has the same flow rate with the acid entering to the reaction unit. The boric acid concentrations of the effluent streams are found from the boron analysis.

$$\text{Flow rate of liquid: } 97 \text{ g/min} \quad \rho_L = \text{density of acid} = 1.03 \text{ g/ml}$$

$$\text{Boric acid at the outlet of the fourth reactor: } 2.66 \text{ mol/l}$$

$$BA_{\text{prod}} = \left(\frac{97 \text{ g. acid}}{\text{min}} \right) \cdot \left(\frac{1 \text{ ml}}{1.03 \text{ g. acid}} \right) \cdot \left(\frac{2.66 \text{ mol H}_3\text{BO}_3}{\text{l}} \right) \cdot \left(\frac{1 \text{ l}}{1000 \text{ ml}} \right)$$

$$BA_{\text{prod}} = 0.250 \text{ mol H}_3\text{BO}_3/\text{min}$$

- By-product

The solid part separated from the product is the by-product of the reaction, namely gypsum. It is analyzed in order to find out if it has some amount of unreacted colemanite in it. But no boron trioxide is detected in the waste.

F.5. CONVERSION CALCULATIONS

This part will be explained by using the data of the material balances part.

- From the incoming colemanite

$$BA_{\text{col}} = \text{Boric acid entering the system by colemanite}$$

$$BA_{\text{tank}} = \text{Boric acid entering the system from the acid tank}$$

$$BA_{\text{prod}} = \text{Boric acid out from the system in solution}$$

$$\begin{aligned} \% \text{ conversion} &= \frac{BA_{\text{prod}} - BA_{\text{tank}}}{BA_{\text{col}}} \cdot 100 = \frac{BA_{\text{conv}}}{BA_{\text{col}}} \cdot 100 \\ &= \frac{\text{Boric acid produced from colemanite}}{\text{Entering colemanite}} \end{aligned}$$

$$\% \text{ conversion} = \frac{0.125}{0.125} \cdot 100 = 100\%$$

- From the incoming sulfate ion

The acid tank contains 5.58 % of sulfuric acid. The colemanite entering the reaction system has a negligible amount of sulfate in it. So, it can be neglected.

The sulfate ion concentration at the outlet of the reaction unit is found from the sulfate analysis.

SI_{in} = Amount of SO_4^{2-} in by the sulfuric acid

SI_{out} = Amount of SO_4^{2-} out from the system

$$SI_{\text{in}} = \left(\frac{97 \text{ g. acid}}{\text{min}} \right) \cdot \left(\frac{0.0558 \text{ g. H}_2\text{SO}_4}{\text{g. acid}} \right) \cdot \left(\frac{1 \text{ mol H}_2\text{SO}_4}{98 \text{ g.}} \right) \cdot \left(\frac{1 \text{ mol SO}_4^{2-}}{1 \text{ mol H}_2\text{SO}_4} \right)$$

$$SI_{\text{in}} = 0.055 \text{ mol /min}$$

$$SI_{\text{out}} = 0.00775 \text{ mol/min}$$

$$\% \text{ conversion} = \frac{SI_{\text{in}} - SI_{\text{out}}}{SI_{\text{in}}} \cdot 100 = \frac{\text{Sulfate ion in solid}}{\text{Entering sulfate ion}}$$

$$\% \text{ conversion} = \frac{0.055 - 0.00775}{0.055} \cdot 100 = 86\%$$

F.6. UNIT CONVERSIONS

- Calcium ion concentration

The calcium ion results have the units of ppm. It should be converted to mol Ca^{2+} /min. In order to do the conversion, the following expression is used.

$$\text{Liquid flow rate} = (97 \text{ g/min}) / (1.03 \text{ g/ml}) = 94.17 \text{ ml/min}$$

Ca^{2+} concentration at the outlet of the fourth reactor: 600 ppm

$$\text{Ca}^{2+} (\text{ppm}) = (600 \text{ ppm}) \cdot \left(\frac{1 \text{ mg/l}}{1 \text{ ppm}} \right) \cdot \left(\frac{94.17 \text{ ml}}{\text{min}} \right) \cdot \left(\frac{1 \text{ mol Ca}^{2+}}{40 \text{ g.}} \right) \cdot \left(\frac{1 \text{ g}}{1000 \text{ mg}} \right) \cdot \left(\frac{1 \text{ l}}{1000 \text{ ml}} \right)$$

$$\text{Ca}^{2+} = 0.0014 \text{ mol/min}$$

- Sulfate ion concentration

The sulfate ion results have the units of ppm. It should be converted to mol SO_4^{2-} /min. In order to do the conversion, the following expression is used.

$$\text{Liquid flow rate} = (97 \text{ g/min}) / (1.03 \text{ g/ml}) = 94.17 \text{ ml/min}$$

SO_4^{2-} concentration at the outlet of the fourth reactor: 7900 ppm

$$\text{SO}_4^{2-} (\text{ppm}) = (7900 \text{ ppm}) \cdot \left(\frac{1 \text{ mg/l}}{1 \text{ ppm}} \right) \cdot \left(\frac{94.17 \text{ ml}}{\text{min}} \right) \cdot \left(\frac{1 \text{ mol SO}_4^{2-}}{96 \text{ g.}} \right) \cdot \left(\frac{1 \text{ g}}{1000 \text{ mg}} \right) \cdot \left(\frac{1 \text{ l}}{1000 \text{ ml}} \right)$$

$$\text{SO}_4^{2-} = 0.00775 \text{ mol/min}$$

- Magnesium ion concentration

The calcium ion results have the units of ppm. It should be converted to mol Mg^{2+} /min. In order to do the conversion, the following expression is used.

$$\text{Liquid flow rate} = (97 \text{ g/min}) / (1.03 \text{ g/ml}) = 94.17 \text{ ml/min}$$

Mg^{2+} concentration at the outlet of the fourth reactor: 332 ppm

$$\text{Mg}^{2+} (\text{ppm}) = (332 \text{ ppm}) \cdot \left(\frac{1 \text{ mg/l}}{1 \text{ ppm}} \right) \cdot \left(\frac{94.17 \text{ ml}}{\text{min}} \right) \cdot \left(\frac{1 \text{ mol Ca}^{2+}}{24.3 \text{ g.}} \right) \cdot \left(\frac{1 \text{ g}}{1000 \text{ mg}} \right) \cdot \left(\frac{1 \text{ l}}{1000 \text{ ml}} \right)$$

$$\text{Mg}^{2+} = 0.00129 \text{ mol/min}$$

APPENDIX G

MODELING

In modeling part of the thesis, macrofluid and microfluid models were simulated utilizing the gypsum crystal growth model obtained from batch reactor experimental data.

In this section Mat Lab Programs of the macrofluid and microfluid models were given for experiments HB2.1 & HB2.2. The function for gypsum crystal growth model and the residence times were changed and the program was executed for the other experiments at different residence times. The representative outputs of the programs were also given in section G.3.

G.1. Macrofluid Model Mat Lab Program

G.2: Microfluid Model Mat Lab Program

G.3. Mat Lab Program Outputs for the Verification of Experimental Data

G.1: MACROFLUID MODEL MAT LAB PROGRAM

```

function conc;
clear;
% Time Constant vector
tao=[20,40,60,100,240];
tao=60*tao;
% Final time values for the integral
maxtime1=150000;
maxtime2=400000;
% -----
results=zeros(5,8);
errort1t2=zeros(5,8);

t=0:0.5:maxtime1;
t2=0:0.5:maxtime2;
fprintf(' Time 1 = %15.0f \n',maxtime1);
fprintf(' Time 2 = %15.0f \n',maxtime2);
for k=1:5
    for n=1:8
        Conc=C(t).*E(t,tao(k)/n,n);
        Conc2=C(t2).*E(t2,tao(k)/n,n);
        results(k,n)=trapz(t2,Conc2);
        errort1t2(k,n)=abs(trapz(t,Conc)-trapz(t2,Conc2));
    end
end
fprintf('-----Results-----\n');
fprintf('          tao1= %3.0f s   tao2= %3.0f s   tao3= %3.0f\n',tao(1),tao(2),tao(3),tao(4),tao(5));
s          tao4=      %3.0f      s          tao5=      %3.0f
s\n',tao(1),tao(2),tao(3),tao(4),tao(5));
for n=1:8
    fprintf('n = %2d -> ',n);
    for k=1:5
        fprintf('%15.6f',results(k,n));
    end
    fprintf('\n');
end
fprintf('-----Errors-----\n');
fprintf('          tao1= %3.0f s   tao2= %3.0f s   tao3= %3.0f s\n',tao(1),tao(2),tao(3),tao(4),tao(5));
tao4=      %3.0f      s          tao5=      %3.0f
s\n',tao(1),tao(2),tao(3),tao(4),tao(5));
for n=1:8
    fprintf('n = %2d -> ',n);
    for k=1:5
        fprintf('%15.6e',errort1t2(k,n));
    end
    fprintf('\n');
end

% Function definitions
function y=C(t)
y=(49.1+0.013.*t)./(925.9+t);

function y2=E(t,taof,n)
y2=( (t.^(n-1)) / (factorial(n-1).*taof.^n) ).*exp(-t/taof);

```

G.2: MICROFLUID MODEL MAT LAB PROGRAM

```
function cstr
clc;
tao=[20 40 60 100 240 ];
tao=60*tao;
n=[1 2 3 4 6 8] ;
Ca0=0.053;
C=zeros(6,6);
fprintf('-----\n');
-----\n');
for i= 1:5
    for j= 1:6
        Ca0=0.053;
        for k=1:n(j)
            C(k,j)=bul (Ca0,tao(i)/n(j));
            Ca0=C(k,j);
        end
    end
    fprintf('tao = %5.2f \n',tao(i));
    fprintf('-----\n');
-----\n');
    disp(C);
    fprintf('-----\n');
-----\n');
end

function y=bul (Ca0,tao)
k=0.027;
Csat=0.013;
x1=1/2/k/tao*(2*k*tao*Csat-1+(-4*k*tao*Csat+1+4*k*tao*Ca0)^(1/2));
x2=1/2/k/tao*(2*k*tao*Csat-1-(-4*k*tao*Csat+1+4*k*tao*Ca0)^(1/2));

if (x1> x2)
    y=x1;
elseif (x2>x1)
    y=x2;
elseif (x1 > 0) & ( x2 > 0),
    fprintf('iki pozitif kök, x1 seçildi') ;
    y=x1;
else
    break
end
```

G.3. MAT LAB PROGRAM OUTPUTS FOR THE VERIFICATION OF EXPERIMENTAL DATA

The residence times selected for the execution of the programs for Experiment HC3.2 was 20, 40, 60 and 80 minutes. For Experiment HC3.1, the residence times were 60, 120, 180 and 240 minutes. These residence times were selected as the residence times in experiments were 60 and 20 min for experiments HC3.1 and HC3.2, respectively. The crystal growth model for Experiment HB3.1 was used in the models. The values used for the verification of the experimental data were put into the borders in Tables G.1- G.4.

Table G.1. Output of Mat Lab Program for microfluid model for the verification of Experiment HC3.1

tao = 3600.00						
1-CSTR	2-CSTR	3-CSTR	4-CSTR	6-CSTR	8-CSTR	
0.0101	0.0117	0.0129	0.0138	0.0152	0.0162	
0	0.0083	0.0090	0.0097	0.0108	0.0117	
0	0	0.0077	0.0081	0.0090	0.0097	
0	0	0	0.0074	0.0080	0.0086	
0	0	0	0	0.0075	0.0079	
0	0	0	0	0.0071	0.0075	
0	0	0	0	0	0.0072	
0	0	0	0	0	0.0070	
tao = 7200.00						
1-CSTR	2-CSTR	3-CSTR	4-CSTR	6-CSTR	8-CSTR	
0.0089	0.0101	0.0110	0.0117	0.0129	0.0138	
0	0.0073	0.0078	0.0083	0.0090	0.0097	
0	0	0.0068	0.0071	0.0077	0.0081	
0	0	0	0.0066	0.0070	0.0074	
0	0	0	0	0.0067	0.0069	
0	0	0	0	0.0064	0.0067	
0	0	0	0	0	0.0065	
0	0	0	0	0	0.0063	
tao = 10800.00						
1-CSTR	2-CSTR	3-CSTR	4-CSTR	6-CSTR	8-CSTR	
0.0083	0.0094	0.0101	0.0107	0.0117	0.0125	
0	0.0069	0.0073	0.0077	0.0083	0.0088	
0	0	0.0065	0.0067	0.0071	0.0075	
0	0	0	0.0063	0.0066	0.0069	
0	0	0	0	0.0064	0.0066	
0	0	0	0	0.0062	0.0064	
0	0	0	0	0	0.0062	

	0	0	0	0	0	0.0061

tao = 14400.00						

1-CSTR	2-CSTR	3-CSTR	4-CSTR	6-CSTR	8-CSTR	

0.0080	0.0089	0.0096	0.0101	0.0110	0.0117	
0	0.0067	0.0070	0.0073	0.0078	0.0083	
0	0	0.0063	0.0065	0.0068	0.0071	
0	0	0	0.0062	0.0064	0.0066	
0	0	0	0	0.0062	0.0064	
0	0	0	0	0.0061	0.0062	
0	0	0	0	0	0.0061	
0	0	0	0	0	0.0060	

tao = 18000.00						

1-CSTR	2-CSTR	3-CSTR	4-CSTR	6-CSTR	8-CSTR	

0.0077	0.0086	0.0092	0.0097	0.0105	0.0112	
0	0.0065	0.0068	0.0071	0.0075	0.0079	
0	0	0.0062	0.0064	0.0066	0.0069	
0	0	0	0.0061	0.0063	0.0065	
0	0	0	0	0.0061	0.0062	
0	0	0	0	0.0060	0.0061	
0	0	0	0	0	0.0060	
0	0	0	0	0	0.0059	

Table G.2. Output of Mat Lab Program for microfluid model for the verification of Experiment HC3.2

tao = 1200.00						

1-CSTR	2-CSTR	3-CSTR	4-CSTR	6-CSTR	8-CSTR	

0.0129	0.0152	0.0167	0.0178	0.0195	0.0207	
0	0.0108	0.0121	0.0132	0.0149	0.0162	
0	0	0.0100	0.0109	0.0124	0.0136	
0	0	0	0.0096	0.0109	0.0120	
0	0	0	0	0.0099	0.0109	
0	0	0	0	0.0092	0.0101	
0	0	0	0	0	0.0095	
0	0	0	0	0	0.0090	

tao = 2400.00						

1-CSTR	2-CSTR	3-CSTR	4-CSTR	6-CSTR	8-CSTR	

0.0110	0.0129	0.0142	0.0152	0.0167	0.0178	
0	0.0090	0.0100	0.0108	0.0121	0.0132	
0	0	0.0084	0.0090	0.0100	0.0109	
0	0	0	0.0080	0.0089	0.0096	
0	0	0	0	0.0082	0.0088	
0	0	0	0	0.0077	0.0082	
0	0	0	0	0	0.0078	
0	0	0	0	0	0.0075	

tao = 3600.00						

1-CSTR	2-CSTR	3-CSTR	4-CSTR	6-CSTR	8-CSTR
0.0101	0.0117	0.0129	0.0138	0.0152	0.0162
0	0.0083	0.0090	0.0097	0.0108	0.0117
0	0	0.0077	0.0081	0.0090	0.0097
0	0	0	0.0074	0.0080	0.0086
0	0	0	0	0.0075	0.0079
0	0	0	0	0.0071	0.0075
0	0	0	0	0	0.0072
0	0	0	0	0	0.0070

tao = 4800.00					

1-CSTR	2-CSTR	3-CSTR	4-CSTR	6-CSTR	8-CSTR
0.0096	0.0110	0.0120	0.0129	0.0142	0.0152
0	0.0078	0.0085	0.0090	0.0100	0.0108
0	0	0.0073	0.0077	0.0084	0.0090
0	0	0	0.0070	0.0075	0.0080
0	0	0	0	0.0071	0.0075
0	0	0	0	0.0068	0.0071
0	0	0	0	0	0.0068
0	0	0	0	0	0.0067

tao = 6000.00					

1-CSTR	2-CSTR	3-CSTR	4-CSTR	6-CSTR	8-CSTR
0.0092	0.0105	0.0115	0.0122	0.0134	0.0144
0	0.0075	0.0081	0.0086	0.0094	0.0102
0	0	0.0070	0.0074	0.0080	0.0085
0	0	0	0.0068	0.0072	0.0076
0	0	0	0	0.0068	0.0072
0	0	0	0	0.0066	0.0068
0	0	0	0	0	0.0066
0	0	0	0	0	0.0065

Table G.3. Output of Mat Lab Program for macrofluid model for the verification of Experiment HC3.1

Time 1 =	150000				
Time 2 =	300000				
-----Results-----					
	tao1= 3600 s	tao2= 7200 s	tao3= 10800 s	tao4= 14400 s	tao5= 18000 s
n = 1 ->	0.008889	0.007579	0.007053	0.006762	0.006574
n = 2 ->	0.007392	0.006548	0.006246	0.006091	0.005996
n = 3 ->	0.007050	0.006348	0.006104	0.005980	0.005905
n = 4 ->	0.006912	0.006272	0.006051	0.005940	0.005873
n = 5 ->	0.006839	0.006232	0.006024	0.005919	0.005856
n = 6 ->	0.006794	0.006208	0.006008	0.005907	0.005846
n = 7 ->	0.006763	0.006192	0.005997	0.005899	0.005839
n = 8 ->	0.006741	0.006180	0.005989	0.005893	0.005834
-----Errors-----					
	tao1= 3600 s	tao2= 7200 s	tao3= 10800 s	tao4= 14400 s	tao5= 18000 s
n = 1 ->	0.000000e+000	5.033225e-012	5.225351e-009	1.682811e-007	1.351114e-006
n = 2 ->	0.000000e+000	0.000000e+000	1.363779e-013	1.099811e-010	5.739970e-009
n = 3 ->	0.000000e+000	0.000000e+000	0.000000e+000	7.545874e-014	2.643398e-011
n = 4 ->	0.000000e+000	0.000000e+000	0.000000e+000	0.000000e+000	1.240509e-013
n = 5 ->	0.000000e+000	0.000000e+000	0.000000e+000	0.000000e+000	0.000000e+000
n = 6 ->	0.000000e+000	0.000000e+000	0.000000e+000	0.000000e+000	0.000000e+000
n = 7 ->	0.000000e+000	0.000000e+000	0.000000e+000	0.000000e+000	0.000000e+000
n = 8 ->	0.000000e+000	0.000000e+000	0.000000e+000	0.000000e+000	0.000000e+000

Table G.4. Output of Mat Lab Program for macrofluid model for the verification of Experiment HC3.2

Time 1 =	150000				
Time 2 =	300000				
-----Results-----					
	tao1= 1200 s	tao2= 2400 s	tao3= 3600 s	tao4= 4800 s	tao5= 6000 s
n = 1 ->	0.012481	0.009965	0.008889	0.008273	0.007868
n = 2 ->	0.010185	0.008164	0.007392	0.006980	0.006723
n = 3 ->	0.009516	0.007713	0.007050	0.006704	0.006492
n = 4 ->	0.009215	0.007524	0.006912	0.006595	0.006402
n = 5 ->	0.009047	0.007422	0.006839	0.006538	0.006355
n = 6 ->	0.008941	0.007359	0.006794	0.006504	0.006327
n = 7 ->	0.008868	0.007315	0.006763	0.006480	0.006308
n = 8 ->	0.008814	0.007284	0.006741	0.006463	0.006294
-----Errors-----					
	tao1= 1200 s	tao2= 2400 s	tao3= 3600 s	tao4= 4800 s	tao5= 6000 s
n = 1 ->	0.000000e+000	0.000000e+000	0.000000e+000	0.000000e+000	7.093978e-014
n = 2 ->	0.000000e+000	0.000000e+000	0.000000e+000	0.000000e+000	0.000000e+000
n = 3 ->	0.000000e+000	0.000000e+000	0.000000e+000	0.000000e+000	0.000000e+000
n = 4 ->	0.000000e+000	0.000000e+000	0.000000e+000	0.000000e+000	0.000000e+000
n = 5 ->	0.000000e+000	0.000000e+000	0.000000e+000	0.000000e+000	0.000000e+000
n = 6 ->	0.000000e+000	0.000000e+000	0.000000e+000	0.000000e+000	0.000000e+000
n = 7 ->	0.000000e+000	0.000000e+000	0.000000e+000	0.000000e+000	0.000000e+000
n = 8 ->	0.000000e+000	0.000000e+000	0.000000e+000	0.000000e+000	0.000000e+000

VITA

Gaye . (Yücel) akal was born in ankaya, Ankara on March 01, 1974. She was graduated in 1991 from the High School of TED Ankara College. She received her B.S. degree in Chemical Engineering from the Middle East Technical University in June 1995. Since 1997 she has been a graduate assistant in the Department of Chemical Engineering. She received her M.Sc. degree from the same department in September 1998. She performed her M.Sc. thesis study on the reactivity of coal in carbonization and gasification by thermogravimetric analysis under the supervision of Prof. Dr. Güniz Gürüz and Prof. Dr. Hayrettin Yücel. Her main areas of interest are the design of slurry reactors, boric acid production in continuous reactors and modeling of industrial reactors. Her research has been published in the international and national proceedings.